1117

TRANSPORTATION RESEARCH RECORD

Pavement Evaluation and Rehabilitation

TRANSPORTATION RESEARCH BOARD
NATIONAL RESEARCH COUNCIL
WASHINGTON, D.C. 1987

Transportation Research Record 1117
Price: $25.00
Typesetter: Lucinda Reeder
Layout: Betty Hawkins

mode
1 highway transportation

subject areas
24 pavement design and performance
40 maintenance

Transportation Research Board publications are available by ordering directly from TRB. They may also be obtained on a regular basis through organizational or individual affiliation with TRB; affiliates or library subscribers are eligible for substantial discounts. For further information, write to the Transportation Research Board, National Research Council, 2101 Constitution Avenue, N.W., Washington, D.C. 20418.

Printed in the United States of America

Library of Congress Cataloging-in-Publication Data
National Research Council. Transportation Research Board.

Pavement evaluation and rehabilitation.

p. cm.—(Transportation research record, ISSN 0361–1981 ; 1117)
ISBN 0-309-04470-7
1. Pavements—Maintenance and repair—Congresses. I. National Research Council (U.S.). Transportation Research Board. II. Series.
TE7.H5 no. 1117
380.5 s—dc19
[625.7'd1] 87–31308
CIP

Sponsorship of Transportation Research Record 1117

GROUP 2—DESIGN AND CONSTRUCTION OF TRANSPORTATION FACILITIES
David S. Gedney, Harland Bartholomew & Associates, chairman

Pavement Management Section
R. G. Hicks, Oregon State University, chairman

Committee on Pavement Rehabilitation
Gordon W. Beecroft, chairman
James F. Shook, ARE, Inc., secretary
Edward Aikman, Ralph W. Allen, Paul Autrel, Martin L. Cawley, G.G. Davison, Paul J. Diethelm, Denis E. Donnelly, Wade L. Gramling, David J. Halpenny, Joseph B. Hannon, W.J. Head, James W. Hill, Walter P. Kilareski, Joe P. Mohoney, Richard W. May, William G. Miley, Gene R. Mooris, Louis G. O'Brien, John C. Potter, R.N. Stubstad, Harvey J. Treybig, Robert L. White, Loren M. Womack

Committee on Strength and Deformation Characteristics of Pavement Sections
J. Brent Rauhut, Brent Rauhut Engineering, Inc., chairman
Joseph H. Amed III, Gilbert Y. Baladi, Richard D. Barksdael, Stephen F. Brown, Albert J. Bush III, George R. Cochran, Billy G. Connor, Amir N. Hanna, R.G. Hicks, Ignat V. Kalcheff, William J. Kenis, Thomas W. Kennedy, Erland Lukanen, Robert L. Lytton, Michael S. Mamlouk, Edwin C. Novak, Jr., Lutfi Raad, Quentin L. Robnett, Byron E. Ruth, Gary Wayne Sharpe, James F. Shook, Roger E. Smith, R.N. Stubstad, Marshall R. Thompson, Ulian I. Tufektchiev, Thomas D. White

Committee on Monitoring, Evaluation and Data Storage
William A. Phang, Ministry of Transportation and Communication, chairman
Don H. Kobi, Paris, Ontario, secretary
A.T. Bergan, Frank V. Botelho, Billy G. Connor, Brian E. Cox, Michael I. Darter, Karl H. Dunn, Wouter Gulden, William H. Highter, James W. Hill, Andris A. Jumikis, Scott A. Kutz, Kenneth J. Law, W.N. Lofroos, K.H. McGhee, Edwain C. Novak, Jr., Freddy L. Roberts, Ivan F. Scazziga, S.C. Shah, Mohamed Y.Shahin, Roger E. Smith, Herbert F. Southgate, Elson B. Spangler, Richard L. Stewart, Loren M. Womack, John P. Zaniewski

Committee on Surface Properties—Vehicle Interaction
A. Scott Parrish, Maryland Department of Transportation, State Highway Administration, chairman
Louis E. Barota, Robert R. Blackburn, James L. Burchett, Gaylord Cumberledge, Thomas D. Gillespie, Wouter Gulden, Lawrence E. Hart, Carlton M. Hayden, Rudolph R. Hegmon, John Jewett Henry, Walter B. Horne, Don L. Ivey, Michael S. Janoff, Kenneth J. Law, Jean Lucas, David C. Mahone, William G. Miley, Robert L. Novak, Bobby G. Page, Richard N. Pierce, John J. Quinn, J. Reichert, Elson B. Spangler, William H. Temple, James C. Wambold

George W. Ring III, Transportation Research Board staff.

Sponsorship is indicated by a footnote at the of each paper.
The organizational units, officers, and members are as of December 31, 1986.

NOTICE: The Transportation Research Board does not endorse products or manufacturers. Trade and manufacturers' names appear in this Record because they are considered essential to its object.

Transportation Research Record 1117

The **Transportation Research Record** series consists of collections of papers on a given subject. Most of the papers in a Transportation Research Record were originally prepared for presentation at a TRB Annual Meeting. All papers (both Annual Meeting papers and those submitted solely for publication) have been reviewed and accepted for publication by TRB's peer review process according to procedures approved by a Report Review Committee consisting of members of the National Academy of Sciences, the National Academy of Engineering, and the Institute of Medicine.

The views expressed in these papers are those of the authors and do not necessarily reflect those of the sponsoring committee, the Transportation Research Board, the National Research Council, or the sponsors of TRB activities.

Transportation Research Records are issued irregularly; approximately 50 are released each year. Each is classified according to the modes and subject areas dealt with in the individual papers it contains. TRB publications are available on direct order from TRB, or they may be obtained on a regular basis through organizational or individual affiliation with TRB. Affiliates or library subscribers are eligible for substantial discounts. For further information, write to the Transportation Research Board, National Research Council, 2101 Constitution Avenue, N.W., Washington, D.C. 20418.

Contents

Foreword

Record 1117 contains 19 papers that address topics related to pavement evaluation and rehabilitation. The papers will be of interest to both researchers and practicing engineers.

Ali and Khosla evaluate layer moduli of three pavement sections by analyzing falling-weight deflectometer data using four methods: VESYS, ELMOD, OAF, and MODCOMP2. Backcalculated data are compared to material properties determined in the laboratory. The VESYS and ELMOD methods exhibited better agreement between backcalculated and laboratory data than did OAF and MODCOMP2.

Johnson and Hicks surprisingly reveal that in Alaska one pavement section having a base course of uncrushed aggregate performed better than another section having a base course of crushed aggregate. Larger maximum-sized aggregate and higher density for the uncrushed aggregate were believed to be responsible for the better performance of the uncrushed base course.

Uzan and Sides present a microcomputer method for the numerical analysis of stresses, strains, and displacements in multilayer systems due to various shapes on contact areas and pressure distributions. The analytical results agreed closely with other analytical and numerical integration solutions except for very thick layers for which the solution may not converge.

Rwebangira et al. investigated the sensitivity of backcalculated pavement layer moduli to variations in input parameters. Application of three computer programs BISDEF, MODCOMP2, and SEARCH revealed that all were sensitive to layer thickness and surface deflection measurements. BISDEF was also sensitive to the depth of the stiff layer and the assumed range of the modulus. Although identical data were input, backcalculated moduli from the procedures were significantly different.

Seven experimental pavement sections in Jamaica are described by Rolt et al. Thicker sections, after 4 years, were not expected to perform as well as predicted by appropriate design charts. Sections with cement-stabilized limestone and mechanically stabilized river shingle (water-worn gravel) performed better than unstabilized limestone bases.

The effectiveness of slab undersealing and load transfer restoration using retrofit dowel bars and double-vee shear devices on concrete pavement at a truck terminal is discussed by Roman and Shahin. The dowel bars appeared to be more appropriate at the site studied.

The development and demonstration of a prototype computerized expert system for evaluating concrete highway pavements are described by Hall et al. Conclusions reached by the expert system and the importance of some particular factors are explained. Further work will add rehabilitation strategies to the system.

Krauthammer and Khanlarzadeh apply a finite element method to the analysis of layered pavement systems. After comparing the results of the analysis of specific pavement systems in Minnesota to experimental data and observations, the authors make recommendations on design of pavement sections and overlays.

Chou and McCullough present a method of analysis for developing the distress index and rehabilitation criteria for CRC pavements in Texas. The method, intended to be used in pavement management network evaluation and rehabilitation scheduling, is believed to be a step forward in the evaluation of pavement distress conditions.

A model for predicting thermally induced reflection cracking in asphalt overlays is presented by Majidzadeh and McLaughlin. The model was tested on two overlaid pavements. Reflection cracking in the overlays has tended to verify the usefulness of the model predictions.

Lorenz discusses seven types of interlayers used experimentally in New Mexico to minimize reflective cracking. Although results were mixed, one type of fabric interlayer and two rubberized asphalt membranes were believed to be beneficial in retarding the onset of, but not eliminating, reflective cracks. Use of the interlayers requires close control to avoid construction

problems. Heater scarifying of badly cracked pavements should be considered as an alternative to cleaning and sealing the cracks.

Evaluation of the South Dakota low-cost profilometer at the 1984 University of Michigan road profilometer meeting is described by Huft et al. After deficiencies were revealed, the measurement system was correspondingly modified. Additional changes were made to permit measurement of rut depth and to include visual ratings with profile measurements.

Clapp and Eberhardt report a preliminary computer study for predicting tire-pavement contact forces for use in exciting dynamic models. Many simplifying assumptions are used; however, detailed tread pattern information can be incorporated into the models.

Kulakowski et al. propose an acceptability criterion for trailers that measure road roughness that is based on the measuring error of the trailer rather than on deviations of trailer parameters from standard values. This proposal would permit larger deviations of shock absorber parameters from standard values while assuring a higher overall accuracy of the measuring system.

In developing pavement distress information, Hajek and Haas find that 60 percent of the variance associated with 15 distress factors can be explained by only 5 basic types of distress. For detailed maintenance requirements, an evaluation of the 15 distress factors is still needed; however, the 5 basic factors can be used for future surface distress predictions.

Stoffels and Lytton formulate a utility analysis framework for evaluating nondistructive testing (NDT) devices used on asphalt concrete pavements. This utility analysis should be useful to firms contemplating the purchase of NDT devices.

A preliminary model for estimating the life of asphalt overlays using long-term pavement performance data is developed by Hajek et al. Benefits and limitations of a long-term pavement performance monitoring program for pavement performance prediction are illustrated.

Moore et al. describe the Kansas DOT system for developing panel pavement ratings, their administration, and their correlations with present serviceability index (PSI) and present serviceability ratings (PSR). An appendix contains rating instructions for the individuals on the panel and procedures of the survey.

An Idaho DOT study to develop a low-cost method to collect pavement distress data is presented by Baker et al. The study determined that high-quality video images of road surfaces can be collected at average speeds and that the images can be used to assign reliable crack characteristics and severity ratings. Further work was to assess costs and benefits.

Determination of Layer Moduli Using a Falling Weight Deflectometer

N. A. ALI AND N. PAUL KHOSLA

The increasing popularity of nondestructive pavement evaluation methods, based on interpretation of surface deflections, has prompted the development of several different types of nondestructive testing (NDT) devices. One such device is the falling weight deflectometer (FWD), which was used in the evaluation of layer moduli of three pavement sections. Several methods are currently available to interpret the FWD deflection data and backcalculate the layer moduli. Four methods selected for analysis of the deflection data included VESYS, ELMOD, OAF, and MODCOMP2. A comparison of the material properties determined in the laboratory and the backcalculated values indicated that two of the four methods, namely, VESYS and ELMOD, had great potential for pavement evaluation.

The failure of a pavement before the end of its designed life generally results from loss of strength in one or more layers in the pavement's structure. One method of identifying the weakened layer is to evaluate the material properties of existing in-service pavements.

There are two possible methods for evaluating the material properties. The first is to conduct laboratory testing on either laboratory-compacted specimens or undisturbed samples taken from the pavement. This method is tedious, time consuming, and destructive to the pavement structure. In addition, coring often delays traffic, which is usually unacceptable to the public. Furthermore, it is difficult, if not impossible, to simulate exact states of stress in the laboratory testing of pavement materials.

The second method of evaluating the material properties is by means of nondestructive testing (NDT). NDT consists of making nondestructive measurements on a pavement's surface and inferring, from these measurements, in situ characteristics related to the structural adequacy or loading behavior. Such evaluation of highway pavements is of particular importance to those responsible for the operation and maintenance of these facilities. Providing a quantitative basis for evaluating the pavement's structural condition at any stage of its life is one of the main objectives of nondestructive testing of flexible pavement.

Among the different load responses (stresses, strains, and deflections), the only practical measurements are deflections. Deflection is a basic response of the whole system to the applied load. Also, surface deflection measurements are rapid, relatively inexpensive, and nondestructive. All these factors make NDT attractive and useful.

The increasing popularity of structural evaluation methods based on interpretation of surface deflections has prompted the development of several different types of NDT devices. One such device is the falling weight deflectometer (FWD). It is believed that the FWD provides realistic deflection basin parameters that can be used as an input into a mechanistic pavement model to quickly and adequately determine the structural condition of a given pavement.

School of Engineering, North Carolina State University, Raleigh, N.C. 27695–7908.

RESEARCH APPROACH

In order to evaluate the pavement performance and pavement structural condition at any stage of its life, engineers must be able to reliably predict pavement behavior at any time. Several methods for predicting pavement behavior are currently in use *(1–4)*. Based on the deflection data, these methods predict the pavement modulus. In order to evaluate the reliability of these methods, a group of three pavement sections out of primary roads in North Carolina were selected for analysis.

Material samples were taken from the pavement sections for laboratory testing. In the laboratory, the mechanical properties of the pavement materials were determined by subjecting specimens to a series of dynamic laboratory tests under different environmental conditions.

NDT of the pavement sections was conducted with the aid of the FWD. Using the prediction models, the measured deflection basin was interpreted and characterized properly in order to backcalculate the properties of the layer materials. These backcalculated values were then compared with those determined in the laboratory.

FIELD AND LABORATORY TESTING PROGRAM

In order to test a wide variety of pavement configurations while assuring maximum uniformity of materials and construction procedures, three sections of primary roads across North Carolina were selected as the test sites. Furthermore, two subsections were selected in each of the sections and the test pits (approximately 2 by 5 ft) were excavated across the wheel path of the traffic lanes at selected locations. Subsection 01 represented a section with poor performance, and Subsection 11 represented a section with relatively better performance. Where performance throughout a section was poor, the two Subsections 01 and 02 were selected for the purpose of getting representative materials. After removing the asphalt surface, base course, and 2–4 in. of subgrade, a soil moisture cell was installed to monitor the variation of moisture in the subgrade. Samples of subgrade soil were collected for moisture determination in the laboratory.

Cores from the asphaltic surface layers were removed for laboratory testing. The actual layer thicknesses in each of the selected test subsections are given in Table 1.

TABLE 1 DESIGN THICKNESS OF TEST SUBSECTIONS

Section No.	Subsection No.	Pavement Layer Thickness (in.)			
		I_2	H	H–B	ABC
US–64	01	3	3	–	7.5
	11	2.80	3	–	7.5
I–40	01	2	3	3	10.0
	02	2	3	3	9.5
US–19	01	2	2	–	13.0
	11	2	2	–	13.0

NOTE: I_2 = asphaltic surface course; H = asphaltic binder course; H–B = asphaltic base course; ABC = aggregate base course.

FWD Testing Procedures

The FWD used in this study was obtained from Dynatest Consulting, Inc., Ojai, California. The FWD provides an impact load to the pavement. A mass is dropped from an operator-selected height onto a plate that is connected to a base plate by springs *(5)*. FWD deflections are measured with velocity transducers. One of these sensors is located at the center of the loading plate. Six additional sensors are movable and can be placed at any desired distance away from the center of the place. During this testing program, the FWD sensors were placed at 7.87, 11.8, 23.3, 39.3, 55.1, and 70.8 in. away from the center of the loading plate.

At four selected points, closed to the test pits, a complete load sweep test was performed at two different dates. The FWD was operated at three load magnitudes ranging from 6,000 to 12,000 lb.

The air temperature was measured during the testing. The Witczak formula was used to determine from the air temperature the mean pavement temperature at the upper third point of the asphalt layer *(6)*.

The FWD deflection basin is characterized by the following equation:

$$Area = \frac{1}{2}\left(\frac{D_0 + D_1}{D_0}\right)(7.87) + \left(\frac{D_1 + D_2}{2}\right)(3.93) + \left(\frac{D_2 + D_3}{2}\right)(11.8) + \left(\frac{D_3 + D_4}{2}\right)(15.7) + \left(\frac{D_4 + D_5}{2}\right)(15.8) + \left(\frac{D_5 + D_6}{2}\right)(15.7) \quad (1)$$

where

D_0 = maximum deflection (at the center of the plate);
D_1, D_2, D_3, D_4, D_5, and D_6 = deflections at 7.87, 11.8, 23.6, 39.3, 55.1, and 70.7 in. from the center of the load plate, respectively; and
$Area$ = normalized deflection basin area (in.^{2}).

Laboratory Testing

Laboratory testing was performed to determine the resilient modulus of each layer of the pavement test sections. Asphalt concrete samples cored from the pavement sections were 4 in. in diameter, with a height equal to the pavement's thickness. A diamond saw was used to cut and slice the cores into sections corresponding to the structure of the layer. The resilient modulus values in the indirect tension mode were determined at temperatures of 0°F, 30°F, 50°F, 70°F, 90°F, and 120°F.

Cylindrical samples of base course and subgrade soil were recompacted and tested under dynamic load in a triaxial cell. The resulting characterization was a stress-dependent resilient modulus for different moisture contents. The test procedures are described by Khosla *(7)*.

MODULI CALCULATION METHODS

Four procedures were used to backcalculate the modulus values. The procedures involve the initial calculation of deflection parameters using the measured deflection profile. Then the estimation of in situ stiffness of pavement layer is carried out using a graphical solution or a computer program. In the following section, various procedures for backcalculating the resilient modulus of the pavement layers are discussed.

Graphical Procedures

The VESYS program was used as part of this research to develop a graphical procedure for backcalculating the pavement parameters. The VESYS model incorporates the viscoelastic and fatigue properties of the pavement materials. For the analysis of existing pavement systems, algorithms were developed that can be used with measured load deflection data and known material thickness or properties.

The algorithms were developed by applying statistical regression analysis techniques to the VESYS-generated response data. The same principle of developing nomographs was used by Hoffman and Thompson *(3)*, except that their nomographs were based on data generated by the finite element program ILLI-PAVE. VESYS data were generated for 1,920 pavement configurations. These included pavements with asphalt concrete (AC) thickness (T_{AC}) of 2, 3.5, 5, 6, and 8 in. Granular base thicknesses (T_{base}) were 5, 7, 9, 11, 13, and 16 in. These thicknesses are representative of the range of typical flexible pavement designs. Four levels of subgrade moduli of resilience (MR_{soil}), (1,000, 3,000, 7,000, and 11,000 psi), four levels of AC modulus of resilience (MR_{AC} = 100,000, 250,000, 500,000, and 1,000,000 psi), and five levels of base course modulus (MR_{base} = 15,000, 20,000, 25,000, 30,000, and 35,000 psi) were evaluated for different group combinations of granular base resilient moduli and asphalt concrete granular base thicknesses.

A constant load of 9,000 lb was maintained throughout the study to account for one-half of the 18-kip, single-wheel load commonly used for design. In mathematical representation, the load was applied on top of the upper layer and uniformly distributed over a circular contact area of 6-in. radius the same as the loading plate on the FWD.

The predictive equations were developed based on multiple regression techniques relating the dependent variables (D_0,

Area) to the four independent variables (MR_{AC}, MR_{soil}, T_{AC}, and T_{base}). The regression equations were optimized to yield good predictive equations. The following groups were obtained (see Table 2):

1. Group A for pavements with base course moduli in the 15,000–20,000 psi range.
2. Group B for pavements with base course moduli in the 20,000–25,000 psi range.
3. Group C for pavements with base course moduli in the 25,000–30,000 psi range.
4. Group D for pavements with base course moduli in the 30,000–35,000 psi range.

Each group was divided into four subgroups according to asphalt concrete and base course thicknesses as follows:

- Subgroup 1 includes pavements with AC layers between 2 and 3.5 in. thick and base course layer thicknesses of 11 in. and less.
- Subgroup 2 includes pavements with AC layers between

TABLE 2 VESYS DEFLECTION BASIN ALGORITHMS

Dependent Variable	R^2	σ	O	*A*	*B*	$C \times 10^{-3}$	$D \times 10^{-3}$
Group A Subgroup A1: $2 \le T_{AC} \le 3.5$ and $5 \le T_{base} \le 11$							
Log D_0	0.8947	0.00660	2.54302	−0.07690	−0.01536	−0.00152	−0.05650
Area	0.8926	3.20000	18.62890	2.35430	0.23410	0.00485	−1.14756
Subgroup A2: $3.5 \le T_{AC} \le 6$ and $5 \le T_{base} \le 13$							
Log D_0	0.8919	0.00711	2.46114	−0.05649	−0.01102	−0.00021	−0.05643
Area	0.9165	2.61170	20.82290	1.74453	0.01079	0.00687	−1.13039
Subgroup A3: $3.5 \le T_{AC} \le 6$ and $7 \le T_{base} \le 16$							
Log D_0	0.8876	0.00709	2.42531	−0.05493	−0.00883	−0.00021	−0.05530
Area	0.9060	2.85970	22.04200	1.70225	0.00829	0.00678	−1.12581
Subgroup A4: $5 \le T_{AC} \le 8$ and $7 \le T_{base} \le 16$							
Log D_0	0.8823	0.00770	2.35864	−0.04227	−0.00770	−0.00023	−0.05632
Area	0.8917	2.98400	24.88840	1.11373	−0.02676	0.00735	−1.03941
Group B Subgroup B1: $2 \le T_{AC} \le 3.5$ and $5 \le T_{base} \le 11$							
Log D_0	0.8859	0.00660	2.51110	−0.07018	−0.01804	−0.00014	−0.05709
Area	0.9067	2.75080	19.43320	2.27395	0.27868	0.00465	−1.16114
Subgroup B2: $3.5 \le T_{AC} \le 6$ and $5 \le T_{base} \le 13$							
Log D_0	0.8933	0.00705	2.42912	−0.05270	−0.01256	−0.000192	−0.05730
Area	0.8878	3.35700	21.84990	1.62080	0.09244	0.00668	−1.09810
Subgroup B3: $3.5 \le T_{AC} \le 6$ and $7 \le T_{base} \le 16$							
Log D_0	0.8886	0.00705	2.38590	−0.05080	−0.00984	−0.00019	−0.05624
Area	0.8886	3.21870	22.71080	1.56320	0.02731	0.00675	−1.08740
Subgroup B4: $5 \le T_{AC} \le 8$ and $7 \le T_{base} \le 16$							
Log D_0	0.8838	0.00767	2.31880	−0.03834	−0.00860	−0.00021	−0.05723
Area	0.8851	2.99180	25.24160	0.96940	0.02407	0.00737	−1.00560
Group C Subgroup C1: $2 \le T_{AC} \le 3.5$ and $5 \le T_{base} \le 11$							
Log D_0	0.8973	0.00650	2.48875	−0.06582	−0.01986	−0.00013	−0.05746
Area	0.9072	2.73640	20.49120	2.07104	0.32778	0.00420	−1.18234
Subgroup C2: $3.5 \le T_{AC} \le 6$ and $5 \le T_{base} \le 13$							
Log D_0	0.8926	0.00710	2.40620	−0.04934	−0.01402	−0.00018	−0.05730
Area	0.9195	2.26060	23.03600	1.44380	0.13460	0.00621	−1.11380

TABLE 2 *continued*

Dependent Variable	R^2	σ	O	*A*	*B*	$C \times 10^{-3}$	$D \times 10^{-3}$
Subgroup C3: $5 \le T_{AC} \le 8$ and $7 \le T_{base} \le 16$							
Log D_0	0.8879	0.00710	2.36110	–0.00047	–0.01109	–0.00018	–0.05652
Area	0.9185	2.19200	24.36950	1.36618	0.02819	0.00627	–1.09390
Subgroup C4: $5 \le T_{AC} \le 8$ and $7 \le T_{base} \le 16$							
Log D_0	0.8829	0.00770	2.30230	–0.03654	–0.00977	–0.00020	–0.05745
Area	0.9066	2.24470	26.54050	–0.89392	–0.00352	–0.00688	–0.99435
Group D Subgroup D1: $2 \le T_{AC} \le 3.5$ and $5 \le T_{base} \le 11$							
Log D_0	0.8981	0.00650	2.46624	–0.06146	–0.02164	–0.00012	–0.05780
Area	0.9096	2.60990	21.43700	1.91125	0.36021	0.00398	–1.18420
Subgroup D2: $3.5 \le T_{AC} \le 6$ and $5 \le T_{base} \le 13$							
Log D_0	0.8927	0.00713	2.3840	–0.04644	–0.01537	–0.00017	–0.05790
Area	0.9116	2.37410	23.9829	1.33270	0.12955	0.00589	–1.09118
Subgroup D3: $3.5 \le T_{AC} \le 6$ and $7 \le T_{base} \le 16$							
Log D_0	0.888	0.00716	2.33571	–0.04432	–0.01213	–0.00017	–0.57017
Area	0.9135	2.19490	25.16870	1.26623	0.03536	0.00592	–1.06948
Subgroup D4: $5 \le T_{AC} \le 8$ and $7 \le T_{base} \le 16$							
Log D_0	0.8833	0.00776	2.28040	–0.03442	–0.01071	–0.00019	–0.05792
Area	0.8951	2.36660	27.14670	0.81903	–0.00324	0.00657	–0.96330

NOTE: Equation of the form: Dependent variable = O + $A\,T_{AC} + B\,T_{base} + C\,MR_{AC} + D\,MR_{soil}$.

3.5 and 6 in. thick and base course layer thicknesses of 13 in. and less.

- Subgroup 3 includes pavements with AC layers between 3.5 and 6 in. thick and base course layers between 7 and 16 in.
- Subgroup 4 includes pavements with AC layers between 5 and 8 in. thick and base course layers between 7 and 16 in.

The equations in Table 2 for Groups A through D are reproduced in nomographical form. A typical set of nomographs is shown in Figures 1 and 2.

The resilient modulus of the granular base course is relatively insensitive to moisture content and temperature when compared with the resilient modulus of asphalt and the subgrade. Therefore, the VESYS model was used to backcalculate MR_{AC} and MR_{soil}, while prediction equations were developed to determine the MR_{base}. Regressions were performed on the re-

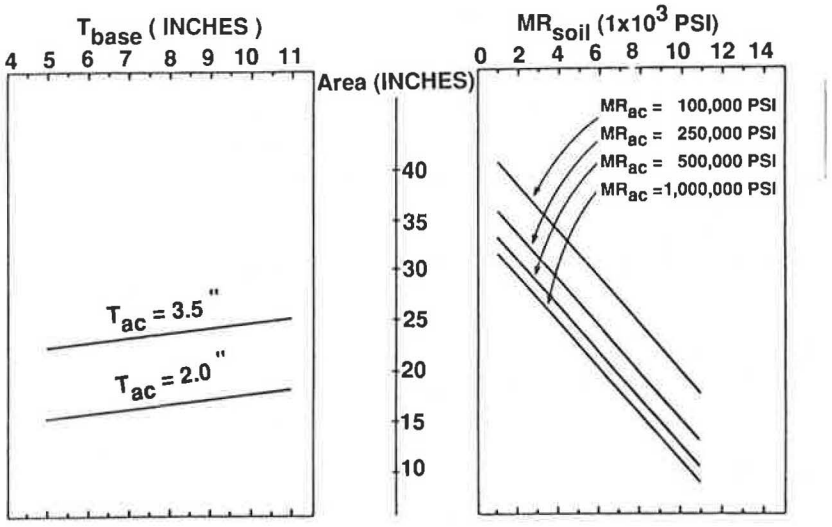

FIGURE 1 Nomograph based on area—Group A1.

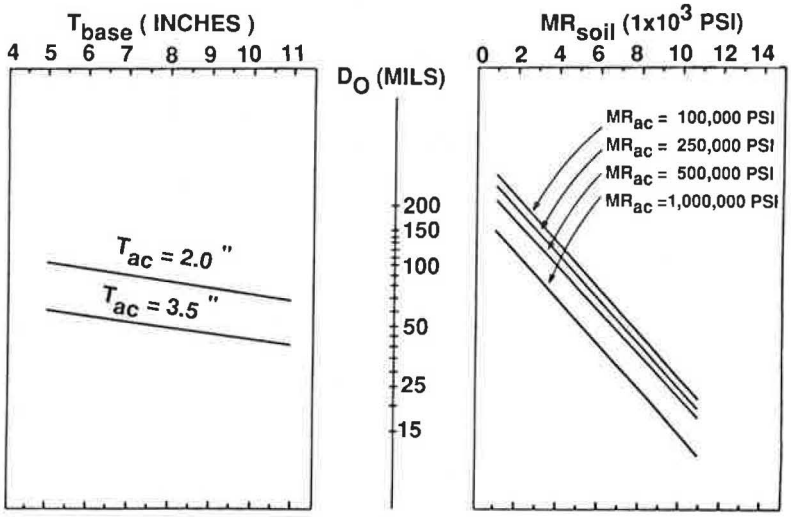

FIGURE 2 Nomograph based on D_0—Group A1.

silient modulus values of the base course to determine the constants of the following relationship for different seasons:

$$\log (MR) = A + B \log \theta \quad (2)$$

where

MR = resilient modulus,
θ = sum of principal stresses, and
A, B = constants.

The values of the regression constants to predict MR_{base} are shown in Table 3.

Moduli Calculation Using Computer Programs

The FWD load deflection was analyzed using the ELMOD computer program. ELMOD is capable of determining the moduli of the asphalt layer, base course, plus the surface modulus, and the nonlinear parameters C_0 and N of the subgrade *(4)*.

The surface modulus is given by the following relationship:

$$E_0 = c_0 \left(\frac{\sigma}{\sigma'}\right)^N \quad (3)$$

where

E_0 = surface modulus,
σ = major principal stress,
σ' = a reference stress, and
C_0, N = constants.

The surface modulus (the modulus of the half-space that would give the same surface deflection as the multilayer structure) is calculated at distance r for the known loading conditions and the measured deflection value of $d(r)$ as follows:

$$E_0 = \frac{(1 - r^2)\,\sigma_0 a^2}{r\,d(r)} \quad (4)$$

where

r = Poisson ratio,
σ_0 = contact stress, and
a = radius of the loaded area.

Using Equation 3 and the following equations, the resilient modulus of the subgrade MR can be calculated.

$$MR = C \left(\frac{\sigma}{\sigma'}\right)^N \quad (5)$$

$$c = \left(\frac{C_0}{1 - 2N}\right) \quad (6)$$

The OAF program has been developed to accommodate the

TABLE 3 SUMMARY OF REGRESSION RESULTS

Section No.	Winter		Spring		Summer		Fall	
	A	B	A	B	A	B	A	B
US–64	3,950.0	0.495	4,470.0	0.450	5,750.0	0.412	3,050.0	0.567
I–40	2,900.0	0.5775	3,350.0	0.522	3,800.0	0.510	1,200.0	0.633
US–19	6,500.0	0.356	6,060.0	0.357	8,300.0	0.350	5,500.0	0.416

deflection results from FWD. The procedure is required to measure deflection at 0, 30, 60, and 100 cm from the applied load.

Layer moduli are determined for a specific site by inputting the following information into a computer program making use of the ELSYM program for stresses and deformations in multilayer elastic systems *(1)*:

1. Surface deflection measurements and load configurations,
2. Base type,
3. Layer thickness,
4. Poisson ratio for all layers, and
5. Asphalt concrete modulus at test temperature.

Essentially, the program solves for the moduli of the various layers by attaining compatibility between measured and computed deflections at the locations for which deflection data were acquired in the field.

The MODCOMP2 program can handle up to eight surface deflections for each load level, measured at various radial distances from the center of the load *(2)*.

1. Surface deflection and radial distances of geophones from the center of the load,
2. Load values,
3. Poisson ratio,
4. Base and soil type, and
5. Seed modulus for the pavement layers.

The computed deflections are compared with measured deflection, and the seed moduli are adjusted as a function of the magnitude of the difference in deflections. This process is repeated until agreement between the difference of the computed and measured deflection is within the specific tolerance. The tolerance specified for this analysis was 5 percent.

VERIFICATION PROCEDURE

All of the six subsections were used to validate and verify the four procedures discussed in the previous section. Each location had the conventional flexible pavement design consisting of an AC surface, granular base, and a fine-grained subgrade.

A comparison of the backcalculated material properties with laboratory values was used in the validation procedure.

The resilient modulus of the base course depends upon the state of stress and moisture content. The resilient modulus corresponding to a representative moisture content and 50 psi of bulk stress was determined. A value of 50 psi represents the state of stress in the field as determined by the CHEV5L multilayer elastic computer program.

The resilient modulus of fine-grained subgrade depends upon the deviator stress and moisture content. The resilient modulus corresponding to the representative moisture content at the time of testing and the deviator stress of 6 psi were selected.

From both laboratory and backcalculated results summarized in Tables 4–9, the following observations could be made:

1. From the backcalculated MR_{AC} values and the pavement temperature at the time of deflection testing, it is evident that the modulus values increase with a reduction in temperature values. Thus, there is a logical trend in the variation of MR_{AC} with the temperature values.
2. From the backcalculated MR_{soil} values by VESYS and the soil moisture condition, it is evident that the modulus values increase with a reduction in moisture content. Thus, there is a logical pattern in the variation of MR_{soil} with the moisture content.
3. The backcalculated MR_{AC} values ranged from 119,750 to 600,200 psi, depending on the testing time and prediction method. There was a significant variation in backcalculated MR_{AC} as determined by different approaches.

TABLE 4 SUMMARY OF FIELD MEASUREMENTS AND LABORATORY-RESILIENT MODULUS VALUES FOR US-64 SECTION

		Field Measurements			Laboratory Resilient Modulus Values (psi)		
Subsection No.	Date of Testing	Pavement Temp (^{0}F)	Base Moisture (%)	Soil Moisture (%)	Asphalt-Concrete	Base	Soil
01	April '85	93	5.3	20.1	258000	26000	6700
	Aug '85	90	4.6	19.17	263000	27000	7500
11	April '85	100	5.3	18.9	200000	26000	4600
	Aug '85	93	4.6	17.9	258000	27000	6500

TABLE 5 SUMMARY OF BACKCALCULATED RESILIENT MODULUS VALUES FOR US-64 BY USING VESYS, ELMOD, MODCOMP2, AND OAF MODELS

		Backcalculated Resilient Modulus Values (psi) Using											
		ELMOD			VESYS			MODCOMP2			OAF		
Sub-section No.	Date of Testing	Asphalt Concrete	Base	Soil	Asphalt-Concrete	Base	Soil	Asphalt-Concrete	Base	Soil	Asphalt-Concrete	Base	Soil
01	April '85	165000	34500	6295	240000	26000	9100	126320	10099	20025	150370	3980	36145
	Aug '85	175000	49500	6785	350000	28000	9500	193000	6260	24720	172970	3990	42840
11	April '85	119750	18000	4370	250000	26000	6000	187900	11380	5870	185350	1760	13740
	Aug '85	143750	32750	4970	300000	28000	7300	314150	5460	9460	251300	2605	18025

TABLE 6 SUMMARY OF FIELD MEASUREMENTS AND LABORATORY-RESILIENT MODULUS VALUES FOR I-40 SECTION

		Field Measurements			Laboratory Resilient Modulus Values (psi)		
Sub-section No.	Date of Testing	Pavement Temp (^{o}F)	Base Moisture (%)	Soil Moisture (%)	Asphalt-Concrete	Base	Soil
01	May '85	78	5.6	10.0	577300	25000	9200
	Sept '85	86	4.8	11.0	384000	26000	7800
02	May '85	90	5.6	18.5	223900	25000	4300
	Sept '85	83.5	4.8	20.4	319000	26000	2500

TABLE 7 SUMMARY OF BACKCALCULATED RESILIENT MODULUS VALUES FOR I-40 BY USING VESYS, ELMOD, MODCOMP2, AND OAF MODELS

		Backcalculated Resilient Modulus Values (psi) Using											
		ELMOD			VESYS			MODCOMP2			OAF		
Sub-section No.	Date of Testing	Asphalt Concrete	Base	Soil	Asphalt-Concrete	Base	Soil	Asphalt-Concrete	Base	Soil	Asphalt-Concrete	Base	Soil
01	May '85	455250	24500	10250	600000	25800	9800	*	*	*	600200	2730	29880
	Sept '85	426250	29250	9500	450000	27400	9200	691230	1423	10104	225880	2650	13840
02	May '85	290250	32000	5500	300000	25800	5800	*	*	*	383000	4630	11110
	Sept '85	350000	29250	3500	400000	27400	5200	425450	48600	3740	515680	2190	13700

*MODCOMP2 could not backcalculate the resilient modulus values from the deflection data because the program would not converge within the tolerance limit (5 to 10%).

TABLE 8 SUMMARY OF FIELD MEASUREMENTS AND LABORATORY RESILIENT MODULUS VALUES FOR US-719 SECTION

		Field Measurements			Laboratory Resilient Modulus Values (psi)		
Subsection No.	Date of Testing	Pavement Temp (°F)	Base Moisture (%)	Soil Moisture (%)	Asphalt-Concrete	Base	Soil
01	May '85	95	6.2	18.4	345000	23500	4000
	Sept '85	88	5.8	18.0	454000	24500	5100
11	May '85	87	6.2	14.8	454600	23500	5200
	Sept '85	85	5.8	15.0	516500	24500	3700

4. The backcalculated resilient moduli of the pavement layers by the ELMOD and VESYS models and laboratory values, for test locations 01 and 11 at different times of testing, were in good agreement.

5. It can be seen that OAF and MODCOMP2 backcalculated lower values of resilient moduli for the base course (MR_{base}) than for the soil, conflicting with the principle of flexible pavements.

CONCLUSIONS

The following conclusions are based on the summary of *MR* methods given in Table 10.

1. ELMOD and VESYS models exhibited greater agreement with the principles of flexible pavement behavior than did OAF and MODCOMP2.

2. In general, backcalculated MR_{AC} values using the four models followed a logical trend in their variation with temperature.

3. The backcalculated MR_{soil} values using the VESYS, ELMOD, and MODCOMP2 models followed a more logical trend in their variation with moisture content as compared with the values arrived at by using the OAF model.

4. The backcalculated *MR* values using the VESYS model had the least variation from laboratory values with the ratio MR_{lab}/MR_{pred} range between 0.48 and 1.08 and most values between 0.77 and 0.97. The values for ELMOD varied between 0.54 and 1.56, with most values between 0.80 and 1.26. The largest variations in the ratio of MR_{lab}/MR_{pred} were exhibited by those values predicted by MODCOMP2 and OAF models. The ratio of MR_{lab}/MR_{pred} for MODCOMP2 ranged from 0.1 to 18.2 with most of the values between 0.55 and 5.61. The MR_{lab}/MR_{pred} ratio for OAF ranged between 0.18 and 14.80, with most values between 0.32 and 9.80. It is possible that developers of these programs could tailor their input in the program to give better results. Perhaps keeping the specified tolerance limit to a low level such as 1 percent or lower, instead of 5–10 percent, could improve the accuracy of the predicted modulus values.

5. From the preceding, it can be seen that VESYS and ELMOD are more suitable for prediction of pavement layer moduli.

TABLE 9 SUMMARY OF BACKCALCULATED RESILIENT MODULUS VALUES FOR US-19 BY USING VESYS, ELMOD, MODCOMP2, AND OAF MODELS

		Backcalculated Resilient Modulus Values (psi) Using											
		ELMOD			VESYS			MODCOMP2			OAF		
Subsection No.	Date of Testing	Asphalt Concrete	Base	Soil	Asphalt-Concrete	Base	Soil	Asphalt-Concrete	Base	Soil	Asphalt-Concrete	Base	Soil
01	May '85	338250	22000	4029	355000	25000	6100	584013	7650	7040	500320	5440	9860
	Sept '85	502400	25500	4825	500000	27900	6000	986320	4360	14685	913810	6330	12800
11	May '85	472500	27750	4871	450000	25000	7500	1118170	1415	51440	650800	5795	11165
	Sept '85	535250	34750	4244	500000	27900	6700	918340	4360	14945	952780	3870	15970

TABLE 10 SUMMARY OF BACKCALCULATED *MR* METHODS

			US 64		I-40		US 19	
			01	11	01	02	01	11
ELMOD	In accordance with the principles of flexible pavement behavior[a]		Yes	Yes	Yes	Yes	Yes	Yes
	Logical backcalculated MR_{ac} versus temperature trend[b]		Yes	Yes	Yes	Yes	Yes	Yes
	Logical backcalculated MR_{soil} versus moisture content[c]		Yes	Yes	Yes	Yes	Yes	Yes
	Range of ratio	Min. Ratio	.54	0.82	0.82	.73	0.90	0.71
	MR_{lab}/MR_{pred}[d]	Max. Ratio	1.56	1.80	1.26	0.91	1.06	1.07
VESYS	In accordance with the principles of flexible pavement behavior[a]		Yes	Yes	Yes	Yes	Yes	Yes
	Logical backcalculated MR_{ac} versus temperature trend[b]		Yes	Yes	Yes	Yes	Yes	Yes
	Logical backcalculated MR_{soil} versus moisture content[c]		Yes	Yes	Yes	Yes	Yes	Yes
	Range of ratio	Min. Ratio	0.74	0.77	0.85	0.48	0.65	0.55
	MR_{lab}/MR_{pred}[d]	Max. Ratio	1.08	1.00	0.97	0.97	0.97	1.03
MODCOMP2	In accordance with the principles of flexible pavement behavior[a]		No	No	No	Yes	No	No
	Logical backcalculated MR_{ac} versus temperature trend[b]		Yes	Yes	N/A	N/A	Yes	No
	Logical backcalculated MR_{soil} versus moisture content[c]		Yes	Yes	N/A	N/A	Yes	Yes
	Range of ratio	Min. Ratio	.23	.68	0.55	0.53	.35	0.1
	MR_{lab}/MR_{pred}[d]	Max. Ratio	4.31	4.94	18.2	0.73	5.61	16.6
OAF	In accordance with the principles of flexible pavement behavior[a]		No	No	No	No	No	No
	Logical backcalculated MR_{ac} versus temperature trend[b]		Yes	Yes	Yes	Yes	Yes	Yes
	Logical backcalculated MR_{soil} versus moisture content[c]		Yes	Yes	Yes	No	Yes	No
	Range of ratio	Min. Ratio	0.18	0.33	0.32	0.18	0.40	0.24
	MR_{lab}/MR_{pred}[d]	Max. Ratio	6.76	14.80	9.80	11.90	4.32	6.33

[a]Flexible pavements consist of a layered load-distributing system with the highest quality (stiffest) materials uppermost.

[b]Since AC is a thermoplastic material, the logical trend for MR_{ac} is inversely proportional to increasing temperature.

[c]The modulus of resilience for fine-grained soils is inversely proportional to increasing moisture content.

[d]The ratio $MR_{lab}/MR_{predicted}$ gives an indication of over/underestimation of the different procedures. Values closest to unity indicate greatest agreement.

REFERENCES

1. K. Majidzadeh and G. Ilves. *Flexible Pavement Overlay Design Procedures,* Vol. 2, *User Manual.* Report FHWA/RD-81/033. FHWA, U.S. Department of Transportation, Aug. 1981.
2. L. H. Irwin. *User's Guide to MODCOMP2* (version 2.1). Report 83–8, Cornell University, Ithaca, N.Y., Nov. 1983.
3. M. S. Hoffman and M. R. Thompson. *Mechanistic Interpretation of Nondestructive Pavement Testing Deflections.* Report FHWA/IL/UI-190. FHWA, U.S. Department of Transportation, June 1981.
4. *ELMOD—Evaluation of Layer Moduli and Overlay Design.* User's Manual, Dynatest Consulting Inc., March 1983.
5. R. E. Smith. *Synthesis Study of Nondestructive Testing Devices for Use in Overlay Thickness Design of Flexible Pavement.* Report

FHWA/RD-83-097. FHWA, U.S. Department of Transportation, April 1984.
6. M. W. Witczak. Design of Full Depth Air Field Pavement. In *Proc., 3rd International Conference on the Structural Design of Asphalt Pavements,* 1972.
7. N. P. Khosla. *Investigation of Premature Distresses in Flexible Pavements.* Research Report FHWA/NC/85-001. Center for Transportation for Transportation Engineer Studies, North Carolina State University, Raleigh, March 1985.
8. W. J. Kenis. *Predictive Design Procedures, VESYS Users Manual.* Report FHWA/RD/77/154. FHWA, U.S. Department of Transportation, 1978.

Publication of this paper sponsored by Committee on Strength and Deformation Characteristics of Pavement Sections.

Evaluation of Effect of Uncrushed Base Layers on Pavement Performance

ERIC G. JOHNSON AND R. G. HICKS

In 1974, the Alaska Department of Highways decided to save money and fuel by removing the base course and placing the asphalt concrete surface directly on the subbase of the Glenn Highway widening project. In 1969, the original two lanes had been constructed with a crushed base course, thus providing an excellent comparison of the performance of the two bases. Laboratory testing showed that the uncrushed base (subbase) was uniformly graded with a maximum size of 2 in. with 37 percent aggregate fracture, whereas the crushed base was uniformly graded with a maximum size of 1 in. with 85 percent aggregate fracture. Base course resilient modulus was back-calculated from falling weight deflectometer readings and subsequently measured in the laboratory. Contrary to previous research and experience in crushed and uncrushed gravel, the uncrushed base course performed better than the crushed base course; the resilient modulus was higher, and the permanent deformation was lower. The uncrushed base is apparently superior because of a larger maximum particle size and greater maximum density. An analysis of the future performance of the roadway with equal thicknesses of asphalt indicates that the pavement over the uncrushed base would have a longer life than the pavement over the crushed base by 54 percent.

In 1974, the Alaska Department of Highways decided to save money and fuel by deleting the base course and placing the asphalt concrete surface directly on the subbase of the Glenn Highway widening project. The original two lanes, constructed in 1969, were built with a crushed base course. The additional two lanes were constructed adjacent to the original roadway, providing an excellent comparison of the performance of the uncrushed subbase and the crushed base course. An investigation was undertaken to analyze the two roadways to see if the difference in fracture led to a difference in performance.

LOCATION

The Glenn Highway is located in south-central Alaska (Figure 1). The project lies between Anchorage and Palmer, just north of Eagle River in the northeast section of the Cook Inlet physiographic region. The northbound lanes were originally constructed in 1969. The 1983 average annual daily two-way traffic was 13,500 vehicles. The cross section consisted of two 14-ft driving lanes with 8-ft shoulders and a 4-ft ditch (Figure 2). The design pavement structure consists of 1.5 in. of hot asphalt concrete over 6 in. of base course Grading D-1 over 6 in. of subbase and 36 in. of select material. Both projects were overlaid with 1.5 in. of hot asphalt concrete (AC) during the summer of 1983. The subgrade soils are predominantly Pleistocene ground moraine (silty gravel and gravelly silt) and outwash deposits (sandy gravel). Surface drainage at the test sites was rated as fair.

The southbound lanes were constructed in 1974. The cross section is the same as the northbound lanes with a 4-ft ditch between them. The design template consisted of 1.5 in. of hot AC over 6 in. of subbase, Grading B, over a variable depth of selected material over unclassified embankment.

Table 1 summarizes the project specification gradation of each of the projects. The crushed base course (D-1) was specified as a 1-in. (or less) uniform gradation, with 3 to 10 percent passing the No. 200 sieve, and the material retained on the No. 4 sieve to have a 75 percent single-faced fracture. The uncrushed base course (Subbase B) was specified as a coarser uniform gradation with a maximum size of 2 in., 3 to 8 percent passing the No. 200 sieve, and no fracture requirement.

Problems were encountered in tight blading the surface before paving because of the 2-in. (or less) unfractured aggregate. Aggregate particles rolled under the grader blade, leaving a loosened scarified surface. A steel wheel roller was used just ahead of the paver to keep the surface tight. It was also necessary to keep the grade well watered. However, it was still difficult to maintain a uniform grade as the pavement haul trucks created troughs and depressions even though no turning movements were permitted. It was believed that this procedure would result in a greater AC thickness than that designed, but cores showed that no excess AC was used.

FIELD INVESTIGATION

Two test sites were selected for evaluation along the project: a 550-ft-long cut section and a 1,000-ft-long embankment fill section. During the spring of 1983, falling weight deflectometer (FWD) deflection tests were performed every 50 ft in the cut section and every 100 ft in the fill section. Four points in each section were selected that represented the average deflection for that section. Test trenches were dug adjacent to these points at the edge of pavement to a depth of 6 ft. Samples of the pavement structure were taken out of the wall of the trench. Bulk disturbed samples of the crushed and uncrushed base courses were also taken from a pavement cut near the test sections. The pavement was cored in the driving lane adjacent to each test trench.

E. G. Johnson, Alaska Department of Transportation and Public Facilities, Box 196900, Anchorage, Alaska 99519–6900. R. G. Hicks, Transportation Research Institute, Oregon State University, Corvallis, Oreg. 97337–2302.

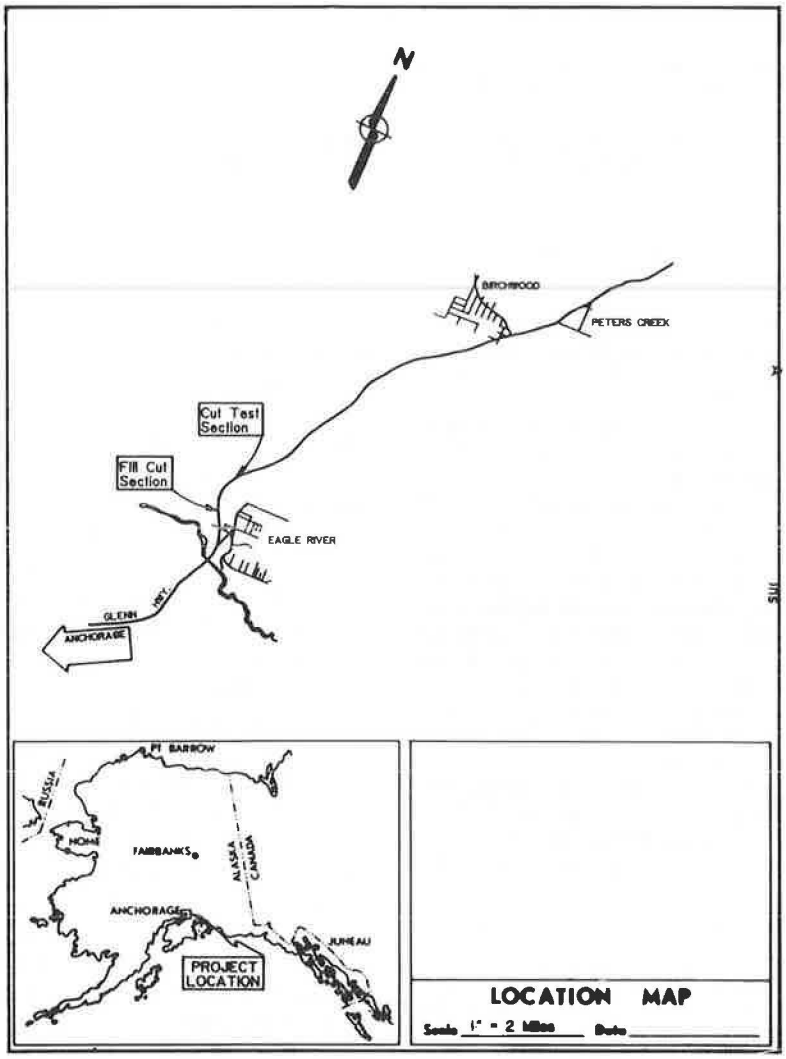

FIGURE 1 Location map.

Pavement Condition

A formal pavement condition survey was not performed as the test sections were overlaid shortly after this investigation was begun in 1983. From a visual inspection prior to the overlay, no major pavement distress was noted in either the northbound or the southbound lanes. No rutting or pavement distortion was apparent and only transverse thermal contraction cracks were noted.

Pavement Structure

Test trenches were used to verify the designed pavement structure. Both the crushed and the uncrushed base courses were

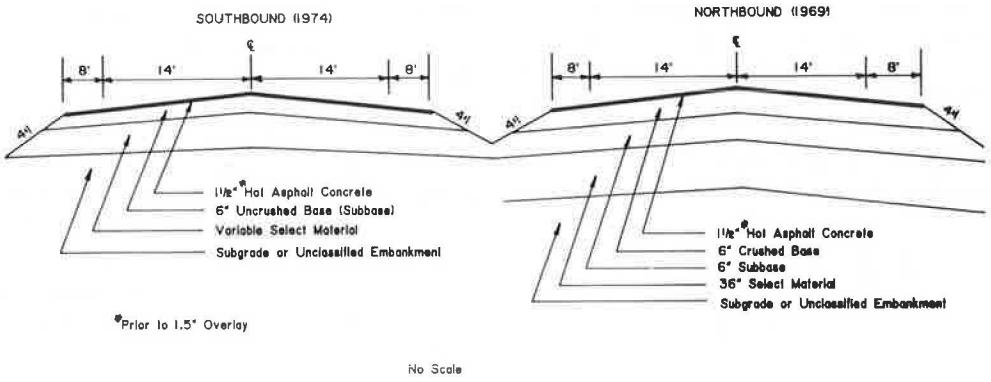

FIGURE 2 As-designed typical sections.

TABLE 1 CRUSHED BASE COURSE AND UNCRUSHED BASE CURSE (SUBBASE) SPECIFICATION AND MEASURED GRADATIONS

	Northbound Lanes, Crushed Base Course			Southbound Lanes, Uncrushed Base Course (Subbase)		
	Specification	Test Results		Specification	Test Results	
Sieve	D-1 (% passing)	Average (% passing)	Range (% passing)	B (% passing)	Average (% passing)	Range (% passing)
2 in.	100	100		100	100	
1.5 in.					97	95–98
1 in.	100	100			80	77–82
3/4 in.	70–100	94	91–95	60–90	69	64–73
1/2 in.		74	72–77		56	52–60
3/8 in.	50–80	62	60–66		48	43–53
No. 4	35–65	43	41–46	30–60	34	29–36
No. 8	20–50	33	29–35		25	21–28
No. 10		30	27–32		23	20–25
No. 40	10–30	14	12–16		9	8–9
No. 200	3–10	7	6–8	3–8	6	4–9
0.02 mm	3–10	4.3	3–5		5.3	3–8
Fracture (%)	75	81	76–85	–	37	19–53
Optimum moisture (wt %)	4.5				4.1	
T180 Proctor density (pcf)	143.9				148.4	

within project specifications (see Table 1). Figure 3 is a 0.45 power plot of the average gradation of the crushed and uncrushed base courses. The crushed base single-faced fracture on the No. 4 sieve averaged 81 percent, whereas the uncrushed base averaged 37 percent. Minor crushing of the uncrushed base was necessary to produce the Subbase B gradation, resulting in some fracture that was not specified. From the project records (Table 1), the T180 Proctor density for the uncrushed base was 148.4 lb/ft^3, much higher than the 143.8 lb/ft^3 for the crushed base.

Table 2 gives a summary of the pavement structure components and their characteristics as measured in the test trenches. The hot AC over the crushed base averaged 4.0 in., whereas the AC over the uncrushed base averaged 3.1 in. (The test sections were overlaid with 1.5-in. AC during the summer of 1983.) The total pavement structure above the subgrade in the cut averaged 42 in. in the crushed-base section (northbound lanes) and 48 in. in the uncrushed-base section (southbound lanes). In the fill sections, the embankment thickness was greater than 60 in. All imported materials are classified as A-1-a and no water was

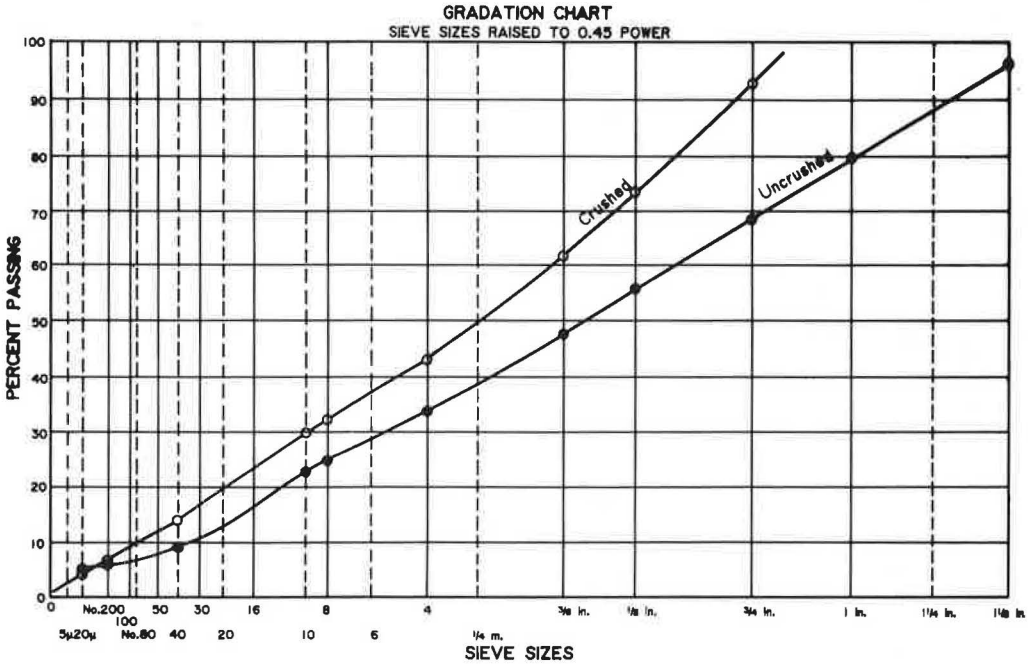

FIGURE 3 A 0.45 power gradation chart of crushed and uncrushed base courses.

TABLE 2 PAVEMENT STRUCTURES (AS-BUILT)

	Northbound Lanes, Crushed Base				Southbound Lanes, Uncrushed Base (Subbase)			
	Average Thickness (in.)	Range (in.)	Maximum Size (in.)	Average P_{200} (%)	Average Thickness (in.)	Range (in.)	Maximum Size (in.)	Average P_{200} (%)
Hot asphalt pavement	4.0[a]	3.4–4.8	–	–	3.1[a]	2.5–3.8	–	–
Base course	6	–	1	7	6	–	2	5
Subbase	6	–	2	7	–	–	–	–
Borrow	30[b]	–	3	7	36[b]	–	4	7
Subgrade	–	–	2	20–29	–	–	2	20–29

[a]After 1.5 in. overlay.
[b]Embankment greater than 60 in. thick.

encountered in any of the trenches. The subgrade in the cut ranged from A-1-b to A-4(0).

Pavement Deflections

An initial series of 20 pavement springtime deflections was measured on each test section using the Dynatest 8000 FWD before the overlay in 1983. Table 3 gives the average springtime deflection and representative basin for each section. For both the cut and embankment sections, the deflections were lower for the uncrushed lanes than for the crushed lanes even though the uncrushed lanes had 1 in. less AC.

In September 1983, after the test sites were overlaid, four test points were selected for additional deflection testing. These sites were adjacent to each test trench. At each site, a series of drops at approximately 45-, 85-, 130-, and 150-psi loadings was performed to investigate the stress sensitivity of the unbound layers. The results of these tests are given in Table 3. Again the deflections were lower for the uncrushed lanes, although the differences were smaller.

TABLE 3 AVERAGE PAVEMENT (DEFLECTION AND REPRESENTATIVE DEFLECTION BASINS (85-psi LOADING)

	Uncrushed (Southbound)		Crushed (Northbound)	
	Cut	Fill	Cut	Fill
Avg. Deflection (April 1983) (Inches 10^{-3})	12.45	10.76	16.30	16.30
Representative Deflection Basin (Inches 10^{-3})				
Sensor 1 (0.00")	13.58	12.01	18.27	16.30
Sensor 2 (7.87")	9.53	7.99	11.54	10.43
Sensor 3 (11.81")	6.77	5.47	7.20	6.38
Sensor 4 (17.72")	3.94	3.11	3.78	3.07
Sensor 5 (25.59")	0.75	1.89	1.81	1.69
Sensor 6 (35.43")	0.68	1.18	0.71	1.10
Sensor 7 (47.24")	0.31	0.75	0.39	0.87
Avg. Deflection (Sept. 1983) (Inches 10^{-3}) (After Overlay)	11.82	8.82	13.08	12.23
Representative Deflection Basin (Inches 10^{-3})				
Sensor 1 (0.00")	12.87	9.17	12.72	10.87
Sensor 2 (7.87")	9.29	7.05	9.72	8.23
Sensor 3 (11.81")	7.13	5.75	8.07	6.69
Sensor 4 (17.72")	4.53	4.02	5.79	4.53
Sensor 5 (25.59")	2.80	2.60	3.82	2.76
Sensor 6 (35.43")	1.69	1.61	2.40	1.57
Sensor 7 (47.24")	1.34	1.14	1.65	1.10

TABLE 4 SUMMARY OF ASPHALT PAVEMENT CORE DIAMETRAL RESILIENT MODULUS TESTING

Sample	Northbound Lanes (Crushed Base) Resilient Modulus (M_r) ksi		Sample	Southbound Lanes (Uncrushed Base) Resilient Modulus (M_r) ksi	
	@ 487 lbs.	@ 974 lbs.		@ 487 lbs.	@ 974 lbs.
221A	509	487	222	611	558
221B	571	465	312	396	380
311	566	503	522	381	381
521A	552	482	812	544	609
521B	410	332			
1011A	468	452			
1011B	121	118			
Average	457	406		483	482
Std. Dev.	159	139		113	119

AC Moduli

Cores at each of the sites were taken in October 1983. The cores were sent to Oregon State University for diametral modulus testing. The samples were tested at 10°C at a frequency of 1 Hz and load duration of 0.1 sec. Table 4 presents the results of the modulus testing. Because of the thickness, three cores had to be sawn to fit the test frame. They are shown as Samples A and B. The average modulus of 483 ksi for the pavement over the uncrushed base is larger than the average of 432 ksi for the pavement over the crushed base.

Base and Subgrade Moduli

The base and subgrade modulus at each test point was backcalculated for each applied load. Two computer programs, ELMOD and MODCOMP2, were used to backcalculate the base modulus. ELMOD uses the method of equivalent thicknesses developed by Dynatest Consultants, Inc.; MODCOMP2 uses elastic layer theory developed by Lynne Irwin *(2)*. The pavement structures were analyzed as a three-layer system, with an AC layer, a base, and subgrade. The AC surface thickness was set equal to the core thickness. The laboratory-determined AC modulus was corrected for temperature based on Van der Poel's nomograph *(1)* and used as an input for each test point for the MODCOMP2 program. ELMOD does not allow user input of the AC moduli for AC thicknesses greater than 3.75 in., but requires user input for AC thicknesses less than 3.75 in.

MODCOMP2, written for a given layer's nonlinear stress-dependent moduli given multiple loads, was unable to obtain a solution for any of the multiple load data from this project. The layer moduli for the unbound layers were solved individually for each load. This was probably because the stress sensitivity of these materials did not fit a power function. In all instances, ELMOD gave higher backcalculated moduli for the base than the MODCOMP2 program. Figure 4 shows a comparison of

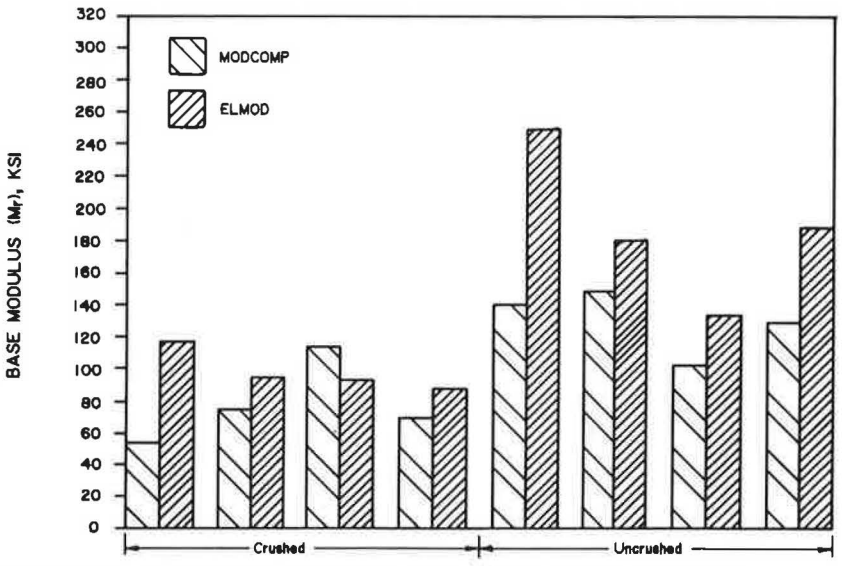

FIGURE 4 Comparison of backcalculation of base course moduli by MODCOMP2 and ELMOD computer programs at 85-psi surface load.

the results from the two programs for the base course at each test point at approximately 85-psi surface loading. The uncrushed-base moduli are higher than the moduli for the crushed base course. Table 5 presents the results of the moduli for all layers at all test points from the MODCOMP2.

Figures 5 and 6 show the base resilient moduli (backcalculated from MODCOMP2) for the crushed and uncrushed base plotted against the average bulk stress for each of the four loads applied by the FWD. The average bulk stress was calculated using PSAD2A *(1)*. Again, the crushed base course exhibited lower moduli than the uncrushed base. The crushed-base moduli also showed more scatter and did not fit the power function for the stress sensitivity of an unbound layer:

$$M_R = K_1\ \theta^n$$

where

M_R = resilient modulus,
θ = bulk stress, and
K_1, n = constants.

TABLE 5 SUMMARY OF BACKCALCULATED MODULI FROM MODCOMP2 (SEPTEMBER 1983 DEFLECTIONS)

Test Point	AC Thickness (inches)	Lab. AC Modus (ksi)	Load (psi)	Base Modulus (ksi)	Subgrade Modulus (ksi)
311					
Crushed, Fill	3.35	581	44.8	47.5	26.0
			86.8	75.5	29.6
			132.4	93.0	31.0
			151.8	99.5	34.2
1011					
Crushed, Fill	4.78	329	42.8	44.1	31.6
			86.1	70.1	33.8
			132.0	85.9	36.6
			149.8	89.0	36.5
221					
Crushed, Cut	3.95	550	43.1	25.2	30.2
			86.1	53.0	30.0
			132.4	69.4	30.8
			149.4	78.3	30.8
521					
Crushed, Cut	3.90	470	42.8	75.5	21.9
			85.1	114.4	24.9
			130.7	137.1	26.1
			147.4	119.6	26.2
312					
Uncrushed, Fill	3.83	438	42.5	100.0	31.5
			84.1	149.2	35.1
			129.7	189.6	39.6
			146.0	202.7	40.8
812					
Uncrushed, Fill	2.50	702	42.2	70.0	27.5
			84.4	129.9	31.9
			130.4	167.2	34.7
			146.8	186.4	35.8
222					
Uncrushed, Cut	2.58	644	41.3	103.6	34.4
			84.6	141.2	43.1
			130.4	178.2	48.1
			147.8	190.7	49.9
522					
Uncrushed, cut	3.43	438	42.5	64.3	20.9
			84.1	101.4	22.9
			130.4	125.4	25.2
			147.4	122.2	26.4

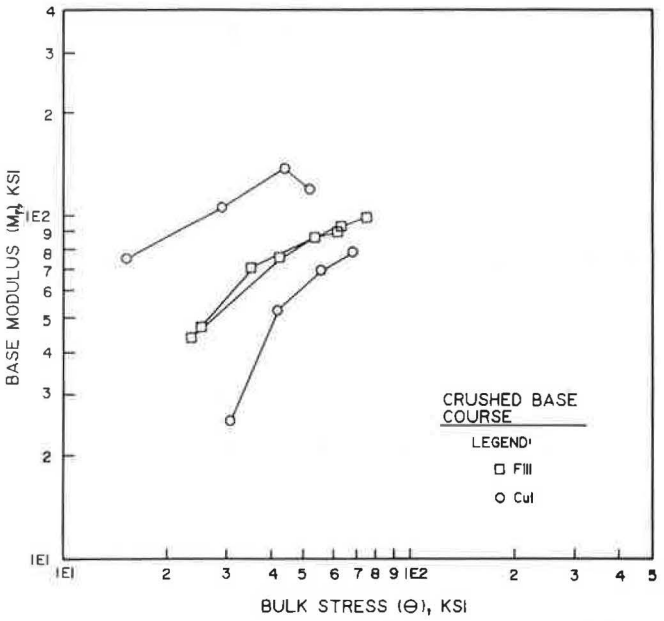

FIGURE 5 Backcalculated, crushed base course moduli from FWD deflections.

LABORATORY INVESTIGATION

To verify the field results, laboratory resilient modulus tests were performed on the two base materials at Oregon State University. The samples were prepared at approximately 96 percent of AASHTO T180 density and at optimum moisture (see Table 1). The test procedures used were in accordance with AASHTO T274-82 as much as possible. The loading frequency was 30 rpm with a load dwell of 0.12 sec. The uncrushed base had a lower optimum moisture content but a higher Proctor density.

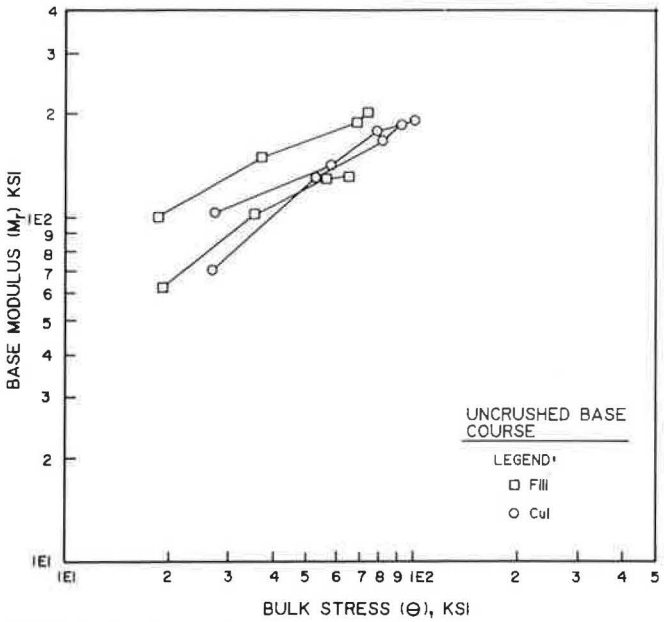

FIGURE 6 Backcalculated, uncrushed base course moduli from FWD deflections.

Modulus Results

The average laboratory values of the resilient modulus versus the bulk stress are presented in Figure 7 along with the average values determined from the field. Although the laboratory values were approximately one-half of those determined in the field, the uncrushed material still performed better than the crushed material. These results, rather surprising in light of past and present research involving crushed and uncrushed gravels, may be attributable to the fact that the maximum size of the uncrushed material is 2 in. whereas the maximum size of the crushed base is only 1 in.

Laboratory resilient modulus tests were also run on samples prepared at 1.5 percent more than the optimum moisture content in an effort to simulate springtime conditions. Figure 8 shows the results of these tests as compared to the average values at optimum. Both materials show a loss in modulus, with the uncrushed material indicating a reduction of 27 percent, higher than the crushed material, which only indicated a reduction of 16 percent. This difference appears to indicate that the fracture may have a benefit during spring thaw when the base course is saturated, as has been suggested by other research *(6)*. Because these percentages are based on only one test each more than optimum, further research should be considered to evaluate the effects of moisture on the base-subbase modulus.

Permanent Deformation Results

Permanent deformation tests were also performed on the field samples using AASHTO T274-82. Samples were tested using a 10-psi confirming stress and a deviator stress of 20 psi. The permanent deformation was measured at logarithmic load repetition intervals for a total of 10,000 repetition. Two tests on

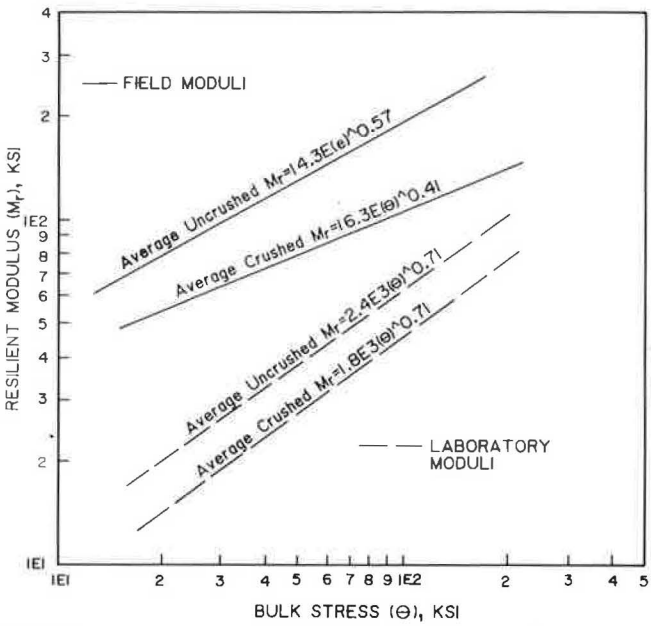

FIGURE 7 Comparison of laboratory-measured base course moduli to backcalculated moduli from FWD deflections.

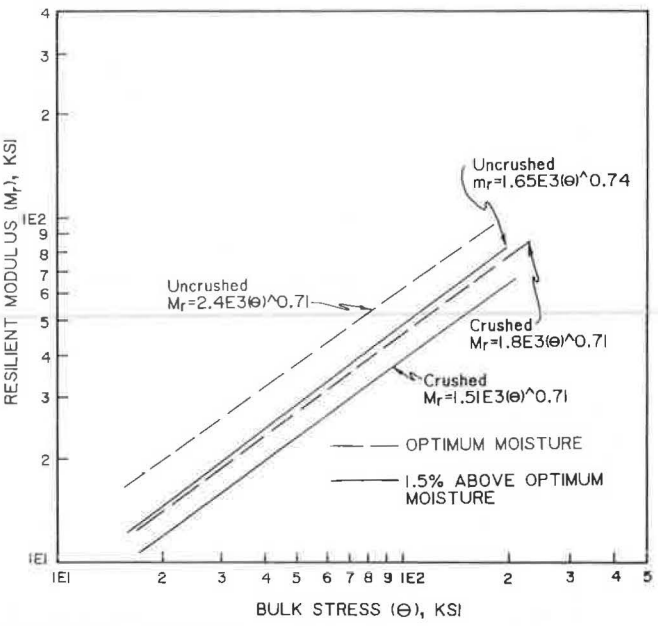

FIGURE 8 Comparison of laboratory-measured base course moduli tested at optimum moisture content and 1.5 percent more than optimum moisture content.

both the crushed and uncrushed bases were run at optimum moisture and one test at 1.5 percent more than optimum moisture. Figure 9 shows the results of the average of two tests at optimum moisture as well as the one at more than optimum moisture for both the crushed and uncrushed bases. Again, the uncrushed base performed better, yielding smaller permanent deformations than the crushed base. Both the crushed and uncrushed bases showed about the same percentage increase in permanent deformation upon saturation. Again, because this result is based on one test of each material, it should be investigated further.

EFFECT OF BASE PROPERTIES ON PAVEMENT LIFE

Analysis Approach

A pavement analysis was performed using the PSAD2A elastic layer computer program to compare the effects on pavement life of using an uncrushed versus a crushed base course. A section with 3 in. of AC, 6 in. of base course, and 12 in. of subbase over a combined embankment and subgrade was selected for analysis (Table 6). The average laboratory AC moduli and the average field backcalculated moduli for the base course for each section were used as given in Table 7. For the summer months, the subbase moduli were made equal to the combined backcalculated moduli for the combined embankment and subgrade.

To simulate springtime conditions, the base course moduli were reduced by the percentages determined in the laboratory on the saturated samples. The subbase moduli were also reduced to 8 ksi. The pavement moduli were adjusted for temperature throughout the spring and summer months (Table 8). No damage to the pavement was assumed when the embankment was frozen during the winter. The fatigue curve recommended in Volume II of the proposed AASHTO *Guide for*

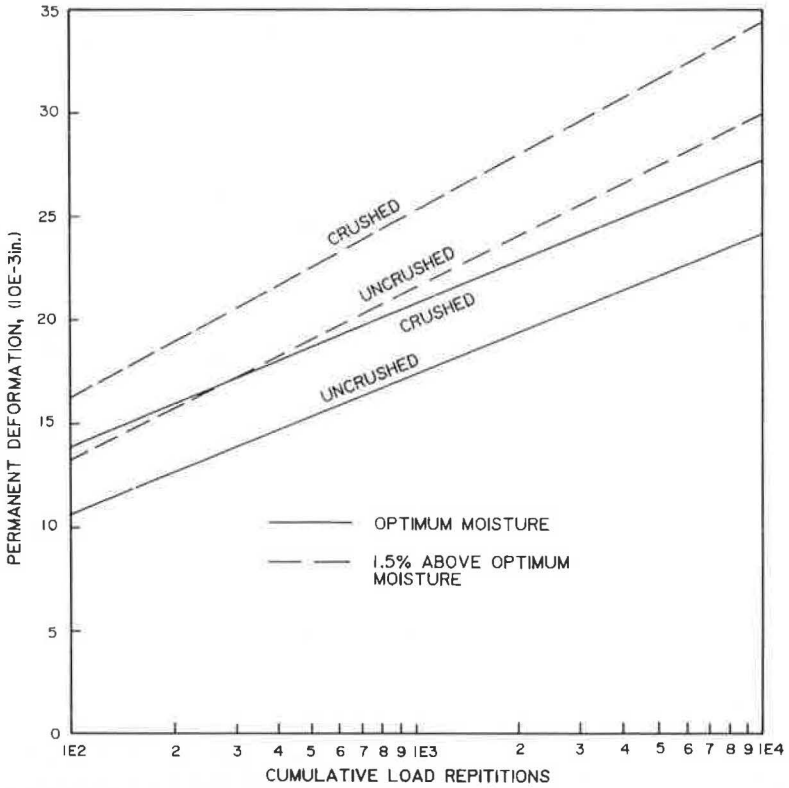

FIGURE 9 Results of laboratory-measured base course permanent deformations at optimum moisture content and 1.5 percent more than optimum moisture content.

TABLE 6 LAYER THICKNESSES USED IN ANALYSIS OF PAVEMENT LIFE

Layer	Thickness (in.)
Asphalt concrete	3.0
Base course	6.0
Subbase	12.0
Subgrade	–

TABLE 7 MATERIALS PROPERTIES USED IN ANALYSIS OF PAVEMENT LIFE

	Modulus (M_R) (ksi)	
Layer	Crushed	Uncrushed
AC at 10°C	468	483
Base course (summer)	$16.3\ \theta^{0.41}$	$14.3\ \theta^{0.57}$
Base course (spring)	$13.7\ \theta^{0.41}$	$10.4\ \theta^{0.57}$
Subbase (summer)	29.6	33.3
Subbase (spring)	8.0	8.0
Subgrade	29.6	33.3

NOTE: θ = Bulk stress.

Design of Pavement Structures (4) was used to determine fatigue life:

$$\log_{10} N_f = 15.988 - 3.291 \log_{10}\left(\frac{t}{10^{-6}}\right) - 0.854 \log\left(\frac{S_{mix}}{10^3}\right)$$

where

N_f = number of allowable load repetitions,
t = strain in the bottom of the AC layer, and
S_{mix} = AC modulus (psi).

The pavement damage was totaled using Miner's hypothesis based on a monthly equivalent axle load (EAL) of 16,000.

Results

The analysis presented in Table 8 shows that with 3.0 in. of AC, the pavement with the uncrushed base would have a life of 12.3 years, whereas the pavement over the crushed base would have a life of only 8.0 years. This represents a 54 percent greater life for the uncrushed base than for the crushed base. However, as constructed with 3.1 in. of AC over the uncrushed base and 4.0 in. over the crushed base, the AC pavement with the crushed base has a longer life than that with an uncrushed base by as much as 31 percent.

DISCUSSION OF RESULTS

It appears that the uncrushed base is superior to the crushed base because of the larger maximum size and higher density. The 0.45 power plots of the gradations on Figure 3 show that the uncrushed base points are closer to a straight line. The crushed base line has a slight upward curve. The straighter plot and the larger maximum size explain the higher density. The higher density apparently results in the uncrushed base being stiffer and having a higher resilient modulus. This stiffness in turn leads to better performance. The uncrushed base also has 1 percent more passing the No. 200 sieve than the crushed base.

TABLE 8 RESULTS OF ANALYSIS OF PAVEMENT LIFE

	Uncrushed Base				Crushed Base			
Month	AC Modulus (ksi)	Strain (10^{-6})	Allowable Repetitions (X1000)	Annual** N_i/N_f	AC Modulus (ksi)	Strain (10^{-6})	Allowable Repetitions (X1000)	Annual** N_i/N_f
April	672	258	435	0.037	690	281	321	0.050
May	600	166	2045	0.008	617	190	1281	0.013
June	391	186	2028	0.008	407	220	1128	0.014
July	333	192	2095	0.008	339	232	1107	0.015
Aug	311	194	2147	0.008	347	230	1117	0.014
Sept	543	171	2020	0.008	560	197	1235	0.013
Oct*	776	152	2195	0.004	793	171	1462	0.006
			TOTAL	0.081			TOTAL	0.125
			Pavement Life	12.3 years				8.0 years

* No damage assumed when embankment is frozen

** 16,000 EALs/month

The optimum moisture of the uncrushed base is also 0.4 percent less than the crushed base. For this project, the uncrushed base has a 37 percent single-faced fracture versus an 81 percent fracture for the crushed base. The larger maximum size and the higher density apparently have a larger beneficial effect than increasing the fracture from 37 to 81 percent.

CONCLUSIONS AND RECOMMENDATIONS

Conclusions

The results of the study indicate the following conclusions are warranted:

1. In all testing, both in the laboratory and in the field, the uncrushed base (subbase, Grading B) performed better than the crushed base (base course, Grading D-1). It had both a higher resilient modulus and a lower permanent deformation. For the project investigated, the uncrushed base had a maximum size of 2 in., 6 percent passed the No. 200 sieve, and the material retained on the No. 4 sieve had a 37 percent single-face fracture. The crushed base had a maximum size of 1 in., 7 percent passed the No. 200 sieve, and there was an 85 percent single-face fracture.
2. The uncrushed base showed a loss of resilient modulus of 27 percent as compared to a 16 percent loss for the crushed base when water content was 1.5 percent more than optimum, but still showed a higher modulus than the crushed base when saturated.
3. Both the crushed and uncrushed base showed about the same percentage increase in permanent deformation at 1.5 percent more than optimum moisture content.
4. In backcalculating the base modulus from the FWD readings, the ELMOD program using the method of equivalent layers gave consistently higher moduli than the MODCOMP2 program using elastic layer analysis.
5. The backcalculated field moduli were approximately two to three times as great as those measured in the laboratory on the same material. It appears that the laboratory resilient modulus test does not adequately reflect the performance of layered pavement structures.
6. For this project, an analysis of the pavement life using the field-backcalculated moduli for the base courses indicated that with the same AC thickness the AC pavement over the uncrushed base would have a 54 percent longer life than that over the crushed base.
7. It appears that the uncrushed base is superior to the crushed base because of the larger maximum size and higher density. This apparently results in the uncrushed base's being stiffer and having a higher resilient modulus. This stiffness in turn leads to the better performance of the uncrushed base.

Recommendations

1. The results presented in this paper are for one project only. Before any conclusions are implemented as to the use of uncrushed base, other test projects should be investigated to verify these results.
2. Further laboratory testing is recommended to determine the effect of maximum size and gradation on resilient modulus.
3. The percentage loss of modulus presented in this paper is based on one sample each of crushed and uncrushed base courses. Also, the springtime damage to the AC as shown in the pavement life analysis is significant. Further testing is recommended to provide a statistical verification of the results presented in this paper.
4. The permanent deformation results presented in this paper are based on one sample each of crushed and uncrushed base courses. Further testing is recommended to provide statistically valid results.
5. Further work appears necessary to adequately predict field performance of layered pavement structures based on laboratory testing of unbound materials.

IMPLEMENTATION STATEMENT

The results of this study are from one project only and are typical of the conditions found on that project. Although the uncrushed base course was shown to perform better than the crushed base course, the general use of uncrushed base courses should not be implemented until more complete testing is performed, both in the laboratory and at field test sites. At this time, the use of uncrushed base can be considered in areas where it is hard to make specification base course because of degradation during the crushing process. These projects should be nonurban and in locations where there are no horizontal forces on the pavement structure due to stopping and starting.

ACKNOWLEDGMENT

The Alaska Department of Transportation and Public Facilities acknowledges the technical assistance and funding assistance provided by the Federal Highway Administration under the Highway Planning and Research Program. Special credit is given to Stuart Albright for conducting the laboratory tests.

REFERENCES

1. R. G. Hicks. Use of Layered Theory in the Design and Evaluation of Pavement Systems. Report FHWA-AK-RD-83-8. Alaska Department of Transportation and Public Facilities, Juneau, July 1982.
2. L. H. Irwin. *User's Guide to MODCOMP1*. Cornell University, Ithaca, N.Y., Nov. 1983.
3. Dynatest Group. *ELMOD Evaluation of Layer Moduli and Overlay Design, User's Manual*. July 1983.
4. *Proposed AASHTO Guide for Design of Pavement Structures*. Vol. II, AASHTO, Washington, D.C., 1985.
5. Alaska Department of Transportation and Public Facilities. *Guide for Flexible Pavement Design and Evaluation*. Juneau, Aug. 1982.
6. R. G. Hicks, S. Albright, and J. R. Lundy. *Evaluation of Percent Fracture and Gradation on Behavior of Asphalt Concrete and Aggregate Base*. Report AK-RD-86-25. Alaska Department of Transportation and Public Facilities, Juneau, Dec. 1985.

Publication of this paper sponsored by Committee on Strength and Deformation Characteristics of Pavement Sections.

The Effect of Contact Area Shape and Pressure Distribution on Multilayer Systems Response

JACOB UZAN AND ARIEH SIDES

Numerical analysis of stresses, strains, and displacements in multilayer systems for any shape of contact area and pressure distribution is presented. The scheme developed for microcomputers is made of two programs: one for evaluating the stresses and deformations under a point load and the second for performing the numerical integration of the point load solution. Results obtained by using the scheme for the uniformly distributed pressure, Boussinesq, and three-layer system cases were compared to those of analytical and other numerical solutions. They were revealed to be in excellent agreement. Results for a rectangular contact area and nonuniform pressure distribution are presented. The effect of the contact area and pressure distribution shapes on the design strains is illustrated and discussed. The scheme presented is preferable to the 3-D finite element analyses. it dispenses with the use of mainframe computers and is highly accurate.

In flexible pavement design the tire contact area is assumed circular and the pressure uniformly distributed. However, there are experimental results that show that the contact area resembles either the circular, elliptical, or even rectangular shape, and the contact pressure distribution is either uniform, parabolic, or irregular depending on the characteristics of the tire, the inflation pressure, and the load *(1, 2)*. It is generally assumed that the difference between pavement response under real loading conditions and under uniform pressure distributed over a circular area is small. This assumption seems adequate for flexible pavement design. Yet, in analyzing trial tests it may be more appropriate to use the real loading conditions for comparing computed and measured stresses and deformations *(3, 4)*. In these cases, the existing multilayer computer programs [BISTRO *(3)* and BISAR *(4)*] were used together with superposition of circular uniform loads to approximately simulate the real loading conditions. In other cases *(5)*, the 3-D finite element computer program was used to calculate strains in a multilayer system. The limitations of both approaches either in representing the real loading conditions or in computer frame size are obvious. As the loads and tire pressures on modern vehicles are increasing, there is an evident need for a scheme for computing the pavement response under these new configurations.

A numerical approach for computing stresses and deformations in elastic multilayer systems for any shape of contact area and pressure distribution is presented. The scheme, developed for microcomputers, includes computer programs for evaluating the stresses and deformations in an elastic multilayer system under the action of a concentrated force and for performing numerical integration over the given contact area.

The paper includes

- A brief description of the theoretical background of the programs,
- A verification of the scheme by comparing the results with other well known solutions, and
- A comparison of the results of analyses using circular and rectangular contact areas and uniform and irregular pressure distributions.

THEORETICAL BACKGROUND

Layered Elastic Systems

The mathematical background of the analysis of stresses and displacements in layered elastic systems was presented by Schiffman *(6)*. The surface loading conditions are those of the axisymmetric case and include the point load condition relevant to the present study.

The computer program developed by Uzan *(7)* for unidirectional horizontal and vertical uniformly distributed loads over a circular area and for different interlayer friction conditions (in a range between fully adhesive and completely frictionless) was modified to include the concentrated force. Near the load, the stresses and deflection tend toward infinity.

The results obtained using the computer program for the Boussinesq case (i.e., a point load applied at the surface of a homogeneous, isotropic, elastic half-space) were compared with the rigorous analytical solutions. They were revealed to be in excellent agreement. The computer program can be used for the numerical integration over the given contact area in calculating stresses and strains in layered elastic systems.

Numerical Integration of the Point Load Solution

The contact area is subdivided into surface elements, with given pressure magnitude at the nodal points. Figure 1 shows a circular area, subdivided into isoparametric elements, with 4 to 6 nodes. Due to symmetry of the circular contact area, only a half-circle, which represents a radius vector, is used to compute stresses and deformations along the x-axis. The integration over the surface element is carried out using the 4 × 4 Gauss quadrature scheme:

$$u_{im} = a_m \sum_{j=1}^{4} \sum_{k=1}^{4} w_j w_k p_{jk} u_{ijk}$$

Technion, Israel Institute of Technology, Technion City, Haifa, Israel 32000.

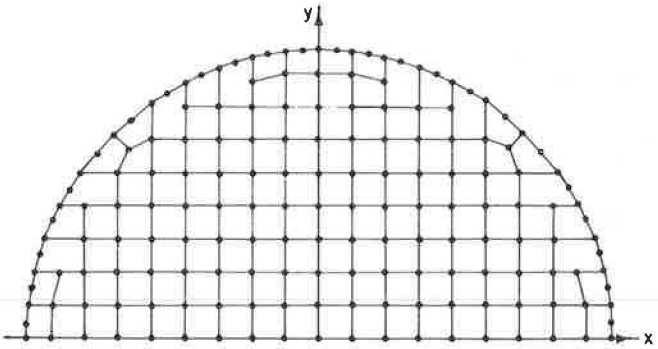

FIGURE 1 Breakdown mesh of a circular area.

where

u_{im} = ith component of the displacement or stress vector at point (x, y) due to the given pressure distribution over element m.
a_m = area of element M.
w_j, w_k = Gauss weighting factors corresponding to the point of integration (x_j, y_k) inside element m.
p_{jk} = pressure evaluated at the integration point (x_j, y_k) using the given values of the pressure at the nodal points, and up to the second-order interpolation polynomial associated with the isoparametric element type.
u_{ijk} = ith component of the displacement or stress vector at point (x, y) due to a unit force applied at the integration point (x_j, y_k).

Summing the contributions of all elements (from $m = 1$ to m = number of elements) leads to the final result of stress, strain, or displacement components. The term u_{ijk} is evaluated numerically by Lagrange interpolation, from tabulated values obtained using the computer code for layered elastic systems with point force loading. Therefore, the numerical integration scheme requires the following steps:

1. Define the layered system, that is, layer thicknesses, elastic parameters (modulus of elasticity and Poisson's ratio), and interface conditions.
2. Define the depth where stresses and displacements are to be evaluated.
3. Run the layered elastic computer program for a unit point load, the given depth, and a number of radial distances. The values of the stresses and displacements obtained are tabulated to permit interpolation in the numerical integration.
4. Define the contact area and subdivide it into isoparametric elements. The size and shape of the element are dictated by the pressure distribution, the regularity of the limits of the contact area, and the regularity of the function u_{ijk}.
5. Run the numerical integration program to get stresses, strains, and displacements for various positions (x, y), at the given depth of the layered system.

The following paragraph show the accuracy of the results obtained with the computer programs.

VERIFICATION

Stresses, strains, and displacements were computed for the following conditions using the procedure developed:

1. One- and three-layer systems. The one-layer system corresponds to the Boussinesq case. The three-layer system variables were (a) layer thicknesses of h_1 = 1.5, 2, 3, and 4 in. and h_2 = 8 in.; (b) moduli of elasticity of E_1 = 400 ksi, E_2 = 60 ksi, and E_3 = 6 ksi; (c) Poisson ratios of μ_1 = 0.35, μ_2 = 0.40, and μ_3 = 0.45, where the indices refer to the layer number sequence. The three-layer systems chosen for the verification are those used by Chen et al. *(5)*.
2. Uniform pressure applied over a circular area. The breakdown mesh of the contact area is shown in Figure 1.
3. Two depths—at the surface and at the bottom of the asphaltic layer in the three-layer system.

The results were compared to those of the analytical or other numerical integration solutions. They were revealed to be in close agreement, with a maximum difference of 0.3 percent. The error associated with most 3-D finite element procedures is expected to be much higher than 0.3 percent. However, the accuracy and efficiency of computations are achieved at the expense of restricting the analysis to linear systems only.

ILLUSTRATIVE RESULTS

The tensile strains at the bottom of the asphalt concrete (AC) layer and the compressive strains at the top of the subgrade were computed for the following loading conditions and layered systems:

Loading Conditions

1. Single-wheel load—4,500 lb.
2. Various contact area shapes and pressure distributions—(a) 75 psi uniformly distributed on a circular area (Figure 1); (b) 63.775 psi uniformly distributed on a rectangular area; and (c) nonuniform pressure distribution on a rectangular area, as reported by Chen et al. *(5)* and shown in Figure 2.

Layered Systems

Three-layer systems as described in the previous section were treated.

The computation results are shown in Figures 3 and 4. It is seen that

1. The maximum tensile strains of the rectangular contact area are similar for the uniformly and nonuniformly applied pressure, except for the thin AC layer (h_1 = 1.5 in.). The maximum strain is found to be under the center of the loading area except for the thin AC layer. In the latter case, the strain reaches its highest value along the transverse (y) direction in Figure 2, close to the high-pressure values.

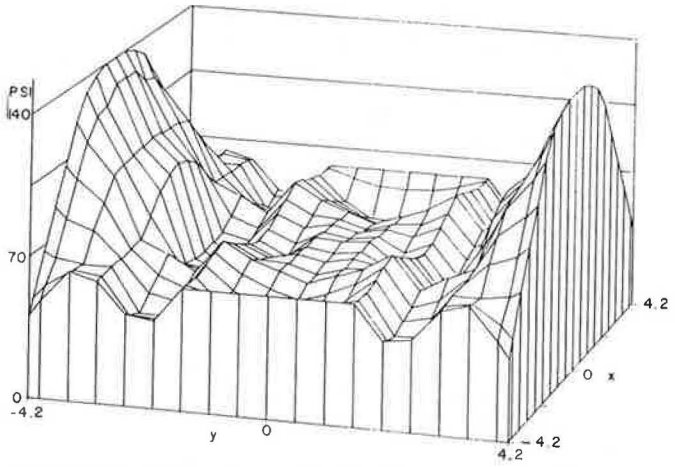

FIGURE 2 3–D pressure distribution on a rectangular contact area.

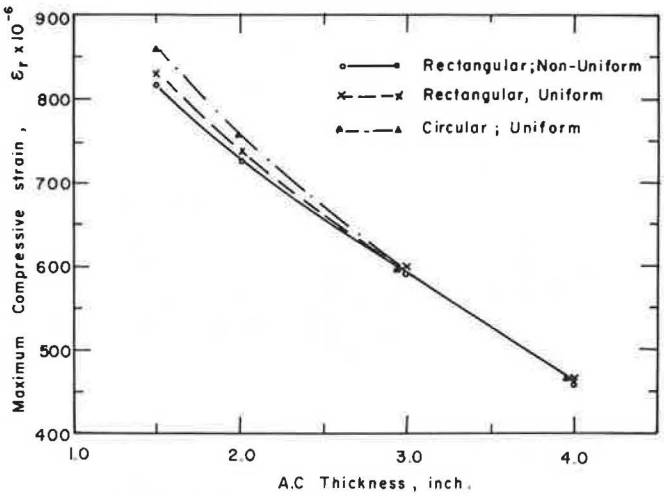

FIGURE 4 Maximum compressive strains at the top of a subgrade.

2. The tensile strains are in general higher for the circular contact area and uniformly distributed pressure than for the rectangular contact area, in cases of both uniform and non-uniform pressure distribution. In the case of a thin AC layer, the particular pressure distribution used in the analysis led to high tensile strains similar to those obtained under the circular area. For the 4-in. thickness, the effect of the contact area shape is smaller than for the 2- and 3-in. thicknesses of AC.

3. The compressive strains at the top of the subgrade are only slightly affected by the contact area shape and pressure distribution. The maximum values for all layered systems were obtained under the center of the loading area.

4. The results suggest that the effect of contact area shape and pressure distribution on the pavement response depends on the depth at which it is computed. This effect is less pronounced as the depth increases.

5. The assumption of circular contact area and uniformly distributed pressure is slightly conservative, and seems adequate for design purposes in the case of thick AC layers and pavements.

The results were compared to those presented by Chen et al. *(5)* using a 3-D finite element program. Both sets of results were obtained for the same multilayer system, wheel load, area shape, and pressure distribution. The tensile strains were similar in both analyses, but the compressive strains of the 3-D finite element were up to 40 percent lower than those of the technique described in the paper. A computation error of that magnitude can lead to an overestimation of the pavement life by a factor of 10.

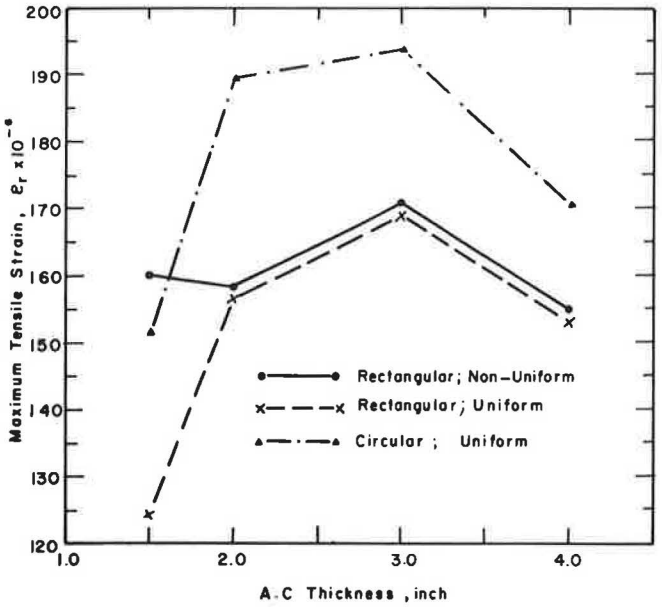

FIGURE 3 Maximum tensile strains at the bottom of the AC layer.

CONCLUSIONS

The computer programs described in this paper can be used for a wide range of problems, including (a) any contact area shape, (b) any pressure distribution, (c) vertical and horizontal loads, and (d) interface conditions varying from rough to frictionless *(7)*.

There are some limitations that should be stressed. In some cases of very thick layers, the solution may not converge. When the pavement response is computed at the surface, the results can be obtained at up to a certain distance from the point force.

The computer programs can be run on microcomputers with 256 kB memory such as the IBM PC or the Digital Rainbow 100+. The programs are written in Fortran and can be used for any pavement or geotechnical purposes. They are very accurate, and superior to the 3-D finite element programs in both accuracy and ease of use.

The theoretical background of two computer programs for analyzing multilayered linear elastic systems, under non-uniformly distributed load over any given contact area shape,

has been presented. The programs, written for microcomputers, dispense with the use of mainframe computers.

The results obtained using the programs are found in close agreement with other analytical or numerical integration solutions. They are more accurate than the 3-D finite elements and other approximations. Illustrative results of the effect of the load distribution and contact area shape are presented.

The computer programs are useful to practicing and research engineers who have restricted or no access to mainframe computers. The programs may be used for analyzing problems involving uncommon load distributions and contact area shapes in both pavement and geotechnical fields.

REFERENCES

1. W. L. Lawton. Static Load Contact Pressure Patterns Under Airplane Tires. *HRB Proc.*, Vol. 37, 1957, pp. 233–239.
2. N. W. Lister and R. Jones. The Behavior of Flexible Pavements Under Moving Wheel Loads. *Proc., 2nd International Conference on the Structural Design of Asphalt Pavements*, University of Michigan, Ann Arbor, 1967, pp. 1021–1035.
3. A. Hofstra and C. P. Valkering. The Modulus of Asphalt Layers at High Temperatures: Comparison of Laboratory Measurements Under Simulated Traffic Conditions with Theory. *Proc., 3rd International Conference on the Structural Design of Asphalt Pavements*, Vol. I, University of Michigan, Ann Arbor, 1972, pp. 430–443.
4. W. G. Bleyenberg, A. I. M. Classen, F. Van Gorkum, W. Heukelom, and A. C. Pronk. Fully Monitored Motorway Trials in the Netherlands Corroborate Linear Elastic Design Theory. *Proc., 4th International Conference on the Structural Design of Asphalt Pavements*, Vol. 1, University of Michigan, Ann Arbor, 1977, pp. 75–98.
5. H. H. Chen, K. M. Marshek, and C. L. Saraf. The Effects of Truck Tire Contact Pressure Distribution on the Design of Flexible Pavements—A 3D Finite Element Approach. In *Transportation Research Record 1095*, TRB, National Research Council, Washington, D.C., 1986. pp. 72–78.
6. R. L. Schiffman. General Analysis of Stresses and Displacements in Layered Elastic Systems. *Proc., 1st International Conference on the Structural Design of Asphalt Pavements*, University of Michigan, Ann Arbor, 1962, pp. 365–375.
7. J. Uzan. The Influence of the Interface Condition on Stress Distribution in a Layered System. In *Transportation Research Record 616*, TRB, National Research Council, Washington, D.C., 1976, pp. 71–73 (Abridgment).

Publication of this paper sponsored by Committee on Strength and Deformation Characteristics of Pavement Sections.

Sensitivity Analysis of Selected Backcalculation Procedures

T. RWEBANGIRA, R. G. HICKS, AND MARK TRUEBE

One major problem facing highway engineers today is the evaluation of existing pavement systems. This evaluation is necessary to meet today's demands for higher magnitudes of traffic loads and intensity. In particular, there exists a need for a reliable, quick, and nondestructive tool that permits the evaluation of pavements to obtain accurate information about existing structural conditions. In response to this need, several types of nondestructive testing equipment and analysis procedures have been developed and are currently available. Their use in predicting pavement layer moduli must be carefully evaluated, as this particular application is now an integral part of the new AASHTO overlay design procedure. BISDEF, MODCOMP2, and SEARCH analysis procedures were evaluated and the sensitivity of the backcalculated moduli to variations in input parameters was investigated. Results obtained for typical asphalt concrete and aggregate-surfaced pavements showed that the backcalculated moduli were sensitive to several of the user-supplied inputs. The backcalculated moduli from BISDEF were sensitive to layer thickness, depth of stiff layer, and assumed range of layer modulus used. For the MODCOMP2 and SEARCH programs, the backcalculated moduli were sensitive to layer thickness. Backcalculated moduli from all three programs were sensitive to variations in surface deflection measurements. Although identical values were input, the backcalculated moduli from the three procedures differed.

One major problem facing highway engineers today is the evaluation of existing pavement systems. This evaluation is necessary to meet today's demands for higher magnitudes of traffic loads and intensity. In particular, there exists a need for a reliable, quick, and nondestructive tool that permits the evaluation of pavements to obtain accurate information about existing structural conditions. In response to this need, several types of nondestructive testing (NDT) equipment and backcalculation procedures have been developed and are currently available *(1–4)*.

These backcalculation procedures are complex, relatively new, and still plagued by problems, including the following *(1)*.

1. The nonuniqueness of the resilient modulus backcalculated from the measured deflection basin,
2. Errors due to possible variation in thickness of pavement layers,
3. Errors involved in assuming a semi-infinite subgrade,
4. Time involved in the iterative process,
5. Errors in backcalculated moduli because of the nonlinear behavior of granular layers and subgrade, and
6. Errors involved in using input values out of the range for which the model was calibrated.

These problems must be dealt with to fully implement the 1986 AASHTO guides for design of pavement structures.

The objective of this paper is to present evaluations of selected procedures currently being used to determine the modulus of pavement layers. The sensitivity of the predicted moduli to various input parameters is also evaluated. The procedures evaluated were the following:

1. BISDEF,
2. MODCOMP2, and
3. SEARCH.

These procedures were selected because of their availability to the authors and the extent of their documentation. They also have been adapted for use on microcomputers and can be run on IBM and IBM-compatible microcomputers.

STUDY APPROACH

Data Collection

The surface deflection measurements used in the analysis were collected from sites located in the Willamette National Forest in Oregon. Typical data from asphalt concrete (AC) and aggregate-surfaced pavements were used. The KUAB falling weight deflectometer (FWD) was used in the collection of surface deflection data. Figure 1 shows the load and deflection sensor layout of the KUAB FWD. Figure 2 shows typical pavement structures used in the analysis.

Procedures Considered

BISDEF

This computer program, developed by the U.S. Army Corps of Engineers, Waterways Experiment Station *(2, 5)*, uses a deflection basin from NDT results to predict the elastic moduli of up to four pavement layers. These determinations are accomplished by matching the calculated deflection basin to the measured deflection basin.

The basic assumption of this method is that dynamic deflections correspond to those predicted from the layered elastic theory. This method uses the BISAR *(6)* layered elastic pro-

T. Rwebangira, Department of Civil Engineering, University of Dar-es-Salaam, P.O. Box 35131, Dar-es-Salaam, Tanzania. R. G. Hicks, Department of Civil Engineering, Oregon State University, Corvallis, Oreg. 97331. M. Truebe, Forest Service, U.S. Department of Agriculture, Eugene, Oreg. 97449.

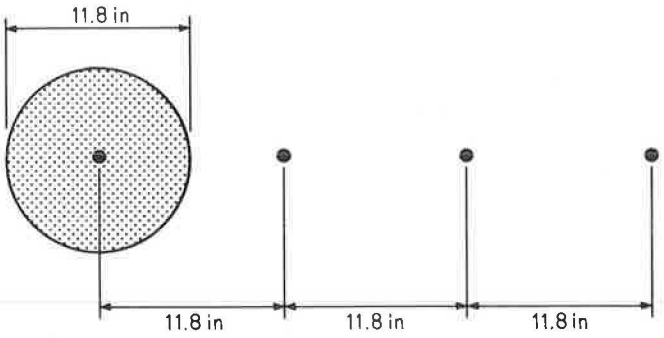

FIGURE 1 Layout of FWD sensor placement.

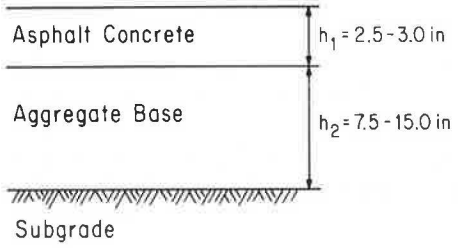

(a) Conventional AC Pavement

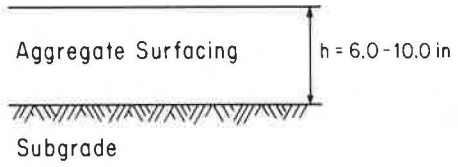

(b) Aggregate Surfaced Pavement

FIGURE 2 Typical pavement structures used in the analysis.

gram to compute the deflections, stresses, and strains of the structures under investigation. The procedure was initially calibrated using data from the Model 2008 Road Rater. There was good agreement between computed and measured deflections when a rigid layer of 240-in. thickness below the surface of the pavement was assumed. The effect of the static load applied to the pavement as a preload was also investigated; for computer modeling this effect was practically negligible for most comparisons.

To determine the layer moduli, the basic inputs include initial estimates of the elastic layer pavement characteristics, as well as deflection basin values. Inputs for each layer include

1. Thickness of each layer,
2. Range of allowable modulus,
3. Initial estimate of modulus, and
4. Poisson ratio.

For the deflection basin, the required inputs are

1. Deflections at a number of sensor locations, and
2. A maximum acceptable error in deflection matching.

The modulus of any layer may be assigned or computed. If assigned, the value is based on the type of material or properties of the material at the time of testing. The number of layers with unknown modulus values cannot exceed the number of measured deflections. The best results are obtained when the moduli of not more than three layers are to be calculated *(5)*.

The program is solved using an iterative process that provides the best fit between measured deflection and computed deflection basins. In this procedure, the set of moduli that minimizes the error sum between the computed deflection and measured deflections is determined. BISDEF, which uses the BISAR *(6)* subroutine for stress and deflection computations, is capable of handling multiple wheel loads and variable interface friction. CHEVDEF, which uses the Chevron elastic layer program, can only handle single-wheel loads *(7)*. The two procedures produce identical results for single-loading cases (e.g., FWD data).

MODCOMP2

MODCOMP2 program specifications, developed by Irwin *(3)*, include the following:

1. Up to eight layers can be included in the pavement system.
2. The layer combinations may be linear elastic or nonlinear stress dependent.
3. The program is capable of accepting data from several typical NDT devices (e.g., FWD, Road Rater, and Dynaflect).
4. It is capable of accepting up to six load levels.

MODCOMP2 uses the Chevron elastic layer computer program for determining the stresses, strains, and deflections in the pavement system. As in BISDEF/CHEVDEF, there is no closed-form solution for determining layer moduli from surface deflection data. Thus, an iterative approach is used that requires an input of initial or estimated moduli for each layer. The basic iterative process is repeated for each layer until the agreement between the calculated and measured deflection is within the specified tolerance or until the maximum number of iterations has been reached.

Because untreated base course and subgrade materials behave as nonlinear materials, the resilient modulus of such materials can be expressed by the equation $M_r = K_1\theta^{K_2}$, where θ is bulk stress and K_1 and K_2 are constants. The program has the added capability to derive K_1 and K_2 parameters for a given layer when they are unknown. In such cases, the user must provide deflection basin data for at least three load levels. The program can accept data for up to six load levels.

SEARCH

This computer program, developed at the Texas Transportation Institute *(4)*, uses a pattern-search technique to fit deflection basins with curves shaped like elliptic integral functions. These curves are solutions to the differential equations used in elastic

layer theory. The theoretical development of the deflection equation used in the program is discussed in detail by Lytton and Michalak *(4)*. The equation is based on the behavior of an elastic layer resting on a rigid incompressible layer, as first postulated by Vlasov and Leont'ev *(8)*. To account for multiple layers, a generalized form of Odemark's assumption *(9)* is used. This assumption transform the thickness of all layers to an equivalent thickness of a material having a single modulus. The input data include

1. Thickness of AC and granular base layers,
2. Force applied and radius of loading plate, and
3. Measured deflection values, and their radial distances, from center of loading plate.

The program searches for the elastic moduli that fit the measured basin to the calculated basin with the least average error. The output includes calculated moduli, computed and measured deflections, force applied, and squared error of the fitted basin.

Type of Deflection Data

The surface deflection values used in this study were obtained from pavements in the Willamette National Forest near Eugene, Oregon. The data were obtained using the KUAB FWD (Figure 1), owned and operated by Pavetech, Inc., of Redmond, Washington. The KUAB FWD *(10, 11)* is a trailer-mounted device towed by a standard-sized automobile. The impulse force is created by dropping a set of two weights from different heights. By varying the drop height, the force is varied from 4,900 to 11,300 lb. The two-mass system is used to create a smooth load pulse similar to that created by a moving wheel load *(10, 11)*. Surface deflections are measured with four seismic transducers (seismometers) that are lowered automatically with the loading plate. Because it can apply a load of a magnitude equal to that produced by a loaded truck, there is no need to correct the determined in situ moduli for stress sensitivity.

Evaluated Input Parameters

The evaluated input parameters included all the user-supplied inputs that could affect the predicted value of the moduli, such as

1. Range of modulus for each unknown layer modulus,
2. Depth of the stiff layer,
3. Seed modulus for each layer,
4. Layer thicknesses for all pavement layers,
5. Magnitude of surface deflection, and
6. Number of iterations and allowable deflection match tolerances.

If applicable, these factors were evaluated for each computer program and for AC and aggregate-surfaced pavements. The evaluation consisted of predicting the unknown modulus of the various pavement layers using different values of each input parameter under consideration. Table 1 summarizes the standard input values.

TABLE 1 STANDARD INPUT VALUES

Variable Name	AC SURFACED PAVEMENTS	AGGREGATE SURFACED PAVEMENTS
Seed Moduli (psi)	Surfacing - 375,000 Base - 30,000 Subgrade - 14,500 Stiff Layer - 1,000,000(1) Used in Tables: 1,2,4,6,8,10 13,15,16	Pavement - 30,000 Subgrade - 14,000 Stiff Layer - 1,000,000(1) Tables: 1,3,7
Layer Thickness (in.)	Surfacing h_1 = 2.5 Base h_2 = 14.5 Subgrade h_3 = 240.0(1) Used for BISDEF in Tables: 1,2, 4,6,8,12,13,16 Surfacing h_1 = 3.0 Base h_2 = 7.0 Subgrade h_3 = Used for MODCOMP2 in Tables: 4,10,13,15	Pavement h_1 = 8.95 Subgrade h_2 = 240 Tables: 1,3,7 9,14 Pavement h_1 = 9.86 Subgrade h = infinity Tables: 5,11
Modulus Range (psi)	Surfacing - 250,000-850,000 Base - 10,000-50,000 Subgrade - 3,000-23,000 Used for BISDEF in Tables: 1,2, 4,6,8,10,13, 15,16 Not required for MODCOMP2 and SEARCH	Pavement - 1,000-100,000 Subgrade - 1,000-100,000 All BISDEF Tables
Deflection Values (mils)	Sensor No.: 1 2 3 4 43.10 26.40 17.80 9.60 Tables: 1,2,6,8, 13,16 34.60 19.80 10.10 4.50 Tables: 4,10,13,15 51.72 31.68 21.36 11.52 Table: 12	Sensor No.: 1 2 3 4 36.70 12.70 4.30 2.40 Tables: 1,3, 7,9,14

(1) Stiff layer not used in MODCOMP2 and SEARCH

RESULTS

Results of the sensitivity analysis are summarized in Tables 2–17. Table 2 presents the effect of modulus range on the predicted moduli for BISDEF for both conventional AC and aggregate-surfaced pavements. The table presents the effect of range class (*A–E*) on the backcalculated moduli and the deflection match difference. Tables 3 and 4 present the effect of the stiff layer position on the predicted moduli and deflection match difference for the BISDEF program for both AC and aggregate-surfaced pavements. The effect of initial moduli values on the backcalculated moduli is presented in Tables 5–8. Both MODCOMP2 and BISDEF were used. In these tables, the initial moduli of the pavement layers and the subgrade are varied. The backcalculated moduli are compared to moduli obtained from the standard input values and their percentage change noted.

Tables 9–13 present the effect of layer thickness on predicted moduli. The values for layer thickness in the tables are varied one at a time, and the backcalculated moduli obtained are compared to moduli obtained from standard input. For this study, all three procedures were used.

Tables 14 and 15 present the effect of variations in deflection measurement on the backcalculated moduli for all three programs. In these tables, the deflection measurements were arbitrarily increased or reduced by 5 and 10 percent from assumed correct values. The backcalculated moduli from these values were compared to the ones obtained from the assumed correct values and the percentage change in moduli was noted. This variation in deflection measurement corresponds to a situation in which the deflection sensors systematically underrecord or overrecord the deflection values.

Tables 16 and 17 present the effect of tolerances and number of iterations on the backcalculated moduli from MODCOMP2 and BISDEF procedures.

DISCUSSION OF RESULTS

The following discussion applies to the results in Tables 2–17. For the values of each variable, the results are compared to a standard. Table 1 presents the standard input values used in the analysis. Variations of input values from those shown in Table 1 are noted on the appropriate table where applicable. The choices of the values in Table 1 were based on the need to get a good match between the measured and calculated deflection basins. This matching produced some different standard structures for different procedures, although most structures were common to all procedures.

Effect of Modulus Range on Predicted Moduli

For a given pavement system, there is a combination of modulus range, initial modulus, and deflection basin that produces the best fit between the measured and calculated deflection basin (see Table 2). The best deflection match occurred at modulus ranges that were the same order of magnitude as typical moduli values of layer materials. When larger modulus ranges were input, the deflection match was not so good. However, very narrow modulus ranges appeared to result in a prediction of the upper or lower boundary deflection values because the predicted value exceeded the given range.

As shown in Figure 3, the deflection match difference for the AC pavements was below the BISDEF-specified value of 10 percent for most of the range values. This difference implies

TABLE 2 EFFECT OF RANGE ON PREDICTED MODULI AND DEFLECTION MATCHING (BISDEF)

AGGREGATE SURFACED PAVEMENT					CONVENTIONAL AC PAVEMENT			
Range Class	Pavement Layer	Modulus Range (psi)	Predicted Moduli, (psi)	Deflection Match Difference,%	Pavement Layer	Modulus Range (psi)	Predicted Moduli, (psi)	Deflection Match Difference,%
A	Pavement	1-1,000,000	30,008	23.4	Surfacing	1-1,000,000	740,474	7.3
	Subgrade	1-1,000,000	13,966		Base	1-1,000,000	17,312	
					Subgrade	1-1,000,000	4,542	
B	Pavement	1-500,000	30,008	23.4	Surfacing	1-500,000	500,000	8.2
	Subgrade	1-500,000	13,966		Base	1-50,000	20,779	
					Subgrade	1-25,000	4,401	
C	Pavement	1,000-100,000	14,200	7.0	Surfacing	250,000-750,000	750,000	5.5
	Subgrade	1,000-100,000	2,232		Base	10,000-50,000	16,428	
					Subgrade	5,000-25,000	5,000	
D	Pavement	5,000-50,000	5,000	11.8	Surfacing	1-1,000,000	693,008	7.5
	Subgrade	5,000-50,000	9,877		Base	1-100,000	18,974	
					Subgrade	1-30,000	4,445	
E	Pavement	7,500-40,000	9,500	13.0	Surfacing	300,000-1,000,000	300,000	10.3
		7,500-40,000	10,000		Base	25,000-75,000	25,000	
					Subgrade	1-30,000	5,263	

Initial Moduli (Aggregate Surfaced)
Pavement - 30,000 psi and subgrade - 14,500 psi

Initial Moduli (AC Surfaced)
Surfacing - 375,000 psi, Base - 30,000 psi, and Subgrade - 14,500 psi

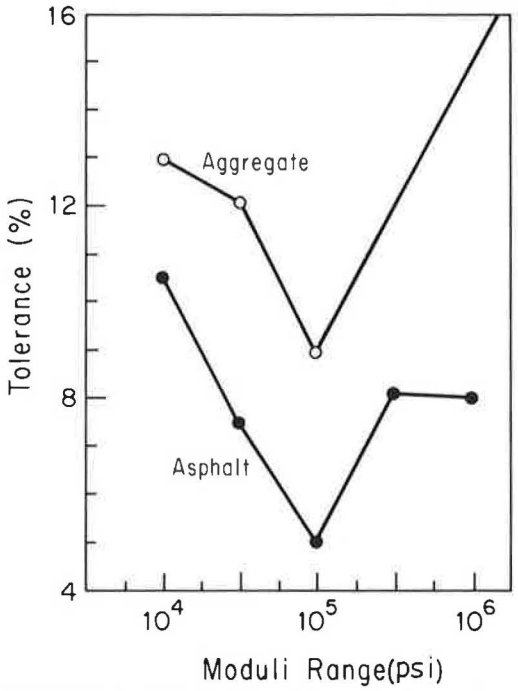

FIGURE 3 Effect of moduli range on deflection matching.

that for practical applications the modulus range does not significantly affect the values of the backcalculated moduli. For aggregate-surfaced pavements, the deflection match difference varied widely with the value of the range. Thus, the modulus range adopted can affect the predicted moduli. This range input parameter applies only for the BISDEF procedure. The range is supposed to improve the speed of convergence to a solution by limiting the range size in which the search for a modulus is to be conducted. Also, because the predicted moduli are not unique (i.e., several combinations of layer moduli can result from the same deflection basin), the range for each layer modulus serves to limit the moduli to their approximate practical values.

Effect of Depth of Stiff Layer

In the development of the BISDEF/CHEVDEF program *(2)*, use of an infinite subgrade layer tended to give larger deflections than measured values. To compensate for this effect, a rigid layer was placed in this system model at a depth of 240 in. (20 ft) below the surface. This placement resulted in a better match between computed deflections and those measured with the Road Rater 2008. In this paper, the position of the stiff layer was varied to determine its effect, if any, on the value of the predicted moduli.

Tables 3 and 4 present the results of the analysis of typical pavement structures using FWD deflection basins. For the conventional AC pavement (Table 3), the deflection match difference did not vary significantly with the depth of the stiff layer. However, the predicted moduli varied substantially from the one predicted at the standard 240-in. depth by as much as 30 percent at a depth of 90 in.

For aggregate-surfaced pavements (Table 4), this effect was more pronounced and variations in modulus of up to 69 percent were observed. Also, percent deflection match tolerances were high. The results point to the fact that there is an optimum depth for a given pavement system and deflection-measuring device stemming from the fact that the stiff layer is required to

TABLE 3 EFFECT OF STIFF LAYER DEPTH ON PREDICTED MODULI AND DEFLECTION MATCHING FOR CONVENTIONAL AC PAVEMENT (BISDEF)

	PREDICTED MODULI (psi)			DEFLECTION MATCH DIFFERENCE, %	% VARIATION IN MODULUS FROM STANDARD(2)		
Position of Stiff Layer,(in)(1)	Surfacing	Base	Subgrade		Surfacing	Base	Subgrade
5	850,000	10,000	3,000	68.8	+6.8	-38.5	-39.5
90	576,884	21,294	3,000	3.9	-27.5	+30.9	-39.5
140	661,549	19,079	4,003	5.0	-16.8	+17.3	-19.2
190	755,360	17,235	4,598	5.4	-5.0	+5.9	-7.2
240(2)	795,154	16,271	4,959	5.6	0.0	0.0	0.0
290	801,392	15,657	5,197	5.8	+0.8	-3.8	+4.8
340	850,000	15,262	5,365	5.9	+6.8	-6.6	+8.2
	850,000	13,969	6,309	6.3	+6.8	-14.1	+27

(1) Depth from the top of subgrade
(2) Standard depth

TABLE 4 EFFECT OF STIFF LAYER DEPTH ON PREDICTED MODULI AND DEFLECTION MATCHING FOR AGGREGATE-SURFACED PAVEMENT (BISDEF)

Position of (1) Stiff Layer	PREDICTED MODULI (psi)		% DEFLECTION MATCH DIFFERENCE	% VARIATION IN MODULUS FROM STANDARD(2)	
	Pavement	Subgrade		Surfacing	Base
24	100,000	7,282	38	150.0	-67.0
60	53,289	16,435	29.8	33.7	-25.6
120	44,703	19,793	13.7	12.2	-10.0
180	41,074	21,270	8.6	3.0	-3.8
200	40,372	21,584	7.6	1.3	-2.3
240(2)	39,850	22,100	6.2	0.0	0.0
300	38,336	22,560	4.8	-3.8	2.1
400	37,116	23,355	3.6	-6.9	5.7
500	34,377	25,036	6.2	-13.7	13.2

(1) Depth from the top of subgrade
(2) Standard depth

limit the depth of summation of vertical strains. If the strains are summed to infinity, the resulting calculated deflections are usually higher than the measured values. Therefore, the position of the stiff layer will vary as a function of the deflection-measuring device and type of pavement structure.

Effect of Seed Moduli

Both BISDEF and MODCOMP2 require the use of initial or seed moduli to begin the iterative process. For the BISDEF/CHEVDEF program, the seed moduli for each layer must be within the range specified for that layer. In MODCOMP2, there is no restriction as to the value of this modulus. Tables 5–8 summarize the results of this evaluation.

Overall, the value of the initial modulus had very little effect on the backcalculated moduli for the paved surface (Tables 5 and 7). When the surfacing seed modulus was doubled, only a 4 percent change in the backcalculated surface modulus occurred. The seed moduli of the surface course had no effect on the backcalculated subgrade or base moduli. Also, changes in the seed moduli of the base and subgrade had a negligible effect on the backcalculated moduli.

These observations also apply to the aggregate-surfaced pavement consisting of granular surfacing over a prepared subgrade (Tables 6 and 8). For MODCOMP2, the backcalculated modulus is relatively more sensitive to the seed moduli of the base layer (Table 5). A maximum change of 9 percent occurred in the predicted base layer moduli when the base layer seed moduli changed by 35 percent.

TABLE 5 EFFECT OF INITIAL MODULUS ON PREDICTED MODULI FOR CONVENTIONAL AC PAVEMENT (MODCOMP2)

Seed Moduli	PREDICTED MODULI (psi)			% CHANGE FROM STANDARD (1)		
	Surfacing	Base	Subgrade	Surfacing	Base	Subgrade
Surfacing						
375,000(1)	585,000	12,653	10,980	0.00	0.00	0.00
450,000	585,998	12,607	10,985	0.17	-0.36	0.05
550,000	587,358	12,544	10,993	0.40	-0.86	0.12
750,000	590,152	12,414	11,011	0.88	-1.89	0.28
850,000						
Base						
10,000	608,993	11,558	11,127	4.10	-8.60	1.34
20,000	594,712	12,205	11,038	1.66	-3.50	0.52
40,000	479,102	12,929	10,945	-1.00	2.18	-0.32
50,000	575,278	13,109	10,923	-1.66	3.60	-0.52
60,000	572,694	13,232	10,908	-2.10	4.58	-0.66
Subgrade						
5,000	577,898	13,028	10,933	-1.2	2.96	-0.43
10,000	589,587	12,441	11,007	0.78	-1.68	0.25
17,500	577,898	12,986	10,938	-1.21	2.60	-0.30
19,500	572,080	13,261	10,905	-2.21	4.80	-0.68

(1) Standard input was: Surfacing - 375,000 psi; Base - 30,000 psi; and Subgrade - 14,500 psi

TABLE 6 EFFECT OF INITIAL MODULUS ON PREDICTED MODULI FOR AGGREGATE-SURFACED PAVEMENT (MODCOMP2)

	PREDICTED MODULI (psi)		% CHANGE FROM STANDARD[1]	
Seed Moduli (psi)	Pavement	Base	Pavement	Base
Pavement				
10,000[1]	73,894	17,478	0.00	0.00
20,000	73,909	17,475	0.02	0.02
30,000	73,902	17,476	0.01	-0.01
50,000	73,895	17,478	0.00	0.00
60,000	73,893	17,478	0.00	0.00
Base				
2,500	73,840	17,488	0.07	0.06
5,000	73,877	17,481	-0.06	0.02
7,500	73,807	17,494	-0.12	0.09
9,000	73,925	17,427	0.12	0.29

(1) Standard: Pavement - 10,000 psi and Base - 1,000 psi

TABLE 7 EFFECT OF INITIAL MODULUS ON PREDICTED MODULI FOR CONVENTIONAL AC PAVEMENT (BISDEF)

	PREDICTED MODULI (psi)			% CHANGE FROM STANDARD [1]		
Seed Moduli (psi)	Surfacing	Base	Subgrade	Surfacing	Base	Subgrade
Surfacing						
375,000[1]	795,154	16,271	4,959	0.00	0.00	0.00
450,000	805,763	16,223	4,966	1.33	-0.29	0.14
550,000	818,504	16,145	4,974	2.94	-0.77	0.30
750,000	826,224	16,054	4,967	3.91	-1.33	0.16
850,000	813,661	16,164	4,963	2.33	-0.66	0.08
Base						
15,500	786,157	16,447	4,950	-1.13	1.08	-0.18
20,000	796,943	16,331	4,954	0.22	0.37	-0.10
40,000	795,622	16,261	4,962	0.06	0.06	0.06
50,000	793,051	16,349	4,953	-0.26	0.48	-0.12
Subgrade						
5,000	799,830	16,312	4,953	0.59	0.25	-0.12
10,000	792,302	16,269	4,962	-0.36	-0.01	0.06
17,500	811,143	16,194	4,960	2.00	-0.47	0.02
22,000	810,775	16,196	4,960	1.96	-0.46	0.02
25,000	809,386	16,211	4,959	1.78	-0.37	0.00

(1) Standard: Surfacing - 375,000 psi; Base - 30,000 psi; and Subgrade - 14,500 psi

TABLE 8 EFFECT OF INITIAL MODULUS VALUE ON PREDICTED MODULI FOR AGGREGATE-SURFACED PAVEMENT (BISDEF)

	PREDICTED MODULI (psi)		% CHANGE FROM STANDARD[1]	
Seed Moduli (psi)	Pavement	Subgrade	Pavement	Subgrade
Pavement				
10,000	14,390	12,217	0.64	0.30
20,000	14,455	12,198	1.09	0.14
30,000[1]	14,299	12,180	0.00	0.00
40,000	14,462	12,194	1.14	0.14
50,000	14,469	12,190	1.19	0.08
Subgrade				
5,000	14,423	12,221	0.88	0.34
10,000	14,469	12,181	1.19	0.00
15,000	14,456	12,197	1.09	0.13
25,000	14,453	12,200	1.08	0.16

Standard: Pavement - 30,000 psi and Subgrade - 14,000 psi

TABLE 9 EFFECT OF LAYER THICKNESS ON PREDICTED MODULI FOR CONVENTIONAL AC PAVEMENT (BISDEF)

	PREDICTED MODULI (PSI)			% CHANGE FROM STANDARD (1)		
Layer Thickness,in.	Surfacing	Base	Subgrade	Surfacing	Base	Subgrade
Surfacing h_1						
1.5	850,000	25,541	4,627	6.9	56.9	-6.7
2.5(1)	795,154	16,271	4,959	0.0	0.0	0.0
3.5	349,372	14,615	5,017	-56.0	-67.1	1.2
4.5	250,000	11,327	5,173	-68.5	-30.4	4.3
5.5	250,000	10,000	4,897	-68.6	-38.5	-1.2
Base h_2						
12.5	693,124	19,199	5,020	-12.8	17.9	1.2
13.5	753,543	17,542	4,988	-5.2	7.8	0.6
14.5(1)	795,154	16,271	4,959	0.0	0.0	0.0
15.5	835,328	15,286	4,927	5.1	-6.1	0.6
16.5	850,000	14,662	4,880	6.9	-9.9	1.6

(1) Standard structure: Surfacing h_1 = 2.5 in. and Base h_2 = 14.5 in.

Effect of Layer Thickness

For all three procedures, pavement layer thickness has to be input, either from the construction data or from cores taken from the pavement. As shown in Tables 9–13, the predicted moduli are sensitive to the variation in thickness of both the surface and base layers. For a conventional AC pavement, the BISDEF-predicted surface and base moduli are very sensitive to the input thickness of the surface layer (Table 9). One inch of change in the surface layer thickness resulted in a change of over 60 percent in the value of the predicted surface modulus and a 60 percent change in the predicted base modulus. The base layer thickness does not have as much effect on the predicted modulus, as only an 18 percent change in predicted modulus occurred for a 2-in. change in the base thickness. The thickness of the layers had little effect on the predicted subgrade modulus. The observed change in predicted subgrade modulus was a maximum of about 7 percent for all the thickness changes considered. As presented in Table 10, the layer thicknesses have little effect on the predicted moduli of the aggregate-surfaced pavement.

For MODCOMP2, the predicted moduli are more sensitive to the input thickness than for BISDEF (Table 11). Both the surface and base moduli are very sensitive to the input surface and base layer thicknesses. The predicted subgrade modulus is also fairly sensitive when compared to the BISDEF-predicted value. For the aggregate-surfaced pavement, the same observations were noted (Table 12).

The predicted moduli from the SEARCH program are also sensitive to the surface and base thicknesses (Table 13). The moduli predicted by SEARCH for the base and subgrade are more sensitive to the surfacing than the base thickness.

Effect of Variations in Deflection Measurements

Tables 14 and 15 present the effect of the accuracy in deflection measurements. In these tables, variation magnitudes of +5 and

TABLE 10 EFFECT OF LAYER THICKNESS ON PREDICTED MODULI FOR AGGREGATE-SURFACED PAVEMENT (BISDEF)

	PREDICTED MODULI (psi)		% DIFFERENCE FROM STANDARD (1)	
Layer Thickness,in	Pavement	Subgrade	Pavement	Subgrade
Base (ho)				
6.95	15,425	11,908	7.92	-2.22
7.95	14,858	12,050	3.93	-1.13
8.00	14,838	12,050	3.74	-1.12
8.50	14,572	12,139	1.92	-0.33
8.95(1)	14,299	12,180	0.00	0.00
9.00	14,441	12,203	0.90	0.20
9.50	14,287	12,276	-0.08	0.80
9.95	14,162	12,344	-0.96	1.30
10.95	13,934	12,493	-2.51	2.60

(1) Standard structure h_o = 8.95 in.

TABLE 11 EFFECT OF LAYER THICKNESS ON PREDICTED MODULI FOR CONVENTIONAL AC PAVEMENT (MODCOMP2)

	PREDICTED MODULI (psi)			% CHANGE FROM STANDARD (1)		
Layer Thickness,in	Surfacing	Base	Subgrade	Surfacing	Base	Subgrade
Surfacing h_1						
2.5	540,790	28,882	9,747	-7.56	128.26	-11.23
3.0(1)	585,000	12,653	10,980	0.00	0.00	0.0
3.5	399,750	11,433	11,043	-31.66	-9.64	0.57
4.5	224,551	9,581	11,117	-61.62	-24.28	1.25
5.0	180,570	8,793	11,144	-69.13	-30.51	1.49
6.0	131,907	6,788	11,358	-77.45	-46.35	3.44
Base h_2						
6.0	469,616	20,176	10,383	-19.72	59.46	-5.44
6.5	470,979	19,525	10,325	-19.49	54.31	-5.96
7.0(1)	585,000	12,653	10,980	0.00	0.00	0.00
7.5	580,544	12,799	10,932	-0.76	1.15	-0.44
8.0	571,670	13,129	10,852	-2.27	3.76	-1.16
14.0	539,842	13,596	10,273	-7.72	7.45	-6.44

(1) Standard structure: Surfacing h_1 = 3.0 in. and Base h_2 = 7.0 in.

TABLE 12 EFFECT OF LAYER THICKNESS ON PREDICTED MODULI FOR AGGREGATE-SURFACED PAVEMENT (MODCOMP2)

	PREDICTED MODULI (psi)		% DIFFERENCE FROM STANDARD (1)	
Layer Thickness,in	Pavement	Subgrade	Pavement	Subgrade
Pavement h_o				
7.86	88,521	18,566	19.79	6.22
8.86	79,668	18,033	7.81	3.18
9.86(1)	73,894	17,478	0.00	0.00
6.86	103,091	19,062	39.51	9.06

(1) Standard Structure h_o = 9.86 in.

TABLE 13 EFFECT OF LAYER THICKNESS ON PREDICTED MODULI FOR CONVENTIONAL AC PAVEMENT (SEARCH)

	PREDICTED MODULI (psi)			% CHANGE FROM STANDARD (1)		
Layer Thickness,in	Surfacing	Base	Subgrade	Surfacing	Base	Subgrade
Surfacing h_1						
2.5(1)	610,700	7,000	7,000	0.0	0.0	0.0
3.0	317,300	7,000	7,000	-48.0	0.0	0.0
3.5	425,300	5,400	6,100	-30.4	-22.8	-12.8
4.0	280,300	5,500	5,900	-54.1	-21.4	-15.7
4.5	508,500	2,100	9,400	-16.7	-70.0	34.4
5.0	371,700	1,900	9,900	-39.1	-72.8	41.4
6.0	290,900	700	18,700	-52.4	-90.0	167.1
Base h_2						
9.0	1,051,900	8,600	6,300	72.2	22.8	-10.0
12.0	612,700	7,000	7,000	0.3	0.0	0.0
14.5(1)	610,700	7,000	7,000	0.0	0.0	0.0
16.0	827,300	6,400	6,400	35.5	-8.5	-8.5
18.0	923,300	6,200	6,200	51.2	-11.4	-11.4
20.0	1,030,900	6,000	6,100	68.8	-14.3	-12.8

(1) Standard structure: Surfacing h_1 = 2.5 in. and Base h_2 = 14.5 in.

TABLE 14 EFFECT OF FWD DEFLECTION MEASUREMENTS VARIATIONS ON PREDICTED MODULI FOR CONVENTIONAL AC PAVEMENT

Procedure Used	Average Variation in Deflection Measurement, %	Deflection Values ($x10^{-3}$) in.				PREDICTED MODULI (psi)			% CHANGE IN MODULI		
		1	2	3	4	Surfacing	Base	Subgrade	Surfacing	Base	Subgrade
MODCOMP2	0	34.60	19.80	10.10	4.50	585,000	12,653	10,980	0.0	0.0	0.0
	+5	36.30	20.79	10.61	4.73	556,408	12,187	10,437	-4.8	-3.7	-4.9
	+10	38.10	21.78	11.11	4.95	525,329	11,683	9,961	-10.2	-7.8	-9.2
	-5	32.87	18.81	9.60	4.28	521,401	14,922	11,895	-10.9	17.9	8.3
	-10	31.14	17.82	9.09	4.05	654,726	13,840	12.228	11.9	9.3	11.4
BISDEF	0	43.10	26.40	17.80	9.60	795,235	16,271	4,959	0.0	0.0	0.0
	+5	45.25	27.72	18.69	10.08	772,506	15,362	4,731	-2.9	-5.6	-4.6
	+10	47.41	29.04	19.58	10.56	747,693	14,631	4,513	-5.9	-10.1	-8.9
	-5	40.95	25.08	16.91	9.02	850,000	17,233	5,239	6.9	5.9	5.6
	-10	38.79	23.76	16.02	8.64	850,000	18,445	5,491	6.9	13.4	10.7
SEARCH	0	43.10	26.40	17.80	9.60	1,313,300	6,900	7,300	0.0	0.0	0.0
	+5	45.25	27.72	18.69	10.08	1,120,200	7,000	7,000	-14.7	1.5	-4.1
	+10	47.41	29.04	19.58	10.56	945,500	6,900	6,900	-28.0	0.0	-5.5
	-5	40.95	25.08	16.91	9.02	1,475,000	7,000	7,900	12.3	1.4	8.2
	-10	38.79	23.76	16.02	8.64	1,903,100	6,400	8,800	44.9	-7.3	20.5

TABLE 15 EFFECT OF FWD DEFLECTION MEASUREMENTS VARIATIONS ON PREDICTED MODULI FOR AGGREGATE-SURFACED PAVEMENTS

Procedure Used	Av. Variation in Deflection Measurement,%	DEFLECTION VALUES ($\times 10^{-3}$) in. 1	2	3	4	PREDICTED MODULI (psi) Pavement	Subgrade	% CHANGE IN MODULI Pavement	Subgrade
BISDEF	0	36.70	12.70	4.30	2.40	25,243	15,757	0.0	0.0
	+5	38.54	13.34	4.52	2.52	24,090	14,992	-4.6	-4.9
	+10	40.37	13.97	4.73	2.77	22,918	14,232	-9.2	-9.7
	-5	34.87	12.07	4.09	2.28	26,535	16,586	5.1	5.3
	-10	33.03	11.43	3.87	2.16	27,961	17,525	10.8	11.2
MODCOMP2	0	36.70	12.70	4.30	2.40	27,291	15,681	0.0	0.0
	+5	38.54	13.34	4.52	2.52	26,051	14,928	-4.5	-4.8
	+10	40.37	13.97	4.73	2.77	24,815	14,254	-9.0	-9.1
	-5	34.87	12.07	4.09	2.28	28,731	16,499	5.3	5.2
	-10	33.03	11.43	3.87	2.16	30,326	17,422	10.0	11.10

+10 percent have been applied to a set of known deflection measurements and the predicted moduli obtained from all three programs. All programs are sensitive to the variations in deflection measurements. The backcalculated surfacing layer moduli using MODCOMP2 and SEARCH show more sensitivity to these variations than the base or subgrade layer moduli, whereas for BISDEF all three backcalculated moduli are equally sensitive.

Effect of Tolerance and Number of Iterations

Table 16 presents the effect of tolerance and number of iterations on the backcalculated moduli. For MODCOMP2, the backcalculated modulus is insensitive to percentage deflection tolerance of less than 0.20 percent. For tolerance levels greater than 5 percent, the predicted modulus changes rapidly with higher values of tolerances. In the case of BISDEF (Table 17), the backcalculated modulus is insensitive to the tolerance level and number of iterations. The backcalculated modulus is insensitive to tolerance level above 5 percent, if the standard three iterations are used. Values of number of iterations greater than two do not have any effect on the backcalculated moduli.

IMPLICATIONS OF FINDINGS

The findings from this study show that the three backcalculation procedures have a number of limitations. The most important is that the predicted modulus is very sensitive to the user-supplied inputs. Some of these inputs cannot be physically measured (e.g., depth of stiff layer and initial moduli). To arrive at a reasonable solution from these procedures, one has to be aware of these limitations and develop methods for dealing with them.

Even with identical input values, the predicted moduli from the three programs are very different. Differences between BISDEF- and MODCOMP2-predicted values occur because BISDEF uses a standard depth to a rigid layer of 240 in. MODCOMP2 does not use such a layer and therefore the vertical strains are summed to infinity. Although not included in the standard input and not investigated in this paper, MOD-

TABLE 16 EFFECT OF TOLERANCES AND NUMBER OF ITERATIONS ON PREDICTED MODULI FOR CONVENTIONAL AC PAVEMENT (MODCOMP2)

	PREDICTED MODULI (psi)			% CHANGE FROM STANDARD (1)		
Tolerance %	Surfacing	Base	Subgrade	Surfacing	Base	Subgrade
0.05	585,000	12,653	10,980	0.00	0.00	0.00
0.15(1)	585,000	12,653	10,980	0.00	0.00	0.00
0.20	585,000	12,653	10,980	0.00	0.00	0.00
5	344,610	26,682	9,771	-41.00	110.00	-11.00
10	344,610	26,682	9,771	-41.00	110.00	-11.00
15	344,610	26,682	9,771	-41.00	110.00	-11.00
No. of Iterations						
5	518,589	15,905	10,622	-11.35	25.70	-3.26
10(1)	585,000	12,653	10,980	0.00	0.00	0.00
15	608,436	11,583	11,124	4.01	-8.46	1.31
20	608,436	11,583	11,124	4.01	-8.46	1.31

(1) Standard: Tolerance = 0.15% and No. of Iterations = 10

TABLE 17 EFFECT OF TOLERANCES AND NUMBER OF ITERATIONS ON PREDICTED MODULI FOR CONVENTIONAL AC PAVEMENT (BISDEF)

	PREDICTED MODULI (psi)			% CHANGE FROM STANDARD (1)		
Tolerance %	Surfacing	Base	Subgrade	Surfacing	Base	Subgrade
0.5	811,263	16,193	4,960	2.00	-0.48	0.02
2.5	811,263	16,193	4,960	2.00	-0.48	0.02
5.0	811,263	16,193	4,960	2.00	-0.48	0.02
10(1)	795,235	16,271	4,959	0.00	0.00	0.00
12.5	795,235	16,271	4,959	0.00	0.00	0.00
15.0	795,235	16,271	4,959	0.00	0.00	0.00
20.0	795,235	16,271	4,959	0.00	0.00	0.00
No. of Iterations						
1	850,000	17,283	5,440	6.89	6.22	9.70
2	795,235	16,271	4,959	0.00	0.00	0.00
3(1)	795,235	16,271	4,959	0.00	0.00	0.00
8	795,235	16,271	4,959	0.00	0.00	0.00
12	795,235	16,271	4,959	0.00	0.00	0.00
18	795,235	16,271	4,959	0.00	0.00	0.00
20	795,235	16,271	4,959	0.00	0.00	0.00

(1) Standard: Tolerance = 10% and No. of Iterations = 3

COMP2 can be used with a rigid layer at an appropriate depth in a manner similar to that of BISDEF. The difference between SEARCH and the other two programs is probably due to the differences in stress distribution between the Vlasov and Leont'ev *(8)* equation and the elastic layer programs used in BISDEF and MODCOMP2. The speed of computation using these programs depends on the hardware support available, but, on a relative scale, SEARCH is the fastest, followed by MODCOMP2 and BISDEF at about the same speed.

One major weakness of the programs used in this analysis is their inability to consider the stress sensitivity of the modulus in any given layer. Although MODCOMP2 has the capability to consider the stress sensitivity of the granular and subgrade layer, this option was not used because of the lack of sufficient data. If the variations in moduli and stress were taken into account, there would be no need to adopt a fictitious rigid layer.

Another major weakness is that the moduli determined with these procedures, indeed with most curve-fitting procedures, are never unique; there are several combinations of layer moduli that can result from the same deflection basin. This problem has been addressed by some researchers *(1)* by using regression equations to determine the seed moduli. However, such approaches are still based on locally developed relationships that cannot be used with confidence outside the area for which they were calibrated.

In general, the results clearly show the problems that might be encountered in attempting to use most of the backcalculation procedures available. A general guideline is that, before adopting any procedures for production or detailed analysis, a sensitivity study should be carried out. This study should look at all user-supplied input data, especially those that cannot be physically measured.

CONCLUSIONS AND RECOMMENDATIONS

The evaluations conducted in this study revealed the following:

1. The range of moduli used as input in BISDEF affects the accuracy of matching the measured and calculated deflection basins.
2. The predicted AC surface modulus by the BISDEF program is sensitive to the depth of the stiff layer and the surfacing and base thicknesses.
3. The predicted base modulus using BISDEF is sensitive to the depth of the stiff layer as well as the layer thicknesses of the surfacing and base layers.
4. The predicted subgrade modulus using BISDEF for the conventional AC pavement is only sensitive to the depth of the stiff layer. For the MODCOMP2 procedure, the predicted subgrade modulus is sensitive only to tolerance and number of iterations.
5. Using BISDEF, the predicted pavement and subgrade moduli for the aggregate-surfaced pavement are highly sensitive only to the depth of the stiff layer. For the same pavement type, the MODCOMP2-predicted modulus is sensitive only to the pavement layer thicknesses.
6. For the two programs requiring them as input, the seed moduli have no significant effect on the backcalculated moduli.
7. The backcalculated AC surfacing modulus using MODCOMP2 is very sensitive to the thickness of the surface and base layers. It is also sensitive to the input percent tolerance.
8. The predicted moduli for all pavement layers using SEARCH are sensitive to the thickness of the pavement layers.
9. The computer program SEARCH requires the least amount of user-supplied inputs and uses the least amount of computer time.

Based on the findings, the following recommendations appear warranted:

1. For all three backcalculation procedures, special attention should be paid to the determination of the pavement layer thicknesses. If possible, a number of cores should be taken at each site to determine the pavement layer thicknesses.
2. When using BISDEF, calibrations should be carried out using typical deflection basins to determine the depth of the stiff layer that gives the smallest deflection match differences. Further, the range of layer moduli used should be as close as possible to the actual modulus range found in practice for the material under consideration.

3. When using MODCOMP2, attention should be paid to deflection match tolerance, which should be kept at or below the suggested value of 0.15 percent.

4. For all three programs, attention should be paid to the variations in surface deflection measurement.

REFERENCES

1. W. Uddin. *A Structural Evaluation Methodology for Pavements Based on Dynamic Deflections.* Ph.D. dissertation, The University of Texas at Austin, Dec. 1984.
2. A. J. Bush III. *Non-Destructive Testing for Light Aircraft Pavements, Phase II, Development of Nondestructive Evaluation Methodology.* Final Report FAA-RD-80-9-II. FAA, U.S. Department of Transportation, Nov. 1980.
3. L. H. Irwin. *User's Guide to MODCOMP2,* Version 2.1. Local Roads Program, Cornell University, Ithaca, N.Y., Nov. 1983.
4. R. L. Lytton and C. H. Michalak. *Flexible Pavement Deflection Using Elastic Moduli and Field Measurements.* Research Report 207-7F. Texas Transportation Institute, Texas A&M University, College Station, Aug. 1979.
5. A. J. Bush and D. R. Alexander. Pavement Evaluation Using Deflection Basin Measurement and Layered Theory. In *Transportation Research Record 1022,* TRB, National Research Council, Washington, D.C., 1985, pp. 16–29.
6. *BISAR Users Manual: Layered System Under Normal and Tangential Loads.* Koninklijke-Shell Laboratorium, Amsterdam, Holland, 1972.
7. J. Michelow. *Analysis of Stresses and Displacement in an N-Layered Elastic System Under a Load Uniformally Distributed Over a Circular Area.* California Research Corporation, Calif., 1963.
8. V. Z. Vlasov and N. N. Leont'ev. *Beams, Plates and Shells on Elastic Foundation.* Translated from Russian, Israel Program for Scientific Translations, Jerusalem, 1966.
9. N. Odemark. *Investigations as to the Elastic Properties of Soils and Design of Pavements According to the Theory of Elasticity.* Staten Vaeginstitut, Stockholm, Sweden, 1949.
10. O. Tholen. *Falling Weight Deflectometer, A Device for Bearing Capacity Measurements: Properties and Performance.* Department of Highway Engineering, Royal Institute of Technology, Stockholm, Sweden, 1980.
11. O. Tholen, J. Sharma, and R. Terrel. Comparison of Falling Weight Deflectometer with Other Deflection Testing Devices. In *Transportation Research Record 1007,* TRB, National Research Council, Washington, D.C., 1985, pp. 20–26.
12. T. Rwebangira, R. G. Hicks, and M. Truebe. *Determination of Pavement Layer Structural Properties for Aggregate Surfaced Roads.* Paper prepared for the 4th International Conference on Low-Volume Roads, Cornell University, Ithaca, N.Y., 1987.

Publication of this paper sponsored by Committee on Strength and Deformation Characteristics of Pavement Sections.

Performance of a Full-Scale Pavement Design Experiment in Jamaica

J. ROLT, S. G. WILLIAMS, C. R. JONES, AND H. R. SMITH

The design, construction, and first 4 years' performance of seven experimental sections of road built on the May-Pen bypass in Jamaica are described. The road sections comprise varying pavement thicknesses of cement-stabilized and unstabilized marly limestones on a relatively weak, imported, clay subgrade having an in situ California bearing ratio (CBR) of 6 percent overlying a granular drainage blanket. One section has a full-depth pavement of locally available river shingle mechanically stabilized with limestone fines. The sections have a common surfacing of 50 mm of asphalt concrete. Traffic to date has been 3.0 million standard axles in one direction and 0.6 million in the other, with an average unidirectional flow of 1,300 vehicles/day. To date the primary mode of failure for the sections with unstabilized limestone bases has been deformation in the wheel tracks (rutting) with no associated cracking. The degree of rutting was revealed to be well correlated with early-life deflection, indicating a traditional mode of failure dependent on vertical stresses and compressive strains throughout the pavement. A rut depth progression model was developed that predicts rutting in terms of deflection and cumulative traffic. The model agrees closely with deflection criteria curves developed in the United Kingdom for roads having naturally cementing roadbases. After 4 years, about 10 percent of the road pavement (unstabilized bases only) reached a failure condition corresponding to a rut depth of 15 mm. From layer thicknesses, strength distributions, and the deflection performance model, it was possible to predict the performance of the thicker sections of road pavement. At the end of the study, the road was performing well in comparison with expectations from appropriate design charts but the predictions indicated that the relationship between overall thickness and traffic-carrying capacity was somewhat steeper than those of the design charts and therefore the thicker sections of road might not perform as well, relatively, as the thinner sections. The sections with cement-stabilized limestone and mechanically stabilized river shingle all performed better (showing no significant deformation) than the unstabilized limestone bases.

In Jamaica, shortages of high-quality stone have meant that marly limestones have been used for roadbases. These materials are variable in quality and are usually chemically stabilized with cement. However, in view of the traffic loadings experienced by the roads it was believed that by suitable thickness design and material selection some of the limestones ought to make satisfactory roadbases without being stabilized. To demonstrate this ability, the Ministry of Construction and the Overseas Unit TRRL agreed to cooperate on the construction and evaluation of a full-scale pavement design experiment to compare the performance of various stabilized and unstabilized marly limestones in roadbases.

J. Rolt, C.TR. Jones, and H. R. Smith, Overseas Unit, Transport and Road Research Laboratory, Crowthorne, Berkshire RG11 6AU, United Kingdom. S. G. Williams, Ministry of Construction, Jamaica.

There are some areas of Jamaica where marly limestone is not readily available. River shingle is potentially an alternative material for use in roadbases provided it can be mechanically stabilized by adding the correct quantity of finer-graded material. Crushed marl ranging in size from 5 mm down to dust is suitable for this purpose, and therefore a base comprising mechanically stabilized river shingle was included in the experiment.

The properties of the materials, the design of the experiment, and an evaluation of the test sections after 4 years' traffic, during which the traffic reached 0.6 million standard axles in one direction and 2.9 million in the other, are described herein.

DESIGN OF THE EXPERIMENT

The experimental sections were constructed as part of the May-Pen bypass situated about 60 km west of Kingston. The original experiment consisted of eight test sections, each 91 m (300 ft) long, separated by nonexperimental transitions of 30 m (100 ft) between sections. The first section was subsequently abandoned because of the unusual traffic patterns arising from the proximity of a junction.

The primary purpose of the experiment was to compare the performance of different types and thicknesses of roadbase. The design of the experiment allowed the following aspects of performance to be studied.

1. The relative performance of different thicknesses of good-quality marly limestone roadbase.
2. A comparison between a roadbase of poor-quality marly limestone stabilized with cement and a good-quality unstabilized limestone of similar thickness.
3. A comparison between a full-depth pavement of river shingle mechanically stabilized with fine-graded limestone and the same total thickness of conventional pavement comprising a base of good-quality limestone and a subbase of lower quality.
4. Comparisons between conventional designs using different qualities of roadbase and subbase materials.

A cross section of the experiment showing the thicknesses of layers and material types is shown in Figure 1.

MATERIALS

Classification and strength tests on all the materials taken from the road after compaction are presented in Table 1; the mean particle size distribution of the materials is shown in Figure 2.

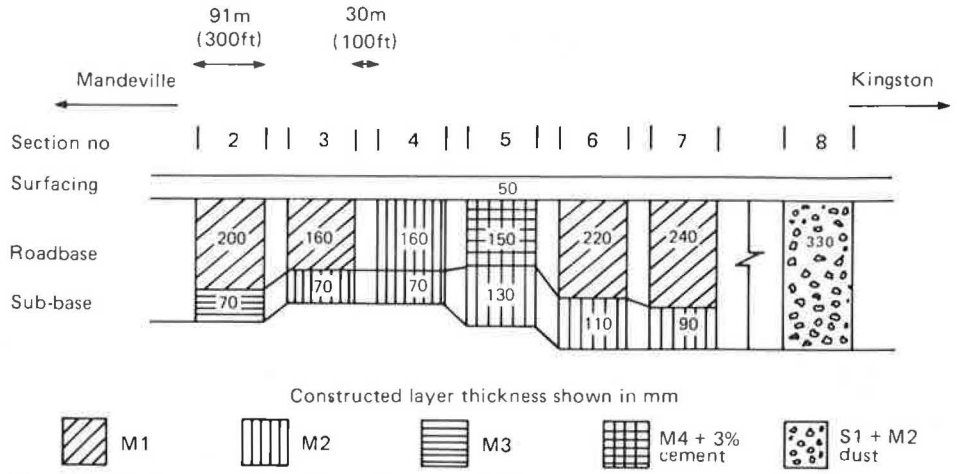

FIGURE 1 Cross section of experiment as built.

Limestone M1 is within Jamaican specifications for roadbases but M2 has a higher plasticity and is too fine to comply with the specifications. The strength of the stabilized limestone M4 exceeded the specifications in Road Note 31 *(1)*. The blended river shingle and crushed limestone used in Section 8 is well graded and nonplastic. The CBR value of this material is lower than that of the corresponding pure limestone used as roadbase on other test sections.

To ensure a uniform and relatively weak subgrade condition, a clay was imported and laid to a minimum thickness of 520 mm (20.5 in.) over a 150-mm (6.0-in.) drainage blanket. The material properties of the clay are shown in Figure 3.

CONSTRUCTION

Field compaction trials indicated that a 14-tonne smooth-wheeled roller was adequate for all base materials. During construction, a day density of 100 percent of the maximum dry density obtained in the modified AASHO compaction test was

TABLE 1 MATERIAL PROPERTIES (LABORATORY TESTS)

MATERIAL	MODIFIED AGGREGATE IMPACT VALUE[1]		LL	PI	LABORATORY COMPACTION AND CBR TESTS BS 1377 : 1975 4.5 kg RAMMER					UNCONFINED COMPRESSIVE STRENGTH[2]
	DRY	WET	%	%	MDD Mg/m³ (lb/ft³)	OMC %	CBR @ OMC %	SOAKED CBR(4 day) %	SWELL @ OMC %	N/mm² (lbf/in²)
M1	35	40	Non-plastic		2.01 (125.5)	10.0	125	100	NIL	-
M2	36	36	27	12	1.98 (123.5)	9.5	140	-	-	-
M3	41	47	21	5	1.96 (122.2)	11.2	48	26	NIL	-
M4	24	-	41	27	2.01 (125.8)	9.9	-	15	2.3	-
M4 + 3% cement			-	-	2.01 (125.9)	7.6	300	270	0.11	1.79 (260)
S1 + M2 dust	18	23	Non plastic		2.16 (135.0)	9.1	62	44	NIL	
Jamaican specification (roadbase)			25	6	-	-	-	80	0.3[3]	
Jamaican specification (subbase)			30	15	-	-	-	30	1.0[3]	

1. Tests carried out on aggregate passing 14mm and retained on 10mm
2. Tests on 150mm (6in) cube
3. BS 1377 : 1975 2.5 kg rammer

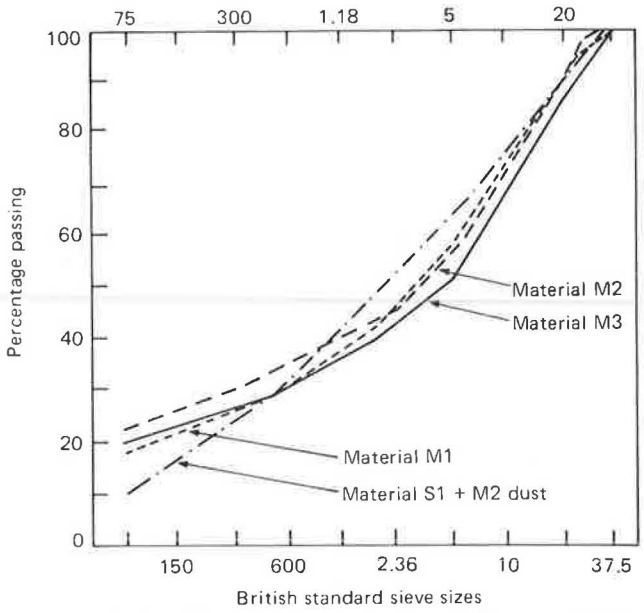

FIGURE 2 Particle size distribution in roadbase materials.

achieved with small standard deviations. The subgrade was compacted to 95 percent of the maximum dry density obtained in the British Standard compaction test (using the 1975 2.5-kg rammer method) *(2)*.

The specifications for the asphalt concrete (AC) surfacing and the results of testing during construction are shown in Figure 4, in which it appears that quality control was good. That air voids were low is notable.

Layer thicknesses, in situ strengths of all layers, and variability in these values for each test section are discussed. The road was completed and opened to traffic by April 1981.

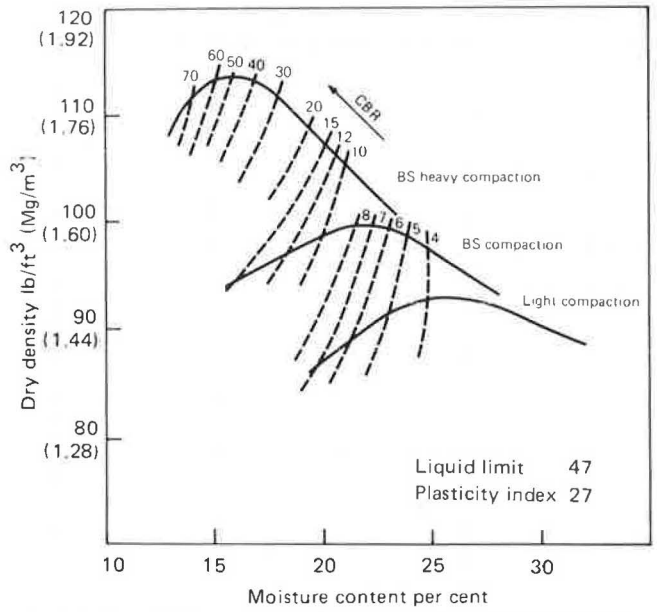

FIGURE 3 CBR-density-moisture content relationship for clay subgrade.

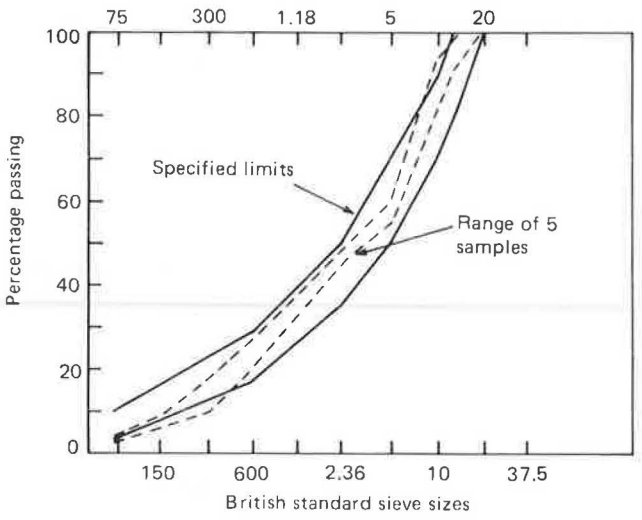

Specification		Measured range
Bitumen content, %	4.5 –7.0	5.8 – 6.3
VMA, %	14 max	13.0 – 13.7
Air voids, %	2 – 5	2.5 –3.4
Stability, kN	>4.45	7.4 – 11.1
lbs	>1000	1650 – 2480
Flow, mm	2.0 – 4.6	2.5 –3.3
1/100ins	8 –18	10 – 13

FIGURE 4 Specification and results for asphalt concrete.

Traffic

The undirectional ADT since construction has been constant at approximately 1,300 vehicles/day; total commercial traffic reached 400,000 by June 1985.

Table 2 presents the percentage flow and average equiv-

TABLE 2 SUMMARY OF CLASSIFIED COUNTS AND AXLE LOAD SURVEYS FOR COMMERCIAL VEHICLES

AXLE CONFIGURATION	TOWARDS KINGSTON		TOWARDS MANDEVILLE	
	PER CENT	EF	PER CENT	EF
1.2	61	0.92	65	6.81
1.22	30	1.97	25	7.40
1.2 - 22	1	3.32	1	5.13
1.22 - 22	8	0.99	9	7.94

PER CENT = Per cent flow of the total number of commercial vehicles
EF = Equivalence factor per vehicle

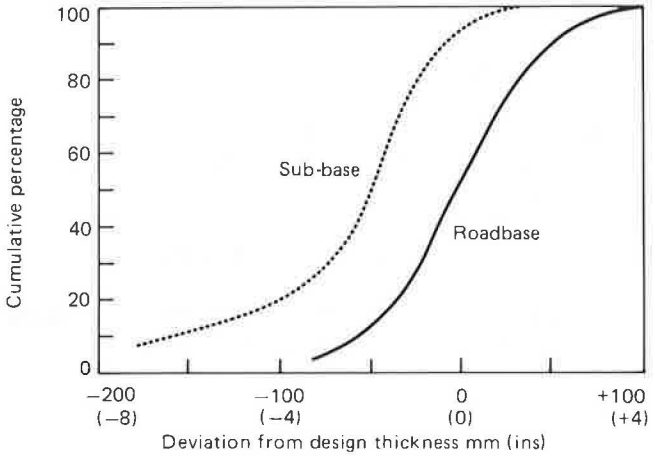

FIGURE 5 Distribution of roadbase and subbase thicknesses.

alence factor for each type of commercial vehicle for each direction. The majority of vehicles traveling toward Mandeville is heavily loaded, whereas the majority of vehicles traveling in the opposite direction is empty or only partially loaded. By June 1986, the cumulative traffic loading since construction reached 0.6 million standard axles toward Kingston and 2.9 million toward Mandeville.

PAVEMENT INVESTIGATIONS

In 1982 and in 1983, subsurface investigations were carried out by digging test pits. Between 1983 and 1985, a total of 72 nondestructive tests were performed using the dynamic cone penetrometer (DCP) to measure layer thicknesses and in situ strengths to a depth of 800 mm *(3)*.

Thickness of Pavement Layers

Although the mean thicknesses of the roadbases were revealed to be close to the design values, there was a shortfall in the thickness of subbase for Sections 2–6; in particular, Sections 4, 5, and 6 were especially thin relative to the design, having thicknesses of 73, 130, and 110 mm, respectively, instead of 200 mm. Of equal importance for the analysis of performance is the variability of thicknesses within sections. Cumulative frequency distributions are shown in Figure 5. The median roadbase thickness equals the design value, but 10 percent of the pavement has a roadbase thickness of 60 mm (2.4 in.) less. The median thickness of subbase is about 50 mm (2 in.) below the original design value, and 10 percent of the pavement has a subbase thickness 150 mm (6 in.) less than the design. If the variability of the subbase is translated into expected life, other things being equal, the lesser thickness implies that 95 percent of the pavement will fail before reaching its expected design life and 10 percent of the pavement could fail before reaching 10 percent of its design life. Variability of this magnitude often occurs for granular layers laid with a grader; it needs to be taken into account explicitly in any structural design method.

In Situ Strength of the Pavement Materials

The in situ strengths of the pavement materials as measured by the DCP are summarized in Table 3.

The minimum CBR values suggested by Road Note 31 *(1)* of 80 and 25 percent for roadbase and subbase, respectively, are soaked values, and therefore some of the in situ readings correspond to material that is weaker than specified, especially for Limestone M2 and the cement-stabilized material M4. The lower CBR value of 53 percent for M2 when used as a subbase material is a result of the lower densities.

The cement-stabilized roadbase used in Section 5 shows a particularly high variability in strength and, although the section appears to be performing well, the test pit results indicate poor mixing of the stabilizer during construction.

Laboratory investigations in 1983 indicated that there was no measurable breakdown of any of the limestones during the first 2 years of traffic.

Strength of the Clay Subgrade

Control testing for density during construction showed that the mean dry density was 96 percent of the maximum dry density achieved in the BS standard compaction test with a relatively

TABLE 3 IN SITU CBR VALUES (DCP METHOD) OF THE PAVEMENT LAYERS

MATERIAL	ROADBASE				SUBBASE			
	NO OF TESTS	$\bar{x}$	SD	RANGE	NO OF TESTS	$\bar{x}$	SD	RANGE
M1	18	119	22.1	88–150	NOT USED			
M2	5	107	34.6	67–150	21	53	18.0	27–99
M3	NOT USED				6	41	13.5	25–62
M4 + 3% Cement	5	103	55.3	33–150	NOT USED			
S1 + M2 Dust	6	97	9.1	80–105	NOT USED			

small standard deviation. Samples of clay subgrade obtained in 1982 had a mean moisture content of 20.3 percent with a standard deviation of 3.1 percent. Results of the in situ strength tests using the DCP showed that the subgrade had a mean CBR value of 9.1 percent in 1983. Using the CBR-density-moisture content relationship (Figure 3), the in situ CBR results at the given field density corresponded to a mean moisture content of 20.2 percent with a standard deviation of 1.4 percent, indicating no change from 1982 and confirming that equilibrium conditions were reached.

The DCP results were analyzed by section. At least five results available for each section showed that the subgrade along the site was particularly uniform with no significant differences at the 5 percent level between any sections. However, there was some indication at the 10 percent level that the subgrade of Section 3 was weaker than that of Section 4, Section 3 being the weakest and Section 4 the strongest along the site, mean CBR values being 7.9 and 9.5 percent, respectively. The distribution of in situ CBR values for the complete site is shown in Figure 6. The overall median value is 8.2 percent; 90 percent of the values are greater than 6.2 percent.

Structural Number

The structural number (SN) is a useful method of comparing the overall structural thickness of similar types of road. Using the thickness and strengths from the DCP tests, the SN has been calculated using the following strength coefficients *(4)*.

1. Surfacing:

$a_1 = 0.4$

2. Granular roadbase:

$$a_2 = [29.14\,(\text{CBR}) - 0.1977(\text{CBR})^2 + 0.00045(\text{CBR})^3] \times 10^{-4}$$

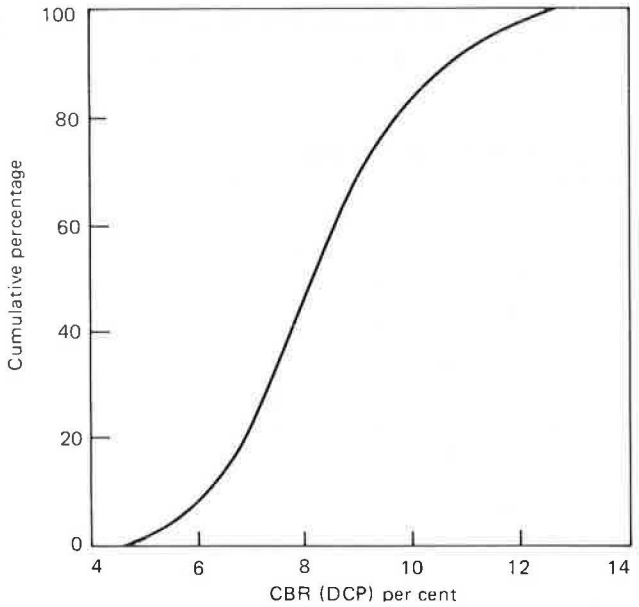

FIGURE 6 Distribution of subgrade strength.

3. Subbase:

$a_3 = 0.01 + 0.065(\log_{10}\text{CBR})$

The contribution that the subgrade makes towards the overall pavement strength is taken into account by calculating the modified structural number (SN_1) using the following equation.

$$SN_1 = SN + 3.51(\log_{10}\text{CBR}) - 0.85(\log_{10}\text{CBR})^2 - 1.43$$

The mean value and range of the modified structural number (SN_1) for each section are shown in Figure 7.

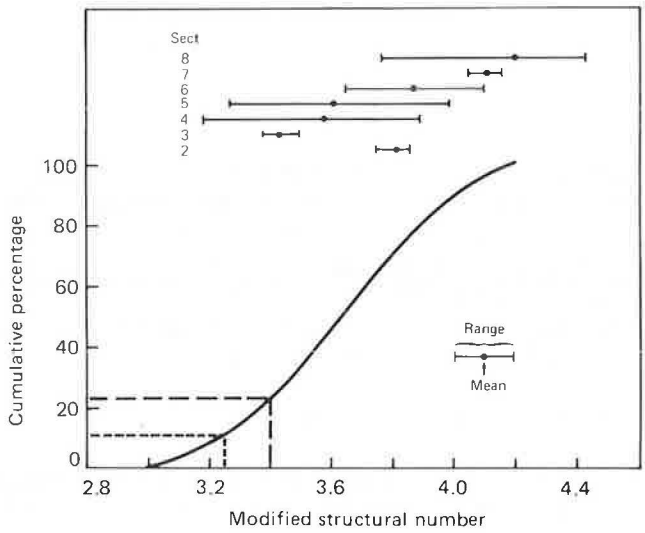

FIGURE 7 Distribution of modified structural number.

Deflection Measurements

Transient deflection measurements at 20 defined locations on each section have been carried out at regular intervals since construction using the standard TRRL method *(5)*. The results show a significant increase over the first year caused by the wetting of the imported clay subgrade. After the first year, the deflection values have remained reasonably constant, indicating that the pavement materials reached equilibrium, thereby lending additional support to the conclusions based on the subgrade strength values measured using the DCP.

That the deflection values correlated extremely well with the performance of each section is shown in the following paragraphs.

PERFORMANCE

Sections with Unstabilized Marly Limestone Roadbases

Pavement deterioration has been monitored by measuring the intensity of cracking and the deformation or rutting under a 2-m straightedge at the 20 deflection test points in each section. The results obtained in June 1985 by wheelpath for Sections 2–8 are summarized in Table 4.

TABLE 4 DEFORMATION AND CRACKING, JUNE 1985

SECTION NO	TOWARDS KINGSTON						TOWARDS MANDEVILLE					
	VERGE SIDE			OFF SIDE			OFF SIDE			VERGE SIDE		
	DEFORMATION mm		CRACKING m/m^2	DEFORMATION mm		CRACKING m/m^2	DEFORMATION mm		CRACKING m/m^2	DEFORMATION mm		CRACKING m/m^2
	MEAN	RANGE		MEAN	RANGE		MEAN	RANGE		MEAN	RANGE	
2	0.4	0-2	0	0	-	0	1.4	0-3	0	6.2	0-9	0
3	4.8	2-7	0	0.4	0-2	0	0.4	0-2	0	15.2	7-21	0
4	3.3	0-8	0.22	0	-	0	0.8	0-4	0	9.0	3-16	0
5	1.6	0-5	0	0	-	0	1.4	0-4	0.37	1.0	0-5	0
6	0.6	0-3	0	0	-	0	2.4	0-6	0	9.0	2-18	0
7	1.8	0-6	0	0	-	0	5.4	4-7	0	6.4	3-10	0
8	1.4	0-7	0.11	0	-	0	0	-	0	0	-	0.01

The predominant mode of failure to date has been deformation (Table 4). Except for Sections 5 and 8, which are discussed in more detail later, the deformation measured in the verge-side wheelpath in the direction toward Mandeville is three to four times greater than in the other, more lightly loaded, direction.

Deformation in the wheelpath depends on vertical stresses in the pavement and the number of times the stresses are repeated. Deflections also depend on vertical stresses, especially those at subgrade level. Provided all the deformation does not occur in the upper layers of the pavement as a result of inadequate shear strength, it would be expected that after a given time or cumulative traffic, deformation would correlate reasonably well with deflection. This correlation was revealed to be true in this experiment. The magnitude of the deformations is expected to increase with traffic or load repetitions. Usually a model is found to fit the data of the form

$$RD = AN^B \quad (1)$$

where

RD = rut depth (mm),
N = number of load repetitions, and
A, B = constant dependent on deflection and other variables.

Attempts were made to fit this and other models to the data, but the model that best explained the variability was

$$RD = -0.51 + TD(0.0027D - 0.080); \quad \text{for } 35 < D < 70 \text{ and } 0 < T < 3.0, \quad (2)$$

where D is deflection (10^{-2} mm) and T is the cumulative number of standard axles (millions).

The multiple correlation coefficient for this model was 0.84, giving an R^2 value of 0.70. An important characteristic of this model is that for no traffic the deformation is close to zero for all values of D. The predicted versus measured deformation is plotted in Figure 8. The model should not be extrapolated for deflection values less than 0.35 mm or greater than 0.70 mm.

Assuming a deformation criterion of 10 mm for defining critical pavement condition as is done in the United Kingdom, the model can be used to predict the life of other road pavements with a similar structure. Figure 9 shows results from Equation 2 superimposed on the deflection performance curve established for roads having naturally cementing roadbases in the United Kingdom. Where the curve has been extrapolated outside the range of data available at present from this study, it should be treated with caution. However, within the present range of data there is reasonable agreement between the two curves, illustrating that the deflection criterion curve established for the Jamaica test sections is similar to that developed in the United Kingdom.

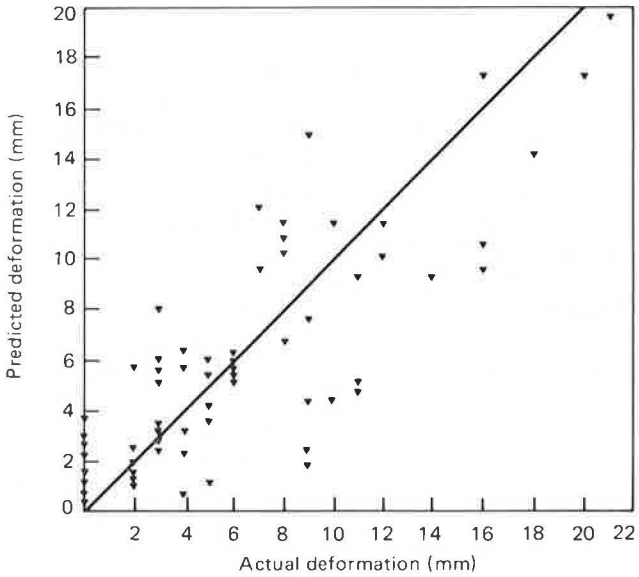

FIGURE 8 Predicted versus actual deformation for Equation 2.

Comparative Performance of Sections

Sections 2, 3, and 7 allow comparison among the performance of different thicknesses of limestone roadbase. The thinnest

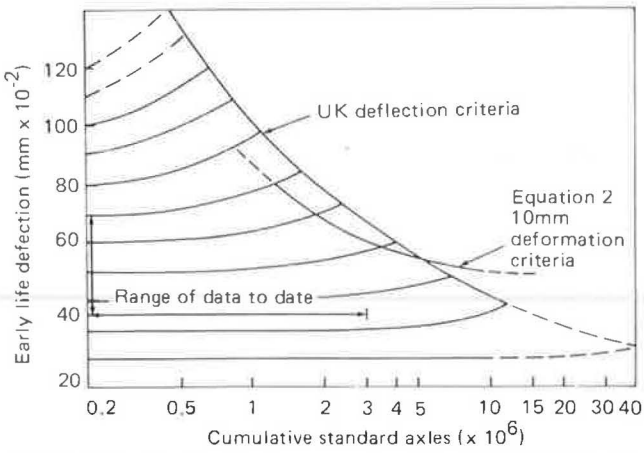

FIGURE 9 Relation between earlier life deflection and life for pavements with granular roadbases whose aggregates exhibit a natural cementing action.

section, Section 3, has performed least well, as expected, but Section 2 has performed at least as well as Section 7 despite being considerably thinner (Figure 1). The reason for this anomalous behavior is not known. The subbase of Section 2 consisted of a different limestone from that used on Sections 3 and 7, but standard tests indicated that its properties were inferior. The DCP tests indicated that the subgrades of Sections 2 and 7 were similar, but the deflections on Section 7 were slightly higher than those on Section 2. Further testing and monitoring are necessary to resolve this apparently anomalous behavior. Both sections performed well and deterioration did not progress far enough to characterize the trends.

Comparison of performance between the section with the stabilized roadbase, Section 5, and the sections with unstabilized roadbases (Sections 2, 3, 4, 6, and 7) shows that Section 5 has performed slightly better than Section 2 and considerably better than Sections 3, 4, 6, and 7, which have deformed extensively.

The mean SN_1 values of Sections 2 and 5 (Figure 7) are similar, but the range of SN_1 is greater on Section 5 with a low minimum value of 3.27 that reflects the poor mixing of the cement. Despite this poor mixing, the roadbase of Section 5 has performed better than that of Sections 6 and 7, which are considerably thicker. Unfortunately, because of the anomalous behavior of Section 2 relative to Sections 6 and 7, it is not possible to derive equivalencies between stabilized and unstabilized limestone. Comparison between Sections 2 and 5 indicates that 1 mm of stabilized limestone is equivalent to 1 mm of unstabilized but better-quality material. However, comparison between Sections 5 and 7 indicates that 1 mm of unstabilized limestone is equivalent to less than 0.75 mm of stabilized material.

It might be expected that the difference in base stiffness would be reflected in the deflection results, but Section 5 is not noticeably different from Sections 2, 3, 4, or 6. Deflection is sensitive to subgrade strength but is not particularly sensitive to the stiffness of the upper layers. It is anticipated that differences between Section 5 and others could be identified from radius of curvature measurements.

Comparison of the performance of the full-depth mechanically stabilized river shingle on Section 8 with that of Sections 6 and 7, which have approximately the same overall mean pavement thickness comprising limestone base and subbase, shows that the river shingle has performed remarkably well, being particularly stable and showing no deformation after 2.9×10^6 equivalent standard axles (esa) in the heavily loaded direction. Neither the DCP CBR values nor the deflection results have identified this effect; indeed the deflection in the verge-side wheelpath toward Mandeville is higher on Section 8 and the SN_1 values show a similar range (Figure 7).

Finally it is not possible to differentiate between the performances of the two roadbase materials used on Sections 3 and 4. Although there is no significant difference between the thickness of material used on Sections 3 and 4, there appears to be a slight difference in subgrade strength as described. This confounding effect masks any differences in performance that could be ascribed to the different materials. Further testing and monitoring are necessary before firm conclusions can be drawn.

Comparison with Appropriate Design Guides

Early-life deflection of the sections with unstabilized limestone roadbases is a good indicator of performance; deformation has been the primary mode of failure. It is also of interest to compare the performance of the sections with that expected from structural design guides.

No in situ thickness or layer strength tests apart from deflection tests were carried out at the precise location of the defined test points because such tests are either destructive or could disturb the equilibrium conditions within the road. Test pits were therefore excavated and DCP tests carried out between test points. It is a reasonable assumption that within each test section the areas showing the highest deformation correspond to the thinnest sections of road, or more accurately, to partly take account of strength differences, to areas of lowest SN_1. If it is assumed that the distribution of SN_1 corresponds to the distribution of deformation (Figures 7 and 10), it is possible to obtain a relationship between SN_1 and traffic-carrying capacity to a defined terminal condition. For example, let a rut depth of 15 mm be chosen as a critical condition. In June 1985 after the passage of 2.9 million esa, 11 percent of the pavement had a rut depth of 15 mm or more (Figure 9). This area of pavement (i.e., the weakest 11 percent) corresponds to the area of pavement with SN_1 values of less than 3.25 (Figure 7).

The expected traffic-carrying capacity of the areas of pavement that have not yet reached 15-mm deformation can be obtained by using the relationship between rut depth and traffic defined by Equation 2. The relationship is linear with traffic; therefore the expected traffic-carrying capacity of an area of pavement currently displaying a rut depth of, say, 10 mm will be 2.9 million × 15/10, that is, 4.35 million esa. Using this method and the distributions shown in Figures 7 and 10, the relationship between traffic-carrying capacity and SN_1 shown in Figure 11 was obtained.

The results show that sections were performing well in comparison with both the Road Note 31 design guide *(1)* and the NAASRA Interim Guide to Pavement Design *(6)*. Two aspects of Figure 11 are important, namely the increased traffic-carrying capacity and the steeper nature of the curve.

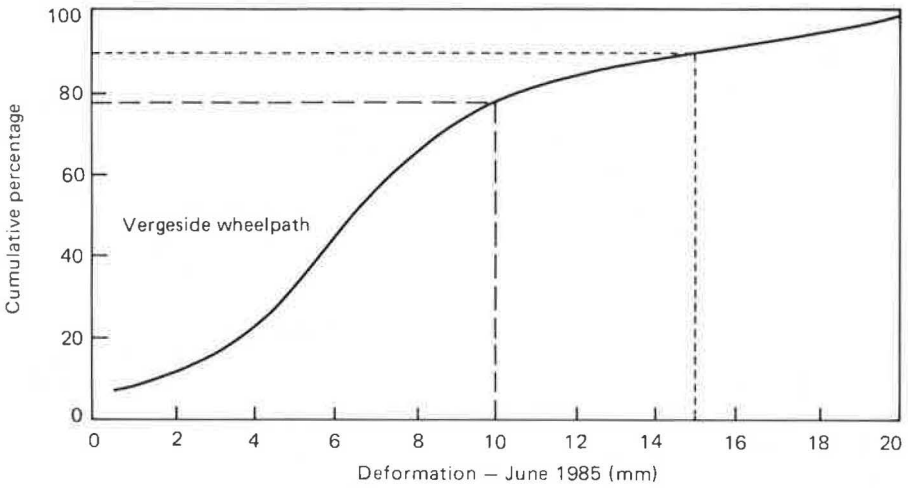

FIGURE 10 Distribution of deformation.

At the low end of the curve, around $SN_1 = 3.2$, the traffic-carrying capacity is 3 to 4 times greater than expected. Although this factor seems large, the relationship is so sensitive to SN that this improvement in capacity is equivalent to an increase in SN of only about 0.3, similar to the range measured over one test section of supposedly uniform thickness. This degree of variability is normal in road construction as demonstrated in numerous full-scale trials and pavement investigations carried out by the Overseas Unit; it must be taken into account by the road designer. Nevertheless, in this analysis the thickness variations are specifically accounted for; hence other explanations for the differences must be sought.

One possible source of systematic error is the measurement of subgrade strength using the DCP. The relationship between DCP and CBR depends to some extent on moisture content, density, and soil type. The maximum likely systematic error for this subgrade material has been estimated to be about 3 percent of CBR; if the subgrade strength has been underestimated by this amount, SN_1 would increase by about 0.3.

The other notable aspect of Figure 11 is that the slope of the relationship is steeper than expected from the design charts. Although the position and scale of the relationships are somewhat different, the slope accords with the analysis of pavement structural designs based on HDM III deterioration relationships carried out by Cox and Rolt *(7)*. However, most of the curve shown in Figure 11 is an extrapolation of existing trends. The analysis has shown that deformation is linearly related to traffic to 3.0 million esa and only 11 percent of the road has reached the 15-mm failure condition up to the present time. There is no guarantee that a similar linear behavior would apply in the future to the areas of pavement that were deforming more slowly. The effect of age hardening of the surface is expected to become apparent and the rate of deformation may therefore begin to decrease, thereby extending the life of the rest of the pavement, at least as far as deformation failure is concerned. This increase in pavement life will flatten the curve in Figure 11 provided no other form of failure (such as cracking) becomes the more dominant mode. Continued monitoring is planned to study the subsequent behavior of the trials.

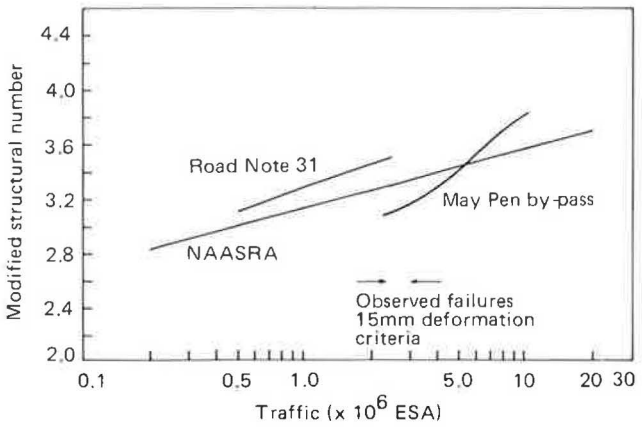

FIGURE 11 Comparison with design guides.

CONCLUSIONS

To date, the experiment has shown that with good-quality AC surfaces, marly limestones can be used to make successful road pavements that deteriorate through the gradual buildup of permanent deformations and whose performance can be predicted reasonably accurately by means of deflection measurements. A model describing the relationship between rut depth, traffic, and deflections has been derived that is applicable up to 3 million esa and for deflections between 0.35 and 0.70 mm measured under an axle load of 62.3 kN (14,000 lb).

The experiment has demonstrated the superior performance of full-depth mechanically stabilized river shingle, but the inconsistent behavior of two sections of standard construction using limestone roadbases and subbases has prevented the estimation of thickness equivalences between unstabilized good-quality limestone, cement-stabilized limestone of lower quality, and mechanically stabilized river shingle.

The overall performance of all sections is better than expected from existing design guides and reliable information for thickness designs capable of carrying up to 10 million esa is expected to be available as the experiment progresses.

The experiment has demonstrated the necessity for taking proper account of variability in subgrade strength and layer thicknesses within the structural design method.

The results have also underlined the importance of good quality control in the manufacture of the premix. The thin premix surface has been both flexible and durable, displaying no fatigue cracking and has also withstood high deformations in the other pavement layers without cracking.

ACKNOWLEDGMENTS

The work described in this paper was carried out in the Overseas Unit (Unit Head, J.S. Yerrell) of the Transport and Road Research Laboratory, United Kingdom. The work forms part of the research program for the Overseas Development Administration, but any views expressed are not necessarily those of the Administration or the Department of Transport.

The project was a joint undertaking with the Jamaican Ministry of Construction. The authors are indebted to the Permanent Secretary, Chief Technical Director, and the staff of the Traffic and Civil Engineering Departments without whose cooperation the work would not have been successful.

REFERENCES

1. *A Guide to the Structural Design of Bitumen-Surfaced Roads in Tropical and Sub-Tropical Countries.* Transport and Road Research Laboratory. Road Note 31, 3rd ed. HMSO, London, England, 1977.
2. *Methods of Test for Soils for Civil Engineering Purposes.* BS 1377. British Standards Institute, London, England, 1975.
3. E. G. Kleyn and P. F. Savage. *The Application of the Pavement DCP to Determine the Bearing Properties and Performance of Road Pavements.* 1st International Conference on the Bearing Capacity of Roads and Airfields, Norwegian Institute of Technology, Trondheim, Norway, 1982.
4. J. W. Hodges, J. Rolt, and T. E. Jones. *The Kenya Road Transport Cost Study: Research on Road Deterioration.* TRRL Report LR 673. Department of the Environment, Transport and Road Research Laboratory, Crowthorne, Berkshire, England, 1975.
5. H. R. Smith and C. R. Jones. *Measurement of Pavement Deflections in Tropical and Sub-Tropical Climates.* TRRL Report LR 935. Department of the Environment, Department of Transport, Transport and Road Research Laboratory, Crowthorne, Berkshire, England, 1980.
6. *Interim Guide to Pavement Thickness Design.* National Association of Australian State Road Authorities, Sydney, Australia, 1979.
7. J. B. Cox and J. Rolt. An Integrated Approach to Pavement Design Based on HDM III Pavement Performance and Vehicle Operating Cost Relationships. *Proc., 13th Australian Road Research Board Conference*, Adelaide, 1986.

Publication of this paper sponsored by the Committee on Strength and Deformation Characteristics of Pavement Sections.

Subsealing and Load Transfer Restoration

R. J. ROMAN, M. Y. SHAHIN, AND J. A. CROVETTI

Presented are the evaluation results of slab subsealing and load transfer restoration using dowel bars and double vee shear devices of a jointed concrete pavement at a large truck terminal facility. Nondestructive deflection testing (NDT) procedures using the falling-weight deflectometer (FWD) were used before and after slab subsealing and installation of the load transfer devices to evaluate the efficiency of the slab subsealing and load transfer devices.

The results of cement grout slab subsealing and load transfer restoration at a large truck terminal facility are presented in this paper. Cement grout subsealing was performed to restore support to slabs exhibiting loss of support due to the presence of voids. Retrofit dowel bars and double vee shear devices were installed on an experimental basis in a small test section of the truck terminal to evaluate the effectiveness of the devices and to answer the following questions:

1. What type of device (e.g., dowel bars or double vee shear devices) is best suited for this facility?
2. What is the relative effectiveness of each device as installed in this facility?
3. Is the slab thickness sufficient to support retrofit load transfer devices?

Based on the performance of the load transfer test section and other areas of the terminal, a decision could be made to expand the load transfer program to other areas of the terminal.

SLAB SUBSEALING

Void Detection

Pumping of base material was observed over much of the terminal. This visual indication of voids was confirmed through nondestructive deflection testing (NDT) procedures using the falling-weight deflectometer (FWD). Void detection procedures developed under NCHRP Project 1-21 *(1)* were used to define the areas for cement grout subsealing and to evaluate the effectiveness of the subsealing operation.

The void detection method used corner deflections measured at three load levels to establish a load versus deflection response for the test location. Corners with no voids cross the deflection axis near the origin, usually at ≤0.002 in. The load versus deflection response line for corners with voids intersects the deflection axis at a point >0.002 in. from the origin.

After a corner that had a void had been subsealed, the load-versus-deflection response line moves back towards the origin.

R. J. Roman and J. A. Crovetti, ERES International, Inc., P.O. Box 1003, Champaign, Ill. M. Y. Shahin, 37 Maple Court, Lake Park, Champaign, Ill.

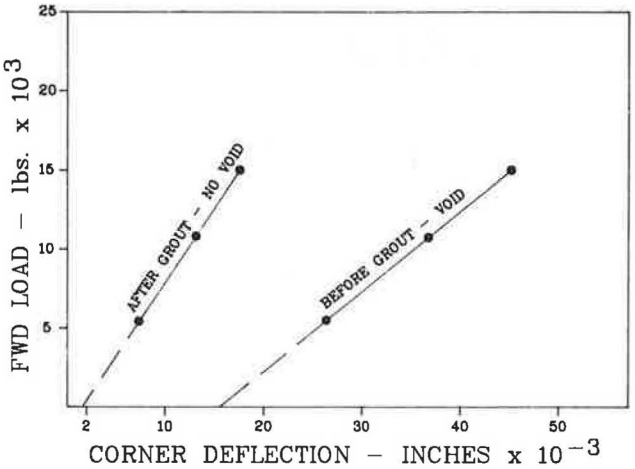

FIGURE 1 Void detection concept.

This void detection concept is shown in Figure 1. The areas selected for subsealing based on this void detection procedure are shown in Figure 2.

Construction Procedures

Several test areas were used to determine a grout injection hole pattern that would provide adequate flow of the cement grout and restoration of support to areas exhibiting voids. Results of the test areas and NDT testing indicated that two grout injection holes per slab would be adequate to restore support to the corner. These holes were located 2 ft off the slab edges as shown in Figure 3.

A cement grout mixture of one part portland cement and three parts pozzolan with a flow within 10 to 16 sec was used. The 7-day strength of the grout mixture was ≥600 psi.

The grout plant consisted of a colloidal mixing machine; maximum pumping pressure was 50 psi. Vertical slab movement detection equipment was used to monitor slab deflection during pumping.

Efficiency of Slab Subsealing

The void detection procedures discussed earlier were used after subsealing to evaluate the effectiveness of the grout in restoring slab support. If a void was present after subsealing, the corner was regrouted. Results of the NDT testing indicated that the subsealing operation was successful in restoring slab support.

In addition to the subsealing operations, a limited test area of load transfer restoration devices was installed to evaluate the effectiveness of the devices in restoring load transfer and retarding further slab deterioration.

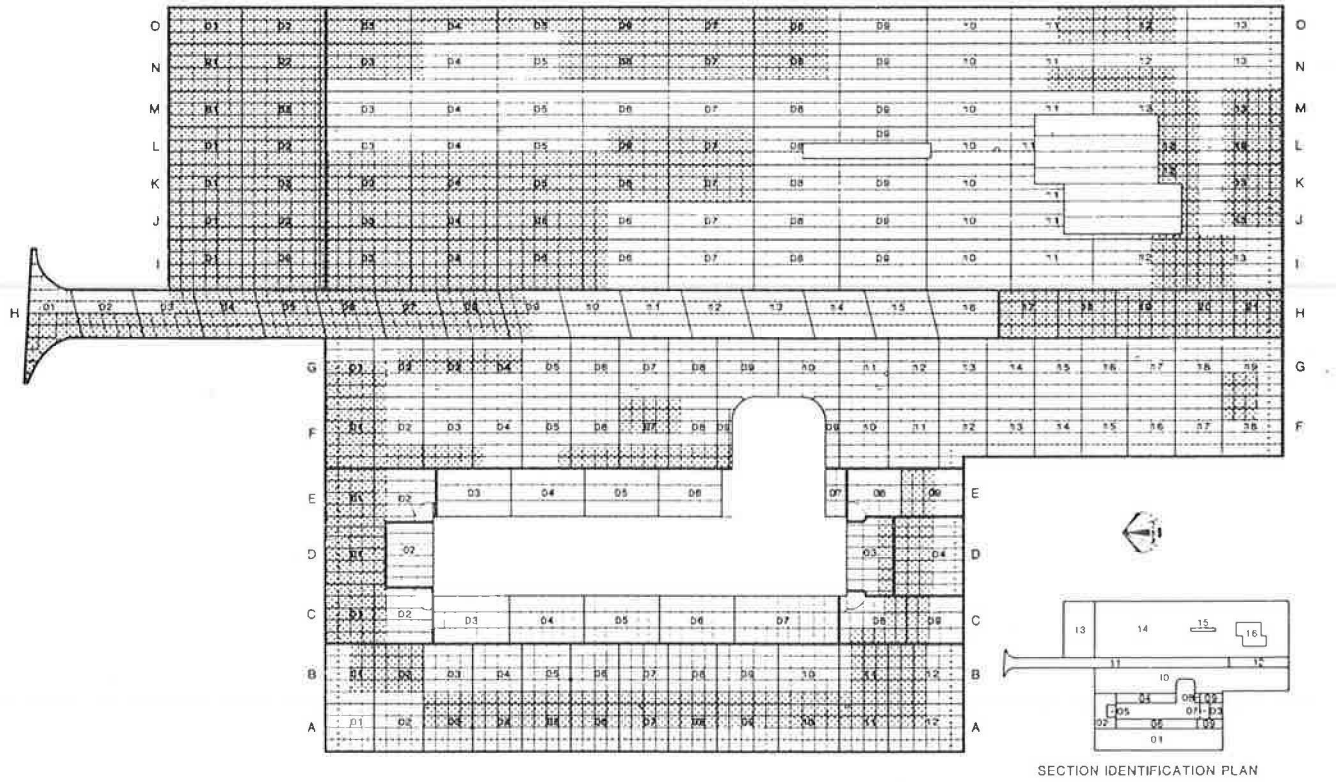

FIGURE 2 Cement grout subseal locations.

LOAD TRANSFER RESTORATION

Load Transfer Efficiency

The ability of a joint or crack to transfer load is a major factor in its structural performance. Load transfer efficiency across a joint or crack may be defined as the ratio of deflection of the unloaded side to the deflection of the loaded side. If perfect load transfer exists, the ratio is 1.00 (100 percent); if no load transfer exists, the ratio is 0.00 (0 percent). Good deflection load transfer efficiencies are in the range 70 to 100 percent. Poor deflection load transfer efficiencies are in the range 0 to 60 percent.

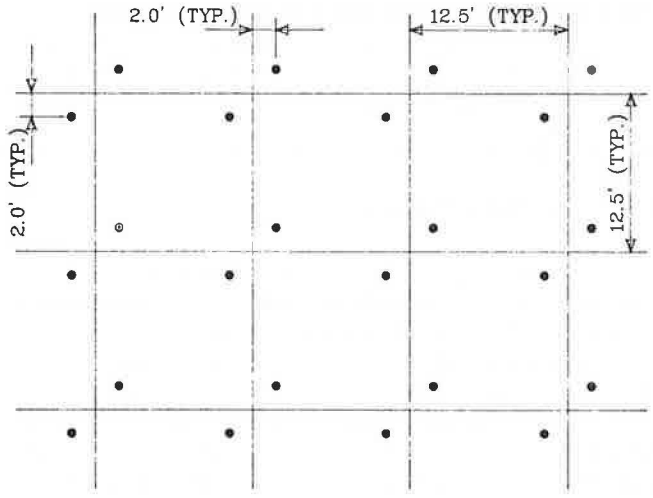

FIGURE 3 Grout injection hole pattern.

Load Transfer Efficiencies at the Terminal

The terminal pavement consists of a 7.7-in. undoweled plain-jointed portland cement concrete (PCC) parking area constructed in early 1982. East-west joints were formed by placing a 2-in.-deep masonite strip into the plastic concrete. North-south joints served as construction joints, and they are keyed with a rounded half-moon keyway. The exception to this is the part of the access drive identified as Sample Units H01–H16 in Figure 2. The east-west joints were also formed with masonite; however, the north-south joints in Section 11 are keyed and tied together with No. 4 deformed tie bars spaced approximately every 2 to 3 ft on center. A summary of the average load transfer efficiency for the pavement sections is presented in Table 1. The values in Table 1 and all load transfer efficiencies in this paper have been corrected for slab bending. The section descriptions refer to Figure 4.

Need For Load Transfer

Restoration of load transfer across a joint is used to retard further deterioration of the concrete slabs. Poor load transfer leads to joint deterioration, including corner breaks, faulting, pumping, and spalling. Load transfer restoration reduces deflections, stresses, and further slab deterioration.

TABLE 1 AVERAGE LOAD TRANSFER EFFICIENCY FOR PAVEMENT SECTIONS

Section	Average Load Transfer Efficiency % N-S Joints	E-W Joints
East of Access	66	45
West of Access 1	63	68
West of Access 2	--	21
West of Access 3	--	37
West of Access 4	--	24
Cargo	--	36
Tied Access	96	43
United Access	--	27

-- Not Tested

Several types of retrofit load transfer devices have been used in the past. However, the procedures to successfully install these devices are still in the experimental stage and cannot be proven effective because of lack of sufficient data on long-term performance. Therefore, although several sections of the terminal were exhibiting poor load transfer, only one test section was selected for retrofit load transfer devices. The test section chosen is part of the untied access as shown in Figure 5. The objectives of limiting installation of load transfer devices to this area were to determine (a) the type of device that will perform adequately, (b) the relative effectiveness of each device as installed at this facility, (c) the slab thickness sufficient to support retrofit load transfer devices, and (d) an adequate repair material.

LOAD TRANSFER RESTORATION TEST AREA

Location of Test Area

The load transfer test area is located in the untied section of the access road as shown in Figure 5. This section had one of the poorest load transfer efficiencies and was also exhibiting pumping.

Layout of Load Transfer Devices

The test area consisted of an area approximately 62 × 48 ft and contained 20 concrete slabs. The locations of the retrofit load

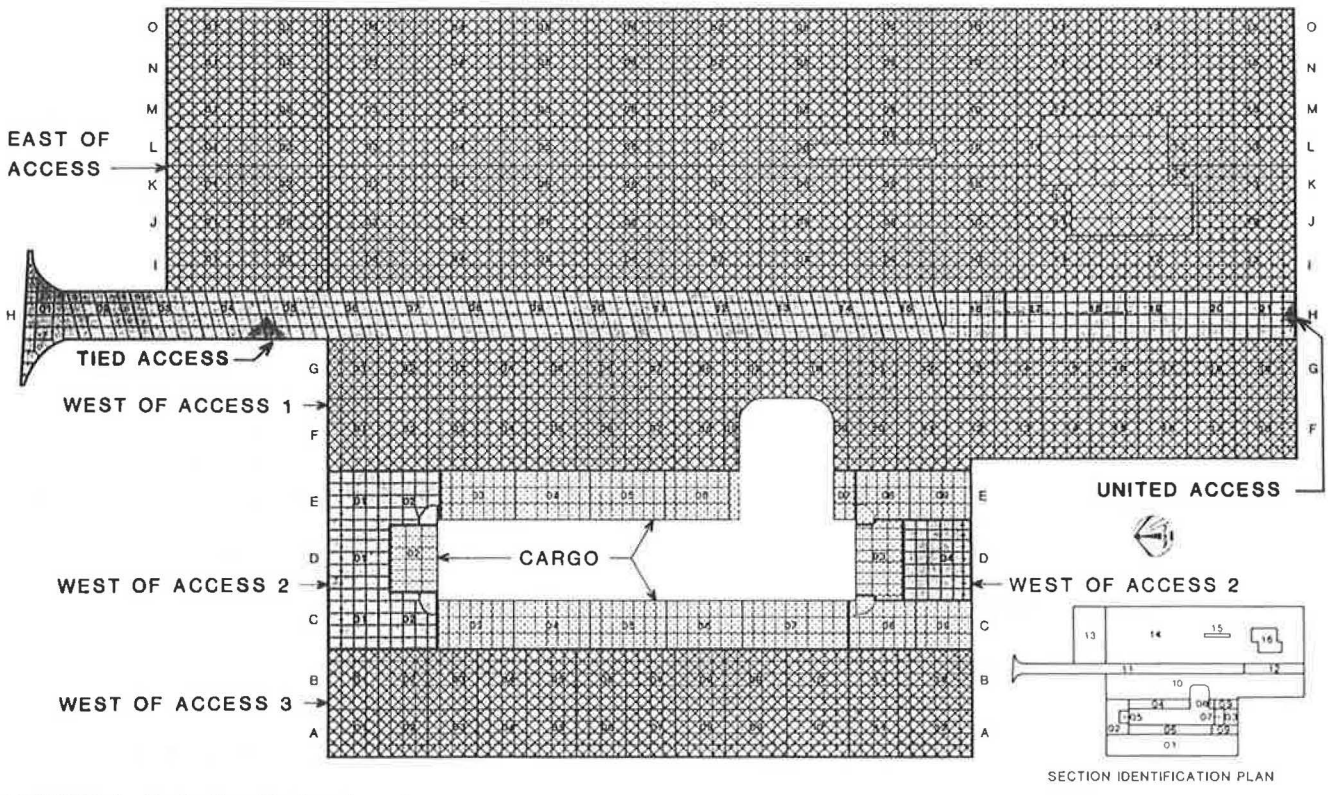

FIGURE 4 Deflection file location plan.

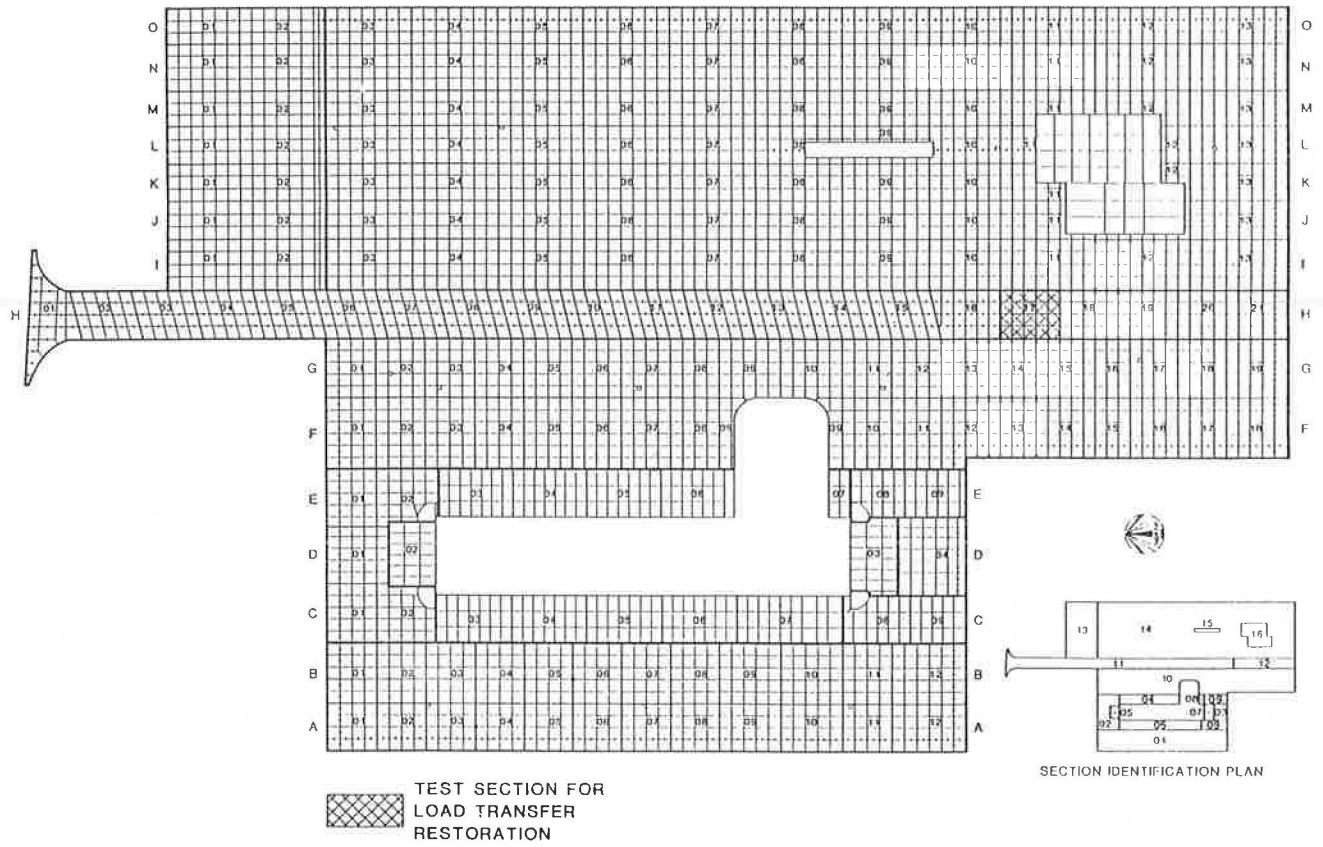

FIGURE 5 Test section for load transfer.

transfer devices as installed in the field are shown in Figure 6. Double vee shear devices were used on two joints. No devices were installed in one joint. This joint served as a control joint. Dowel bars were installed in the last joint in the test section.

LOAD TRANSFER DEVICES

Double Vee Device

The double vee device is a shear device for transferring load across joints. This device is illustrated in Figure 7. Load transfer restoration across joints is accomplished through a bond between the device, the concrete slab, and the repair material. This device is installed in a core hole of 6-in. diameter and is designed to allow for joint movements due to expansion and contraction. The center section of the device is filled with foam to prevent debris and incompressibles from entering the device. The devices used on this project were 6¾ in. in length and 6¼ in. in diameter. The device was precompressed and dropped into the core hole of 6-in. diameter. Maintaining a thoroughly dry core hole during installation was difficult because of a high water table at the site. A particle board was inserted on top of the double vee device to maintain the joint and prevent the repair material from being continuous across the joint. The double vee devices were installed at a cost of $52.00 each.

Dowel Bars

Dowel bars are an effective alternative to using shear devices to restore load transfer across joints. The dowel bars used in the test section were 1 in. in diameter, 18 in. in length, and epoxy coated to protect the dowel bar against corrosion. The dowel bar is installed in a kerf that is saw cut, and the joint is maintained with a fiberboard material as shown in Figure 8. The dowel bars were installed at a cost of $79.00 each.

REPAIR MATERIALS

Several repair materials have been used on past load transfer projects including polymer concretes and high early-strength concrete. Repair materials must be able to develop sufficient bond between the load transfer device and repair material as well as between the existing concrete and the repair material to carry the traffic loads and movement from thermal changes. A high early-strength concrete and a polymer concrete were chosen for this project.

High Early-Strength Concrete

Dayton Superior HD-50 concrete patch is a prepackaged cement-based repair material and was used as the repair material

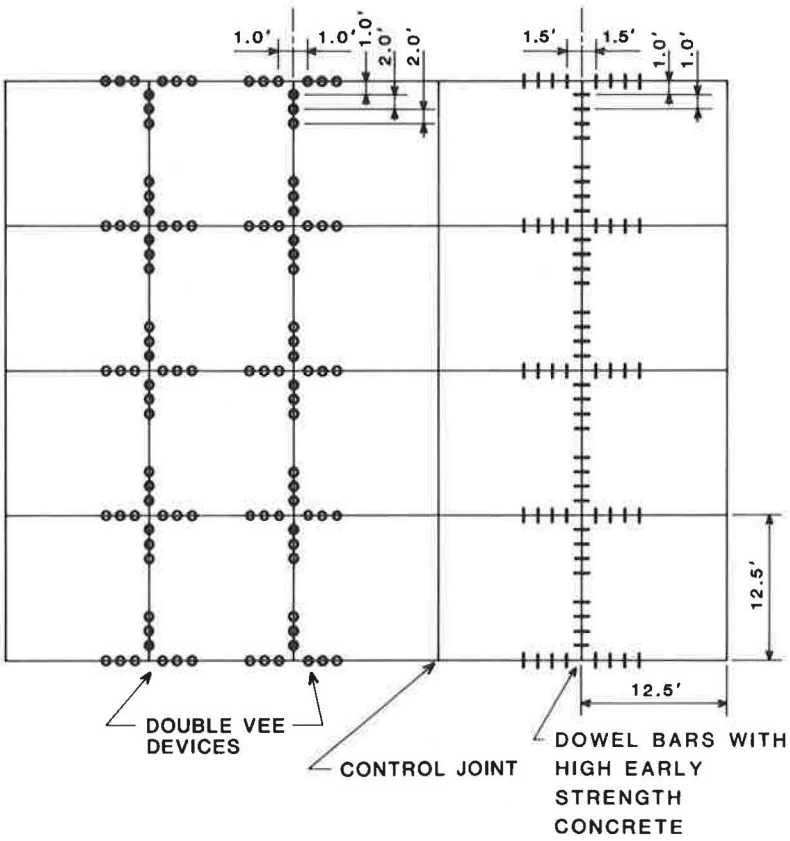

FIGURE 6 Layout of load transfer device test area.

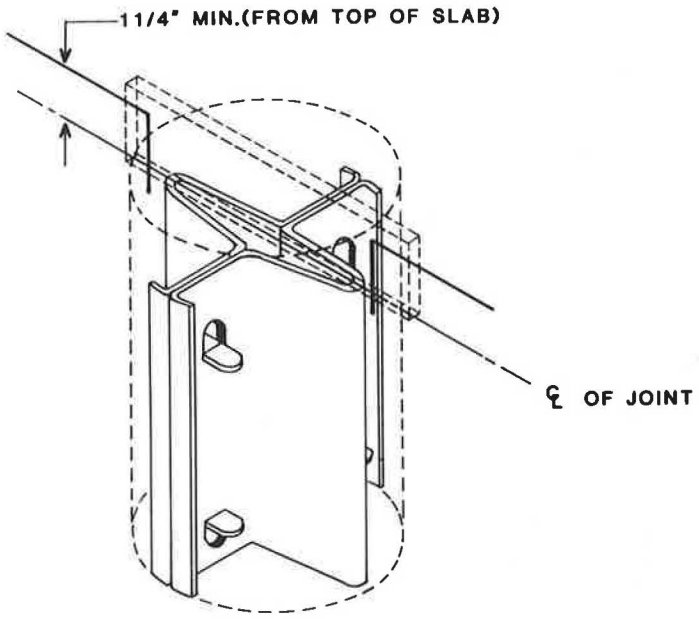

FIGURE 7 Double vee load transfer device.

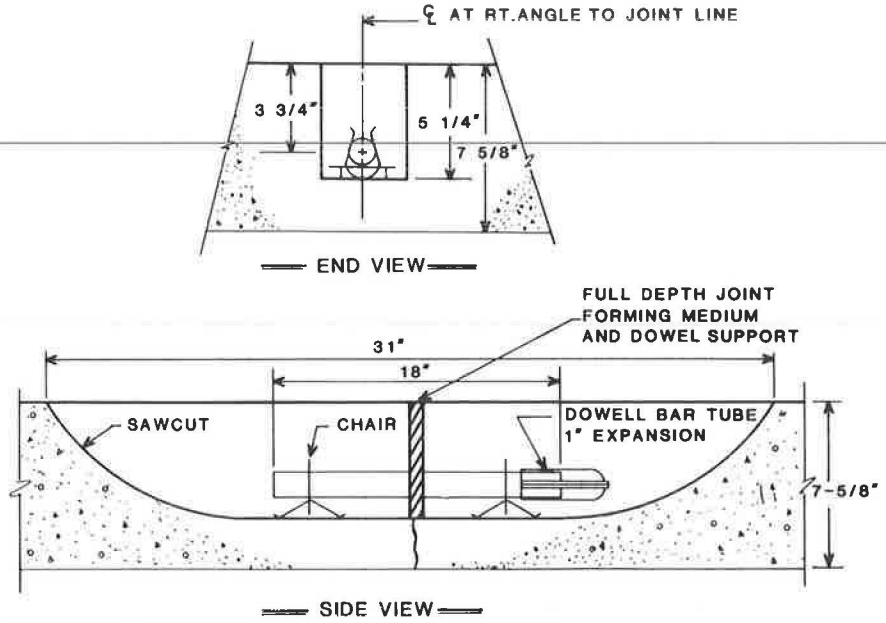

FIGURE 8 Retrofit dowel bar load transfer device.

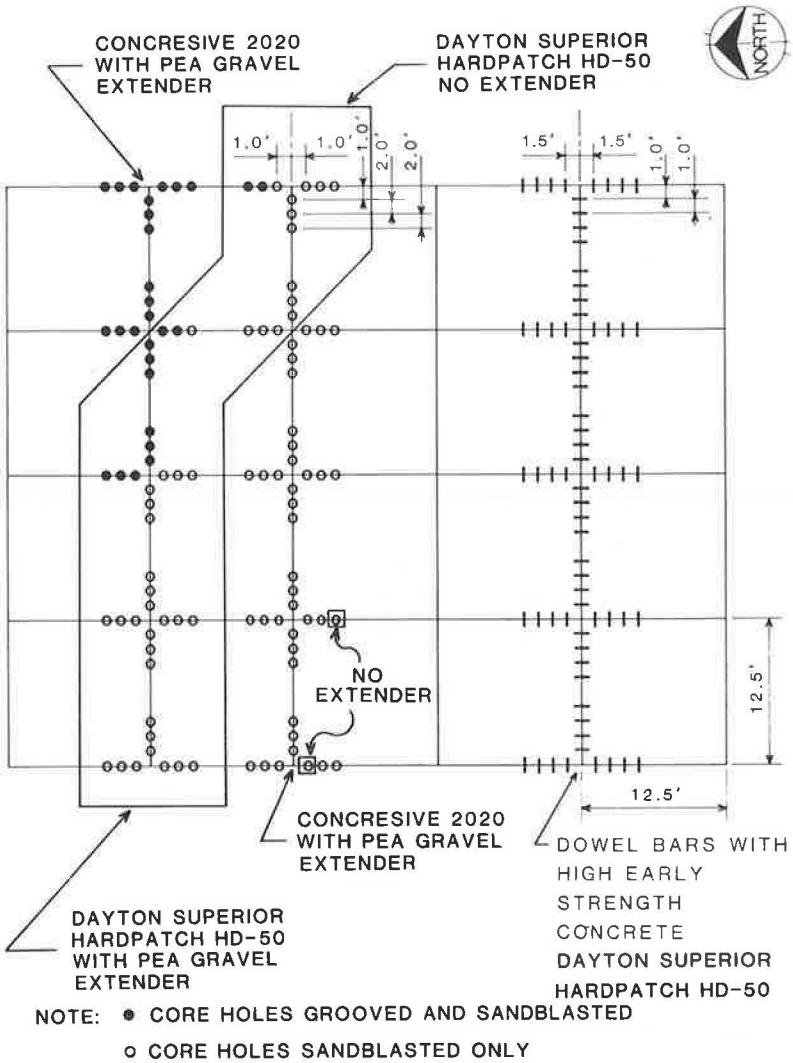

FIGURE 9 Combinations of device type and repair material type.

for the dowel bars and one-half of the double vee devices. Dayton Superior HD-50 is a one-component material that requires only the addition of water. Typical compressive strengths for this material are 2,000 psi within 45 min, 4,000 psi after 3 hr, and 7,000 psi after 7 days.

Polymer Concrete

A polymer concrete called Concresive 2020 was used with one-half of the double vee devices. This material consists of a liquid component and powder component mixed together. After 3 days, the compressive strength of this material is approximately 8,000 psi. This material can be used as is or can be extended with a clean kiln-dried aggregate.

Location of Repair Materials

The combinations of device type and repair material type are shown in Figure 9. The Dayton Superior HD-50 concrete patch used with the dowel bars was extended using 1 quart of sandblasting sand with each two-bag (100-lb) batch of HD-50.

Twenty-one double vee devices were placed with Dayton Superior HD-50 and no extender. Thirty-three double vee devices were placed with Dayton Superior HD-50 extended with a washed, air-dried 3/8-in. pea gravel.

The polymer concrete used to place the double vee devices was extended with the same 3/8-in. washed and air-dried aggregate for all but two double vee devices that were placed with no aggregate extender.

Carter Waters concrete bonding agent compound No. 202 Type I was applied to all core walls and bottoms and sides of kerfs before the repair materials were placed to facilitate bond between the concrete and repair material.

EVALUATION OF PERFORMANCE

Nondestructive Deflection Testing Program

An NDT program was conducted using an FWD to evaluate the effectiveness of the load transfer devices in restoring load transfer across the joints. Test points were established along each of the four joints in the test area. The test points were assigned station numbers as shown in Figure 10. Each test

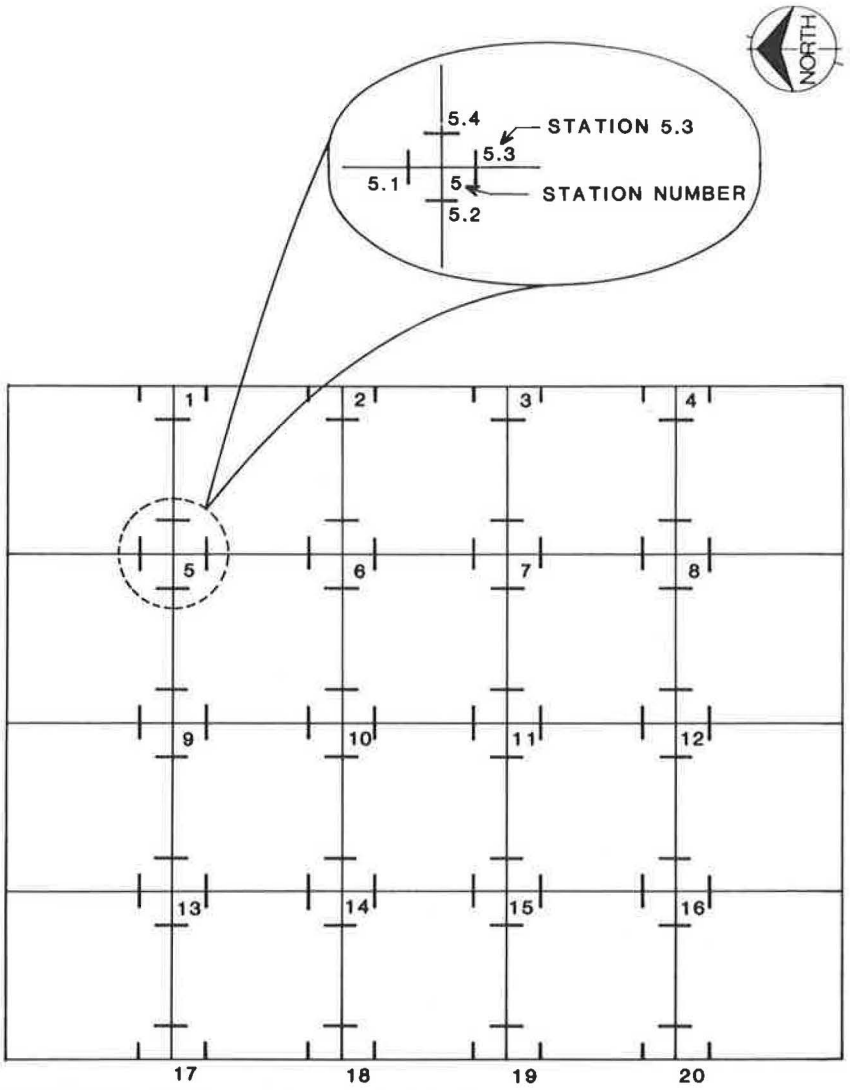

FIGURE 10 Station numbers for load transfer test area.

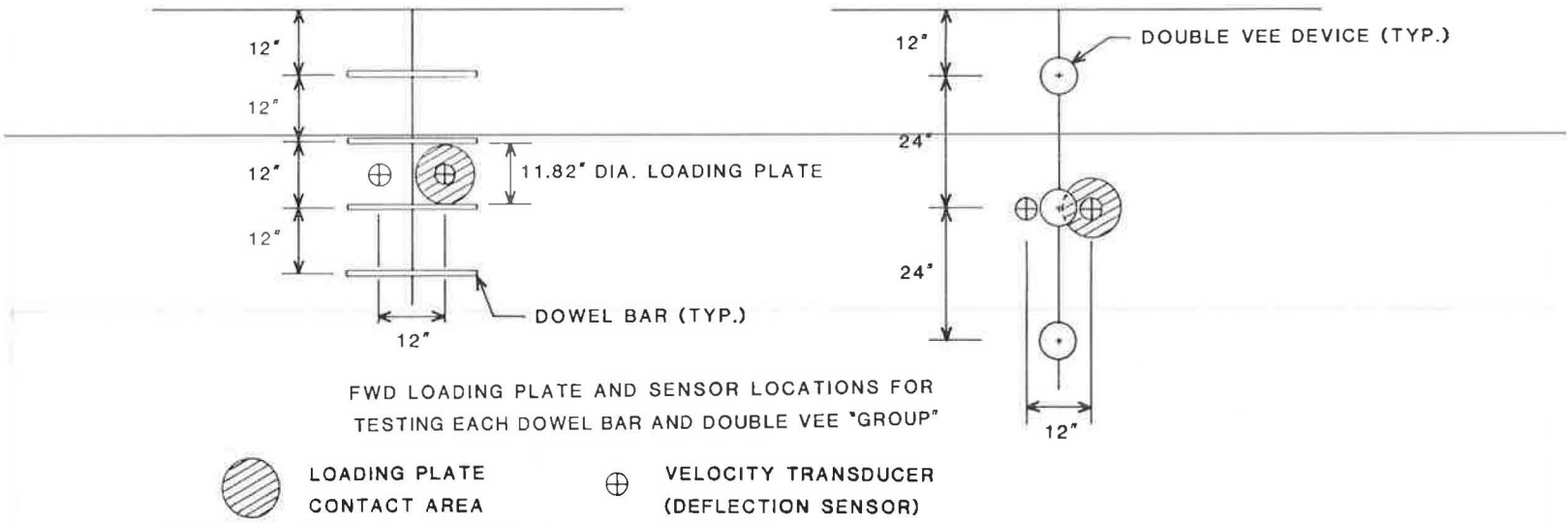

FIGURE 11 Positioning of FWD load plate during testing.

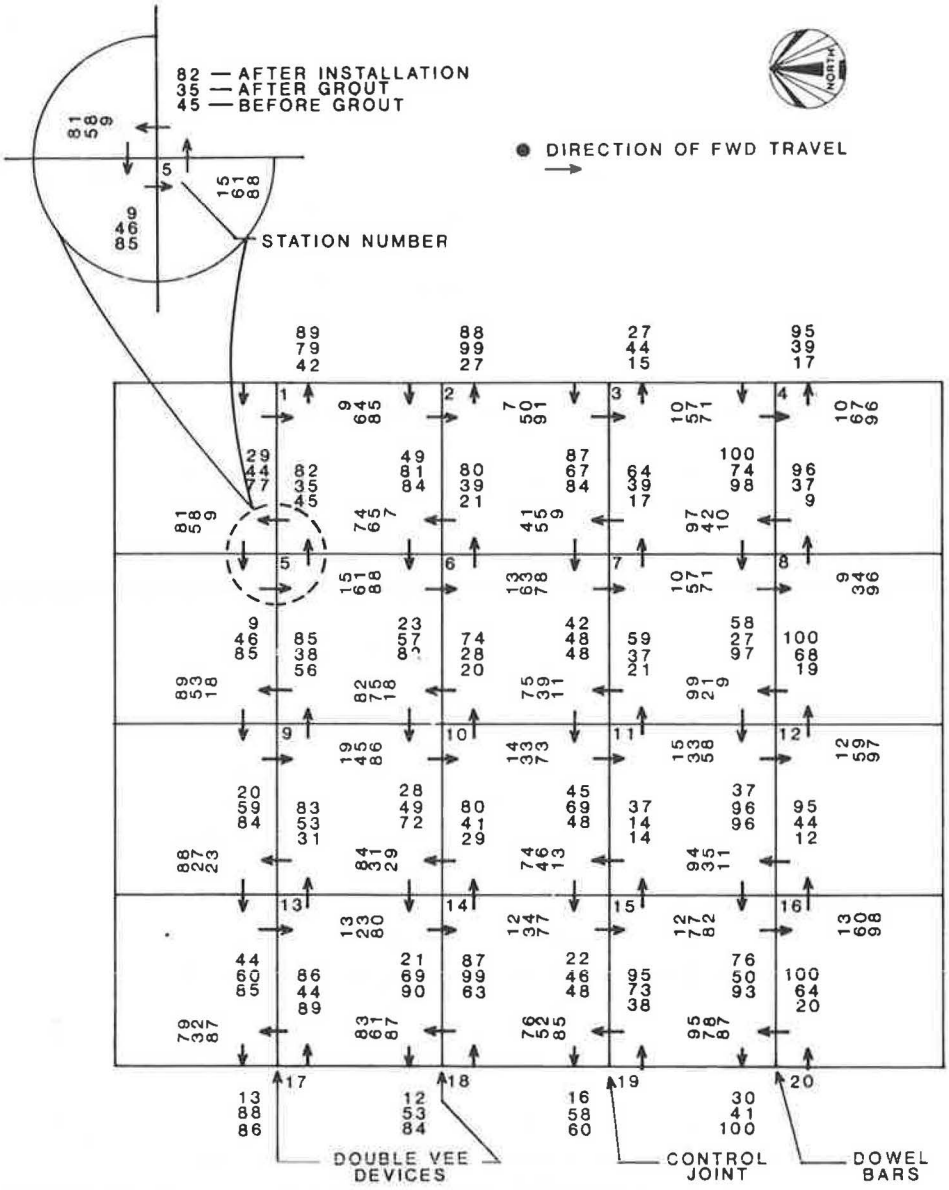

FIGURE 12 Summary of load transfer efficiencies.

point was tested with the FWD before subsealing, after subsealing, and after installation of the load transfer devices. The typical location of the FWD load plate in relation to the installed load transfer devices is shown in Figure 11. A summary of load transfer efficiencies as measured before subsealing, after subsealing, and after installation of the load transfer devices is shown in Figure 12. Additional NDT data are being collected on the test section so that the performance of the devices after 1 year of service can be evaluated.

Effectiveness of Double Vee Devices

The double vee devices were effective in restoring load transfer efficiency across the joint. The two joints where double vee devices were installed had an average load transfer efficiency of 29 percent before subsealing, 54 percent after subsealing, and 83 percent after installation of the load transfer devices. The increase in load transfer efficiencies after subsealing can be attributed to the filling of voids and restoration of slab support and an increased amount of mechanical interlock at the joints from grout's being forced out of the joints during the subsealing operation. A summary of load transfer efficiencies for each station is presented in Table 2.

Effectiveness of Dowel Bars

The dowel bars were also effective in restoring load transfer across the joints and appear to be more effective than the double vee device. The joint where dowel bars were installed had a load transfer efficiency of 29 percent before subsealing, 52 percent after subsealing, and 97 percent after installation of the dowel bars. The increase in load transfer efficiencies after subsealing can be attributed to the filling of voids and restoration of slab support and an increased amount of mechanical

TABLE 2 LOAD TRANSFER EFFICIENCIES FOR STATIONS WITH DOUBLE VEE DEVICES

Station	Grooved	Repair Material Type	Load Transfer Efficiency Before Subsealing	After Subsealing	After LTD Installation
1.1	+	2020	29	44	77
1.2	+	2020	9	64	85
1.3	+	2020	42	79	89
2.1	+	HD-50	49	81	84
2.2		HD-50	7	50	91
2.3		HD-50	27	99	88
5.1	+	2020	9	46	85
5.2	+	HD-50	15	61	88
5.3	+	HD-50	45	35	82
5.4	+	2020	9	58	81
6.1		HD-50	23	57	82
6.2		2020	13	63	78
6.3		2020	21	39	80
6.4		HD-50	7	65	74
9.1	+	HD-50*	20	59	84
9.2		HD-50*	19	45	86
9.3		HD-50*	56	38	85
9.4	+	HD-50*	18	53	89
10.1		2020	28	49	72
10.2		2020	14	33	73
10.3		2020	20	28	74
10.4		2020	18	75	82
13.1		HD-50*	44	60	85
13.2		HD-50*	13	23	80
13.3		HD-50*	31	53	83
13.4		HD-50*	23	27	88
14.1		2020	21	69	90
14.2		2020	12	34	77
14.3		2020	29	41	80
14.4		2020	29	31	84
17.1		HD-50*	13	88	86
17.3		HD-50*	89	44	86
17.4		HD-50*	87	32	79
18.1		2020	12	53	84
18.3		2020	63	99	87
18.4		2020	87	61	83
Average Load Transfer Efficiency			29.2	53.8	82.8

* Hardpatch HD-50 Extended With Pea Gravel

TABLE 3 LOAD TRANSFER EFFICIENCIES FOR STATIONS WITH DOWEL BARS

Station	Load Transfer Efficiency Before Subsealing	After Subsealing	After Dowel Installation
4.1	100	74	98
4.2	10	67	96
4.3	17	39	95
8.1	58	27	97
8.2	9	34	96
8.3	9	37	96
8.4	10	42	97
12.1	37	96	96
12.2	12	59	97
12.3	19	68	100
12.4	9	21	99
16.1	76	50	93
16.2	13	60	98
16.3	12	44	95
16.4	11	35	94
20.1	30	41	100
20.3	20	64	100
20.4	87	78	95
Average Load Transfer Efficiency	29.2	52.0	96.8

Note: Patch Material, Dayton Superior Hardpatch HD–50; Bonding Agent, Carter Waters concrete bonding agent compound No. 202 Type I; Extender, Sandblasting sand (one pint per 2 bags HD–50).

interlock at the joints from grout's being forced out of the joints during the subsealing operation. Table 3 presents a summary of the load transfer efficiencies for stations where dowel bars were installed.

Control Joint

A control joint was maintained in the load transfer test area as shown in Figure 4. The control section was maintained to compare a joint with no load transfer device to those with the retrofit load transfer devices. The measured load transfer efficiencies before subsealing, after subsealing, and at the time load transfer devices were installed in the other joints are presented in Table 4. The average load transfer efficiency increased from 25 percent before subsealing to 47 percent after subsealing. The increase in load transfer efficiencies after subsealing can be attributed to the filling of voids and restoration of slab support and an increased amount of mechanical inter-

TABLE 4 LOAD TRANSFER EFFICIENCIES FOR CONTROL JOINT

Station	Load Transfer Efficiency Before Slab Subsealing 9-16-85	After Slab Subsealing 9-25-85	10-07-85
3.1	87	67	84
3.2	10	57	71
3.3	15	44	27
7.1	42	48	48
7.2	10	57	71
7.3	17	39	64
7.4	9	55	41
11.1	45	69	48
11.2	15	33	58
11.3	21	37	59
11.4	11	39	75
15.1	22	46	48
15.2	12	77	82
15.3	14	14	37
15.4	13	46	74
19.1	16	58	60
19.3	38	73	95
19.4	85	52	76
Average	26.8	50.6	62.1

lock at the joints from grout's being forced out of the joints during the subsealing operation. The amount of mechanical interlock will decrease with time and traffic, resulting in a loss of load transfer efficiency due to mechanical interlock.

Evaluation of Repair Materials for Double Vee Devices

Two repair materials were used with the double vee devices, Dayton Superior HD-50 concrete patch and Concresive 2020 polymer concrete. In addition to the two repair materials, two techniques were used to prepare the core wall, grooving and sandblasting and sandblasting only. Results of deflection testing after installation of the double vee devices indicate that at this early date there is no significant difference in load transfer efficiencies between repair materials or between those core walls that were grooved and sandblasted and those that were sandblasted only. The use of an aggregate extender also appears to have no effect on the performance of the double vee device.

CONCLUSIONS AND RECOMMENDATIONS

The following conclusions and recommendations are presented as a summary of the load transfer restoration effort:

1. Both the double vee devices and dowel bars are capable of restoring load transfer across a joint.
2. Dowel bars are a more appropriate device to restore load transfer at this particular site because of the high water table and moisture problems encountered when installing the double vee devices.
3. A visual and nondestructive deflection survey should be conducted approximately every 2 years to evaluate long-term performance of the load transfer devices and patching materials.
4. A pavement condition index *(2)* of the load transfer test area and the remainder of Section 12 as shown in Figure 4 should be conducted every 2 years after installation of the load transfer devices to evaluate any differences in pavement condition between the load transfer test area and remaining pavement section.

REFERENCES

1. J. A. Crovetti and M. I. Darter. *NCHRP Report 281: Void Detection Procedures*. TRB, National Research Council, Washington, D.C., 1985.
2. M. Y. Shahin and S. D. Kohn. *Pavement Maintenance Management for Roads and Parking Lots*. Technical Report M-294. U.S. Army Construction Engineering Research Laboratory, Champaign, Ill., 1981.

Publication of this paper sponsored by Committee on Pavement Rehabilitation.

Development of a Demonstration Prototype Expert System for Concrete Pavement Evaluation

KATHLEEN T. HALL, MICHAEL I. DARTER, SAMUEL H. CARPENTER, AND JAMES M. CONNOR

A computerized system has been developed to assist state highway engineers in evaluating concrete highway pavements. The system uses information collected by the engineer to determine what mechanisms have caused the distresses present in the pavement, so that the rehabilitation techniques that would be most effective in repairing the distresses and preventing their recurrence can be identified. The evaluation procedure has been developed in the form of an expert system that simulates a consultation between the engineer and an expert in concrete pavement evaluation and rehabilitation. The system was developed through extensive interviewing of concrete pavement experts. The system operates on an IBM-compatible personal computer with two disk drives. The steps in the development of the expert system are described for the benefit of those interested in improved pavement evaluation procedures and in exploring expert systems applications in pavement design, evaluation, and rehabilitation. The work performed demonstrates that an expert system capable of diagnosing pavement deficiencies and their causes at a level approaching that of a human expert in the field can be developed and applied as a component of a practical engineering procedure for comprehensive evaluation and rehabilitation of concrete pavements.

Concrete pavement evaluation is a difficult engineering problem that defies traditional solution methods because of the large number of factors that must be considered, the interactions of these factors, and the shortage of organized information on the ways in which these interacting factors influence performance *(1, 2)*. Although analytical techniques are available to examine particular factors that are known to influence performance, comprehensive pavement evaluation requires the consideration of so many factors that it is still a task best performed by individuals in the pavement field with considerable knowledge about pavement performance and considerable experience in evaluating pavements.

The most appropriate way to develop a formal concrete pavement evaluation procedure thus appears to be through studying and attempting to duplicate the way in which pavement experts evaluate pavements. Two knowledgeable and experienced pavement engineers, whose combined areas of expertise encompass all aspects of concrete pavement evaluation and performance, were involved in the development of this evaluation procedure. Through every step in the development of the procedure, these experts submitted to exhaustive questioning on their reasoning methods.

Department of Civil Engineering, University of Illinois at Urbana-Champaign, Champaign, Ill. 61801.

For the initial development of the evaluation procedure, the scope of the problem was limited to jointed, reinforced, concrete pavement (JRCP). Adaptation of the procedure for jointed plain and continuously reinforced concrete pavements is also under way.

The system was developed for use on an IBM-compatible personal computer using the Insight 2+ expert system shell developed by Level V Research, Inc. An expert system shell is a software tool that allows the expert system developers to concentrate on acquiring knowledge from the experts and expressing it in the form of rules. The shell provides a suitable development environment (with text editor, compiler, etc.) and a control structure to access and use the rules.

SOLUTION APPROACH

Major Problem Areas

The experts identified 12 problem areas that they felt must be considered in an evaluation of a jointed reinforced concrete highway pavement:

1. Structural capacity,
2. Drainage,
3. Foundation stability,
4. Roughness,
5. Concrete durability,
6. Skid resistance,
7. Transverse joint condition,
8. Longitudinal and transverse joint construction,
9. Load transfer,
10. Slab support,
11. Joint sealant reservoir design, and
12. Shoulder condition.

The experts agreed that a thorough assessment of a pavement's present condition required a determination of whether or not one or more deficiencies serious enough to warrant corrective measures existed in each of the 12 major problem areas.

Interviewing Pavement Experts

By far the most difficult task in developing the evaluation procedure was formalizing the reasoning processes by which

the experts determined whether or not a particular pavement deficiency existed. As is typical of difficult problems in any field, the irony exists that the individuals best able to solve problems are often the least able to explain how they solved them. This is a natural result of having solved similar problems so often that the answers become intuitive. Extensive interviewing of the experts is required to learn how they reach conclusions from the information made available to them.

The process of acquiring the knowledge possessed by the experts began with asking the experts to identify the information needed to determine which deficiencies were present in a pavement. These discussions were guided with questions such as

- What facts do you need to know to determine whether a particular pavement deficiency exists?
- If a piece of information is unavailable, can you still guess at whether or not the pavement deficiency exists, or are you unable to reach a conclusion?
- How precise do you need a piece of quantitative information to be? (For example, is the amount of annual precipitation essential information, or would designation as a wet climate suffice?)
- Why is a particular piece of information important?

Questions such as these prompted the experts to think about the relative significance they attached to various data items. In answering such questions, experts rely heavily on heuristic rules, commonly referred to as rules of thumb. Examples of heuristic rules related to concrete pavement evaluation are

- Longitudinal cracks between the centers of two adjacent lanes are due to either foundation movement or poor longitudinal joint construction.
- Standing water or cattails in the ditches indicate an inadequate ditch grade.

Heuristic rules are generalizations that are true in most, but not necessarily all, cases. By relying on them even though strictly speaking they are not always valid, the expert's reasoning moves rapidly to a tentative conclusion of which the expert is reasonably confident. In applying these rules, what differentiates the expert from less knowledgeable people in the field is that the expert knows from problem-solving experience the ranges of validity of the rules and what other factors that are not included in the rules might also be important.

Decision Trees

As discussions with the experts continued, it became increasingly apparent that a problem solution could not be achieved by extracting as many heuristic rules as possible from the experts and applying these rules to evaluating pavement projects in a random fashion. It appeared far preferable to organize the rules in a manner that simulated the patterns in which the experts used them. In other words, not only the knowledge but also the reasoning used by experts in performing concrete pavement evaluation had to be incorporated in the system.

Decision trees were selected as an appropriate means of exploring the experts' reasoning and incorporating it into the expert system. For each of the 12 major deficiency areas, a decision tree was developed that used the pieces of information identified as important for that area, in order of importance. The use of decision tress was welcomed by the experts as a means of ensuring that the many possible combinations of the data items were investigated to the fullest extent possible.

As stated earlier, problem solving on an expert level is highly intuitive. Research in education and psychology *(3)* indicates that experience in solving a particular type of problem contributes to the development of expertise in solving that type of problem (and to a limited extent, increased skill in solving similar problems in different domains), but does not contribute significantly to increased ability to articulate problem-solving approaches. The ability to explain one's line of reasoning appears to be possessed by different people to different degrees independently of their level of expertise in a particular field.

This reflects the experience of the project staff in developing the decision trees for the 12 major problem areas. The number of times that a decision tree had to be revised before it met with a experts' approval was generally more dependent on its complexity than on who had originally drafted it.

Needed Information

Each of the capabilities envisioned for the expert system had associated with it a need for some type and amount of data. The most significant of these capabilities and their associated data needs are as follows:

1. Expert-level performance. In order to perform at a level approaching that of a human expert, the expert system had to collect sufficient data to determine whether one or more deficiencies existed in each of the 12 major problem areas.
2. Data collection effort. In order for users to consider the system a useful tool for project-level evaluation, the system had to operate with information that was readily accessible to a state highway engineer from office records and an inspection of the project site.
3. Efficiency. In order to make efficient use of engineering resources and computer facilities, the system could collect only data essential to the problem solution.
4. Rehabilitation selection. In order to select appropriate rehabilitation techniques, data on specific distress types and severities were necessary.
5. Cost analysis. Ranking of rehabilitation strategies according to cost requires quantity estimates for the individual rehabilitation techniques, and thus data on specific distress quantities and measurements were necessary.
6. Representative sampling. A 100 percent project survey is unreasonable for preliminary project-level evaluation. Data had to be collected for a smaller portion of a project (e.g., 10 to 30 percent) and extrapolated to represent overall project condition and produce reasonable rehabilitation cost estimates.

Meeting all of these data needs was accomplished in the following way. The experts identified the specific data items they would need in order to determine whether or not the pavement was deficient in any of the 12 major problem areas. They were asked to select only data items that they definitely

needed in order to make a decision, and not include information that would simply be "nice to have." They were also asked to consider whether the data items they were requesting would be accessible to state highway engineers.

Project Survey

The data items that were identified as important were summarized in a project survey for JRCP. The project survey consisted of two parts: inventory data and monitoring data. Inventory data included

- Project identification (state, highway designation, direction of survey, and project limits),
- Climate,
- Thickness design,
- Layer materials,
- Joint design and construction,
- Shoulder design and construction,
- Shoulder design, and
- Traffic.

Monitoring data consists of all the information about the pavement's present condition that must be collected during a field inspection of the project, including

- Ride quality,
- Cracking and corner breaks,
- Transverse and longitudinal joint condition,
- Settlements and heaves,
- Drainage conditions,
- Pumping and faulting,
- Concrete surface condition,
- Joint sealant condition,
- Concrete durability,
- Previous repair, and
- Shoulder condition (AC or PCC).

All inventory data and the ride quality portion of the monitoring data are collected for the project as a whole. The remaining monitoring data are collected on sample units within the project. The recommended procedure is to survey a minimum of 500 ft at each milepost, equal to approximately 10 percent of the project length. However, the expert system can accommodate any number and length of sample units that the engineer feels adequately represent the overall project condition. A set of monitoring data sheets must be completed for each sample unit surveyed; extrapolating overall project condition is then performed by the expert system.

Distress types, severities, and quantities are recorded on the monitoring data sheets in a manner consistent with standard distress identification procedures. Monitoring data must be collected for each traffic lane and shoulder. Each of the lanes and shoulders is evaluated separately by the expert system.

Survey Data Entry

In the office, the data recorded on the project survey sheets are entered into a computer using a full-screen data entry program. The screens created by the program follow the format of the project survey sheets. The data entry program writes the inventory data for the project and the monitoring data for each sample unit to computer files for permanent storage.

A separate data summary program converts the data into the form needed for evaluation by the expert system. The major purpose of the data summary program is to read the distress quantities entered for each sample unit, compute their averages, and extrapolate distress quantities for the entire project length. The data summary program then writes the computed overall project information to file for evaluation by the expert system.

Refining the Solution Approach

Initial development of the project survey sheets and the pavement deficiency decision trees was followed by a painstaking process of review and refinement. In developing the decision trees, additional data items of importance that had to be added to the survey were uncovered. Some data items were not used. Had they been unintentionally omitted, or were they really not as significant as originally thought? Every line of reasoning used in every flowchart was reviewed, discussed, and challenged. If two different values of a data item led to the same conclusion, did that imply that the data item was not significant, or that the reasoning leading to the conclusion was faulty? In some cases, decision trees that were not reasonable or efficient were discarded entirely and redrawn from scratch, using a totally different approach. The project survey sheets were also revised repeatedly, as the system developed and the data needs cited previously became more apparent.

During this refinement period, both the decision trees and the project survey sheets were revised many times. This refining process resulted in dozens of major changes and hundreds of smaller changes that greatly improved the quality of the expert system.

EVALUATION CONCLUSIONS

Need for Evaluation Conclusions

It was originally intended that the evaluation procedure would reach a determination of whether or not a deficiency existed in each of the major problem areas. This intention posed two problems. First, the experts found it too restrictive; they wanted the system to explain to the users how conclusions were reached and why particular factors were important in reaching the conclusions. Second, it was not specific enough to make the evaluation results useful in selecting appropriate rehabilitation techniques and estimating costs.

For these reasons, individual evaluation conclusions were written by the experts for most of the paths in the decision trees. In some cases, the conclusions were written generally enough to apply to more than one combination of the data items.

The decision trees and evaluation conclusions developed for roughness and for transverse and longitudinal joint construction are shown in Figures 1 and 2. Roughness evaluation ratings are defined as follows.

RGH 1: Rideability is acceptable.
RGH 2: Poor rideability is indicated by more than 50 in. of faulting per mile and an unacceptably low PSR for pavement ADT level.
RGH 3: Poor rideability is indicated by 5 in. or more of settlements per mile and an unacceptably low PSR for pavement ADT level.
RGH 4: Poor rideability is indicated by 5 heaves or more per mile and an unacceptably low PSR for pavement ADT level.
RGH 5: Poor rideability is indicated by 25 deteriorated joints per mile or more and an unacceptably low PSR for pavement ADT level.
RGH 6: Poor rideability is indicated by an unacceptably low PSR for pavement ADT level.

Longitudinal joint construction evaluation ratings are defined as follows.

JTC 1: Pavement deterioration may be accelerated by infiltration of water permitted by poor longitudinal joint sealant condition.
JTC 2: A longitudinal joint construction deficiency is indicated by longitudinal joint spalling.
JTC 3: A longitudinal joint construction deficiency, likely because of an inadequate depth of saw cut, is indicated by more than 100 ft of longitudinal cracking per mile.
JTC 4: A longitudinal joint construction deficiency, likely because of late sawing, is indicated by more than 100 ft of longitudinal cracking per mile.
JTC 5: A longitudinal joint construction deficiency, likely because of an inadequate depth of plastic insert placement, is indicated by more than 100 ft of longitudinal cracking per mile.
JTC 6: A longitudinal joint construction deficiency, likely because of use of a plastic joint forming insert, is indicated by more than 100 ft of longitudinal cracking per mile.

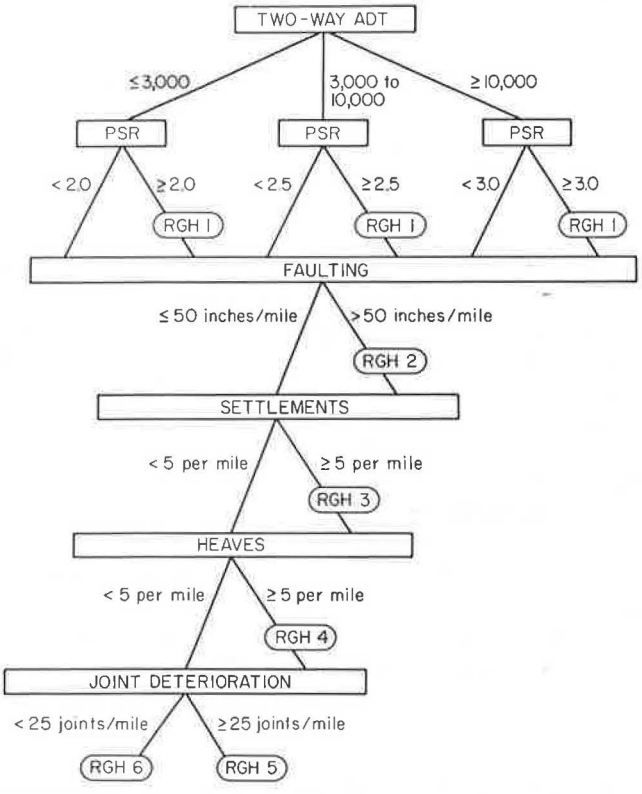

FIGURE 1 Roughness decision tree.

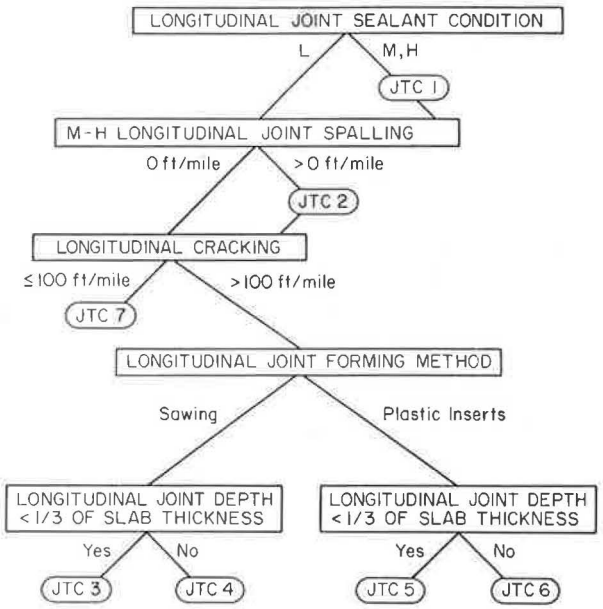

FIGURE 2 Longitudinal joint construction decision tree.

Types of Conclusions

All of the conclusions state as a minimum whether or not a deficiency is indicated by the data and, if so, what factors were significant in reaching this decision. The following conclusion from the drainage decision tree is an example:

> A drainage deficiency is indicated by a wet climate, absence or poor functioning of longitudinal subdrains, and a fine-grained soil base.

An example of multiple paths to a conclusion is the following, from the roughness decision tree. This conclusion can be reached through three different paths, because a difference minimum acceptable PSR is assigned to each of three different ranges of ADT.

> Poor rideability is indicated by 25 or more spalled joints per mile and an unacceptably low PSR for the pavement's ADT level.

The experts believed that some of the conclusions required a little more explanation to justify to the user that the deficiency

was significant enough to warrant corrective action. The following conclusion from the shoulder condition decision tree is an example:

> Excessive dropoff along the lane-shoulder joint constitutes a safety hazard.

In some cases, the experts felt that the evaluation conclusions could not be stated with absolute certainty. In these cases, the conclusions were presented accordingly, with descriptive explanations about the deficiencies and their probable causes. The following conclusion from the transverse joint condition decision tree is an example:

> A high potential for compressive stress buildup and joint deterioration exists, due to the use of Unitube joint forming inserts, the presence of expansive reactive aggregate, and large joint movements associated with the long joint spacing. This may lead to joint blowups and/or spalling.

Number of Possible Conclusions

A total of 114 different evaluation conclusions were written for the 12 decision trees. For a pavement with two lanes in the direction of survey, at least 11 conclusions are reached for the outer traffic lane, at least 10 for the inner lane (longitudinal joint construction and sealant condition are evaluated for the outer traffic lane), and at least 1 for each shoulder, for a total of at least 23 conclusions. More than 23 conclusions are possible because many of the decision trees are capable of reaching multiple conclusions. This multiplicity was permitted in order to indicate when two or more different specific problems grouped within a single deficiency category required corrective action, or when the presence of a single deficiency was supported by two or more lines of reasoning.

EXAMPLE EXPERT SYSTEM PAVEMENT EVALUATION

A 1-mi section of I-74 north of Urbana, Illinois, was surveyed by members of the project staff on August 1, 1986. The pavement consists of 10 in. of jointed reinforced concrete over a dense-graded aggregate base and a silty clay (A-6) subgrade. The joints are doweled and spaced uniformly at 100 ft. The shoulders are asphalt concrete (AC).

This section of I-74 was constructed in 1957. Its current two-way ADT is 26,100 (with 17 percent commercial trucks). Approximately 13 and 3.9 million ESALs have been accumulated in the outer and inner lanes, respectively, over the life of the pavement.

On initial passes over the surveyed section at the posted speed limit, ride quality was rated in each of the two traffic lanes. On subsequent passes, the car was driven slowly along the shoulder while pavement distresses, joint condition, and previous repairs were noted. The condition of the inner and outer shoulders was also noted. The entire project was treated as one sample unit due to its short length. The survey required about 60 min to conduct.

Expert System Evaluation

The survey data were entered into the computer using the full-screen editor and stored on disk. The expert system evaluated the project by reading the data file and solving each of the 12 decision trees to identify deficiencies. Deficiencies were identified in the following areas:

Problem	*Outer Lane*	*Inner Lane*
Structural capacity	yes	yes
Drainage	yes	yes
Foundation movement	no	no
Roughness	yes	no
Concrete durability	no	no
Skid resistance	yes	yes
Joint deterioration	yes	yes
Joint construction	no	no
Load transfer	yes	no
Loss of support	yes	no
Joint sealant deterioration	yes	yes
Shoulder deterioration	yes	yes

The evaluation conclusions generated by the expert system from the survey data for this 1-mi section of I-74 are as follows.

Outer Lane

- Structural deficiency of the pavement is indicated by 700 ft or more of deteriorated transverse cracks per mile.
- Structural deficiency is indicated by a wet or wet-dry climate, a slab thickness of 10 in., and 0.7 million annual 18-kip ESALs.
- A drainage deficiency is indicated by pumping that occurs in a wet climate.
- The pavement shows no indications of either a frost heave problem or swelling soil problem.
- Poor rideability is indicated by an unacceptably low PSR for the pavement's ADT level.
- The pavement shows no indications of significant surface or concrete durability deficiencies.
- Loss of skid resistance is indicated by polished wheel paths.
- A high potential exists for joint deterioration due to poor joint sealant condition permitting infiltration of incompressibles, and large joint movements associated with the long joint spacing.
- Pavement deterioration may be accelerated by water infiltration permitted by poor longitudinal joint sealant condition.
- The pavement shows no indications of a longitudinal joint construction deficiency.
- The pavement shows no indications of a transverse joint construction deficiency.
- Dowels are providing inadequate load transfer at the transverse joints, as indicated by mean transverse joint faulting of more than 0.20 in.
- A load transfer deficiency is indicated at deteriorated transverse cracks by mean crack faulting of more than 0.20 in.
- A load transfer deficiency is indicated at undowelled full-

depth repairs by mean full-depth repair faulting of more than 0.20 in.

- Loss of slab support is indicated by average faulting greater than 0.20 in. at joints and cracks.
- A joint sealant deficiency is indicated by poor joint sealant condition and an inadequate joint sealant reservoir width for the existing sealant type.

Inner Lane

- Structural deficiency of the pavement is indicated by 700 ft or more of deteriorated transverse cracks per mile.
- A drainage deficiency is indicated by a wet or wet-dry climate, absence or poor functioning of longitudinal subdrains, a dense-graded untreated aggregate base, an A-6 subgrade, and heavy traffic of 0.9 million annual 18-kip ESALs.
- The pavement shows no indications of either a frost heave problem or swelling soil problem.
- Rideability is acceptable.
- The pavement shows no indications of significant surface or concrete durability deficiencies.
- Loss of skid resistance is indicated by polished wheel paths.
- A high potential exists for joint deterioration due to poor joint sealant condition permitting infiltration of incompressibles, and large joint movements associated with the long joint spacings.
- The pavement shows no indications of a transverse joint construction deficiency.
- No load transfer deficiency is indicated at transverse joints.
- No load transfer deficiency is indicated at deteriorated transverse cracks.
- No undoweled full-depth repairs are present.
- The pavement shows no indications of loss of slab support.
- A joint sealant deficiency is indicated by poor joint sealant condition and an inadequate joint sealant reservoir width for the existing sealant type.

Outer Shoulder

- Structural deterioration of the AC shoulder is indicated by extensive alligator cracking.
- Deterioration of the AC shoulder is indicated by extensive linear cracking.
- Pumping has resulted in extensive blowhole formation in the AC shoulder.
- Excessive infiltration of water beneath the pavement and AC shoulder is indicated by poor lane-shoulder joint condition.

Inner Shoulder

- Deterioration of the AC shoulder is indicated by extensive linear cracking.
- Pumping has resulted in extensive blowhole formation in the AC shoulder.
- Excessive infiltration of water beneath the pavement and AC shoulder is indicated by poor lane-shoulder joint sealant condition.

Future Pavement Condition

The expert system performed an evaluation of the current condition of this 1-mi section of I-74. Projection of the future condition of the pavement was performed using the concrete pavement evaluation system (COPES) models *(4)*. Using these models, future distress quantities are extrapolated from the current distress data collected during the project survey. Figure 3 shows the predicted progression of joint deterioration over the next 20 years.

The future condition of the inner and outer lanes expressed in terms of number of years remaining before critical levels are reached as predicted by the COPES models is summarized as follows:

	Time to Critical Level (years)	
Distress/PSR	*Outer Lane*	*Inner Lane*
Pumping	now	12
Faulting	now	15
Joint deterioration	10	12
Cracking	now	now
PSR	now	5

Rehabilitation is needed now to correct deficiencies triggered by distress levels that are already critical. The future condition predictions identify the times at which additional deficiencies will exist and will require rehabilitation. This information, along with the actual current distress quantities and projected future distress quantities, is necessary to plan and design rehabilitation needed on the project over the next 20 years.

CURRENT AND FUTURE WORK

Current Work

The expert system for JRCP evaluation is a portion of a larger expert system being developed for evaluation and rehabilitation of all three types of concrete highway pavement (JPCP, JRCP, and CRCP). Future pavement condition prediction will be performed for JRCP and JPCP using models developed under the COPES study *(4)*. The expert system will also use performance prediction models currently being developed for several jointed concrete pavement rehabilitation techniques from data collected on 161 rehabilitated concrete pavements in 24 states. Performance prediction of techniques in the expert system other than these eight (e.g., AC overlay) will use models developed in other studies. Future condition prediction and rehabilitation performance prediction for CRCP will rely on models that have been or are currently being developed for CRCP.

The expert system is currently being documented in manual

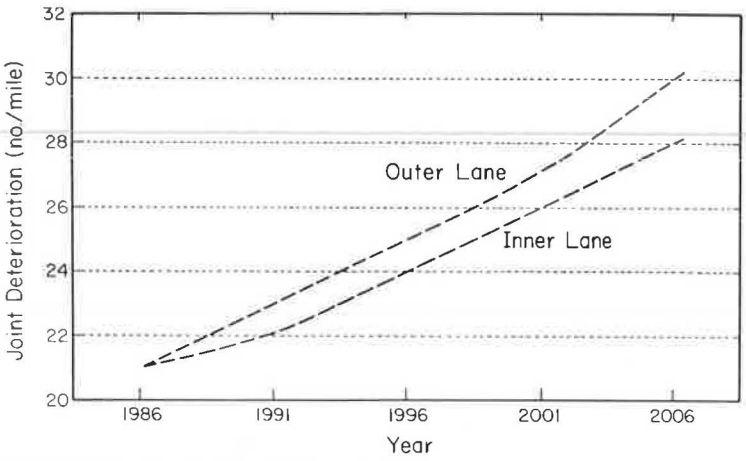

FIGURE 3 Prediction of future joint deterioration for I–74 example.

form and programmed to operate on an IBM-compatible personal computer.

Future Work

Development of large expert systems for research and education purposes is a long-term process. David Waterman, author of *Building Expert Systems (5)*, describes five stages in the evolution of an expert system:

1. Demonstration prototype—a small demonstration system that solves a portion of the problem that will eventually be addressed, suggesting that the approach is viable and full system development is achievable.
2. Research prototype—a medium-sized system capable of credible performance on a number of test cases, but that may be fragile due to incomplete testing and revision.
3. Field prototype—a medium- to large-sized system that has been tested by users in the field and revised until it displays good performance with adequate reliability.
4. Production model—a large system that has been extensively field tested and displays high-quality, reliable, fast, and efficient performance in actual field applications.
5. Commercial system—a production model used on a regular basis in the field that displays near-optimum quality, reliability, speed, and efficiency.

To date, few engineering expert systems have progressed beyond the research prototype stage. This expert system, which is in the demonstration prototype stage, needs to be validated and improved by means of a thorough program of field testing by several state transportation department personnel. Such a testing program would answer the following questions:

- Does the system make decisions with which concrete pavement experts would generally agree?
- Is the logic used in the decision trees correct, consistent, and complete?
- Are the evaluation conclusions adequate for explaining how and why conclusions are reached?
- Are the rehabilitation techniques appropriate for the evaluation conclusions with which they are matched?
- Are the system's outputs well organized, well presented, valid, and of value to the user?
- Is the system efficient and easy to use?

Field testing is a cyclic process that continues through the research prototype stage until the system achieves levels of quality, reliability, speed, and efficiency sufficient to qualify it as a field prototype, suitable for public release.

CONCLUSIONS

1. Concrete pavement evaluation is a complex engineering problem that defies traditional analytical solutions because of the large number of interacting factors involved, suggesting the desirability of a computerized solution method.
2. Concrete pavement evaluation relies heavily on the knowledge and experience of experts in the field for accurate and complete diagnosis of the causes of distress and other pavement deficiencies.
3. Concrete pavement evaluation is an ideal problem for expert system application by which human expertise in pavement evaluation is compiled, formalized, and applied to pavement evaluation problems.
4. A concrete pavement evaluation expert system must incorporate not only the rules but also the reasoning processes used by experts in order to reach conclusions about the presence of several possible pavement deficiencies in an efficient manner.
5. An expert system for concrete pavement evaluation has been developed to the demonstration prototype stage, and application on example problems has demonstrated its feasibility.
6. Extensive field testing and review are needed to improve the quality, reliability, speed, and efficiency of the expert system to the level of a research prototype.

ACKNOWLEDGMENT

The work described in this paper was conducted as part of a study entitled "Determination of Rehabilitation Methods for Rigid Pavements" being conducted for the FHWA by the Civil Engineering Department of the University of Illinois at Ur-

bana-Champaign. The authors wish to express their appreciation to Stephen Forster of FHWA for his assistance.

REFERENCES

1. M. I. Darter, S. H. Carpenter, M. Herrin, E. J. Barenberg, M. R. Thompson, B. J. Dempsey, R. E. Smith, and M. B. Snyder. *Techniques for Pavement Rehabilitation.* National Highway Institute, FHWA, U.S. Department of Transportation, June 1984.
2. M. I. Darter. *Concrete Pavement Condition Survey and Criteria for Method Selection.* National Seminar on PCC Pavement Rehabilitation and Recycling, St. Louis, Mo., 1981.
3. What Makes You an Expert? *Psychology Today*, Vol. 20, No. 7, July 1986.
4. M. I. Darter, J. M. Becker, and M. B. Snyder. *NCHRP Report 277: Concrete Pavement Evaluation System (COPES).* TRB, National Research Council, Washington, D.C., 1985.
5. D. A. Waterman. *A Guide to Expert Systems.* Addison-Wesley Publishing Co., Reading, Mass., 1986.

Publication of this paper sponsored by Committee on Pavement Rehabilitation.

Numerical Assessment of Pavement Test Sections

T. KRAUTHAMMER AND H. KHANLARZADEH

A numerical study was performed at the University of Minnesota for the Minnesota Department of Transportation for assessing and explaining the observed performance of several highway pavement test sections. The test sections that were considered in this study are located in Minnesota near Rothsay, on I-94, and near Olivia, on Trunk Highway 71. For the Olivia site, the objective was to investigate the effect of a thin layer of bituminous bond breaker on the reflective cracking of the new pavement slab, whereas for the Rothsay site the goal was to understand the differences between bituminous-treated bases (BTBs), cement-treated bases (CTBs), and aggregate bases in affecting the pavement behavior and to determine the causes for a relatively poor behavior of pavements on BTBs as compared to pavements on CTBs and aggregate bases. The approach was to use the finite element method and to perform falling-weight deflectometer (FWD) simulations on the test sections. The results from those simulations were compared to FWD test data for model correlation, and finally parametric studies were performed in order to assess the long-term behavior of the pavements under consideration. As a result of the study, preliminary relationships were derived between stress ratios and pavement properties that could affect the long-term pavement behavior. Based on these results, it was possible to provide rational explanations of observed pavement conditions, and to draw significant conclusions on improved procedures for pavement rehabilitation.

This paper is based on a recent study at the Department of Civil and Mineral Engineering at the University of Minnesota for the Minnesota Department of Transportation (MNDOT) in which the performance of several pavement test sections was assessed *(1)*. The general objective of the study was to assist MNDOT to develop optimal methods for rehabilitation of the highway system under its jurisdiction. Two test section sites were considered, one located in the northwestern part of the state on I-94 near Rothsay and the second near Olivia on Trunk Highway (TH) 71 in the southwestern part of the state. At Rothsay, the effect of various types of base materials and thickness on the pavement performance was studied. At the Olivia site in 1977, a 5.5-in. concrete slab over a 1-in. bituminous interlayer as bond breaker was placed on a tapered concrete pavement constructed in 1947. The original pavement consisted of a 22-ft-wide slab, 9 in. thick at the edge and 7 in. thick at the center. The purpose of this test section was to investigate the effect of a bituminous bond breaker on the reflective cracking of the new slab. No further cracking of the old slab was done before placing the new pavement, and after a pavement survey in 1984 it was concluded that virtually no distress existed after nearly 7 years of service. At the Rothsay site, test sections with bituminous-treated bases (BTBs) have performed rather poorly as compared to other sections with aggregate bases or cement-treated bases (CTBs). The purpose of this analytical study was to assist MNDOT in determining the causes for the observed pavement behavior by using an analytical approach based on the finite element method.

Department of Civil and Mineral Engineering, University of Minnesota, 500 Pillsbury Drive S.E., Minneapolis, Minn. 55455.

Previous studies on the analysis of concrete pavement slabs included the work by Chou *(2, 3)* in which the development of a finite element approach for such analyses was described and demonstrated, including the consideration of pavement joint behavior on the slab response. Other researchers also used the finite element method for studying pavement performance and the relationships to design applications. Huang and Wang *(4)* used the modulus of subgrade reaction k obtained from the plate load test for the subgrade characterization, an approach similar to procedures in other studies *(2)*. Tabatabaie and Barenberg *(5, 6)* reported on the development and validation of a finite element code that used a Winkler-type subgrade for studying two-layered cracked pavement sections, including shear transfer across joints or cracks due to aggregate interlock or dowel action. There, too, the initial assumption about the modulus of subgrade reaction was similar to that reported by Chou *(2)* and Huang and Wang *(4)*, but it was later modified by Ioannidis et al. *(7)* who used the concept of the resilient modulus of subgrade reaction K_R, which was based on the subgrade response characterization under repeated impulsive loads.

Extensive information on the finite element method used in this study can be found in books, for example, by Bathe *(8)*. For this study, it was decided to use the commercially available finite element code ADINA *(9)*, which is generally similar to other available multipurpose finite element codes that could be used in a design office environment. The background information on structural dynamics can be obtained from the book by Newmark and Rosenblueth *(10)*, on reinforced concrete structures from the book by Park and Paulay *(11)*, and on foundation dynamics from the texts by Barkan *(12)*, and by Richart et al. *(13)*. The loading conditions used for the experimental part were generated by the well-known falling-weight deflectometer (FWD) method, as discussed in a recent paper by Boutros et al. *(14)* and in the extensive thesis by Foxworthy *(15)*. These loading conditions were later simulated for the finite element analysis based on complete time histories that were obtained experimentally at the sites by MNDOT personnel.

The load from the FWD system is generated by dropping a mass from a selected height. There are four weight levels of 110, 220, 440, and 660 lb, with drop heights from 0.8 to 15 in. for generating equivalent traffic loads of 1,500 to 24,000 lb, respectively. The load induces deflections in the pavement that are derived by integrating velocity-time histories over the load duration. The FWD system produces loads that can be approxi-

mated by a half-sine wave with a duration of 25 to 30 msec, whereas a truck moving at 50 mph creates a loading pulse with durations of about 100 msec *(14)*. Hoffman *(16)* concluded that a stationary nondestructive testing device cannot simulate accurately moving traffic loads; however, the deflections induced by a moving truck compared well with those measured during an FWD test.

APPROACH

The analytical approach for the present study consisted of applying the finite element method for the numerical analyses of the pavement test sections under consideration and comparing the results with experimental data from FWD tests. Once a reasonable agreement was reached between numerical and experimental data and after possible adjustments of the finite element models, it was assumed that the particular model represented accurately the site conditions, and parametric studies of that site were performed for assessing the pavement behavior under given conditions.

FWD LOAD SIMULATION

In structural analysis, the first step is to identify the loading intensity and loading pattern, or configuration. This step includes determination of whether the load is concentrated or distributed and if it is static or dynamic in character. If a dynamic loading condition is present, the load-time history must be known in order to perform the structural or soil-structure interaction analysis. Therefore, it is of utmost importance to have a clear understanding of the loads affecting the pavement. The primary loading on pavements comes from wheel loads on a tire-pavement contact area, and such loads can be simulated using a deflection-based criterion by the FWD equipment *(14, 15)* in which the load is applied dynamically to the pavement while obtaining deflection measurements. The load applied by the FWD was on a circular area, and the problem had to be addressed in three-dimensional (3-D) space. However, in the present modeling the system was assumed to be two dimensional (2-D), and for this reason it was required to convert a 3-D loading case to an equivalent 2-D loading strip configuration for the purpose of comparing the numerical results to those obtained experimentally, as shown in Figure 1. Using the theory of elastic foundation behavior and assuming equal deflections under the two loading cases, an equivalent pressure load for the 2-D case can be found, as follows:

$$(P_{ST}/P_{CR}) = \sqrt{(A_{CR}/A_{ST})} \times (M_{CR}/M_{ST}) \quad (1)$$

where

P_{ST} = pressure applied to strip footing,
P_{CR} = pressure applied to circular footing,
A_{ST} = area of strip footing (1,728 in.^{2}),
A_{CR} = area of circular footing (110 in.^{2})
M_{ST} = influence factor for strip footing (0.68), and
M_{CR} = influence factor for circular footing (0.96).

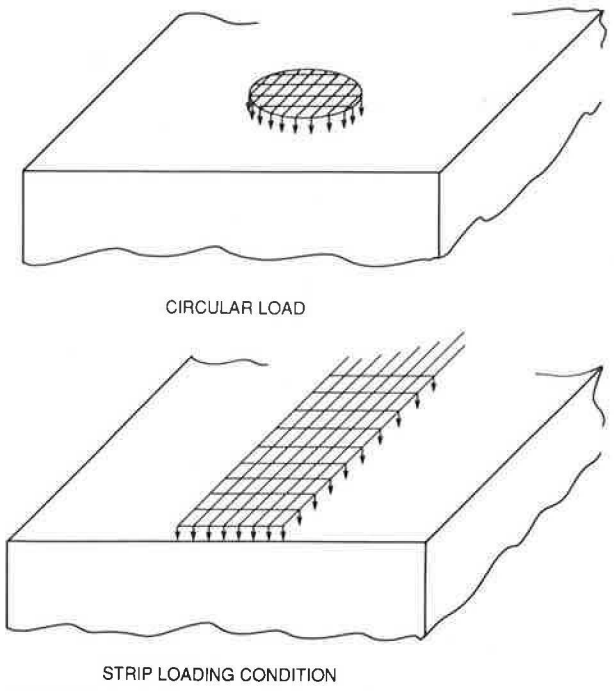

FIGURE 1 3–D versus 2–D loading configurations.

When Equation 1 was applied, it was found that

$$P_{2D} = 0.36P_{3D} \quad (2)$$

In a similar method presented by Bowles *(17)*, the pressure is a function of an influence factor I_W and the least dimension of the footing that leads to a similar solution to the problem.

DAMPING

In dynamic analyses, damping is known to affect the results. Several different methods for obtaining values of damping were examined, for example, those presented by Kuhlemeyer and Lysmer *(18)* and Barkan *(12)*. In order to implement an accurate concept for damping, it was required to obtain a value for a natural frequency of the system ω_n, and to calculate the damping C at each node using the approach proposed by Newmark and Rosenblueth *(10)*, as follows:

$$C = \xi C_{CR} = \xi(2m_E\omega_n) = 2\xi A_E \rho_E \omega_n \quad (3)$$

where

C_{CR} = critical damping of model,
ξ = percent of critical damping,
m_E = mass of the element,
A_E = area of the element, and
ρ_E = mass density of element.

For boundary damping, a value of 100 percent of critical damping was assumed, providing the effect of complete damping in one cycle. For internal nodes, the damping ratios were assumed to be 3, 5, and 7 percent for concrete, asphalt concrete,

and granular materials, respectively. Based on the available information on material properties for the test sites under consideration, the fundamental natural frequencies ω_n were computed with finite element code ADINA *(9)*. The lowest natural frequency of the present model was 1,899 rad/sec for the Rothsay site; this value was inserted into Equation 3 to obtain the damping. The damping was calculated only in the vertical direction because the velocities in the horizontal direction were expected to be small because of the boundary conditions, for which no horizontal motion was allowed. Theoretically, any change in material properties requires the natural frequencies and damping to be recomputed, but it was determined in this study that the largest change in the natural frequency was on the order of 20 percent, and according to Equation 3 it would have an insignificant effect on the nodal damping values. The preceding value for the natural frequency was used to compute the damping and the percentage of the critical damping at every node as required for the ADINA finite element program.

SITE INFORMATION

Rothsay

Twelve test sections with the following properties are located on I-94 near Rothsay, Minnesota.

For the 8-in. slab: dowel diameter = 1 in.; dowel length = 18 in.; dowel spacing = 12 in.; yield strength f_y = 60 ksi. For the 9-in. slab: dowel diameter = 1.25 in.; dowel length = 18 in.; dowel spacing = 12 in. Joints Type C1 were undoweled (first 25 joints in the northern part of each section), whereas joints Type C4 were doweled. Temperature reinforcement, according to AASHTO M55 or M2: dimensions 11 × 18 ft; wire fabric 12 × 6 ft mesh D25 × W23, with f_y = 70 ksi. Tie bars: $^5/_8$ in. in diameter, 30 in. long, and 36 in. of spacing for the L1 joint.

Slab thicknesses: 8 and 9 in.; concrete uniaxial compressive strengths f_C' were from about 3,000 to 7,000 psi with a mean value of 4,944 psi. Slab dimensions: 27 × 12 ft; base thicknesses 5 and 6 in.; base static modulus 15 to 3,000 ksi; and subgrade static modulus 7 to 35 ksi.

Olivia

Test sections were located on TH 71 where 5.5-in.-thick concrete slabs were placed in 1977 over a tapered concrete pavement constructed in 1947. The old pavement consisted of slabs 22 ft wide and 9 in. thick at the edge and 7 in. thick at the center. A 1-in. thickness of bituminous interlayer was placed between the old and the new slabs to serve as bond breaker. The material properties of that site were not well known at the initiation of this study; therefore, a parametric assessment had to be conducted to obtain an accurate set of material properties. The procedure used for this purpose was to simulate FWD tests for the site numerically, to compute the pavement responses for various site conditions, and to determine the site properties from a comparison with experimental data. This approach yielded the following set of material properties, assumed to closely represent those of the actual site conditions, for the present model.

Overlay slab: thickness t_C = 5.5 in.; modulus of elasticity $E_C = 4.5 \times 10^6$ psi; and Poisson ratio $\nu = 0.17$. Bituminous bond breaker: thickness, t_{AC} = 1 in.; E_{AC} = 400 ksi; $\nu = 0.40$. Old slab: thickness, t_{OC} = 8 in. (on average); $E_C = 4.5 \times 10^6$ psi; $\nu = 0.17$. Subgrade soil: thickness t_{SG} = 20 in.; E_{SG} = 140 ksi; $\nu = 0.35$.

THE FINITE ELEMENT MODELS

Rothsay

The model was 64 in. long and had fixed boundaries at the sides and at the bottom, as shown in Figure 2. This finite element mesh consisted of 240 quadrilateral 2-D elements mostly with 4 nodes and 16 quadrilateral elements each having 5 nodes. The mesh was formed to accommodate changes in the thickness of various layers while keeping the element dimension aspect ratios within the 2:1 range. For ease of manipulation and reduction of the computation time, the mesh was divided into 9 element groups. Element Groups 1–4 covered the concrete (32 elements each), Groups 5 and 6 the base (32

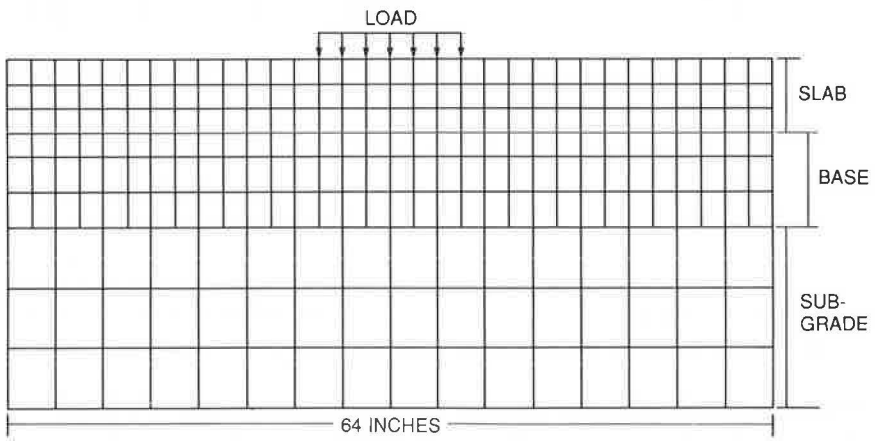

FIGURE 2 Rothsay FE model with element groups.

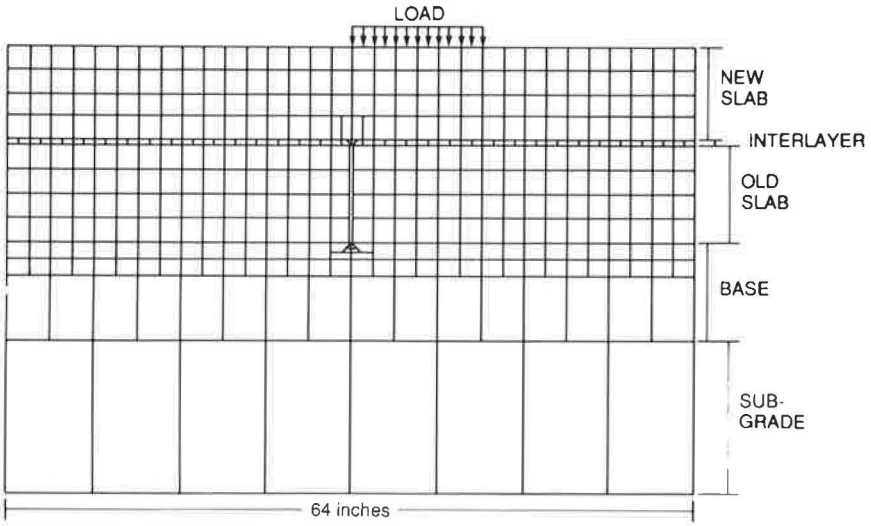

FIGURE 3 Oliva FE model with joint.

elements each), and Groups 7–9 the subgrade soil (16 elements each).

Olivia

This two-dimensional model consisted of 540 nodes with 1,080 degrees of freedom. It was 64 in. long and fixed at its boundaries, as shown in Figure 3. The mesh was divided into 14 element groups in order to reduce computation time as well as for ease of changing layer properties, as follows: 4 element groups for the concrete overlay, 2 for the interlayer (bond breaker), 4 for the old slab, and 4 for the soil. All element dimensions were restricted not to exceed the 2:1 aspect ratio. One joint with an opening of 0.2 in. was introduced at the middle of the old slab with no shear transfer capacity in order to represent an advanced damaged condition.

One of the issues that was addressed during the development of the finite element model was related to the determination of the depth under the pavement that had to be considered in the analysis. Normally, this depth can be determined by computing the distance that a wave would travel in the known simulation time (about 30 msec for the FWD test) from the known seismic velocities of the corresponding materials. Because the seismic wave speed in the present subgrade material is about 2,000 ft/sec, a depth of about 60 ft would be required in the model. This value is not a practical one, and therefore, most of the required 60 ft could be replaced with linear springs having the same stiffness. When this replacement is combined with nonreflecting boundary conditions that can eliminate artificial wave reflections from the model boundaries, the simulation of the problem is expected to be accurate. Furthermore, in the present case the aim was to understand the pavement response as affected by the base material; therefore, although the model considers only changes in the pavement and base, if the subgrade simulation is maintained the same for each site, it may be expected that the relative responses would represent the observed site conditions.

RESULTS

Rothsay Test Sections

Because the elastic properties of concrete, aggregate, soil, and treated bases exhibited a range of values depending on the state of stresses, temperature, compositions, and so forth, the exact properties of the pavement layer at the time of the FWD tests were not known. As a result, an attempt was made to converge numerically to these material properties by performing the numerically simulated FWD tests with the finite element code. Several ranges of these values were tried until both analytical deflection (under the center of applied load) and measured deflection (at the center of the loading plate and at the middle of the slab) were in good agreement. At that time, it was assumed that the material properties that corresponded to the closest numerical values would represent a reasonable approximation of the real site conditions. One of the test sections was chosen for verifying the material properties for this site, and for that section the average measured deflection was equal to 6.22 milli-in., whereas the computed deflection was equal to 6.3 milli-in. for the following material combination: slab thickness $t_C = 9$ in.; $E_C = 5 \times 10^6$ psi; aggregate base thickness $t_{AGG} = 6$ in.; $E_B = 25 \times 10^4$ psi (including dynamic enhancement); subgrade thickness $t_{SG} = 10$ in.; and $E_{SG} = 14 \times 10^4$ psi. Once the site properties were chosen, it was possible to perform a parametric study for assessing the causes for the observed site performance *(19, 20, 22)*.

The criteria selected for assessing the concrete pavement performance were related to the concrete behavior under fatigue conditions. It is an established fact that the concrete fatigue life is a function of the tensile stress ratio (as will be further defined herein). It was shown *(19)* that when this ratio was under 0.55 the concrete could endure virtually an unlimited number of stress repetitions. A similar assumption was adopted for the shear stress ratio, and conclusions regarding the pavement behavior were based on these criteria. The objective of selecting a number of variations of layer thicknesses and

their elastic properties was to examine their effect on the maximum stresses produced by the application of numerically simulated FWD loads.

The variation of the layer properties considered here was in the following range: thickness of concrete slab 8 and 9 in.; concrete modulus of elasticity 4×10^6 and 5×10^6 psi; base thickness 5 and 6 in.; base dynamic modulus 100 to 4,000 ksi; subgrade thickness 10 in.; and subgrade static elastic modulus 35 to 70 ksi. Based on deflection correlation, selected subgrade thickness and its dynamic modulus were 10 in. and 140 ksi, respectively, kept constant for all test sections. Therefore, only four variables were left to be considered, as follows:

1. Concrete thickness t_C (2 values),
2. Concrete modulus of elasticity E_c (2 values),
3. Base thickness t_B (2 values), and
4. Base elastic modulus E_B (100, 150, 250, 300, 500, 750, 1,000, 1,500, 2,000, 2,500, 3,000, 3,500, and 4,000 ksi).

This set of variables brought the total number of combinations to $2 \times 2 \times 2 \times 13 = 104$. However, Variables 1 and 3 (concrete and base thicknesses) were independent, and there was one additional constraint placed on E_B, that when 6 in. of base were used, E_B assumed only two values (150 and 250 ksi, representing the aggregate base), but when 5 in. of base were used, only 11 different values of E_B were considered. Taking these constraints into account and using a partial factorial plan *(20)*, 52 combinations remained, but only 39 out of these combinations were considered in this part of the study. These cases were analyzed, and each finite element computation required 130 to 140 sec of CPU time on an IBM 4341.

As was mentioned earlier, two criteria were selected for assessing the pavement performance, as follows:

1. The ratio of maximum tensile stress (σ_{yy}) of the concrete slab to the tensile strength of concrete represented by the modulus of rupture MR, and
2. The ratio of maximum shear stress (σ_{zy}) to the concrete shear strength v_C represented by $3.5\sqrt{F_C'}$.

After the stress ratios and maximum deflections were computed as functions of base moduli, regression analysis was performed to relate each of the stress ratios to the pavement variables. For the data, a linear regression equation produced the best results.

$$Y = a_0 + a_1X_1 + a_2X_2 + a_3X_3 + a_4X_4 \tag{4}$$

For the tensile stress ratio σ_{yy}/MR, the relationship derived was

$$\sigma_{yy}/MR = 0.55839 - 3.3525 \times 10^{-2}\ t_C - 2.9616 \times 10^{-8}\ E_C + 0.1428\ t_B - 2.0975 \times 10^{-7}\ E_B \tag{5}$$

For this relationship, the sample index of correlation was 0.9133 and the standard error was 0.0284; the standard errors of the coefficients were $\sigma_{a0} = 0.5022$, $\sigma_{a1} = 0.0044$, $\sigma_{a2} = 4.4 \times 10^{-8}$, $\sigma_{a3} = 6.21 \times 10^{-8}$, and $\sigma_{a4} = 1.8 \times 10^{-8}$.

For the shear stress ratio σ_{zy}/v_C, the relationship derived was

$$\sigma_{zy}/v_C = 1.0832 - 4.4281 \times 10^{-2}\ t_C - 7.7 \times 10^{-8}\ E_C + 1.85 \times 10^{-2}\ t_B + 7.6322 \times 10^{-9}\ E_B \tag{6}$$

For this case, the sample index of correlation was 0.8803 with a standard error of 0.0284; the standard errors of the coefficients were $\sigma_{a0} = 0.0946$, $\sigma_{a1} = 0.00826$, $\sigma_{a2} = 8.273 \times 10^{-9}$, $\sigma_{a3} = 1.1698 \times 10^{-2}$, and $\sigma_{a4} = 3.391 \times 10^{-9}$.

The present relationships are in a preliminary form, representing an attempt to verify whether the approach leads to useful results. These are purely descriptive equations and the standard error of the coefficients should not be interpreted in a usual statistical sense because of the fact that the random sampling assumptions were not met. The two relationships represent the effects of changes in any one of four variables on the stress ratios, and may have many useful applications in the future, but only after a more fundamental statistical study is performed. In their modified form, such relationships could be

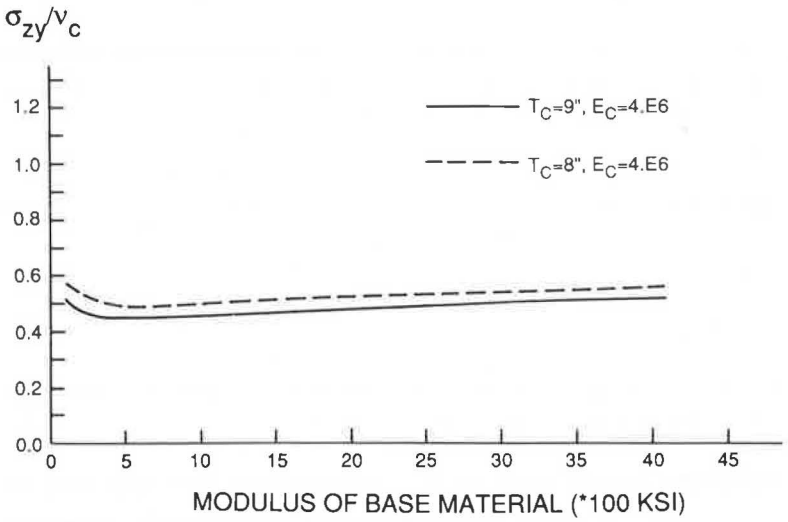

FIGURE 4 Shear stress ratios for various base materials and lower concrete strength.

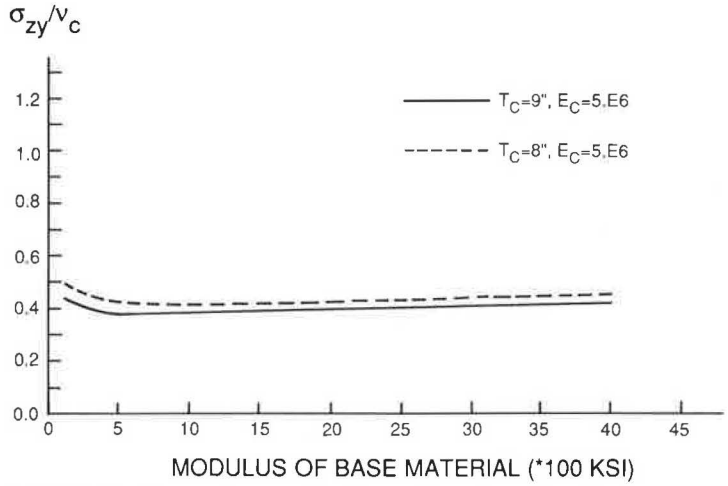

FIGURE 5 Shear stress ratios for various base materials and higher concrete stregth.

used to relate pavement life to the traffic data by using, for example, the Portland Cement Association procedure in which the number and intensity of traffic loads are related to the fatigue life of the pavement system. They may also be used for deriving equivalency factors to convert one type of material to another. For example, one may wish to know for a given pavement life how many inches of a base material could be replaced by 1 in. of concrete slab, and vice versa. However, the use of these equations is not recommended until a complete statistical combination of pavement layer properties is included in the analysis, because equations of this type are considered adequate only when the sample index of correlation is not lower than 0.95. For the present relationship, values were 0.9133 and 0.8803.

As shown in Figure 4 and 5, the shear stress ratio seldom exceeds the value 0.55. This value was attained only once, when slab thickness was 8 in., concrete modulus 4×10^6 psi, and base modulus ≤200 ksi; consequently, one should pay more attention to the tensile stress ratio. Plots of maximum tensile stress over modulus of rupture versus base elastic dynamic modulus, as presented in Figures 6 and 7, revealed that when the dynamic modulus of the base was larger than 900 ksi, the stress ratio was smaller than 0.55; therefore, the pavement slabs should be able to endure virtually an unlimited number of load repetitions.

CTBs normally have moduli in excess of 900 ksi (the range of CTB moduli is 1,000 to 34,000 ksi under static loading conditions); therefore, there should not be a considerable slab deterioration due to base support values. On the other hand, BTBs normally exhibit support moduli in the range of 100 to 2,000 ksi, depending on the mix composition and temperature. Typical values of BTB moduli are 400 to 500 ksi. This range is particularly important during hot summers when BTB moduli decrease to their lower values. In the late spring and early summer, there could be large temperature differentials between day and night. When the base is warm while the top slab

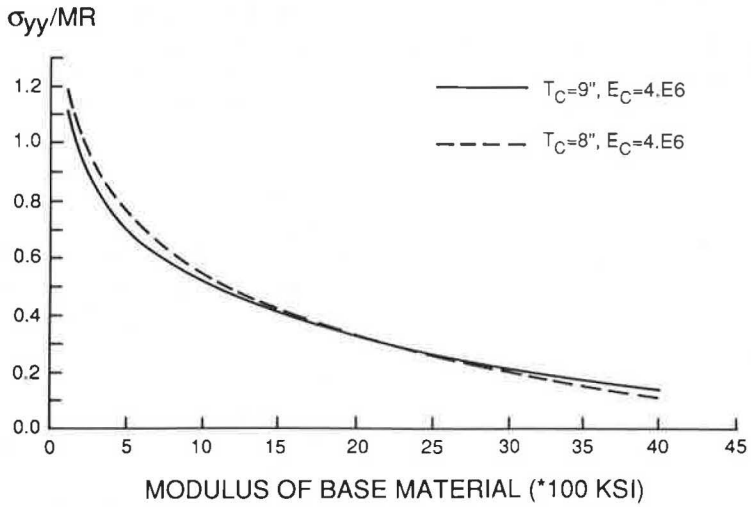

FIGURE 6 Tensile stress ratio for various base materials and lower concrete strength.

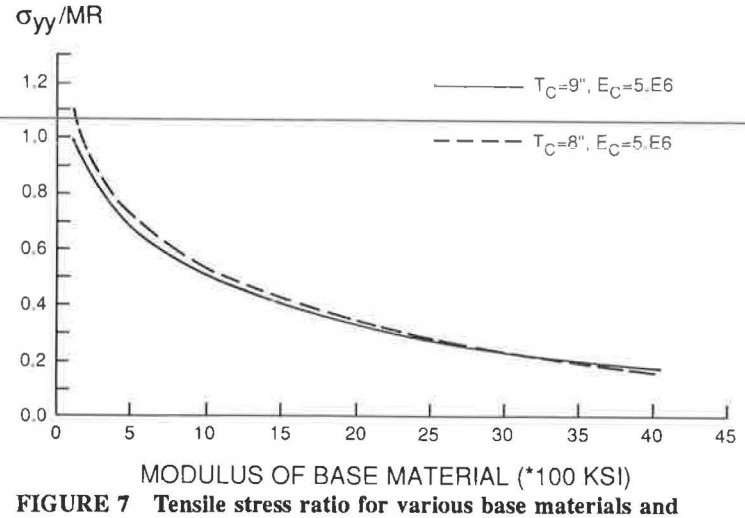

FIGURE 7 Tensile stress ratio for various base materials and higher concrete strength.

surface is cold, the temperature gradient across the thickness of the slab causes the slab to curl up and produces tensile stresses at the top of the slab. At the same time, the base retains a higher temperature, hence, a low modulus. When the traffic load is applied to the pavement as shown in Figures 8a and 8b, the combination of curling stress and loading stresses may cause enhanced stresses along a line parallel to the traffic flow in the slab central region, cracking the slab. This type of crack was observed at the Rothsay test site where the slab was constructed over BTBs. Because the stresses induced by the traffic loads at the surface of the slab tended to be higher for lower base moduli, it became clear that the warmer the base the more severe would be the damage. For example, it was observed from the present results that when E_B was 100 ksi the peak tensile stress at the surface of the slab was 709 psi, whereas when E_B was 1,000 ksi the stress was only 417.9 psi.

The results shown in Figures 6 and 7 suggest that the benefit of a thicker slab diminishes as the base support value increases. For example, increasing the slab thickness from 8 to 9 in. (an increase of 12.5 percent) results in a decrease of about 9 percent in the tensile stress ratio for $E_B \leq 100$ ksi, whereas the same change in slab thickness decreases the stress ratio only by 3.6 percent when E_B is about 850 ksi. The beneficial effect of the thicker slab continuously decreases as the base modulus increases and totally vanishes when E_B is about 1,800 ksi. From this point on, there is a negative effect on the tensile stress ratio as a result of increasing the slab thickness. This phenomenon can be explained by using the theory of beams on elastic foundations *(21)* in which a plot of the tensile stress in the beam as a function of the base reaction modulus for various beam thicknesses yields curves that are not parallel to each other. Therefore, locations on these curves can be defined where increasing the beam thickness results in an increase of the tensile stress for a given base material.

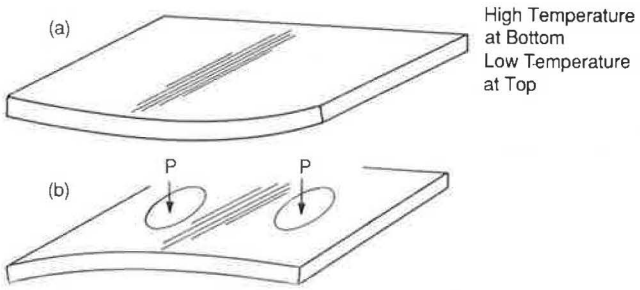

FIGURE 8 Combination of (a) curling effects and (b) traffic loads.

Olivia Test Section

The goal of this part of the analytical study was to investigate the effectiveness of the rehabilitation procedure that had been used, and to demonstrate qualitatively how changes in slab and bond breaker thicknesses and their elastic properties in overlaying materials affect the stresses in the pavement and its long-term behavior. For this task, an approach similar to that used at the Rothsay site was adopted. The preliminary frequency analysis was performed, the natural frequencies were determined, and the fundamental natural frequency (2,580 rad/sec) was used for the damping computations. After the finite element mesh was updated accordingly, the maximum deflection at the center of the slab was computed and compared to the measured data obtained by FWD tests for the same location. Elastic material properties were adjusted until a reasonable match was achieved between the measured and computed deflections. At that point, the model was ready for the parametric analysis in which the old pavement properties were kept constant while changes were made in the thicknesses and material properties of the new slab and the bituminous bond breaker, as follows. New slab thicknesses of 5.5, 6, 7, and 8 in.; bituminous interlayer thicknesses of 0, 0.5, and 1 in.; and bitumen moduli of elasticity of 100, 300, 500, 800, and 1,000 ksi.

A full factorial plan was implemented to account for all combinations of the layer properties, their interaction effects were obtained, and the computations were performed for a total of 33 combinations. (Each computation required about 140 sec of CPU time on an IBM 4341.) The results are presented in

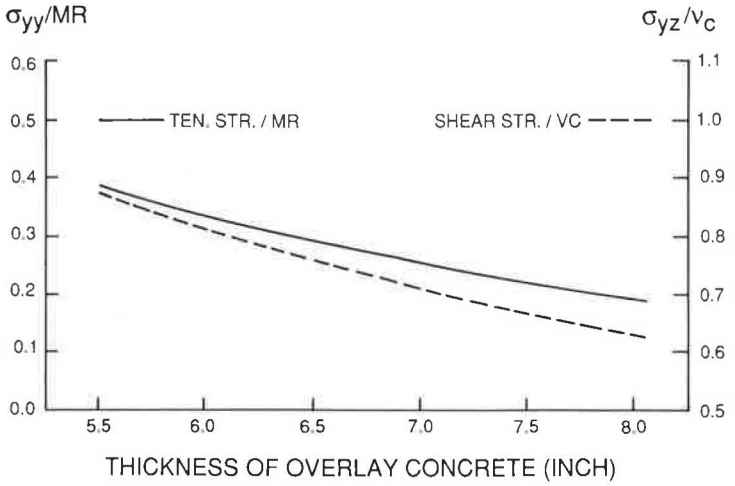

FIGURE 9 Stress ratios without AC interlayer at Oliva.

Figures 9–13. The load was modeled in the same way as were the Rothsay test sections. However, for this section it was determined that the location of the load that produced the most critical stresses was not at the center of the model, but as a result of introducing the pavement joint the critical stresses were obtained when the load was placed next to the joint.

It is shown in Figure 9 that when no bituminous bond breaker was provided the tension stress at the bottom of the new slab was insignificant as far as concrete fatigue was concerned. This result was noticed also in the analysis of the Rothsay site. At Rothsay, it was determined that when the base modulus exceeded 900 ksi the tensile stress ratio at the critical location was less than the fatigue limit of 0.55 at which damage to the concrete would accumulate because of load repetitions. However, at the Olivia site the shear stress ratio for any thickness of new slab was >0.85; therefore, a high shear stress ratio was the dominant factor in determining the life of the structure and the crack propagation when no interlayer was provided.

Change in the tensile stress ratio as a function of overlay thickness and modulus of interlayer is shown in Figure 10. For the thicker slab, the tensile stress ratio was smaller when the modulus of interlayer was 300 ksi or more. Also, the tensile stress ratio under this condition remained less than the 0.55 limit, and should not be of concern even when 1 in. of AC interlayer is provided, as shown in Figure 10. When 1 in. of interlayer bond breaker was provided, the tensile stress ratio exceeded the 0.55 limit only when the interlayer modulus was in the range of up to 150 ksi (Figure 10). This modulus of interlayer is seldom achieved in the northern part of the United States because of the cooler climate. Also, the stresses due to temperature gradient across the slab thickness and those induced by the traffic load tend to cancel part of the tensile stresses at the bottom of the slab. The tensile stress at the top of the slab due to traffic load was limited because of interlayer confinement that resulted in small deflections. When the interlayer thickness was reduced to 0.5 in., the tensile stress ratio

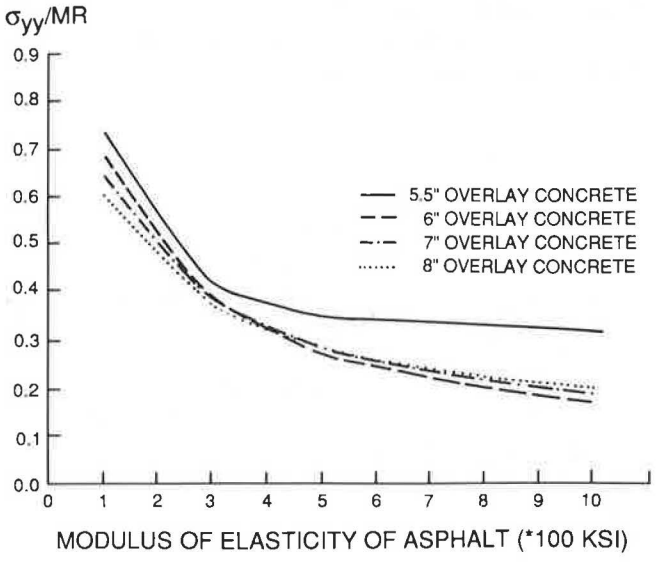

FIGURE 10 Tensile stress ratios for 1.0-in. AC interlayer.

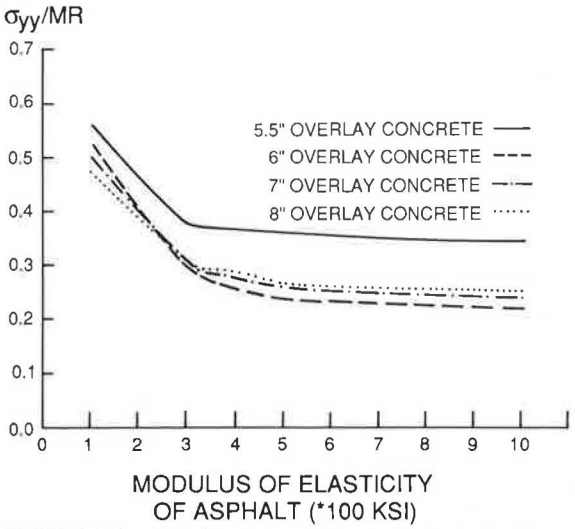

FIGURE 11 Tensile stress ratios for pavement with 0.5 in. of AC interlayer.

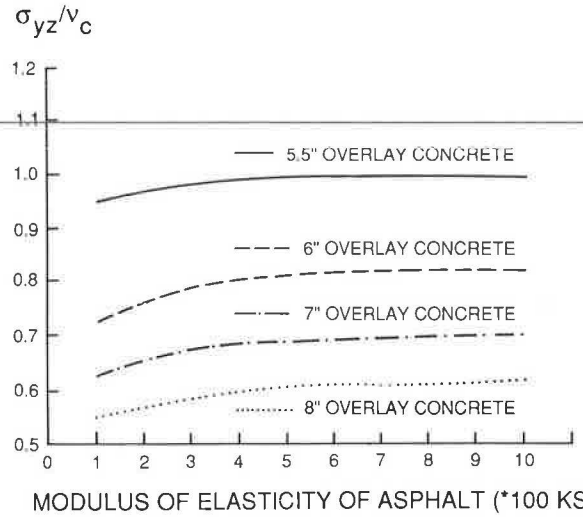

FIGURE 12 Shear stress ratios for pavement with 1.0-in. AC interlayer.

improved as shown in Figure 11. Having a too-thick AC interlayer would increase the tensile stress ratio, so this condition should be assessed for each site during the overlay design.

The modulus of bond breaker and its thickness affected the shear stress ratio as shown in Figures 12 and 13, in which 1 in. of interlayer and 8 in. of concrete slab exhibit a much lower shear stress ratio at every temperature (i.e., at any modulus of interlayer bond breaker), and a greater modulus of interlayer has a small effect on the shear stress ratio when 1 in. of AC interlayer is provided. Under this condition (large E_{AC} and thin interlayer), the effect of bond breaker diminishes and approaches that of no stress relief layer as shown in Figure 9. Therefore, when designing the mix for a stress relief layer, the negative effect of stiff AC mixes on the shear stress ratios should be considered.

All these cases were computed with an open joint; that is, there was no shear transfer across the joint. This assumption may not be correct for all cases, but because the old pavement was assumed to be damaged significantly, it seemed to be justified. Furthermore, any introduction of shear transfer would lead to lower shear stress ratios; thus the present results can be considered to represent relatively more severe pavement damage conditions at the site.

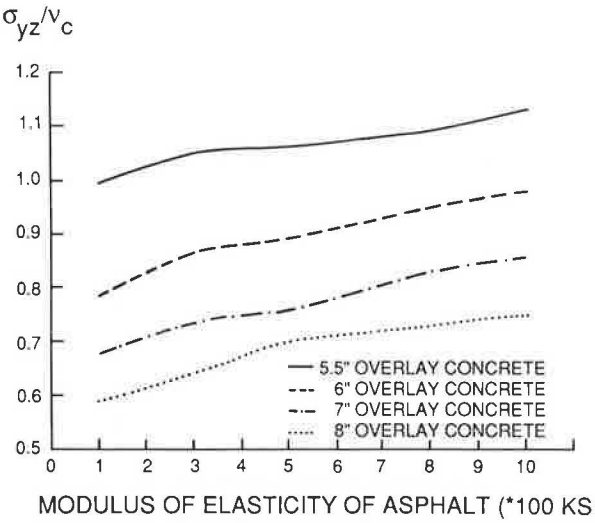

FIGURE 13 Shear stress ratios for pavement with 0.5-in. AC interlayer.

CONCLUSIONS AND RECOMMENDATIONS

The application of the finite element method has been demonstrated for the analysis of layered pavement systems that included several types of materials and site conditions. In this analysis, the loading condition that was used simulated in two dimensions the three-dimensional FWD-induced loads. Special attention was devoted to preserving the dynamic characteristics of the problem and the site geometry. The results obtained appear to be reasonable compared to those reported from previous studies. They compared well with the experimental data and observations at the test sites. Based on the calculated results, the following recommendations were suggested:

1. For a new pavement that may have a low subgrade support, using a cement-treated base for economical crack control is recommended. The experiences gained in Minnesota and Michigan do not support the use of BTBs. When BTBs are deemed to be the only viable option, the designer should take into account the potential temperature differences over various 24-hr periods. When the temperature variation is relatively large, the use of less temperature-susceptible bituminous materials is urged. Also, substantial saving could be realized by providing a thinner slab when CTBs with moduli of 900 ksi or more are used.
2. In overlay design, it appears that the best policy of controlling either tensile- or shear-induced reflective cracking is to provide 1 in. of bituminous interlayer with a small (under 500 ksi) modulus of elasticity as bond breaker.
3. The results of this parametric study suggest that in overlay design tensile stresses are usually of little importance, and that only shear stresses may reach a damaging magnitude. The thicker the slab the less is the shear stress ratio. However, because of economical considerations slabs of more than 7 in. are not constructed; therefore, the interlayer modulus should be decreased as the slab thickness is reduced.

ACKNOWLEDGMENTS

This paper was prepared from a study performed at the Department of Civil and Mineral Engineering, University of Minnesota. The project was sponsored by the Minnesota Department of Transportation (MNDOT) with G. Cochran as project coordinator.

The authors express their appreciation to the personnel at MNDOT for their cooperation and support during this study. The computations were performed on an IBM 4341 at the Department of Civil and Mineral Engineering, University of Minnesota. The authors wish to thank the computer facilities personnel for their cooperation. Also, thanks are due to M. I. Darter and to M. R. Thompson of the University of Illinois at

Urbana for their comments during several discussions on the subject. Finally, the authors wish to thank J. Lin for his assistance.

REFERENCES

1. T. Krauthammer and H. Khanlarzadeh. *Pavement Rehabilitation Evaluation by Analysis of Minnesota Test Sections*. Report ST-86-03. Department of Civil and Mineral Engineering, University of Minnesota, Minneapolis, Aug. 1986.
2. Y. T. Chou. *Structural Analysis Computer Program for Rigid Multicomponent Pavement Structures with Discontinuities—WESLIQID and WESLAYER*. Report GL-81-6, Parts 1–3. U.S. Army Corps of Engineers Waterways Experiment Station, Vicksburg, Miss., May 1981.
3. Y. T. Chou. Stress Analysis of Small Concrete Slabs on Grade. *ASCE Journal of Transportation Engineering*, Vol. 110, No. 5, Sept. 1984, pp. 481–491.
4. Y. Huang and S. T. Wang. Finite Element Analysis of Concrete Slabs and Its Implications for Rigid Pavement Design. In *Highway Research Record 466*, HRB, National Research Council, Washington, D.C., 1973, pp. 55–69.
5. A. M. Tabatabaie and E. J. Barenberg. Finite Element Analysis of Jointed or Cracked Concrete Pavements. In *Transportation Research Record 671*, TRB, National Research Council, Washington, D.C., 1978, pp. 11–19.
6. A. M. Tabatabaie and E. J. Barenberg. Structural Analysis of Concrete Pavement Systems. *ASCE Journal of Transportation Engineering*, Vol. 106, No. TE5, Sept. 1980.
7. A. M. Ioannidis, E. J. Barenberg, and M. R. Thompson. Finite Element Model with Stress Dependent Support. In *Transportation Research Record 954*, TRB, National Research Council, Washington, D.C., 1984, pp. 10–16.
8. K. J. Bathe. *Finite Element Procedures in Engineering Analysis*. Prentice-Hall, Englewood Cliffs, N.J., 1982.
9. *ADINAT: A Finite Element Program for Automatic Dynamic Incremental Nonlinear Analysis*. Report AE 81-1. ADINA Engineering, Watertown, Mass., Sept. 1981.
10. N. M. Newmark and E. Rosenblueth. *Fundamentals of Earthquake Engineering*. Prentice-Hall, Englewood Cliffs, N.J., 1971.
11. R. Park and T. Paulay. *Reinforced Concrete Structures*. John Wiley & Sons, New York, 1975.
12. D. D. Barkan. *Dynamics of Bases and Foundations*. McGraw-Hill, New York, 1962.
13. F. E. Richart, Jr., J. R. Hall, Jr., and R. D. Woods. *Vibrations of Soils and Foundations*. Prentice-Hall, Englewood Cliffs, N.J., 1970.
14. S. Boutrus, T. G. Davis, and M. S. Mamlouk. Dynamics of Falling Weight Deflectometer. *ASCE Journal of Transportation Engineering*, Vol. 111, No. 6, Nov. 1985, pp. 618–632.
15. P. T. Foxworthy. *Concepts for the Development of a Nondestructive Testing and Evaluation System for Rigid Airfield Pavements*. Ph.D. thesis, Department of Civil Engineering, University of Illinois at Urbana-Champaign, June 1985.
16. M. S. Hoffman and M. R. Thompson. Comparative Study of Selected Nondestructive Testing Devices. In *Transportation Research Record 852*, TRB, National Research Council, Washington, D.C., 1982, pp. 32–41.
17. J. E. Bowles. *Foundation Analysis and Design*, 3rd ed. McGraw-Hill, New York, 1982.
18. R. L. Kuhlemeyer and J. Lysmer. Finite Dynamical Model for Infinite Media. *Journal of the Soil Mechanics and Foundations Division*, ASCE, Aug. 1969, pp. 859–877.
19. E. J. Yoder and M. W. Witczak. *Principles of Pavement Design*, 2nd ed. John Wiley & Sons, New York, 1975.
20. W. G. Cochran and G. M. Cox. *Experimental Design*, 2nd ed. John Wiley & Sons, New York, 1957.
21. M. Hetenyi. *Beams on Elastic Foundations*. The University of Michigan Press, Ann Arbor, 1979.
22. H. Lotfi and M. W. Witczak. Dynamic Characterization of Cement-Treated Bases and Subbase Materials. In *Transportation Research Record 1031*, TRB National Research Council, Washington, D.C., 1984, pp. 41–45.

Publication of this paper sponsored by Committee on Pavement Rehabilitation.

Development of a Distress Index and Rehabilitation Criteria for Continuously Reinforced Concrete Pavements Using Discriminant Analysis

CHIA-PEI CHOU AND B. FRANK MCCULLOUGH

Discriminant analysis is applied to developing the distress index and rehabilitation criteria of the network-level pavement management system for continuously reinforced concrete pavements in Texas. The results are intended to provide the Texas State Department of Highways and Public Transportation with guidelines for evaluating the present pavement conditions and for scheduling rehabilitation. For the discriminant analysis, historical condition survey data were evaluated and separated into two groups, overlaid and nonoverlaid pavements, for which detailed descriptions were given. Each set of data comprised several distress manifestations. A discriminant equation was derived from the analysis that linearly combined the distress manifestations and forced the calculated scores Z″ of the two pavement groups to be as statistically different as possible. The relative magnitudes of Z″ could then be used as a distress index. Several modifications were made in the derivation of the discriminant equation in order to minimize the overlapping area of the distribution of the Z″ scores of the two groups. For the final equation developed, the Z″ scores ranged from −1.8 to 1.0, with zero as the criterion for rehabilitation. Thus, a pavement would be classified as a candidate to be overlaid if its distress index was less than zero. With these results, there was a 92.6 percent confidence that any pavement section would be assigned to the group it actually belonged to. Although some unrealistic assumptions were made in this study, the prediction results obtained were encouraging. It is believed that this approach is a further step in the evaluation of pavement distress condition.

The total expenditures required to maintain and rehabilitate pavements in the United States have been increasing rapidly in the past years primarily because most highway sections that were built in the 1960s and 1970s have gradually reached their terminal serviceability condition. Because of the large amount of money involved, improvements in management and technology for the maintenance and rehabilitation of pavements result in significant savings.

In this paper, the use of distress concepts in the pavement management system (PMS) for rigid pavements is discussed. Special emphasis is focused on the application of discriminant analysis techniques *(1)* to the evaluation of the distress condition of continuously reinforced concrete pavement (CRCP) for the purpose of defining the level of pavement performance and determining criteria for major rehabilitation. This scheme is intended to help the Texas State Department of Highways and Public Transportation (SDHPT) in the management of its highway network.

Department of Civil Engineering, The University of Texas at Austin, Austin, Tex. 78712.

BACKGROUND

Review of existing schemes for maintenance and rehabilitation management revealed that the present serviceability index (PSI) was used nationwide for deciding whether a major rehabilitation or an overlay was necessary. The PSI measure developed by Carey and Irick was used at the AASHO road test *(2)*. They showed that the serviceability of a pavement is largely a function of its roughness.

However, a study has been made of a sample of the different degrees of complexity in the existing network-level maintenance and rehabilitation prioritization methods *(3)*. It was concluded that a scheme that uses only the serviceability index is not applicable to CRCP in Texas. The serviceability history of a pavement with heavy maintenance does not appear to change with time or traffic, whereas the distress condition does (Figures 1 and 2). Each point in the figure represents a surveyed section of CRCP in Texas *(4, 5)*. The number of failures (punchouts and patches) per mile was obtained from the records of the CRCP condition surveys performed in Texas in 1974 and 1978 and described in the following sections. The most likely reason for the consistency over time of the serviceability index is the continuous repair of the highway sections by SDHPT staff. This routine maintenance provided tre-

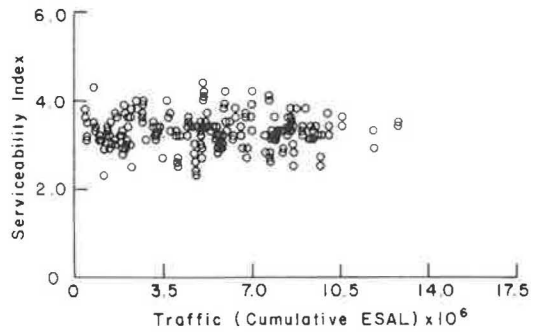

FIGURE 1 Serviceability index versus traffic applications in both directions for Texas CRCP sections surveyed in 1974 and 1978.

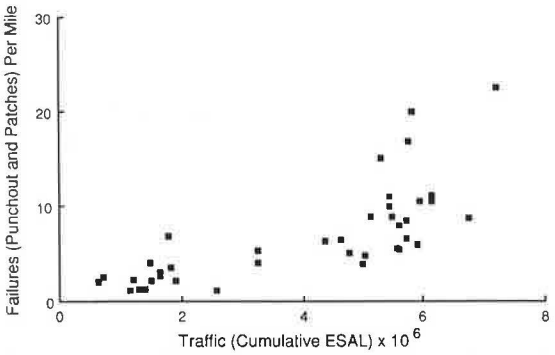

FIGURE 2 Number of failures (punchouts and patches) per mile versus traffic applications in both directions for Texas CRCP sections surveyed in 1974 and 1978.

mendous improvements in pavement roughness, which plays a relatively important role in the serviceability index. Therefore, it is not uncommon for a pavement section to be approaching the end of its life from the structural or economical point of view while the riding quality remains unchanged. Thus, the use of distress measures may be a more realistic way to evaluate a pavement's terminal condition. The development of a distress index to indicate the present pavement condition, therefore, becomes an important task.

In order to obtain a complete data base on the changes in highway distress, a comprehensive condition survey of the CRCP in Texas has been conducted biyearly since 1974. Figure 3 shows the SDHPT districts that were included in the distress condition survey. Several distress manifestations were collected, namely, minor spalling, severe spalling, minor punchout, severe punchout, and repaired patches; the latter were further grouped into asphalt cement, portland cement concrete, and failure patches. Patches result from pavement maintenance. Because the number of patches affects the decision to overlay any particular pavement section, a patch is considered as a distress manifestation in this study.

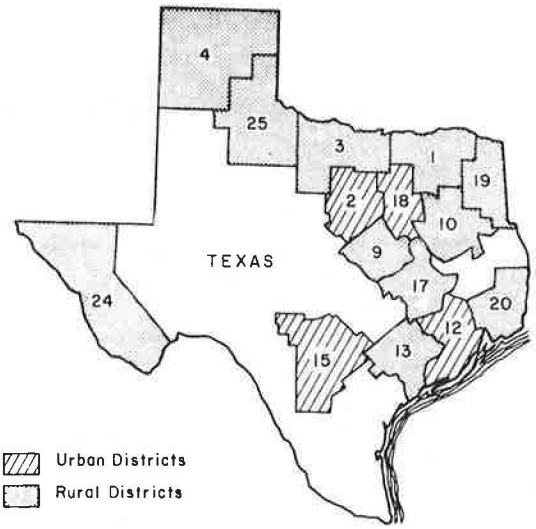

FIGURE 3 Location of rural and urban districts surveyed to collect CRCP information.

The classification of minor or severe is dependent on the size and severity of the distress. For example, a minor punchout is defined as a condition where, although closely spaced transverse cracks are linked by longitudinal cracks to form a block, no sign of movement under traffic is apparent. A severe punchout is recorded when the block moves under traffic. The surrounding cracks will be fairly wide and signs of pumping around the edge of the block may be apparent.

Data were recorded as the cumulative amount of various distress manifestations for every 0.2 mi from the starting point of each surveyed section. Section lengths vary from a fraction of a mile to more than 15 mi. After the condition survey data had been collected and stored, data were reduced for the preparation of the statistical analysis, as follows.

First, the average value of each distress manifestation of every pavement section for each survey year was calculated. This reduced the original survey data of a 10-year period to 1,365 data points. Each datum, representing a pavement section of a certain survey year, was composed of five numbers; each number represented the mean value of a distress manifestation.

It was found that some pavement sections were overlaid in the interval between two successive survey years. No data could be collected after the overlay because the distress could not be seen. Therefore, surveyed sections were grouped into two categories, overlaid and nonoverlaid pavements, and data collected before overlay were used to determine reasons leading to the decision to overlay. Several data points were removed from the database because of the zero values after overlay. Also, survey data of 1984 were removed because no following data were available to check which category the pavement sections of 1984 should be grouped into. Therefore, the final database consisted of 882 data points, 56 overlaid and 826 nonoverlaid. A sample of the summary of reduced data is shown in Figure 4.

Several methods used to calculate the distress index revealed in the literature were evaluated. The proposed methods are

1. Subjective parameters *(6)*,
2. Regression analysis *(7)*,
3. Factor analysis *(8)*, and
4. Discriminant analysis *(9, 10)*.

After the various methods were reviewed, discriminant analysis was selected for the development of the distress index used in this study, because it appeared to be the most appropriate technique for the data available and because of its encouraging results.

DISCRIMINANT ANALYSIS

Discriminant analysis is a statistical technique used to classify data into groups by maximizing the differences between group means. To distinguish between the groups, a collection of discriminating variables that measure characteristics for which the groups are expected to differ is made. The mathematical objective of discriminant analysis is to weight and linearly combine the discriminating variables in some fashion so that the groups are forced to be as statistically distinct as possible.

($\log_e$) minor spall	($\log_e$) severe spall	($\log_e$) minor punchout	($\log_e$) severe punchout	($\log_e$) patch	group
5.2	.5	1.4	.5	.5	2.0
5.2	.5	0	.5	0	2.0
0	0	0	0	0	2.0
5.0	.5	.9	0	.5	2.0
5.0	.5	0	0	.5	2.0
0	0	0	0	0	2.0
5.5	0	0	0	0	2.0
4.4	0	0	0	0	2.0
5.1	0	0	0	0	2.0
4.7	0	0	0	0	2.0
5.2	.7	.3	0	.2	2.0
5.2	.7	.3	.1	0	2.0
0	0	.3	0	0	2.0
5.3	.5	.5	.1	.3	2.0
5.3	.5	.3	0	.1	2.0
0	0	1.1	0	0	2.0
5.6	1.3	2.9	.3	1.0	2.0
5.6	1.3	1.9	0	0	2.0
0	0	2.1	0	0	2.0
5.5	.9	3.2	1.2	.6	2.0
5.6	.9	3.0	.3	0	2.0
0	0	.4	.1	0	2.0
5.2	1.5	1.9	1.0	2.5	1.0
5.1	1.2	1.6	.7	2.2	1.0
5.9	1.4	2.3	0	1.9	1.0
6.2	1.6	4.2	.8	1.7	1.0
6.2	0	3.3	.9	1.5	1.0
4.7	2.2	4.0	0	1.4	1.0
5.2	2.7	4.0	.3	2.3	1.0
5.2	2.5	3.2	.2	1.9	1.0
0	0	1.5	1.1	3.2	1.0
0	0	2.0	1.0	3.3	1.0
0	0	2.6	.9	3.0	1.0
0	0	2.7	.4	3.5	1.0
5.1	3.9	1.4	1.8	3.5	1.0
5.3	4.1	2.4	1.6	4.0	1.0
6.2	4.1	1.5	1.4	2.0	1.0
6.1	3.1	2.4	2.4	3.0	1.0
5.6	1.1	3.1	2.0	2.7	1.0
5.8	2.1	2.7	.2	2.2	1.0
6.2	1.9	2.4	1.9	2.4	1.0
6.2	4.2	2.2	1.9	2.6	1.0
5.6	5.0	1.1	.8	2.2	1.0

FIGURE 4 Sample of data used in discriminant analysis.

In this study, the historical data are separated into two groups, overlaid and nonoverlaid pavements. Each group of data consists of several distress manifestations, as mentioned in the earlier section, which represent the distress condition of a specific section in a specific survey year. By using discriminant analysis, one or more composites or discriminant functions, the distress variables, are derived so that the composites yield boundaries that minimize the overlap in the distribution of the a discriminant scores of the different groups. The discriminant score is the value of the composite function for a particular datum. Ideally, the discriminant scores for cases within a particular group are similar. The maximum number of discriminant functions that can be derived is either one less than the number of groups or equal to the number of discriminant variables, if there are more groups than variables. Therefore, only one function is derived in this study.

The inputs of the discriminant analysis are historical condition survey data, including various distress types and their corresponding groups. The outcomes of the analysis are the discriminant function and its relative magnitudes that can be used as a distress index. In addition, the percentages of analyzed data that were correctly classified into either correspondent group are given. Once the equation is developed, data for any new section can be assigned to one of the predetermined groups by calculating its discriminant score and comparing it with the boundary between the groups.

In the development of the discriminant function, the discriminant subprogram of the statistical package SPSS was used *(9)*.

At this stage, it is important to mention several assumptions inherent to the approach used in this study.

1. The distress variables are considered normally distributed.
2. The SDHPT district's decisions for overlaying the sections were assumed to be correct and consistent.
3. The total cost of overlaying a pavement when it should not be overlaid is equal to the total cost of not overlaying a pavement when it should be.

ANALYSIS AND RESULTS

The discriminant function developed in the analysis to discriminate between groups is of the form

$$Z_i = \sum_{j=1}^{m} a_j z_{ij}; \quad \text{for } i = 1, \ldots n \tag{1}$$

where

Z_i = discriminant score of the ith pavement section datum,
a_i = weighting coefficient,
z_{ij} = standardized value for the ith discriminating variable with respect to the jth distress manifestation,
n = number of data, and
m = number of the discriminant variables.

The standardized values z_i are calculated as follows:

$$z_{ij} = \frac{x_{ij} - \overline{x}_j}{\sigma_{\overline{x}_j}}; \quad \text{for } i = 1, \ldots n; \quad j = 1, \ldots m \tag{2}$$

where

x_{ij} = value of the distress manifestation j for the datum i being classified,
x_j = mean value of the distress manifestation j for all n data, and
$\sigma_{\overline{x}_j}$ = standard deviation of $\overline{x}_j$.

As can be seen in Equation 1, the discriminant function is linear, but it may not produce a realistic situation. However, the statistical program requires a linear form and any nonlinear transformation of the discriminating variables should be made before this program is used. Several transformation models have been tested, including multiple linear, second-degree polynomial, and natural logarithm. The logarithm method, which shows the best results of analysis, is also the most commonly used transformation for growth-type data, for example, distress evolution, and for cases in which the mean is proportional to the standard deviation, which is the case in this study.

TABLE 1 CONSTANTS TO BE USED IN EQUATIONS 1 AND 3, WITH MINOR SPALLING AND SEVERE SPALLING

i	Distress Manifestation	a_i	$\bar{x}_i'$	$\sigma_{x'_i}$
1	Minor spalling (MSP)	–0.04248	3.558	2.5075
2	Severe spalling (SSP)	–0.09866	1.4191	1.6301
3	Minor punchout (MPUNT)	0.05373	1.0853	1.0502
4	Severe punchout (SPUNT)	0.47223	0.3015	0.5044
5	Patch (PATCH)	0.72323	0.6313	0.8281

Based on the findings of the analysis, Equation 2 is modified to the following form (although Equation 1 remains unchanged).

$$z_{ij} = \frac{\ln(x_{ij} + 1) - \bar{x}_j'}{\sigma_{\bar{x}_j'}} \tag{3}$$

where

x_{ij} = same as defined before;

$\bar{x}_j' = \sum_{j=1}^{n} \ln(x_{ij} + 1)/n$;

n = number of data, both overlaid and nonoverlaid groups; and

$\sigma_{\bar{x}_j'}$ = standard deviation for $\bar{x}_j'$.

Table 1 summarizes the parameters to be used in Equation 3. The variable PATCH is the sum of asphalt cement, portland cement concrete, and failure patches. Inclusion of the minor and severe spalling terms in the equation would have been misleading because of their counter signs. In addition, the two terms have relatively small values of coefficients compared to the other three variables. Thus, another equation was developed without considering the terms of minor and severe spalling. Table 2 presents the coefficients, mean values, and standard deviations of analyzed discriminant variables used in the improved discriminant equation. This equation can be further simplified by introducing the total means and deviations of the distress variables in Equations 1 and 3 to obtain

$$Z = -1.02544 + 0.01872(\text{MPUNT}) + 1.04429(\text{SPUNT}) + 1.09347(\text{PATCH}) \tag{4}$$

where

Z = discriminant score (or Z score),

MPUNT = ln(minor punches per mile + 1),

SPUNT = ln(severe punchouts per mile + 1), and

PATCH = ln(total patches per mile + 1).

There were 882 data points for the population of historical surveyed data of the CRCP network in Texas included in the derivation of the discriminant equation. This data set comprises 56 overlaid and 826 nonoverlaid sections.

Hence, for any particular pavement, data on each distress manifestation should be substituted into Equation 4 in order to obtain a value of Z, the score for that pavement.

As noted in Equation 4, the score has a minimum value of –1.02544 and it increases with the quantity of various distresses. It was always thought that pavements in good condition should have higher scores than those in poor condition. Thus, the signs of constant terms and coefficients are reversed and Equation 4 is rewritten as Equation 5 with the same variable definitions:

$$Z' = 1.02544 - 0.01872(\text{MPUNT}) - 1.04429(\text{SPUNT}) - 1.09347(\text{PATCH}) \tag{5}$$

The Z' scores for all the pavements in the original (historical) data are calculated and the mean scores of each group are also computed. Table 3 summarizes the mean scores of each group and the probability of correct prediction by the discriminant equation.

It should be emphasized that the individual Z' score will not have the same distribution pattern about each group mean because of the different characteristics. The historical distress record of any specific pavement section always from its best condition, that is, no distress, and increases with time and traffic until the unacceptable condition before overlay. Thus, there exists a high bound, the best condition, in the Z' score distribution of the nonoverlaid group, whereas the Z' score of the overlaid group tends to be distributed normally. A frequency distribution for each of the two groups is plotted (against the Z' score) on one continuous horizontal axis (Figure

TABLE 2 STATISTICAL PARAMETERS OF THE CRCP DATA USED IN EQUATIONS 1 AND 3, WITHOUT MINOR SPALLING OR SEVERE SPALLING

i	Distress Manifestation	a_i	$\bar{x}_i'$	$\sigma_{x'_i}$
1	Minor punchout (MPUNT)	0.01869	1.0853	1.502
2	Severe punchout (SPUNT)	0.44885	0.3015	0.5044
3	Patch (PATCH)	0.72391	0.6313	0.8281

TABLE 3 GROUP MEANS OF DISCRIMINAT Z″ SCORE AND NUMBER OF CASES CORRECTLY PREDICTED BY THE DISCRIMINANT EQUATION 5

Group	Mean	Number of Cases	Number of Correct Classifications	Percent
Overlaid	−3.1736	56	56	92.9
Nonoverlaid	0.2151	826	757	91.6
Total	0.0	882	809	91.72

5). The shadowed area indicates the overlap of the two distributions. In the discriminant analysis, the grand mean of the groups will always be zero, which falls between the two group means but is not necessarily the average of these two means. A special case happens only when the groups have an equal amount of data and each has a normal distribution of the Z′ score. Overlapping of the Z′ scores between the two groups is not preventable. However, this area can be reduced by transforming the input data or it can be balanced for both sides by seeking a specific value of the Z′ score that will give 50 percent probability to assigning a pavement having a Z′ score with the overlapping area to the nonoverlaid and the overlaid groups. For the equation formed by using the data for the whole population of Figure 4, this specific Z′ score is calculated to be −1.60.

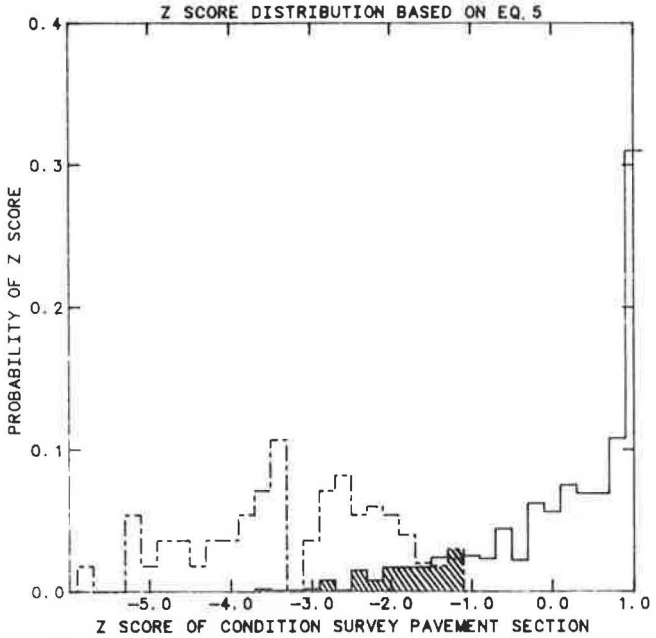

FIGURE 5 Frequency distribution of Z′ scores for the data set used in the discriminant analysis.

Therefore, if Z′ of any pavement is less than −1.60, there is a strong probability that the pavement will be a good candidate for an overlay. Similarly, a pavement with a Z′ value larger than −1.60 has a large probability of being in good condition so that no overlay is necessary. Under the analysis, when Z′ has the value of −1.60, the overlap area is equally divided in two parts. The right half represents the probability α that a pavement that should be overlaid is misclassified into the nonoverlaid group. Likewise, the left half indicates the probability β that a pavement is classified into the overlaid group although it is still better than the acceptable level. In order to simplify decision making about which value the Z′ should be, an assumption was made. It was assumed that the total cost, including agency and user costs, of overlaying a pavement when it should not be overlaid is equivalent to the total cost of not overlaying a pavement when it should be. The Z′ score of −1.60 is, therefore, considered to be the appropriate value to separate the two groups in this study. This decision results in α = β = minimum possible value = 7.4 percent.

Equation 5 can be modified so that the Z scores are compared to zero rather than to −1.60, by using the equation

$$Z'' = Z' + 1.60$$
$$= 2.62544 - 0.01872(\text{MPUNT}) - 1.04429(\text{SPUNT}) - 1.09347(\text{PATCH}) \quad (6)$$

or also dividing by 2.62544 so that the equation is of the form

$$Z'' = 1.0 - 0.0071(\text{MPUNT}) - 0.3978(\text{SPUNT}) - 0.4165(\text{PATCH}) \quad (7)$$

where Z″ = modified zero score, and MPUNT, SPUNT, and PATCH are as defined in Equation 4.

If Z″ ≥ 0, pavement does not need overlay; if Z″ < 0, pavement needs overlay immediately. A plot of the Z″ frequency distributions of the two groups, based on Equation 7, is represented in Figure 6.

In Equation 7, the most important variable that affects the Z″ score is PATCH (patching), followed by SPUNT (severe punchout), and MPUNT (minor punchout). The required numbers of patches and severe punchouts, respectively, that will cause a pavement section to be overlaid when the other distress variables are all zeros are as follows:

Distress Manifestation	*Number/Lane/Mile*
Severe punchouts	11.3
Patches	10.0

If (minor punchout) = (severe punchout) = 0, then the number of patches/lane/mile to cause overlay of a pavement is exp(1/0.4165) = 10.0.

The number of minor punchouts is not presented herein because a situation in which a pavement section is overlaid due to millions of minor punchouts but no severe punchouts or patches is not realistic.

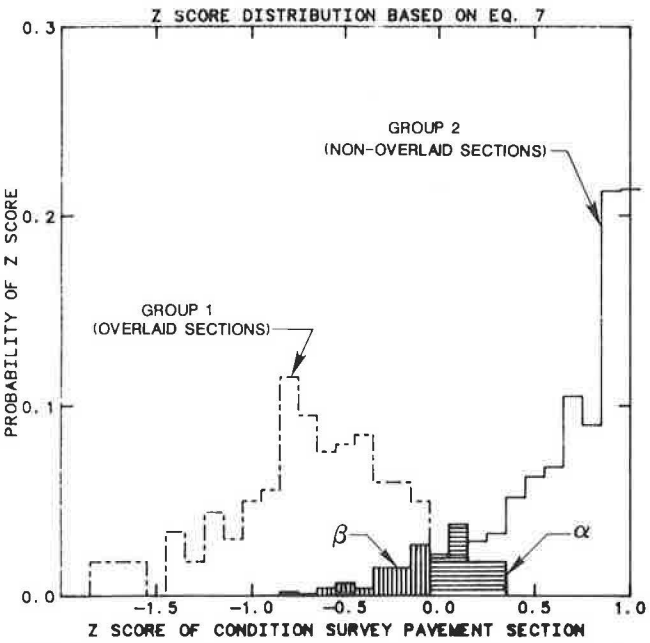

FIGURE 6 Modified frequency distribution of Z′ scores for the nonoverlaid and overlaid groups.

The final equation correctly classified 92.6 percent $(1 - \alpha)$ of the 882 cases. The cases used to test the prediction capability of the discriminant equations were the same as the ones used to develop the equation.

SUMMARY

Because of the rapid expansion of expenditures in pavement maintenance and rehabilitation, improvements to the PMS have become more and more important. A good evaluation system for pavement performance can not only efficiently use the available annual maintenance budgets at the network level but also economically plan the best rehabilitation timing of any specific pavement at the project level. This study is, therefore, focused on the derivation of distress index and rehabilitation criteria for the CRCP network in Texas. Several approximate methods aimed at developing a distress index have been studied. Discriminant analysis was chosen because its technique is appropriate for the available data. The historical condition survey data of the comprehensive CRCP network were used in the discriminant analysis. The logarithmic method was selected to transform the original distress data before applying the discriminant technique because it resulted in the best fit for the data groupings.

After several modifications, the final equation used to calculate the distress index Z score is

$$Z'' = 1.0 - 0.0071(\text{MPUNT}) - 0.3978(\text{SPUNT}) - 0.4165(\text{PATCH})$$

where

Z'' = distress index (or Z score),
MPUNT = ln(minor punchouts per mile + 1),
SPUNT = ln(severe punchouts per mile + 1), and
PATCH = ln(total patches per mile + 1).

The criterion for major rehabilitation is that a pavement would be classified as a candidate to be overlaid if its distress index Z'' is negative.

CONCLUSIONS

The principal conclusions derived from this study concerning the development of distress index and rehabilitation criteria for CRCP at the network level are summarized as follows.

1. PSI values did not correlate with the rehabilitation decision.
2. A distress index Z'' was developed using 10 years of condition survey data with the discriminant analysis method.
3. Punchouts and patches were the primary distress manifestations included in the distress index equation.
4. Z'' ranged from +1.0 to −1.8 with zero as the rehabilitation criterion with a confidence level of 92.6 percent.
5. The Z'' equation provides a ranking method for rehabilitation needs for network analysis and maintenance programming.
6. It is recommended that the economics analysis of the overlay timing be studied. The specific number of 1.60 in Equation 6 can be revised by changing the ratio of α to β. This ratio is proportional to the value of the cost of overlaying a pavement when it should not be overlaid divided by the cost of not overlaying a pavement when it should be.
7. Although the distress index and rehabilitation criterion developed in this study were based on the condition survey data of Texas, it is strongly believed that the results can be applied to other states. However, the rehabilitation criterion may be shifted from zero (Figure 6) to new points for different states because the SDHPT district's decision to overlay the pavement sections is highly dependent on budget constraints that vary from state to state.

ACKNOWLEDGMENT

The authors are pleased to acknowledge the combined support of the Center for Transportation Research at the University of Texas at Austin and the Texas State Department of Highways and Public Transportation, in cooperation with FHWA. Special acknowledgment is made to the staff of the Center for Transportation Research of the University of Texas at Austin for their assistance in preparing the drafts and figures of this paper.

REFERENCES

1. R. M. Thorndike. *Correlational Procedure for Research.* Garden Press, Inc., New York, 1972.
2. W. N. Carey and P. E. Irick. The Pavement Serviceability-Performance Concept. *Bulletin 250,* HRB, National Research Council, Washington, D.C., 1960.
3. M. de V. Guiterrez and B. F. McCullough. *Rigid Pavement Network Rehabilitation Scheduling Using Distress Quantities.* Research Report 249-5. Center for Transportation Research, The University of Texas at Austin, 1983.

4. M. de V. Guiterrez and B. F. McCullough. *Summary Report for 1978 CRCP Condition Survey in Texas.* Research Report 177-20. Center for Transportation Research, The University of Texas at Austin, 1969.
5. J. P. Machado, B. F. McCullough, and W. R. Hudson. *CRCP: Predictions of Distress Quantities.* Research Report 177-8. Center for Transportation Research, The University of Texas at Austin, 1977 (unpublished).
6. R. D. Pedigo and W. R. Hudson. *Simplified Pavement Management at the Network Level.* Report NA-3/1. ARE, Inc., Austin, Tex., 1981.
7. N. R. Draper and H. Smith. *Applied Regression Analysis.* John Wiley and Sons, New York, 1966.
8. L. T. Oehler and L. F. Holbrook. *Performance of Michigan's Postwar Concrete Pavements.* Research Report 711. Michigan Department of State Highways, Lansing, June 1970.
9. M. M. Tatsuako. *Multivariate Analysis: Techniques for Education and Psychological Research.* John Wiley and Sons, New York, 1971.
10. N. G. Nie et al. *Statistical Package for the Social Sciences (SPSS),* 2nd ed. McGraw-Hill Book Co., New York, 1970.

Publication of this paper sponsored by Committee on Pavement Rehabilitation.

A Mechanistic Model for Thermally Induced Reflection Cracking of Portland Cement Concrete Pavement with Reinforced Asphalt Concrete Overlay

K. MAJIDZADEH, A. ABDULSHAFI, G. J. ILVES, AND ASTON MCLAUGHLIN

A new model is presented to analyze the phenomenon of thermally induced reflection cracking of asphalt concrete overlays over portland cement concrete pavements. The model is based on fundamental material properties of creep compliance, fracture toughness, and indirect tensile strength and does not depend on any empirical distress functions. When applied to fabric-reinforced overlays, however, a fabric effectiveness factor is required. This factor is obtained from single laboratory thermal simulation tests on beams and is defined as the ratio of failure times of reinforced and unreinforced (control) beams. The developed model has been validated by application to laboratory specimens of small-scale and large-scale beams and to field pavements. The model predicted the formation of thermally induced reflection cracks to within a few months of their actual occurrence on four out of five field projects. The models also predicted that the fifth project would not experience reflection cracking for a considerable time (75 years). After two winters and almost two years in service, not a single reflection crack has appeared in this project. The reflection cracking analysis model has been computer coded as RECK. Only the RECK program is required for the analysis of laboratory beams, but application to field pavements requires that another computer program (EFRON) be used first to develop some inputs required by RECK. RECK is considered a significant advance in the analysis of the reflection cracking phenomenon because the dependence on empirically developed distress functions has been eliminated, and treatment of the asphaltic concrete as a viscoelastic material is considered.

The theoretical work of Schapery *(1)* and others on analyzing fracture of a viscoelastic material appeared to have some bearing on the search for a mechanistic approach to the problem of reflective cracking. Schapery *(1)* has successfully applied this approach to fracture characterization of materials. In the application of this theory to asphaltic concrete, however, there is a need to use caution in the mathematical treatment of the developed model along three lines: first, that the simplifying assumptions do not violate the theory while at the same time realistically modeling the mechanics of beam fracture; second, that the developed model should require easy-to-find input parameters that could be obtained from the laboratory testing data to be obtained in this study; and third, that some modification to the model is required because this study is dealing with different materials such as asphaltic mixtures and fabrics than were used by the previously cited researchers.

K. Majidzadeh, A. Abdulshafi, and G. J. Ilves, Resource International, Inc., 281 Enterprise Drive, Westerville, Ohio 43081. A. McLaughlin, Federal Aviation Administration, U.S. Department of Transportation, Washington, D.C. 20590.

DEVELOPMENT OF RECK MECHANISTIC MODEL

To date, most fracture mechanics approaches assumed that material behavior was either linear elastic or viscoelastic. The stress field in a plane viscoelastic body subjected only to prescribed traction forces is the same as that in an elastic body of the same geometry and loading, provided that the resultant force on any closed boundary vanishes. It follows as a corollary that the stress intensity factors K for similarly loaded linear elastic and viscoelastic bodies satisfying this condition are equal. For an elastic material, the stress intensity factor K is independent of the crack growth rate $\dot{a}$. However, for linear viscoelastic material two cases arise: (a) for a very slowly growing crack (the quasielastic case), the material will respond with long-decade-time creep compliance $J(\infty)$ being the material-characterizing parameter; and (b) for a very rapidly propagating crack growth (the dynamic case), $a \rightarrow \infty$, the material will respond with the short-decade-time creep compliance $J(0)$ being the material-characterizing parameter. Therefore, the viscoelastic stress analysis solution will not only depend on the appropriate use of the correspondence principle but also on what crack speed will develop, or can reasonably be assumed, under the specified loading conditions, that is, whether quasielastic or dynamic analysis is used *(2)*.

Consider Figure 1 for a viscoelastic medium subjected to stresses acting along the crack plane (Mode I) in the neighborhood of a crack tip indicated by O, and located at $x = a(t)$, where the crack plane is defined by $y = 0$. It is convenient to define a reference system attached to the moving crack tip as $r = x = a(t)$. The region $0 < r < \alpha$ is termed the cohesive zone where the material exhibits nonlinear material behavior (more precisely, nonproportional stress-strain-time behavior). This zone was first recognized by Dugdale in his cohesive fracture model *(3)*. The material behavior outside this zone is assumed to be linear viscoelastic. The basic problem is to find the following.:

1. The size of the cohesive zone α (which is not addressed in this paper),

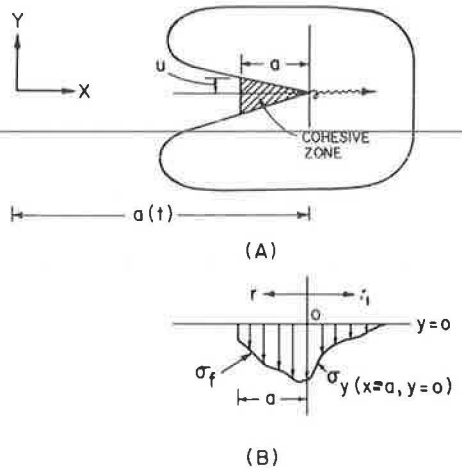

FIGURE 1 Crack in a viscoelastic medium.

2. The crack opening displacement U, and
3. The crack growth rate $\dot{a}$

The Boundary Value Problem and Its Solution

When a solution for the equivalent elastic problem is known, the solution to the viscoelastic problem could be found using the correspondence principle method *(2)*. This principle emerged from observing that the only difference between formulating a boundary value problem for a linear elastic or viscoelastic medium is in the assignment of the Young's modulus of elasticity E and Poisson's ratio μ. In other words, if the elastic solution exists for a boundary value problem, then the corresponding viscoelastic solutions could be found by simply replacing the material constants E, μ, G, and K of the elastic solutions by their viscoelastic equivalents. This principle applies in the case of a stationary crack; however, two conditions have to be met in order to use the correspondence principle for growing cracks. The first condition is that the cohesive stresses σ_f are independent of the material constants. Such a requirement could be met by prescribing σ_f a priori, as is the case in the Dugdale model *(3)*. The second condition is that the displacement in the plane of the crack could be expressed in separable form of two multiplicable functions: one for the material constants and the other for the geometry. Such a requirement could be met if the resultant force on any closed loop is identically zero.

It follows that if U_e is the elastic displacement field for a unit value of creep compliance $J(t)$, then the corresponding viscoelastic displacement U_{ve} can be written as

$$U_{ve}(t) = \int_0^t \left[J(t-\tau) - \frac{\delta U_e}{\delta \tau} \right] d\tau \tag{1}$$

Using the condition of small scale yielding [$a << a(t)$] and considering Figure 1, the elastic solution following Dugdale's approach *(3)* can be written as

$$\sigma_y(r) = \frac{H(r_1)}{2\pi r}\left[K - \int_0^\alpha \sigma_f(\zeta)/\zeta^{1/2} d\zeta \right]; \quad r_1 > 0 \tag{2}$$

$$U_y(r) = 4KH(r)\,(r/2\pi)^{1/2} - \frac{2}{\pi} H(r_1) \int_0^\alpha \sigma_f(\zeta) \ln \frac{\zeta^{1/2} + r^{1/2}}{\zeta^{1/2} - r^{1/2}} d\zeta; \quad r \to 0 \tag{3}$$

where

r_1 = extension of crack beyond the cohesive zone,
σ_y = crack plane stress,
$H(r)$ = unit step function,
σ_f = stress in the cohesive zone,
ζ = dummy variable,
U_y = crack opening displacement,
K = stress intensity factor, and
α = size of the cohesive zone.

The requirement that the stress σ_y be nonsingular at the crack tip ($r = 0$) implies

$$K = \left(\frac{2}{\pi}\right)^{1/2} \int_0^\alpha \frac{\sigma_f(\zeta)}{\zeta} d\zeta \tag{4}$$

Substituting Equation 4 in Equation 3,

$$U_y(r) = \frac{2H(r)}{\pi} \int_0^\alpha \sigma_f(\zeta) \left[2\left(\frac{r}{\zeta}\right) - \ln \frac{\zeta^{1/2} + r^{1/2}}{\zeta^{1/2} - r^{1/2}} \right] d\tau \tag{5}$$

Determination of the Viscoelastic Displacement U_{ve}

Using the correspondence principle typified by Equation 1 as applied to the elastic crack opening displacement U_y in Equation 5 yields

$$U_{ve}(t) = \frac{8}{\pi} \sigma_{f_{max}} \times \int_{t_1}^t \left[J(t-\tau) \frac{\partial}{\partial \tau} [a(\tau) - x]^{1/2} - \left(\frac{\alpha x - a\tau}{2} \ln \frac{\{\alpha^{1/2} + [a(t) - x]^{1/2}\}}{\{\alpha^{1/2} - [a(t) - x]^{1/2}\}} \right) \right] d\tau \tag{6}$$

Here $t \geq t_1$ and t_1 is the time at which the crack tip reaches the generic point x; that is $r(x, t_1) = a(t_1) - x = 0$. Although not explicitly shown in Equation 6, x and σ_f may also be time dependent.

It follows from Equation 6 that the viscoelastic displacement could be obtained if the quantities $\sigma_{f_{max}}$, $J(t)$, and α are determined. For a constant cohesive stress, α depends only on the stress intensity factor K. Therefore, if information on the creep compliance $J(t)$, fracture strength $\sigma_{f_{max}}$, and stress intensity factor K could be determined experimentally or from field measurements, then Equation 6 would establish a relationship

between the crack opening displacement in a viscoelastic material and crack length $a(t)$ as function of time.

Determination of the Failure Time

Equation 6 specifies two bounds t_1 and t. The lower bound t_1 defines the time required to initiate a crack and advance its tip to a point $x = a(t_1)$. Schapery *(1)* indicated that the time t_1 required to propagate the crack the distance α is approximately three times the initiation time. The upper bound t defines the time required to advance the crack or equivalently increase the crack opening displacement any specified length. At the time of rupture, the crack opening displacement reaches a critical value U_c, and the time elapsed is defined as the failure time t_f. The work of fracture γ of an element in the cohesive zone until rupture occurs can be expressed as

$$\gamma = \frac{1}{2} \int_{t_1}^{t_2} \sigma_f \frac{\delta U_y}{\delta_t} \, dt \tag{7}$$

or equivalently, using a change of variable, as

$$\gamma = \frac{1}{2} \int_0^C \sigma_f \frac{\delta U}{\delta r} \, dr; \quad \dot{a} > 0 \tag{8}$$

where C is the crack length at failure.

If σ_f is constant, Equation 7 reduces to

$$\gamma = \frac{1}{2} \sigma U_c = \frac{1}{2} \sigma \, \Delta t_f \tag{9}$$

where U_c is the initial joint opening displacement at failure. If the creep compliance of the asphaltic overlay could be written in the form

$$J(t) = J_0 + J_2 t^m \tag{10}$$

Then using Equations 6, 9, and 10 and making the change of variable $S = a(t - t_1)$ lead to the following equation for the crack growth rate $\dot{a}$:

$$\dot{a} = \frac{\pi}{8} \left\{ \frac{J_2 I}{2\gamma[1 - (K^2/K_\infty^2)]^2} \right\}^{1/m} \frac{K^{2+2/m}}{\sigma_y^2} \tag{11}$$

where

$$I = \frac{1}{2} \int_1^0 S^m \ln \frac{1 - (1 - S)^{1/2}}{1 + (1 - S)^{1/2}} \, dS \tag{12}$$

J_0, J_2, and m are the creep compliance constants and K and K_∞ are the initial and unbound stress intensity factors.

Equation 11 is the general equation for the crack opening rate. The derivation of this equation is given by Majidzadeh and Ilves *(4)*. However, because the parameter measured in the laboratory tests is the time of failure at a specific joint opening rate, it is convenient to rewrite this equation to yield the failure time t_f.

The work of fracture 2γ required to produce a unit of surface area is given by

$$2\gamma = J_0 K_\infty^2 \tag{13}$$

Introducing Equation 13 into Equation 11 and rearranging terms yields

$$t_f = t_0 + \frac{8\sigma_f^2}{\pi} \left(\frac{C_0}{C_2 I} \right)^{1/m} \int_{a_0}^{a_\infty} \left(\frac{K_\infty^2}{K^2} - 1 \right)^{1/m} \frac{1}{K^2} \, da \tag{14}$$

where

t_f = failure time;
t_0 = crack initiation time, assumed to be zero;
a_0 = initial crack length;
a_∞ = crack length for which the crack propagation rate becomes unbounded;
K = stress intensity factor corresponding to crack length a;
K_∞ = stress intensity factor corresponding to crack length a; and
I = constant defined in Equation 12.

The developed model requires easy-to-find input parameters that could be obtained from laboratory test. These parameters are the properties of the overlay material such as the creep compliance $J(t)$, the fracture strength σ_f, the joint opening rate as a function of time, and the fracture toughness KIC. The determination of KIC also requires the applied horizontal load on the bean (slab) that results in the same stresses as those developed as a result of thermal load. Other input data, required only for model verification, are measured values of the applied load $P(t)$ and the corresponding values of the crack length $a(t)$ at different time intervals. Using these input parameters, the model predicts the time t_f at which failure occurs and the crack opening displacement $U(t)$ at different time intervals.

MODIFICATION AND VALIDATION OF RECK MODEL

Modification for Fabric or Interlayer Inclusion

The inclusion of a fabric layer within the overlay pavement structure is expected to prevent or delay reflection cracking. The purpose of this fabric, as a reinforcing layer, is to physically restrain the opening movement of the crack as the joint underneath opens. As has been indicated in the literature, there are several approaches to the reflection cracking problem, including stress-relieving interlayers such as SAMI, crack-arresting interlayers such as the Arkansas open-graded layer, and preoverlay rehabilitation.

A mechanistic approach to determining the effect of fabrics or interlayers on crack growth rate includes these layers in stress analysis; the EFRON program is capable of handling up to five such interlayers, which may be of any width. The difficulty with this approach is that the in situ properties of the interlayers (creep modulus, Poisson ratio, tensile strength, and fracture toughness) are very difficult to determine. It was hoped that these properties could be deduced from the results of fatigue tests; however, the analysis of small-scale beam data *(5)* showed that this was not possible within an elastic system—the interlayer properties would have to be a function of the applied

stress as well. Therefore, an empirical approach was used here to include the effect of interlayers; namely, the analysis was conducted by assuming that the interlayers (fabric or SAMI) were not present and by comparing the predicted failure time with the actual failure time to obtain a fabric effectiveness factor.

Analysis of Field Pavement

Daily variation of temperature gradients and seasonal variation of average pavement temperature result in changes in the joint opening, that is, in U_{ve}. The crack opening displacement can be calculated using the EFRON program provided that the rate of change of temperature (average or curling gradient) is known. Thus, the field case is identical to the laboratory beam case with the exception that the load developed as a result of the temperature drop will have to be computed using EFRON for the field case instead of using the measured values for the laboratory case. The load is required to evaluate the opening mode *I* and stress intensity factor *KI*. The following procedure is used to evaluate field pavements:

1. The joint opening and the resulting stress in the asphalt above the joint are determined using the EFRON program for monthly increments of temperature drop.
2. EFRON is rerun using a load applied horizontally to the ends of the slab in order to find the horizontal pull required to reach the same critical stress in the asphalt above the joint as in Step 1.
3. The results of Step 1 and Step 2 computations are input into the RECK program and the incremental crack growth is determined.

Laboratory Validation

An attempt was made to test the membrane-reinforced beams under simulated thermal stress, but the tests could not be completed due to debonding of the overlay. Six beams were tested at room temperature and at 40°F in this mode; all debonded before any distress was visible in the asphalt overlay. However, in order to illustrate the theory, the specimens tested were analyzed with the model described in previous sections. To further illustrate the use of the theory, large-scale beams *(4)* were also analyzed. These series of tests were intended to simulate the effect of the seasonal temperature drop on joint openings and crack formation. The test setup consisted of the beam's being pulled apart at a constant rate while the joint opening was observed, and while load and crack propagation developed as a function of time.

The test results for time to failure are plotted as a function of the asphaltic concrete cross section (beam width × overlay thickness) in Figure 2. The solid lines represent the best-fit lines through the data points with the constraint that the lines must go through zero. The equations of the regression lines along with the root mean square error are also shown in this figure. Although there is scatter in the data, it is apparent that the high-modulus fabric increases the time to failure significantly (1.95 times), whereas the fiber material SAMI appears to have a very small affect; the effectiveness from this analysis is about 1.08. (The fiber SAMI used by Majidzadeh and Ilves *(4)* is somewhat different from that used in this research in that the stone chip layer was absent in the former study.) When considering the scatter in the data, the effectiveness of 1.08 is not significant. It is, however, encouraging that this effect is positive (and greater than one) rather than negative.

Because the in situ fabric properties were not known, the analysis was conducted assuming that the fabric had the same properties as the overlay. Thus, if the prediction model (RECK) is successful and if the fabrics have a beneficial effect, the predicted failure time should agree with the actual failure time for the control samples and should be lower by the fabric effectiveness factor for the treated specimens.

The results of this analysis are given in Table 1. The significant values in this table are under the column heading *T/T'*; that is, the ratio of actual failure time to the predicted failure

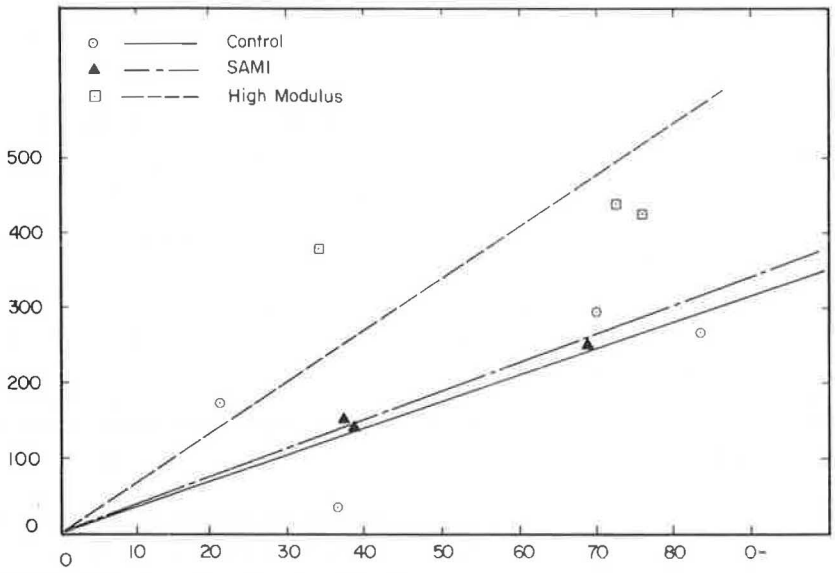

FIGURE 2 Results of horizontal pull tests.

TABLE 1 RESULTS OF HORIZONTAL PULL TESTS

Sample No.	Width in.	Hov in.	Lab T Hrs.	Pred T' Hrs.	T/T'
9C	14.2	5.89	265.0	241.3	1.098
10C	14.0	5.00	295.0	212.3	1.390
21C	14.0	2.00	171.0	152.9	1.118
45C	14.5	2.50	31.0	44.8	0.692
6H	13.8	5.00	250.0	225.4	1.109
13H	14.0	2.75	143.5	127.8	1.115
14H	13.8	2.68	150.0	131.2	1.144
7O	14.5	5.00	440.0	238.7	1.843
8O	14.3	5.30	424.0	235.2	1.803
17O	14.0	2.30	217.0	119.0	1.824
18O	14.0	2.43	379.0	206.9	1.832

C = Control
H = SAMI
O = High Modulus Fabric

time. It can be seen that these data are remarkably consistent (the results for the control beam have somewhat greater scatter, but the average of the two outliers is close to that of the other two results) and the fabric effectiveness, as measured by the time ratio, is close to that obtained from Figure 2. Although the RECK model appears to underpredict the time to failure by about 10 percent, partly because of the fact that the program considers failure to occur when the crack length reaches 90 percent of the overlay thickness (the stress intensity factor becomes unbounded at the surface), the agreement with the measurements is good.

The input data to the RECK program for these cases were the applied load and the crack length as a function of time. Other pertinent information for these tests was fracture toughness KIC = 800 psi; indirect tensile strength σ_y = 150 psi; and creep compliance

$$J(t) = 0.000001(0.25 + 5t^{0.33}) \quad (15)$$

where t is the transformed time. The output from these analyses was the predicted joint opening as a function of time and the time to failure. Figure 3 shows a typical result, and the other

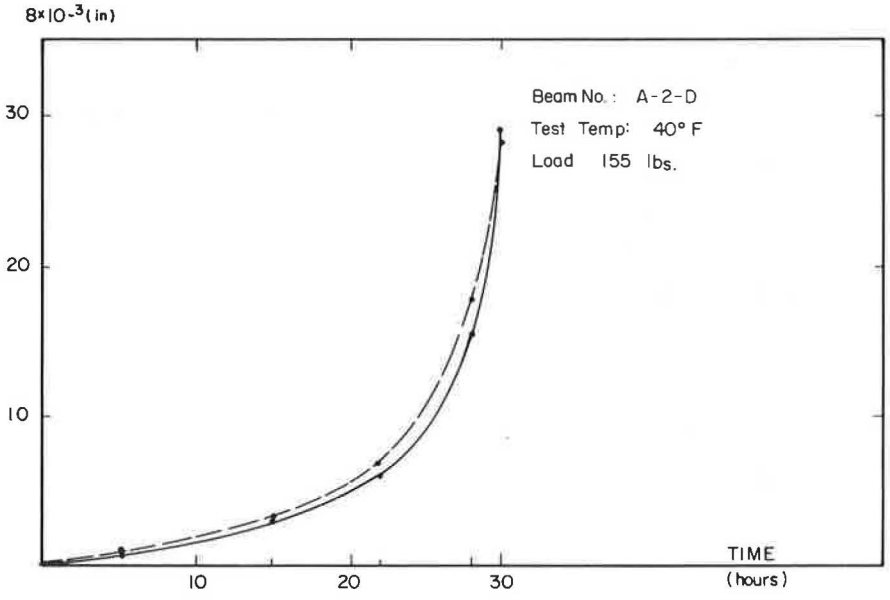

FIGURE 3 Comparison of actual and predicted joint opening for small-scale beams.

data are presented in the figures in Majidzadeh et al. *(6)*—again the agreement is excellent.

Field Validation

Introduction

As discussed before, two of the mechanisms contributing to reflection crack formation are thermal stresses resulting from daily variation in vertical temperature gradient of the concrete slab and seasonal change in average concrete temperature. It was shown *(5)* that both mechanisms result in changing the joint opening, which can be calculated using the EFRON program.

The change in joint opening is the result of variation in temperature over a period of time; that is, the rate at which the joint opening changes can be calculated if the time rate of change of temperature (either seasonal or daily temperature gradient) is known. This change in joint opening is precisely the parameter required for the failure analysis. Thus, the same theory and models used to analyze the laboratory test response to thermal loading are directly applicable to the analysis of full-scale pavements. Of course, this analysis requires certain input data such as the elastic material properties (modulus and Poisson ratio), the asphaltic concrete creep compliance, the master creep compliance, indirect tensile strength, fracture toughness, the equivalent horizontal load that produces the same stress in the asphalt over the joint as thermal contraction, pavement geometry (thickness, overlay thickness, and joint-crack spacing), and coefficient of friction between concrete slab and subbase or subgrade. One method of obtaining the friction value is to make the joint movement measurements as a function of slab temperature as recommended by the ARE method *(7)*; however, because the coefficient of friction is variable from location to location, the values presented in Table 2 may be used without appreciable loss of accuracy *(8)*.

Application to Pavement

A literature search was undertaken to find highway projects that could be used for this purpose. The literature was full of references to reflection cracking studies; however, few of these studies also contained the data required for a rational analysis of performance and fewer still had the data described in the previous section. A thorough search using the TRIS system yielded a New York study by McCullagh *(9)* that contained three highway overlay projects without fabric that could be used with the developed model; but even this report did not contain the pertinent asphaltic concrete properties (modulus, creep compliance, fracture toughness, and indirect tensile strength) required by the model. The literature also indicates that the Rochester International Airport is a candidate for the analysis because it has concrete pavement sections where a fabric was used under the overlay. Further, an overlay project on I-271 near Cleveland, Ohio, was selected to be used along with the Rochester International Airport and the New York Study data. The following assumptions were made in these analyses:

1. The master creep compliance is given by the expression

$$J(t') = 0.000001[0.25 + 5(t\ 10^{-7.91 + 0.113T})^{1/3}] \quad (16)$$

where

t' = transformed time,
t = time (sec), and
T = temperature (°F).

Equation 16 is a modification of Schapery's equation *(1)* to include the average time-temperature shift factor of Kenis *(10)*.

2. The indirect tensile strength (in psi) as a function of temperature T is given by the expression *(11)*:

$$\sigma_y = 1{,}205\ e^{-0.0136T} \quad (17)$$

TABLE 2 COEFFICIENT OF FRICTION FOR VARIOUS MATERIALS

Subbase Type	Coef. of Friction
Surface treatment	2.2
Lime stabilization	1.8
Asphalt stabilization	1.8
Cement stabilization	1.8
River gravel	1.5
Crushed stone	1.5
Sandstone	1.2
Clay subgrade	1.0
Sandy soil	0.9
Tar paper	1.6
Polyethylene sheet	0.5

3. The fracture toughness KIC is 1,200 psi. This value represents an average over the temperature range considered.
4. The friction coefficient between the slab and subbase is 0.9. (The results are rather insensitive to variations of this value.)
5. The 1983–1984 temperature history *(6)* is applicable.
6. The temperature drops at a uniform rate from the maximum to the minimum average daily temperature in 6 months.
7. It is assumed that the crack grows only during the time the temperature is decreasing.

Overlays Without Fabric Reinforcement

Table 3 gives the data for the three New York projects. Although the seven assumptions regarding asphalt properties had to be made, it was nevertheless felt that these projects could be used for model validation. They are also included to illustrate the use of the new method.

The first step in this analysis is to divide the design period of 6 months for seasonal temperature change into intervals of 1 month and determine the average temperature during the intervals. If the temperature is assumed to drop uniformly according to Assumption 6, then the loading time t per analysis interval is proportional to the average temperature at that interval; that is,

$$t = t_0 (T_h - T)/(T_h - T_1) \quad (18)$$

where

T_h = maximum average daily temperature (°F),
T_1 = minimum average daily temperature (°F),
T = current temperature (°F), and
t_0 = time (sec) for temperature to drop from T_h to T_1 (6 months).

The next step is to determine the creep compliance and the creep modulus (the inverse of compliance), and use these values with the EFRON program to compute the joint opening and critical stress in the asphalt layer above the joint as a result of the temperature drop.

The EFRON program is also used to determine the equivalent horizontal load (pull) required to generate the same critical stress above the joint as was found in the previous step. This computation can be done by assuming a load, calculating the resultant stress, and taking the ratio of stresses from this step and the previous step. The iterative process should be used rigorously because iteration is required whenever the shear stress exceeds the maximum shear at the slab-subbase interface; however, this effect is negligible for all practical purposes.

Results of EFRON analysis are given in Table 4. Projects 5S, 9L, and 29 are actual projects *(9)*, and Project 29′ is the same as Project 29 except that the joint spacing has been reduced to 45 ft to illustrate the effect of joint spacing. Also given in Table 4 (under the column heading percent of joints cracked) is the history of reflection cracking development.

The joint opening and load results of the EFRON analysis are input into RECK along with temperatures, indirect tensile strength, fracture toughness, and geometry of the pavement. The output of the RECK program is the predicted time in hours for the reflection crack to grow to 90 percent of the way through the overlay. The 90 percent value rather than 100 percent is used because the stress intensity factor becomes unbounded at the surface; in any case, the crack growth rate beyond 90 percent is very rapid.

Because of Assumption 7, if the time to failure is less than 4,320 hr the failure time in months is obtained simply by dividing the time by 720. However, if the failure time is between 4,320 and 8,640 hr, the time in months is 6 + time/720; if the time is between 8,640 and 12,960 hr, the time in months is 12 + time/720 and so forth.

Table 5 gives the predicted time in months for failure and the corresponding percentage of reflection cracking that actually occurred. Although the agreement between predicted and actual failure times is not perfect, the predicted times are reasonably consistent with observed cracking. Also, comparison of results for Projects 29 and 29′ indicates that shortening joint spacing decreases the amount of joint opening and increases the time to failure, as expected.

Comparison of Projects 5S, 9L, and 29′ shows the effect of temperature although the temperatures effect is somewhat more difficult to isolate because both maximum and minimum temperatures change for these projects. However, comparison of Projects 9L and 29′, for which the temperature drops are nearly the same, shows that lower minimum temperature results in a reduction of the time to failure; that is, reflection cracking is more severe in colder climates.

Overlays with Fabric Reinforcement

Fabric reinforcement of overlays of rigid pavements was used on selected joints of I-271 in Cleveland, Ohio, and on sections

TABLE 3 PROJECT DATA FOR UNREINFORCED OVERLAYS

Property	5S	9L	29
Overlay thickness, in.	2.5	2.5	2.5
Concrete Thickness, in.	8.0	8.0	8.0
Joint/Crack Spacing, ft.	45.0	45.0	94.0
Max. Daily Temp. *°F	76.0	81.5	80.0
Min. Daily Temp. *°F	3.5	-1.5	-6.0

*Average of daily high and low temperatures.

TABLE 4 EFRON PROJECT ANALYSIS

Project	Time Mo.	Avg. Temp. °F	Avg. Modulus ksi	Joint Opng. in	Load lb	% Joints Cracked
	0	76.0	2.15	0		0
	1	70.0	2.20	.0371	198	***
	2	57.9	3.60	.0734	255	64.0
5S	3	45.8	9.00	.1066	454	72.0
	4	33.8	23.00	.1339	841	96.0
	5	21.7	58.00	.1526	1396	96.0
	6	9.5	153.00	.1628	1975	96.0
	0	81.5	0.94	0	0	0
	1	74.6	1.26	.0432	182	***
	2	60.7	2.85	.0858	257	23.1
9L	3	46.9	7.85	.1240	474	61.5
	4	33.1	23.50	.1550	976	42.3
	5	19.2	70.00	.1774	1736	80.3
	6	5.4	200.00	.1838	2414	88.5
	0	80.0	1.15	0	0	0
	1	72.8	1.50	.0878	693	***
	2	58.5	3.40	.1700	863	***
29	3	44.2	10.10	.2374	1326	72.5
	4	29.9	30.90	.2805	2082	74.5
	5	15.5	100.00	.3000	2829	98.0
	6	1.2	290.00	.3077	3240	98.0
	0	80.0	1.15	0	0	N/A
	1	72.8	1.50	.0446	195	N/A
	2	58.5	3.40	.0878	293	N/A
29'	3	44.2	10.10	.1265	573	N/A
	4	29.9	30.90	.1559	1192	N/A
	5	15.5	100.00	.1720	2060	N/A
	6	1.2	290.00	.1792	2660	N/A

of the main runway at the Rochester International Airport. The pertinent data for these projects are presented in Table 6. The same analysis procedure discussed in the previous section was again used. The results of EFRON analysis are presented in Tables 7 and 8 for I-271 and the Rochester International Airport, respectively. These data were input into the RECK program to obtain the predicted failure times. The program predicts that reflection cracking should occur in the I-271 pavement in 15.3 months (approximately 1.5 winters) and in the Rochester International Airport runway pavement in approximately 75 years; that is, thermally induced reflection cracking will not soon be a problem at the Rochester International Airport.

The overlay on I-271 was placed during May 1984; the performance rating was made during December 1985 and again during March 1986. It was found during the December 1985 rating that approximately 85 percent of the joints had reflected through the overlay; the March 1986 rating showed the value to be nearly 100 percent. Thus, the predicted time of 15.3 months agrees very well with the observed value of 19 to 22 months

TABLE 5 PREDICTED FAILURE TIMES

	5S	9L	29	29'
Jnt. Opening in	.163	.285	.308	.179
Predicted Time Hrs.	8986	4830	1622	4120
Predicted Time Mo	24.5	12.7	2.3	5.7
% Cracking at Time	100	100	<72.5	N/A
Time at 100% Crack	15	7	8	N/A

N/A = Not Applicable

(1.5 to 2 winters). The predicted time for reflection cracking to occur in an unreinforced overlay is 3.0 months (0.5 winters). This analysis indicates that the 2.5-in. overlay is too thin for fabrics to be of any significant benefit. The overlay thickness for the prevention of thermally induced reflection cracking could be determine using this analysis method.

The fabric-reinforced overlay at the Rochester International Airport had been in service about two winters at the time of rating. A detailed inspection of the main runway where fabric was used showed that not a single joint had reflected through. Although this observation does not validate the 75-year prediction, it is encouraging. It is necessary to monitor the performance of this pavement over the next several years to further verify the prediction model. The monitoring should be conducted in areas of low traffic to isolate thermally induced cracking from fatigue effects.

TABLE 6 PROJECT DATA FOR FABRIC-REINFORCED OVERLAYS

Property	I-271	Rochester
Overlay thickness, in	3.0	6.0
Concrete thickness, in	10.0	11.0
Joint/crack spacing, ft	60.0	25.0
Max. daily temp. * ^{o}F	80.5	80.0
Min. daily temp. * ^{o}F	-11.5	3.0
Fabric Type	Petromat	
Fabric Effectiveness	3.05	3.05

*Average daily high and low temperatures.

TABLE 7 EFRON ANALYSIS OF I-271

Time Mo.	Avg. Temp. ^{o}F	Avg. Modulus ksi	Joint Opng. in	Load lb	% Joints Cracked
0	80.5	0.27	0	0	0
1	72.8	0.56	.0601	268	**
2	57.5	2.12	.1228	368	**
3	42.2	7.95	.1802	701	**
4	26.8	30.00	.2233	1571	**
5	11.5	112.00	.2457	2864	**
6	-3.8	390.00	.2541	3809	**

TABLE 8 EFRON ANALYSIS OF ROCHESTER INTERNATIONAL AIRPORT

Time Mo.	Avg. Temp. °F	Avg. Modulus ksi	Joint Opng. in	Load lb	% Joints Cracked
0	80.0	0.70	0	0	0
1	73.6	1.21	.0228	64	**
2	60.8	3.75	.0452	126	**
3	47.9	11.50	.0664	304	**
4	35.1	35.60	.0845	756	**
5	22.3	105.00	.0974	1564	**
6	9.4	295.00	.1044	2517	**

SUMMARY, CONCLUSIONS, AND RECOMMENDATIONS

Summary

A newly developed thermally induced reflection cracking prediction model was applied to four highway and one airport pavement overlay projects. The model is mechanistic in that only material properties and pertinent pavement geometry are required as input. The model has been verified in both laboratory and field settings. In the laboratory, agreement between predicted and measured failure time is excellent. In the field, the model predicted the time for reflection cracking to occur to within a few months for the period when 100 percent reflection cracking actually took place for the four highway projects. This agreement is excellent, especially in view of the fact that several assumptions had to be made about the overlay properties.

The model also predicted that thermally induced reflection cracking would not develop in the overlay at Rochester International Airport for 75 years. This overlay was built during the 1984 construction season and has been in service through two winters; at the last rating not a single joint had reflected through this overlay. While survival through two winters does not necessarily validate that 75-year prediction, it does strongly suggest that reflection cracking is not expected soon to be a problem with this overlay. Thus, all five field validation projects are in strong accord with the prediction model.

Conclusions

1. The reflection cracking model developed in this study represents a significant advance in the analysis of the reflection cracking phenomenon because it is based on sound principles of the laws for fracture mechanics.
2. The model does not require developing empirical distress functions as an input to the prediction of reflection cracking failure time.
3. The asphalt concrete overlay is characterized as viscoelastic material where the creep compliance function is an input. This is especially important for thermally induced cracking. However, if this function is not available, the model has a typical master creep compliance function as a user option.
4. The model requires easy-to-find input parameters.
5. The application of the model to the prediction of reflection cracking in both the laboratory and the field settings shows that these predictions could be made with good accuracy.

Recommendations

The model developed in this study to predict the formation of thermally induced reflection cracking appears to be successful when applied to flexible overlays of rigid pavements. It is, however, not applicable to the analysis of overlays over flexible pavements where thermally induced movements may be significant (i.e., for flexible pavements with low-temperature cracking) because a model to predict thermal movements of viscoelastic pavements is needed. The EFRON program is able to predict these movements in an elastic pavement including a viscoelastic overlay but needs to be modified to include the effect of subgrade friction on a viscoelastic slab. The RECK program can then be used with the inputs from a modified EFRON analysis to predict thermally induced reflective cracking in asphaltic concrete overlays of both rigid and flexible pavements.

Fabric effectiveness factors have been developed for a few nonwoven fabrics including the fiber SAMI layer; similar data are needed for woven fabrics. Testing them requires laboratory testing of beams under fatigue and simulated thermal loading conditions. The testing procedure developed for use in this study is recommended for this purpose.

REFERENCES

1. R. A. Schapery. A Theory of Crack Initiation and Growth in Viscoealstic Media, I. Theoretical Development. *International Journal of Fracture*, Vol. II, No. 1, Feb. 1975.
2. G. A. C. Grahma. The Correspondence Principle of Linear Time-Dependent Boundary Regions. *Quarterly of Applied Mechanics*, Vol. 26, 1968, pp. 167–174.
3. D. S. Dugdale. Yielding of Steel Sheets Containing Slits. *Journal of the Mechanics and Physics of Solids*, Vol. 8, 1960.

4. K. Majidzadeh and G. J. Ilves. *Improved Methods to Eliminate Reflection Cracking*. Final Report, FHWA/RD-86/075. FHWA, U.S. Department of Transportation, June 1985.
5. K. Majidzadeh, G. J. Ilves, H. Sklyut, and V. R. Kumar. *Mechanistic Methodology for Airport Pavement Design with Engineering Fabrics, Vol. I: Theoretical and Experimental Bases*. DOT/FAA/PM-84/9. FAA, U.S. Department of Transportation, Aug. 1984.
6. K. Majidzadeh, G. J. Ilves, and V. R. Kumar. *Mechanistic Methodology for Airport Pavement Design with Engineering Fabrics. Vol. II: Advanced Concepts, Validation and Criteria*. DOT/FAA/PM-84/9. FAA, U.S. Department of Transportation, July 1986.
7. K. Majidzadeh, C. Buranarom, and M. Karahouzian. *Application of Fracture Mechanics for Improved Design of Bituminous Concrete*. Final Report, FHWA-RD-76-91. FHWA, U.S. Department of Transportation, June 1976.
8. H. J. Treybig B. F. McCullough, P. Smith, and H. Von Quintus. *Overlay Design and Reflection Cracking Analysis of Rigid Pavements*. Vol. 1, Final Report, FHWA-RD-77-66. FHWA, U.S. Department of Transportation, Aug. 1977.
9. F. R. McCullagh. *Reflection Cracking of Bituminous Overlay of Rigid Pavements*. Special Report 16. Engineering Research and Development Bureau, New York State Department of Transportation, State Campus, Albany, N.Y., Feb. 1973.
10. W. J. Kenis. *Predictive Design Procedures, VESYS User's Manual*. FHWA-RD-154. FHWA, U.S. Department of Transportation, Jan. 1978.
11. A. Karaki. *Engineering Characteristics of Hot-Recycling Asphalt Materials*. M.S. thesis. Ohio State University, Columbus, 1984.

Publication of this paper sponsored by Committee on Pavement Rehabilitation.

New Mexico Study of Interlayers Used in Reflective Crack Control

VIRGINIA M. LORENZ

The application of an overlay restores the riding quality and skid properties and prolongs the service life of a roadway that has deteriorated. This type of rehabilitation may result in a new problem, reflective cracking, where subsurface cracks propagate into and through the protective overlay. By placing some form of interlayer between the old deteriorated pavement and the new overlay, reflective cracking may be reduced or even prevented. Thus, the useful life of the overlay is increased, resulting in a savings in maintenance costs. New Mexico established several experimental projects under Category 2 experimental projects under Category 2 experimental construction in which different forms of interlayers were used. A description is provided for seven types of interlayers incorporated into the reported four of the original six projects located throughout the state. For each project, the original pavement structure, the new overlay, and the type of interlayer is given. Also, inspections made at different intervals are summarized. Conclusions derived from the studied projects indicate that interlayers do retard the rate of reflective cracks, implying a savings in maintenance cost. Interlayers do not necessarily prevent crack reflection. Of all the types of interlayers used in the reported projects, one type of paving fabric (Mirafi 140) performed the best at reducing reflective cracks whereas the two types of rubberized asphalt membranes performed second and third best. On one project, it was revealed that two control sections performed just as well as the fabric and the two rubberized asphalt membranes. Out of the three projects with similar weather data, two projects had similar results, and the aforementioned fabric performed best.

The primary objective of any pavement design system is to provide a roadway that is not only safe and rides comfortably, but also extends these characteristics over a maximum useful life with a minimum amount of required maintenance. Because the pavement generally deteriorates in the forms of cracking, rutting, and other surface deformations, rehabilitation frequently involves applying a thin overlay over a properly prepared cracked pavement. This method of restoration may subsequently result in a new problem—that of reflective cracking patterns that migrate into and eventually through the overlay. Once the overlay is fractured, erosion can occur rapidly. the ride and safety performance of the roadway are eventually severely affected, resulting in further costly maintenance. Many highway agencies perceive that placing some form of interlayer between the old deteriorated pavement and the new overlay will prevent, or at least retard, reflective cracking, thereby increasing the life of the overlay and resulting in a savings in maintenance costs.

New Mexico Highway Department, P.O. Box 1149, Santa Fe, N. Mex. 87504–1149.

The objective of this study was to finalize the evaluation of several New Mexico experimental projects that were established under Category 2 experimental construction and to provide an overall evaluation of several interlayer systems that New Mexico has implemented for the purpose of retarding reflective cracking. Only the first four of the original six reported projects are discussed.

MECHANISMS OF REFLECTIVE CRACKING *(1, 2)*

Horizontal and vertical movements between the original pavement and the overlay are the basic mechanisms that result in the development of reflective cracking. Although several field observations and theoretical analysis of reflective cracking have been made, there have not been many controlled projects in which sufficient data were taken to accurately determine the cause or factors associated with this type of cracking. Most of the projects studied consisted of an asphalt overlay over a portland cement concrete pavement. Hence, a generally accepted well-developed description of the mechanisms and response variables is not available.

Reflective cracking is generally accepted to be partially due to horizontal movements resulting from the expansion and contraction of the existing pavement as a result of temperature and moisture changes. Tensile stresses produced from movements at the joints or cracks become critical because of the bond between the overlay and the existing pavement. The amount and rate of temperature change, slab length, gauge length across the joint or crack, and properties of the overlay materials are all contributing factors to the development of reflective cracking.

Repeated traffic loadings produce differential vertical movements at joints and cracks that result in shear stress concentrations at the joints and cracks in the overlay. The magnitude of load, the amount of load transfer across the joint or crack, and the differential subgrade support under the existing pavement are important factors involved in differential deflections.

INTERLAYER SYSTEMS

Several projects have been undertaken in New Mexico in which interlayers were used in the hopes of reflective crack retardation. The types of interlayers incorporated into the four experimental project locations are as follows:

The Arizona rubberized asphalt membrane is produced by the Arizona Refining Co., Phoenix, Arizona. An 85-100 pen asphalt was combined with 20 percent reclaimed replasticized rubber and 2 percent extender oil and then heated to 410°F. A

120-150 pen asphalt was used in lieu of the 85-100 pen asphalt on one of the projects. As the material was uniformly applied at an average rate of 0.63 gal/yd^2 across the roadway, the small cracks were filled. Chips were then spread across the membrane at an average rate of 38 lb/yd^2.

Arkansas mix consists of an open-graded bituminous pavement with a coarse gradation with aggregate less than 2 in. in size and 3 percent AC-20 grade asphalt. The material is placed in one 3½-in. lift and then rolled by a 5-ton roller.

Heater-scarification is carried out by two units used to preheat the pavement. One unit scarifies the existing mat to a depth of ¾ in. The rejuvenating agent Reclamite is then applied to the scarified surface by a distributor at a rate of 0.08 gal/yd^2. A steel roller follows the distributor to compact the material.

Mirafi 140, manufactured by Celanese Fibers Marketing Co., is a nonwoven fabric uniquely constructed from two types of continuous filament fibers. One type of fiber consists of a polypropylene homofilament, and the other is a heterofilament composed of a polypropylene core covered with a nylon sheath. During the webmaking process, the heterofilaments are heat bonded or fused together where they intersect. During this process, the homofilament polypropylene, which is unaffected by the heat, becomes mechanically interlocked with the other fibers, thereby giving the fabric its high tear strength and elongation capability.

Petromat, a nonwoven fabric, is manufactured by Philips Fibers Corp. A needlepunching process uses polypropylene filameters to form the fabric.

The Sahuaro rubberized asphalt membrane is produced by the Sahuaro Petroleum and Asphalt Co., Phoenix, Arizona. The rubberized asphalt, which is blended at 350°F, consists of 25 percent vulcanized granulated rubber and 120-150 pen asphalt. The mixture is diluted to between 5.5 and 7.5 percent by volume with kerosene. The mixture is applied at 325°F on the roadway at an average rate of 0.6 gal/yd^2. Chips are then spread across the membrane at an average rate of 38 lb/yd^2.

The standard base course, which is placed directly on top of the existing mat, consists of a finer gradation with aggregate ¾ in. in size and smaller. The moisture content is maintained at 5 percent; a vibratory roller is used for compacting the 4-in. layer.

EXPERIMENTAL PROJECTS

The four experimental projects in which these interlayers were used, located as shown in Figure 1, were the following:

1. I-25, 7.0 mi south of Raton, in north Colfax County;
2. I-40, 4.5 mi east of Clines Corners, in east Torrance County;
3. I-25, 8.2 mi north of Truth or Consequences and North and Mitchel Point Interchanges, in north Sierra County; and
4. I-40 west of Grants, mileposts 70.15 to 79.0, Bluewater Interchange to Milan Interchange, in Cibola County.

Environmental conditions that affect the pavement structure were collected for a 3-year period (1980–1982) at national weather stations located in close proximity to each project site. Provided by the National Climatic Data Center in Asheville, North Carolina, the data were compared and found to be similar for the following projects: I-25 at Raton, I-40 at Corners, and I-40 at Grants.

Project on I-25, South of Raton

Discussion of Project

The original roadway was completed in 1968 with thicknesses and types of layers as follows: ⅝-in. plant mix seal coat, 4½-in. plant mix bituminous pavement, 6-in. untreated base, 6-in. cement-treated base course, and 4-in. untreated subbase. The project was designed using the *R*-value, traffic index, and gravel equivalent design concept rather than the AASHTO Interim Design Guide procedures for pavement design.

The experimental project consisted of overlaying the existing roadway and using two types of crack relief systems. Prior to construction, several pavement distresses were observed. Some rutting had occurred in the wheelpaths of the driving lanes. Extensive longitudinal and transverse cracking could be seen as well as some localized alligator-type cracking. There was no indication that the pavement failed structurally, requiring the removal and replacement of the underlying structure. Six 600-ft monitor sections were demarcated so that each of the types of crack relief systems was represented in the construction of two sections, whereas the remaining four sections were constructed as control sections with different thicknesses of plant mix bituminous pavement (PMBP) layers and without the use of an interlayer. All cracks in each monitor section were photographed and logged in a field book for future reference. The overlay thicknesses consisted of 2½ and 4 in. for the no-interlayer sections and 2 in. for the Mirafi 140 and Petromat sections. A ⅝-in. plant mix seal coat was constructed on the entire project.

This experimental project was completed in November 1978 at an initial cost of $72,212/lane-mi. All cracks in the existing pavement had been blown clean and filled with 120-150 pen asphalt. An 85-100 pen asphalt was spread as a tack coat before the Mirafi 140 fabric was placed at a rate of 0.15 to 0.20 gal/yd^2 and at an approximate temperature of 375°F. Before the Petromat fabric was placed, the 85-100 pen asphalt was applied as a tack coat at a rate of 0.25 gal/yd^2 and at an approximate temperature of 325°F. No specific problems were reported during construction.

This project has since been inspected several different times with the last inspection occurring on October 18, 1983. Only the monitor sections were inspected and all cracks were noted in the log book. The primary distresses that occurred in one or all of the monitor sections were rutting, raveling, and fatigue cracking. Table 1 summarizes the number of cracks observed before the overlay construction and during each inspection after the construction, and the percent of the reflective cracks of the original cracks for each monitor section.

Summary and Conclusions

Cracks were first observed during the final inspection, which

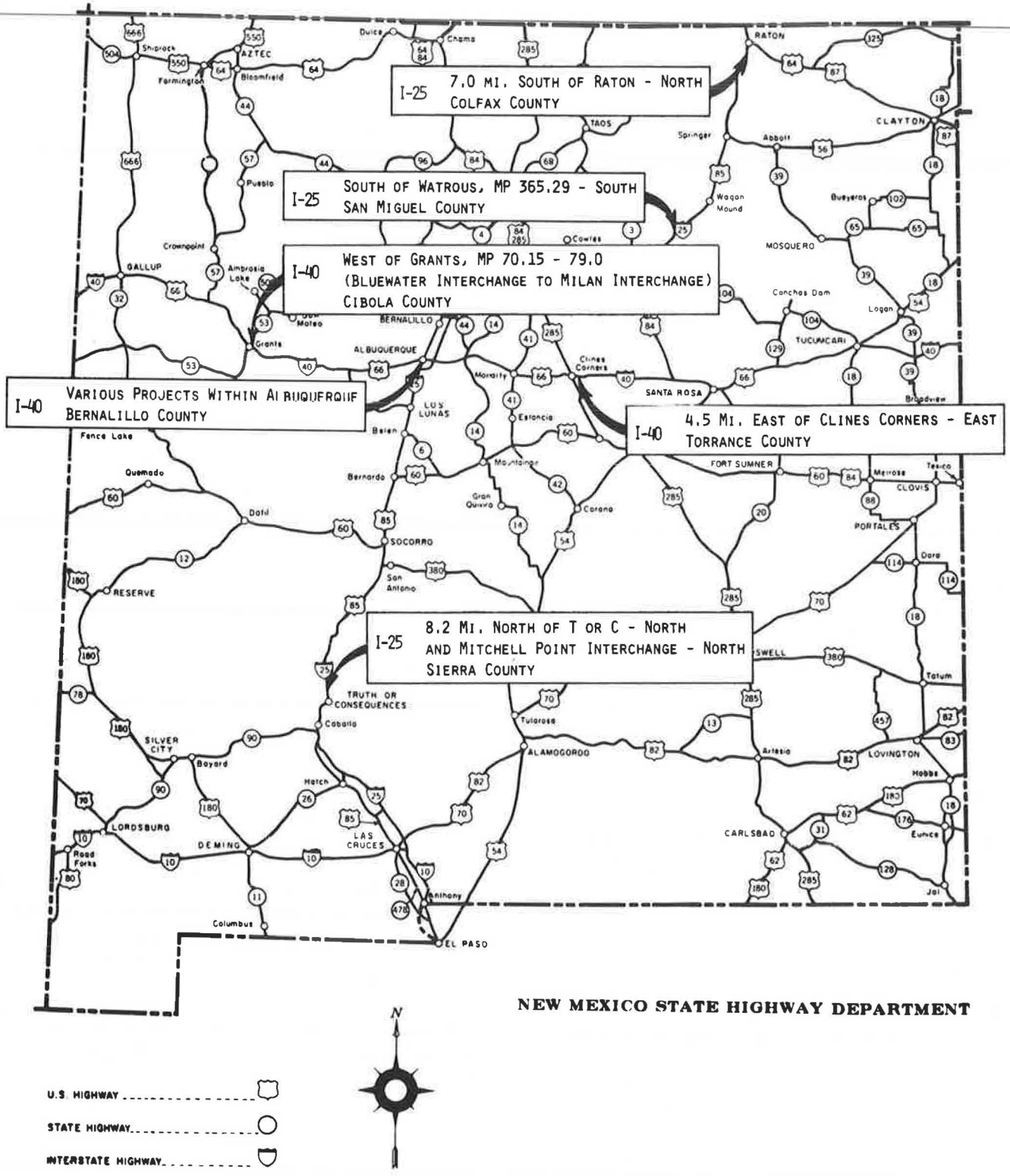

FIGURE 1 New Mexico experimental project locations.

TABLE 1 REFLECTIVE CRACKS, I-25 SOUTH OF RATON

TEST SECTION NUMBER Type of Interlayer	Total No. of Original Cracks	Number of Cracks Observed Percent of Total Number of Original Cracks Date of Inspection (Age of Overlay in Years) 4/26/79 (0.4)	1/22/80 (1.2)	10/15/81 (2.9)	10/18/83 (4.9)
SECTION I					
Control Section	23	0	0	0	9
No Interlayer		0%	0%	0%	39%
SECTION II					
Mirafi 140	32	0	0	0	9
Fabric		0%	0%	0%	28%
SECTION III					
Petromat	37	0	0	0	10
Fabric		0%	0%	0%	27%
SECTION IV					
Control Section	46	0	0	0	9
No Interlayer		0%	0%	0%	20%
SECTION V					
Control Section	35	0	0	0	8
No Interlayer		0%	0%	0%	23%
SECTION VI					
Control Section	32	0	0	0	9
No Interlayer		0%	0%	0%	28%

took place almost 5 years after the overlay construction. The two monitor sections with 4 in. of PMBP and no interlayer have both the greatest percentage (39 percent) and the smallest percentage (20 percent) of reflective cracks. The section using Mirafi 140 fabric had 28 percent of the cracks return. The section constructed with Petromat fabric had 27 percent of the original cracks return. Where a 2½-in. layer of PMBP was built without an interlayer, 23 percent of the original cracks reflected through in one section and 28 percent occurred in the other section. Figure 2 is a graph of the percent of cracks returned versus the number of years since the overlay was constructed. As shown, after almost 5 years of service, fewer than 30 percent of the cracks reflected through the overlay in five out of the six sections. The pavement distresses that developed indicate that the reflective cracks could be caused by repeated traffic loads. The Petromat section and two control sections had the best performance of all the experimental sections in reducing reflective cracking.

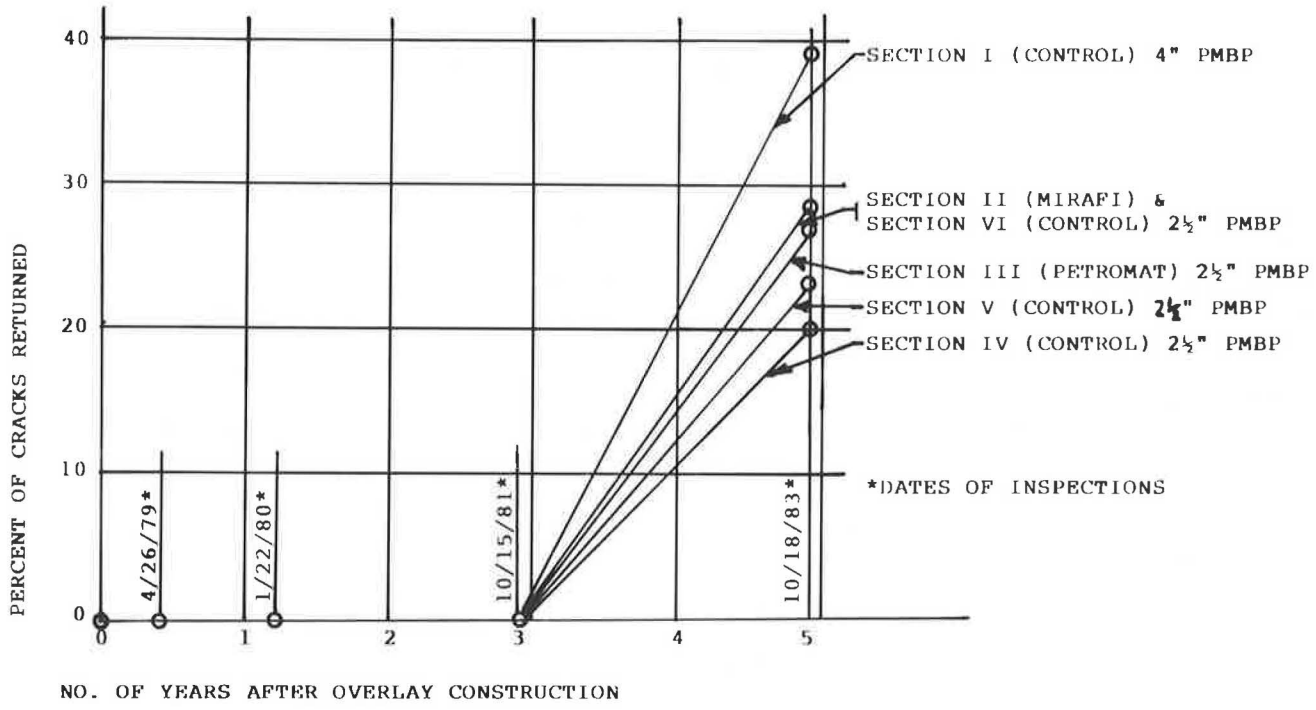

FIGURE 2 Reflective cracks versus overlay life, I-27, 7.0 mi south of Raton.

Project on I-40, East of Clines Corners

Discussion of Project

Completed under three contracts, the original roadway was built in 1956–1958 with layer thicknesses and types of materials used in the construction as follows: 5/8-in. plant mix seal coat, 3-in. PMBP, 4-in. base course, and 4-in. subbase. Stage construction surfacing was designed using an *R*-value, traffic index, and gravel equivalent. Records indicated that a 2-in. overlay was anticipated to be structurally sufficient to complete the stage construction for the anticipated life expectancy.

The entire experimental project, which was completed at a cost of $102,297/lane-mi, consisted of overlaying the existing roadway with 5 1/2 in. of PMBP and implementing four different types of crack relief systems: Sahuaro rubberized asphalt, Arizona rubberized asphalt, Mirafi 140, and Petromat. Extensive transverse, longitudinal, and alligator cracks observed before construction were photographed and logged in a field book for future reference. Some pavement areas were removed and replaced because they were so badly deteriorated.

Six 600-ft sections completed by July 1978 were selected to be monitored. Sections I–V were constructed with one type of crack relief system and one of these sections was built without an interlayer.

Several problems arose during construction of the overlay project. An investigation attributed the raveling of the rubberized asphalt mixture to incorrect mixing times. An incomplete reaction between the rubber and the asphalt resulted in the stripping of the rubberized material. Section VI was added to the project when these problems occurred during the construction of the section with Sahuaro rubberized asphalt. Section VI was constructed with the same interlayer but with only a 4-in. PMBP layer. The tack coat for the fabrics was 120-150 pen asphalt. For Mirafi 140, the application rate varied from 0.15 to 0.20 gal/yd^2.

Problems occurred in other sections. When the chips that were spread over the rubberized asphalt were too fine, a poor bond to the next layer resulted. The problem disappeared after the chips were rescreened.

Other problems experienced were related to fabric blowing and parachuting because it was not adhering to the tack coat. Additional labor was used to straighten, cut, and replace the fabric. Because the spray bar on the distributor was not long enough to apply the full width required for the Mirafi 140 fabric, a second pass was made that resulted in an excess of asphalt where the two passes overlapped. In addition, the tack coat was not spread uniformly. The laydown machine had a tendency to pull on the fabric, thereby wrinkling it or pulling it apart at the joints. Because shoving of the PMBP occurred in some areas, those sections were removed and replaced. Throughout the entire project, the contractor made an attempt to fill the existing cracks with 120-150 pen asphalt, but it was estimated that only half the cracks were partially filled and the other half were left unfilled.

Flushing occurring in the initial lifts on top of one fabric was attributed to the segregation of the aggregate that occurred during several handling operations. The percentages of asphalt and fines were both increased in an attempt to reduce segregation, but the voids in the mix were reduced thus producing a dense mix. Segregation became a cumulative situation because of improper storage of the aggregate, and improper loading, unloading, and placing of the PMBP. The flushing was eventually eliminated by reducing the percent of asphalt, and the percent of fines was reduced to provide voids in the mix.

Since construction was completed, this project has been inspected several times with the most recent inspection occurring on September 8, 1983. All new cracks were logged in the book for only the monitor sections. Pavement distresses observed in one or more sections included severe bleeding, rutting, and transverse and longitudinal cracking.

Core samples taken in each monitor section in this project and analyzed to verify the causes of the observed pavement distresses indicated the following:

1. Bleeding occurring in the pavement surface resulted from too high an asphalt content in the plant mix seal coat or PMBP, or the asphalt stripped from the aggregate.
2. The original cracks had not been properly cleaned and sealed.
3. Stripping of the asphalt from the aggregate caused portions of the cores to disintegrate.
4. In most cases, the interlayer remained intact, even though the original crack propagated through the pavement layers to the top.

Table 2 indicates the number of cracks observed before the overlay construction and during each inspection.

Summary and Conclusions

Cracks began appearing as early as 19 months after the overlay construction in the Arizona rubberized asphalt section. After 2 years, cracks were observed in the first Sahuaro rubberized asphalt section. Cracks appeared in the control section and the second Sahuaro rubberized asphalt section after almost 2 1/2 years. After more than 5 years, cracks were observed in all sections. The greatest percentage (51 percent) of reflective cracks that were observed during the final inspection occurred in the control section where no interlayer was used. The smallest percentage (22 percent) of cracks that returned was observed in the Petromat section. The percent of cracks in the remaining sections ranged from 25 to 44 percent. Figure 3 is a graph of the percent of cracks returned versus the number of years since the overlay was constructed for each monitor section. After more than 5 years of service, less than 30 percent of the cracks returned in three out of the six sections. The pavement distresses observed indicated that repeated traffic loads and temperature and moisture changes possibly aided in the development of the reflective cracking. The Petromat, Sahuaro, and Arizona sections performed the best in reducing the number of reflective cracks.

Project on I-25, North of Truth or Consequences

Discussion of Project

The original roadway was built in July 1966 with the configuration of materials and layer thicknesses as follows: 1 1/2-in.

TABLE 2 REFLECTIVE CRACKS, I-40 EAST OF CLINES CORNERS

TEST SECTION NUMBER Type of Interlayer	Total No. of Original Cracks	Number of Cracks Observed Percent of Total Number of Original Cracks Date of Inspection (Age of Overlay in Years) 1/15/80 (1.4)	7/31/80 (2)	2/19/81 (2.4)	10/6/81 (3.2)	9/8/83 (5.1)
SECTION I Sahuaro Rubberized Asphalt	25	0 0%	1 4%	2 8%	3 12%	11 44%
SECTION II Arizona Ref. Co. Rubberized Asphalt	28	1 4%	0 0%	1 4%	1 4%	7 25%
SECTION III Mirafi 140 Fabric	40	0 0%	0 0%	0 0%	0 0%	12 30%
SECTION IV Petromat Fabric	37	0 0%	0 0%	0 0%	0 0%	8 22%
SECTION V Control Section No Interlayer	41	0 0%	0 0%	5 18%	6 15%	21 51%
SECTION VI Sahuaro Rubberized Asphalt	53	0 0%	0 0%	3 6%	3 6%	15 28%

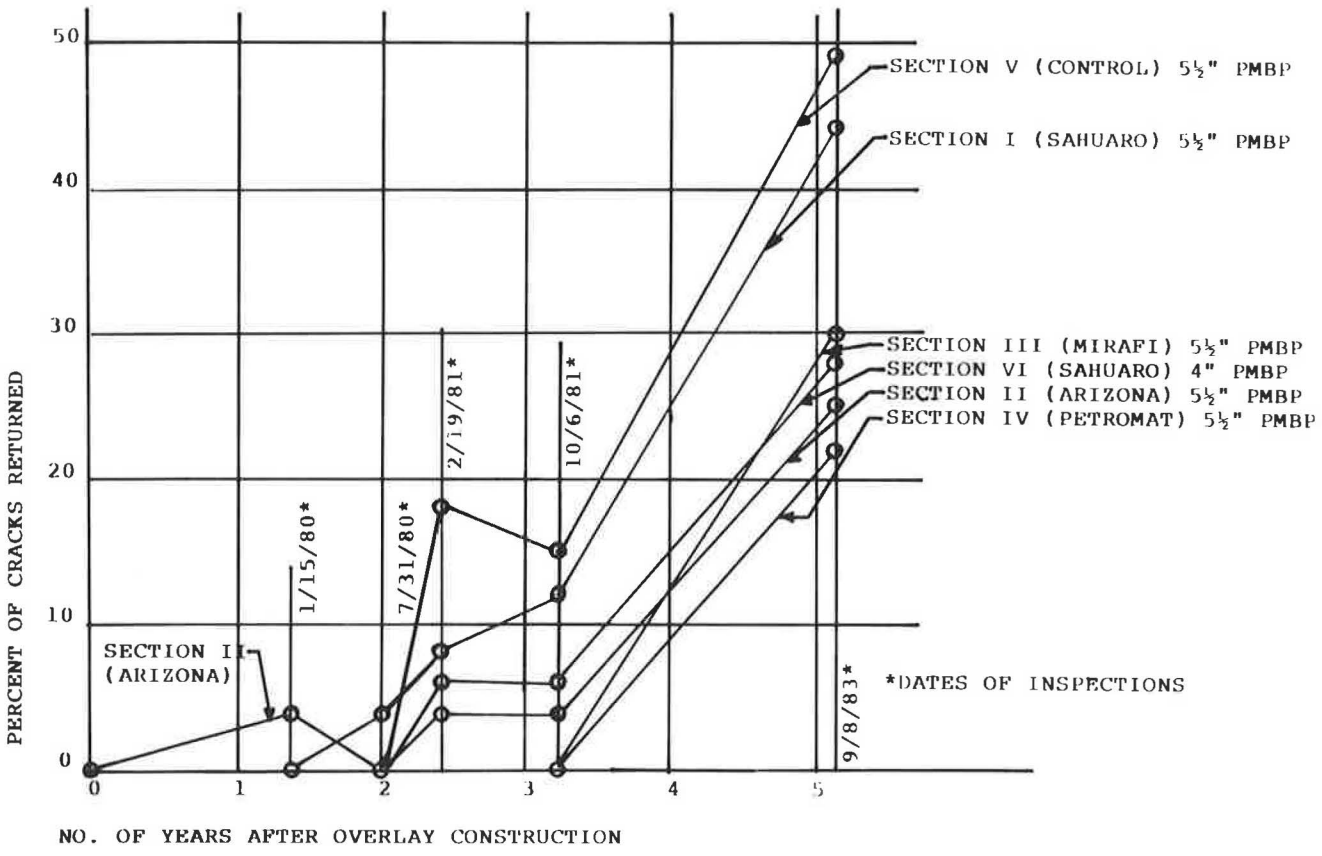

FIGURE 3 Reflective cracks versus overlay life, I-40, 4.5 mi east of Clines Corners.

surface course, 2-in. binder course, 4-in. asphalt-treated base, and 4-in. subbase. Design data were not available in the project files.

The experimental project consisted of incorporating four crack relief systems (Sahuaro rubberized asphalt, Arizona rubberized asphalt, Petromat, and Mirafi 140) and the heater-scarification process with a 2-in. PMBP overlay.

Prior to construction, numerous transverse cracks were observed with widths ranging from 1/4 to 1 in. and with depths of approximately 8 in. No alligator cracking was apparent. One 500-ft monitor section was laid out in each experimental test section and one in the control section. All cracks in each monitor section were photographed and logged in a field book for future reference.

This experimental project was completed in July 1979 at an initial cost of $112,434/lane-mi. The contractor attempted to fill all cracks in the existing pavement with 120-150 pen asphalt; however, because of the depth and width of each crack, not all cracks were filled. Other problems occurred during construction. In the heater-scarification section, while the second heater unit was scarifying the old pavement, the asphalt in the previously filled cracks began to bleed through the scarified material. Excessive asphalt from crack sealing also caused a problem in the Sahuaro section. Bleeding occurred through the chips when the hot rubberized asphalt blend was applied to the area where cracks had been filled. Minor wrinkles that occurred in both fabric sections did not present any problems.

Since the date when construction was completed, several inspections have taken place. During an interim inspection, several cores were sampled. An analysis resulted in the following comments:

1. The rubberized asphalt membranes and the fabrics appeared to be intact.
2. Small cracks remained filled with crack sealant while large cracks had voids as deep as 2 in. between the interlayer and PMBP. Where no crack sealant was used, the cores fell apart into pieces.
3. Old cracks in the control section reflected through the new surfacing.
4. There was no evidence of reflective cracking in the heater-scarification section.

The final inspection was performed on September 27, 1983, when the monitor sections were observed in detail and all new cracks were noted in the log book. The pavement distresses observed in one or more sections were raveling, rutting, and transverse and longitudinal cracks.

The data in Table 3 show the number of cracks and the percent of original cracks observed during all reported inspections. Figure 4 shows the increase of percent of cracks returned versus the age of the overlay construction.

Summary and Conclusions

Cracks began to appear within the first year after the overlay construction in four of the six monitor sections. Cracks appeared in the remaining two sections within the next 6 months following that first year. The pavement distresses indicate that both vertical and horizontal movements possibly contributed to the development of reflective cracking. The heater-scarification section and the Mirafi 140 section had the best performances for reducing reflective cracking after 4 years with cracks returning at 77 and 80 percent, respectively.

TABLE 3 REFLECTIVE CRACKS, I-25 NORTH OF TRUTH OR CONSEQUENCES

TEST SECTION NUMBER Type of Interlayer	Total No. of Original Cracks	Number of Cracks Observed Percent of Total Number of Original Cracks Date of Inspection (Age of Overlay in Years) 9/12/79 (0.1)	1/7/80 (0.4)	12/11/80 (1.4)	10/13/81 (2.2)	10/12/83 (4.2)
SECTION I Heater-Scarify & Rejuvenate	30	0 0%	0 0%	3 10%	6 20%	23 77%
SECTION II Sahuaro Rubberized Asphalt	22	0 0%	0 0%	7 32%	9 41%	23 100%
SECTION III Arizona Ref. Co. Rubberized Asphalt	25	0 0%	5 20%	14 56%	15 60%	28 100%
SECTION IV Petromat Fabric	19	0 0%	1 5%	9 47%	11 58%	20 100%
SECTION V Mirafi 140 Fabric	25	0 0%	3 12%	8 32%	9 36%	20 80%
SECTION VI Control Section No Interlay	31	0 0%	13 42%	19 61%	19 61%	31 100%

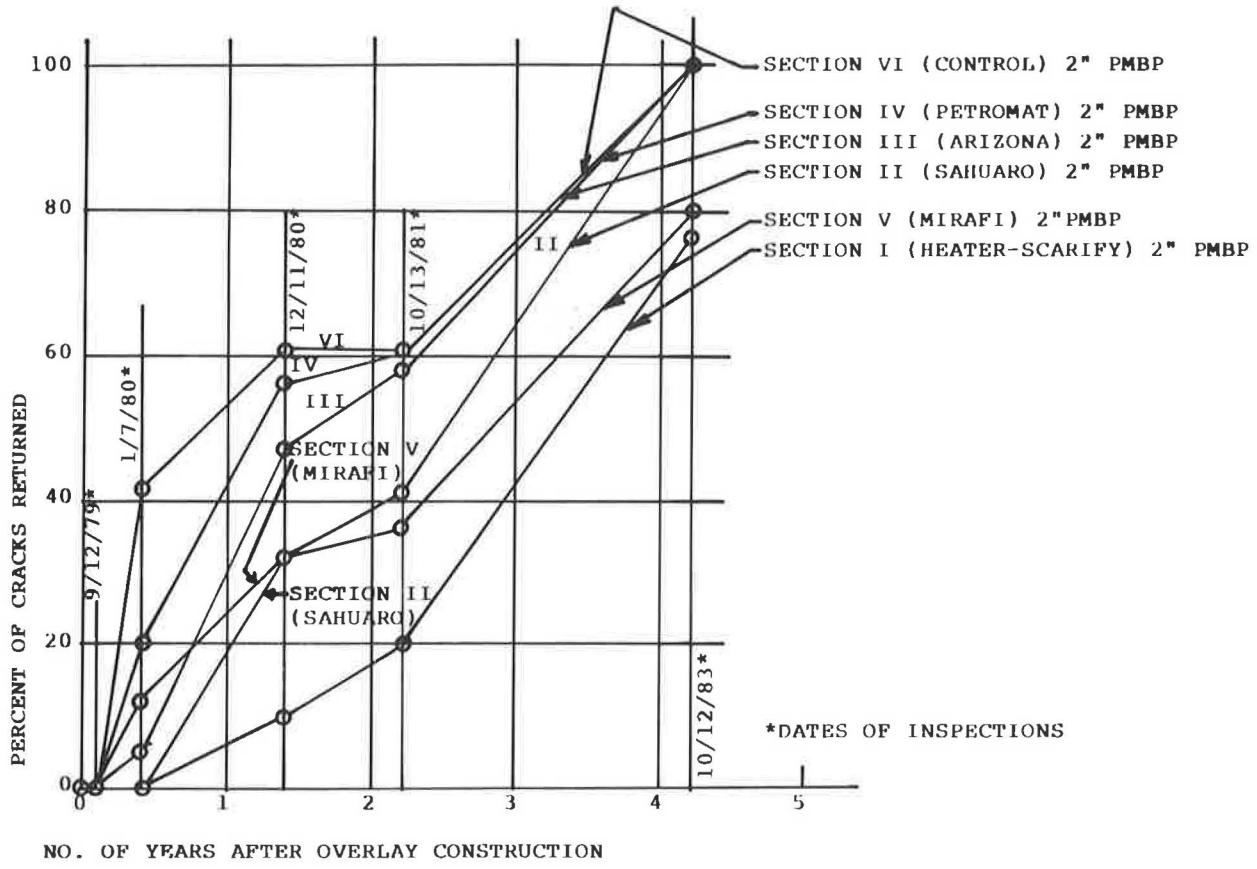

FIGURE 4 Reflective cracks versus overlay life, I-25, 8.2 mi north of Truth or Consequences.

Project on I-40 West of Grants

Discussion of Project

The project for constructing the original pavement was completed in 1970 with the following configuration of the thicknesses and materials: 3 in of asphalt concrete, 6 in. of cement-treated base, and 4 in. of subbase. Design data were not available for this project.

Two types of systems were incorporated as stress-relieving interlayers in this experimental project. The Arkansas mix was overlaid with 2½ in. of PMBP and the standard base course was overlaid with 3½ in of PMBP. A 500-ft monitor section was laid out in each experimental test section for which all major cracks were photographed and logged in a field book.

This project was completed in November 1979 at a cost of $76,044/lane-mi. No major problems developed during the construction of the standard base course or the Arkansas mix. Only construction traffic was allowed on these sections prior to placement of the hot mix; all traffic was discouraged on the Arkansas mix until it had completely cooled.

Since project completion, three inspections have been documented. The last inspection occurred on October 5, 1983, in which the monitor sections only were observed in detail. New cracks that appeared since the overlay construction were logged in the field book. The primary pavement distress that occurred in each section was rutting with an average depth of 3/8 in.

Some flushing or bleeding also occurred in both sections of the driving lane. In addition, transverse and longitudinal cracks were observed.

Table 4 presents the number of cracks returned for each inspection and the percent of the original cracks. Figure 5 is a graph showing the percent of reflective cracks versus the time in years after the overlay construction.

Summary and Conclusions

Cracks first began appearing in each section after slightly less than 4 years. Pavement distresses indicate that the reflective cracks were possibly developed by repeated traffic loads. A total of 37 percent of the cracks had returned in the Arkansas mix section. The standard base course performed better with only 5 percent reflective cracks.

CONCLUSIONS AND RECOMMENDATIONS

The following conclusions were derived from this study.

1. Interlayers do retard the rate of reflective cracks, and can therefore produce a savings in maintenance costs.

TABLE 4 REFLECTIVE CRACKS, I-40 WEST OF GRANTS

TEST SECTION NUMBER Type of Interlayer	Total No. of Original Cracks	Number of Cracks Observed Percent of Total Number of Original Cracks Date of Inspection (Age of Overlay in Years) 2/6/80 (0.3)	4/80 (0.4)	10/8/81 (1.9)	10/5/83 (3.9)
SECTION I					
Arkansas Mix	24	0	0	0	9
		0%	0%	0%	37%
SECTION II					
Standard	41	0	0	0	2
Base Course		0%	0%	0%	5%

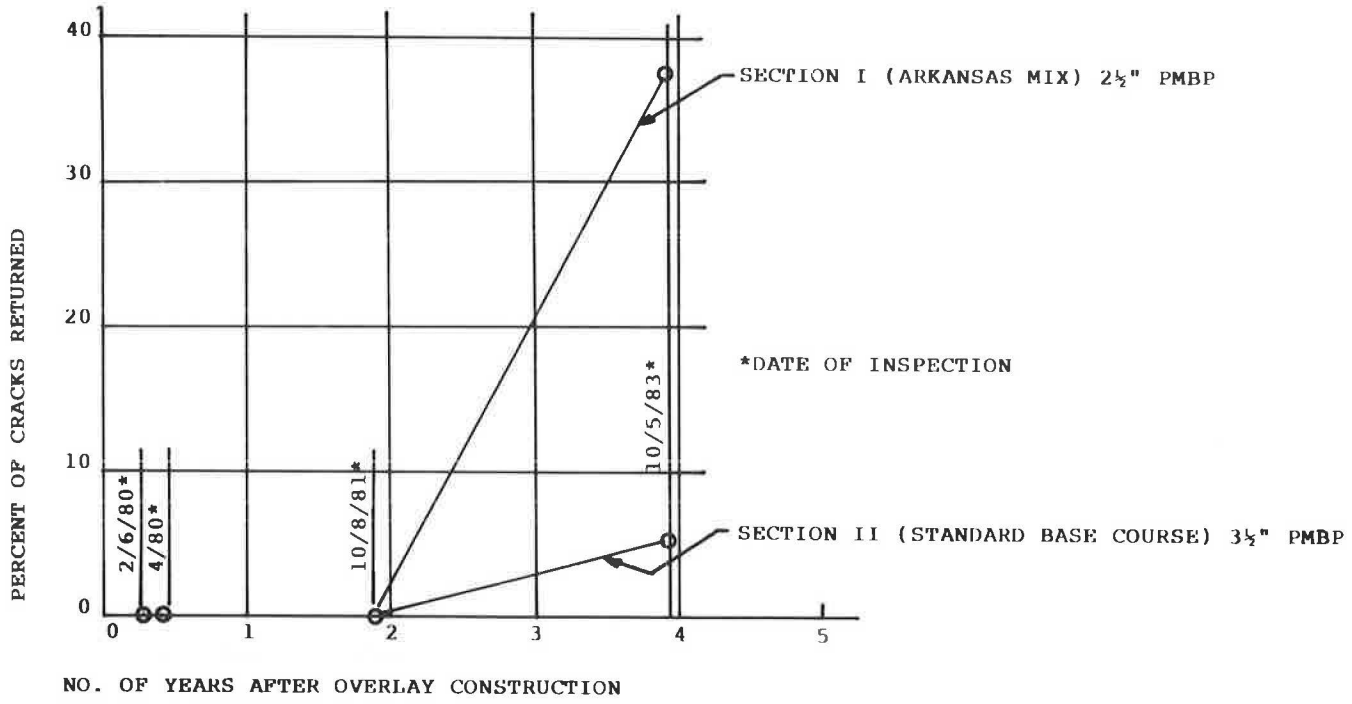

FIGURE 5 Reflective cracks versus overlay life, I-40, Mileposts 70.15 to 79.00, west of Grants.

2. Interlayers do not necessarily prevent crack reflection.
3. Petromat fabric performed the best when all of the New Mexico experimental projects were compared.
4. Arizona and Sahuaro rubberized asphalt membranes were close competitors to Petromat in reducing reflective cracking.
5. Two control sections on I-25 at Raton performed just as well as the Petromat fabric and the Arizona and Sahuaro rubberized asphalt membranes on the project on I-40 at Clines Corners. One section had a 4-in. overlay and the other section had only a 2½-in. overlay. A thicker overlay appears to reduce crack propagation, but it would not be as cost-effective as the fabric or rubberized asphalt membrane.
6. Two of the three projects with similar weather data had similar results. The results from both the I-40 project at Clines Corners and the I-25 project at Raton indicated that Petromat fabric performed the best with 30 percent or less reflective cracks.

The following are recommendations for future experimental research and routine construction projects:

1. Tighter control is needed in construction of projects. Numerous problems occurred during construction of these projects that probably affected the actual performance of the interlayers. To achieve the expected results of a reduction of reflective cracks, the interlayers must be constructed according to specifications.
2. Interlayers consisting of a paving fabric or a rubberized asphalt membrane are highly recommended for reducing reflective cracks in an overlay construction project. For the interlayer to be successful, the existing surface needs to be patched, cleaned, free of irregularities, and dry. All cracks wider than ½ in. are to be cleaned and sealed. In the case of fabrics, the tack coat application rate should consist of a total of the asphalt retention required by the fabric as tested, and an amount of

asphalt needed to satisfy the surface hunger of the existing pavement.

3. Heater-scarification is a plausible alternative if cracking in the existing pavement is excessive. The initial cost of this process could be less than cleaning and sealing the cracks followed by the placement of an interlayer.

ACKNOWLEDGMENT

The author expresses appreciation to Douglas I. Hanson, Robert D. Williams, and Robert G. Ringer for their critical reviews and suggestions; to H. Gerald Boxberger, Robert D. Williams, Robert L. Wheeler, Lloyd Buchwald, L. Linson, Dan Sowle, John Gonzales, Ruben C. Garcia, and Thomas J. Koglin for their assistance in the collection and documentation of field information; to Arthur Palmer for his assistance in the collection of historical data; to William Gonzales for his graphical work; and to Ray Pavlovich, Orlando P. Garcia, Susan Q. Gallaher, and Connie Maestas for their assistance in assembling and editing the printed portion of the paper.

REFERENCES

1. G. Sherman. *NCHRP Synthesis of Highway Practice 92:Minimizing Reflection Cracking of Pavement Overlays*. TRB, National Research Council, Washington, D.C., Sept. 1982.
2. H. J. Treybig, B. F. McCullough, P. Smith, and H. Von Quintus. *Overlay Design and Reflection Cracking Analysis for Rigid Pavements*. FHWA-RD-77-66. FHWA, U.S. Department of Transportation, Aug. 1977.

Publication of this paper sponsored by Committee on Pavement Rehabilitation.

Status of the South Dakota Profilometer

DAVID L. HUFT, DEBRA C. CORCORAN, BLAIR A. LUNDE, AND PAUL A. ORTH

During 1981–1982, the South Dakota Department of Transportation (SDDOT) developed a low-cost profilometer system to replace its response-type roughometer. Since then, the unit has been used to conduct annual statewide profile surveys primarily for pavement management purposes. In September 1984, SDDOT participated in the University of Michigan Transportation Research Institute (UMTRI) Road Profilometer Meeting. The UMTRI draft report of October 1985 showed that the performance of the SDDOT profilometer was deficient in two respects. First, the beginnings of measured profiles showed extraneous long-wavelength content. Second, the system underestimated the profile magnitudes generally, but most severely on smooth highway sections, at lower test speeds, and at longer wavelengths. After the draft report was reviewed, the system was examined to determine whether these deficiencies were symptoms of inherent system shortcomings, or whether they resulted from correctable implementation errors. The errors were in fact determined to be correctable, and the system was modified accordingly. In addition, other changes have been made to allow rut depth measurement and visual rating of highway condition parameters to occur simultaneously with profile measurement.

In 1981–1982, the South Dakota Department of Transportation (SDDOT) developed a low-cost, high-speed road profilometer that has been used to conduct annual statewide surveys for highway roughness evaluation. In 1984, SDDOT was invited to participate in the University of Michigan Transportation Research Institute (UMTRI) Road Profilometer Meeting. The tests, summarized in an UMTRI draft report of October 1985 *(1)*, showed the profilometer performance to be deficient, first because the beginnings of recorded profiles tended to exhibit extraneous long-wavelength content, and more important, because the system tended to underestimate profiles, especially on smooth highway sections, at low test speeds, and at long wavelengths.

After discovery of these problems, SDDOT initiated a complete reexamination of the profilometer system to determine their cause. The purpose of this paper is to describe the profilometer system in greater technical detail than has been published previously *(2)*, explain the causes of the problems cited in the draft report, and describe modifications that have been made both to correct the problems and to extend the usefulness of the system.

DESCRIPTION OF PROFILOMETER

The SDDOT profilometer is an inertial profilometer—that is, it uses an accelerometer to establish an inertial reference plane from which vertical deviations in vehicle displacement are measured. A roadway profile referenced to this plane may be computed as the difference between this displacement and the distance between the vehicle and the pavement.

Conceptually, profile measurement can be divided into the six operations summarized by Figure 1: measurement of the vertical displacement of the vehicle as a function of time; measurement of the horizontal distance the vehicle has traveled; measurement of the vehicle's height above the pavement surface at equally spaced intervals of highway distance; synchronized subtraction of the vehicle displacement and height measurements to compute the relative highway profile; storage of the computed profile on magnetic media; and reconstruction of a filtered profile from the stored profile for purposes of inspection or analysis. The first five operations are performed in real time, as the test vehicle drives down the highway at normal traffic speeds. Profile reconstruction and analysis are performed after the data are returned to the laboratory.

Vehicle Displacement Measurement

Although direct measurement of the test vehicle's vertical displacement through space is impractical, it is possible to measure its vertical acceleration as a function of time and then doubly integrate the acceleration to generate the displacement record. A Schaevitz model LSBC-2 linear servo accelerometer measures the vehicle's vertical acceleration. The unit is biased for 1 g to eliminate the acceleration due to earth's gravity from the signal output. Its range of ± 2 g and frequency response of 0 to 110 Hz are adequate to measure significant vehicle motions in the range of ± 1 g at 0 to 5 Hz.

Besides the significant accelerations, the acceleration signal contains higher-frequency components corresponding to extraneous vibrations in the vehicle body. A low-pass, linear phase filter is used to attenuate these components before the acceleration signal is digitized. According to the Nyquist criterion of sampling, the acceleration signal must not contain any frequency components higher than one-half of the 125-Hz sampling frequency used by the profilometer. The filter should, however, pass the frequencies of interest with as little attenuation as possible. A Frequency Devices Model 757L8L 20-Hz eight-pole filter is mounted on a printed circuit card located within the profilometer computer, along with an operational amplifier that multiplies the acceleration signal by a factor of two to increase the signal level to 5 volts per g. The same card contains a bipolar 15-volt power supply module that powers the accelerometer, filter module, and operational amplifier.

Figure 2 shows the attenuation and delay introduced by the low-pass filter. Below 2 Hz, where the most significant vehicle accelerations occur, the signal loss is less than 0.7 percent. At 4

South Dakota Department of Transportation, 700 East Broadway, Pierre, S. Dak. 57501.

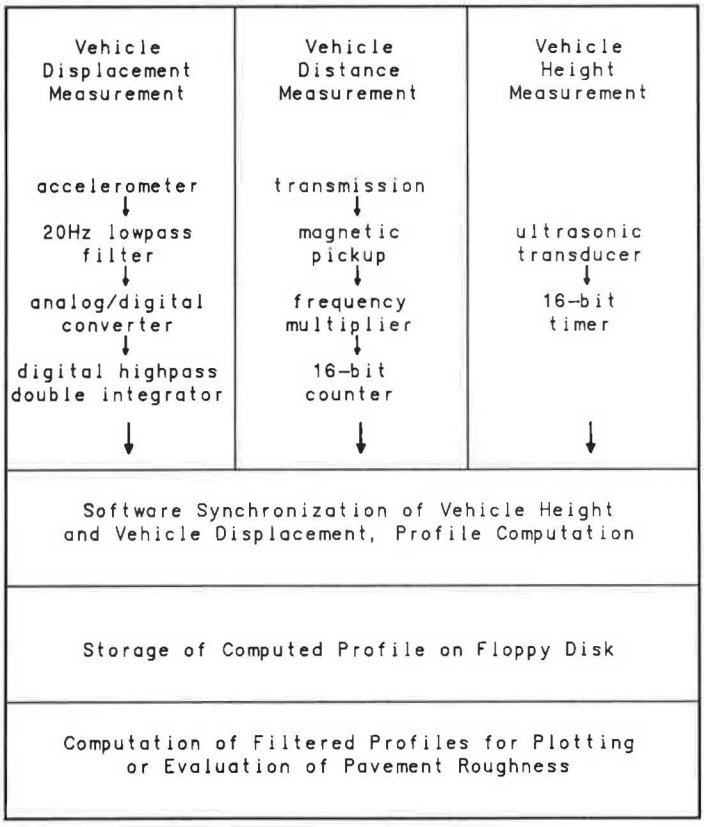

FIGURE 1 Profilometer block diagram, listing major hardware and software components. All processes except the last are done in real time, as the test vehicle drives at normal highway speed.

Hz, the high edge of possible vehicle motion, the loss is approximately 2.7 percent. At 20 Hz, the signal is attenuated by 50 percent, and at the Nyquist frequency of 62.5 Hz, the signal is attenuated by 99.95 percent. The delay introduced by the filter is approximately 25.3 msec and is essentially constant for signals in the frequency range of 0 to 40 Hz, decreasing to 12.3 msec at 62.5 Hz.

After the acceleration signal is filtered, it is converted into numbers that may be manipulated by the profilometer computer. An ADAC Model 1012 12-bit analog-to-digital converter installed in the computer samples the signal at 8-msec intervals, converting signal levels between −5 and +5 volts (corresponding to accelerations of −1 and +1 *g*) into integers between −2047 and +2047. The resolution of the acceleration signal is 1 *g* divided by 2048, or 0.01571 ft/sec^2. The analog-to-digital converter's stated accuracy is ±0.025 percent of full scale reading, or approximately one-half of the resolution.

Acceleration sampling must occur at precisely timed intervals to ensure accuracy in the subsequent integration. Measurements are initiated by an ADAC Model 1601GPT clock programmed to generate interrupts at intervals of 8.000 msec. The clock is equipped with an error flag to indicate whether interrupts are being serviced by software as quickly as they are being generated. Profile measurement software monitors the flag and would abort profile measurement if an error were detected. Tests have shown that the profilometer hardware and software are capable of sustaining the 125-Hz sampling rate under every conceivable operating condition.

The digitized acceleration signal is doubly integrated to yield a record of vehicle displacement. The SDDOT profilometer integrates numerically rather than with electronic circuits in order to avoid problems of integrator saturation.

The growth of errors due to offsets is a problem inherent to both analog and numerical integration. When an acceleration signal composed of a true acceleration $a(t)$ plus some offset b is doubly integrated, the computed displacement $u^*(t)$ consists of the true displacement $u(t)$, one error term linear in time due to the initial (unknown) vertical velocity, and another error term proportional to the square of time t^2. That is,

$$u^*(t) = u(t) + v(0)t + 0.5bt^2 \quad (1)$$

For even small values of offset b, the second error term predominates as time increases. For a profile 10 mi in length, the value of t^2 exceeds 0.5 million sec^2 assuming a test speed of 50 mph. Even for an offset of only 10^{-3} *g*, the displacement error is approximately 8,300 ft, more than 1.5 mi, in elevation. Although the error term involving initial velocity is proportional to time and grows more slowly, it, too, can overwhelm the true displacement. Fortunately, because both error terms vary slowly, they may be controlled by removing very low frequencies from the integrated displacement signal.

A numerical process, a type of digital filter, has been devised to both doubly integrate and high-pass filter the acceleration signal as it is being measured. It is useful to describe the filter's performance in terms of transfer functions that define ratios of

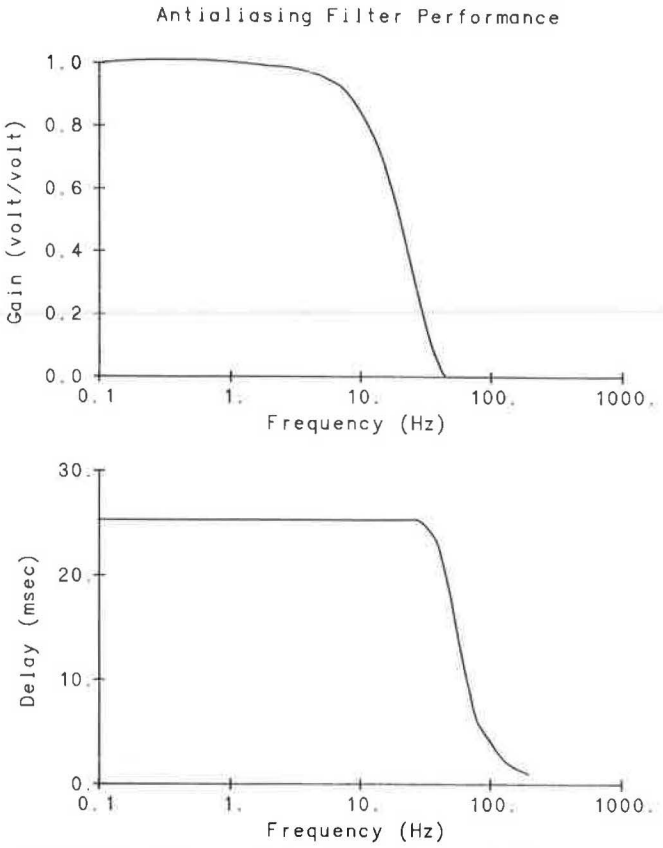

FIGURE 2 Characteristics of the eight-pole, linear-phase, 20-Hz low-pass antialiasing filter used to condition the accelerometer signal.

its output to input within the frequency range of interest. The composite transfer function can be expressed as the product of an integration transfer function $I(f)$ and a high-pass filtering transfer function $H(f)$, where f is the frequency of the signal:

$$F(f) = I(f) * H(f) \tag{2}$$

The ideal double integrator transfer function

$$D(f) = -(1/2\pi f)^2 \tag{3}$$

is numerically approximated by the transfer function

$$I(f) = -[h/2 \sin (\pi f h)]^2 \tag{4}$$

The quality of this approximation depends on the signal frequency f and the sampling interval h; the ratio of actual to ideal integration is given by the relation

$$R(f) = I(f)/D(f) = [\pi f h/\sin (\pi f h)]^2 \tag{5}$$

which is exactly 1 for a frequency of 0, but reaches a maximum value of 2.47 when the frequency equals the Nyquist frequency (one-half of the sampling frequency). At 5 Hz, below which vertical acceleration signals of interest lie, the approximation overestimates the displacement magnitude by 0.5 percent. Although the integration increasingly overestimates at high frequency, the low-pass antialiasing filter so strongly attenuates with increasing frequency that no net overestimation occurs.

The high-pass filtering transfer function is

$$H(f) = 1/[1 + \cot^2 (\pi f h)/\cot^2 (\pi f_0 h)] \tag{6}$$

which has complete attenuation at zero frequency, 50 percent attenuation at the cutoff frequency f_0 (0.01 Hz for the profilometer system), and no attenuation at the Nyquist frequency. Because the transfer function is only second order, the filter does not exhibit sharp roll-off. Its performance is sufficient, however, to limit the growth of integration errors.

The combination of integration and high-pass filtering is accomplished by a second-order recursive digital filter of the form

$$u_n = Au_{n-2} + Bu_{n-1} + Ch_2a_{n-2} \tag{7}$$

where the constants A, B, and C are determined analytically from the sampling interval h and the cutoff frequency f_0. That is, the displacement u_n is given as a linear combination of the two previously computed displacements u_{n-1} and u_{n-2} and the acceleration a_{n-2} measured two sampling intervals previously.

The integration algorithm introduces a signal delay of two sampling intervals at all frequencies, so that the computed displacement at time t actually corresponds to the vehicle displacement two intervals earlier. In addition, the high-pass

filtering introduces delay that increases rapidly as frequency decreases. Thus, longwave vehicle displacement components are shifted significantly.

Figure 3 shows the composite effect of the high-pass double integration, assuming a vehicle speed of 55 mph. The gain ratio—that is, the ratio of computed displacement to true displacement—varies within ±2 percent over the frequency range of 8 to 0.0 Hz, corresponding to wavelengths of 10 to 1,000 ft. At frequencies greater than 1 Hz, the signal delay is nearly constant and equal to a distance equivalent to two sampling intervals, or about 1.3 ft. At lower frequencies, the signal delay increases significantly; at a frequency of 0.0114 Hz, corresponding to a wavelength of 7,000 ft, the signal delay exceeds 1,000 ft.

The practical significance of Figure 3 is that for the sampling frequency, high-pass frequency, and vehicle speed normally used by the profilometer, the high-pass integration accurately estimates the amplitude of vehicle motion at wavelengths up to 1,000 ft, although not without phase distortion and delay at longer wavelengths. Because the vertical motion of the vehicle is restricted to frequencies less than 5 Hz, the integration's overestimation at higher frequencies is not significant.

Because the integration and filtering are based in time rather than distance, lower vehicle speeds alter the wavelength and delay distances. Figure 4 is similar to Figure 3, except that a slower vehicle speed is assumed. As expected, the range of accurate operation is altered in proportion to the ratio of vehicle speeds.

Vehicle Distance Measurement

Accurate determination of the horizontal vehicle travel is required to ensure correct data location. A magnetic pick-up mounted between the profilometer vehicle's transmission and speedometer cable generates electronic pulses at 0.873-ft intervals. At any speed greater than 5 mph, a frequency multiplier located on an interface board within the profilometer computer multiplies the pulse frequency by 512, improving the distance resolution to 0.00190 ft per count. The interface board accumulates these counts in a 16-bit counter until the count matches a software-programmable count equivalent to the desired data interval, then generates a program interrupt that causes the software to accumulate the distance, initiate vehicle height measurement, and compute profile. Normally, an interval of 1.0 ft is specified, but other intervals may be selected so long as they are consistent with the operating speed of the system.

Calibration is determined automatically by measurement of the number of counts required to travel a known distance, allowing periodic adjustment to correct for tire wear.

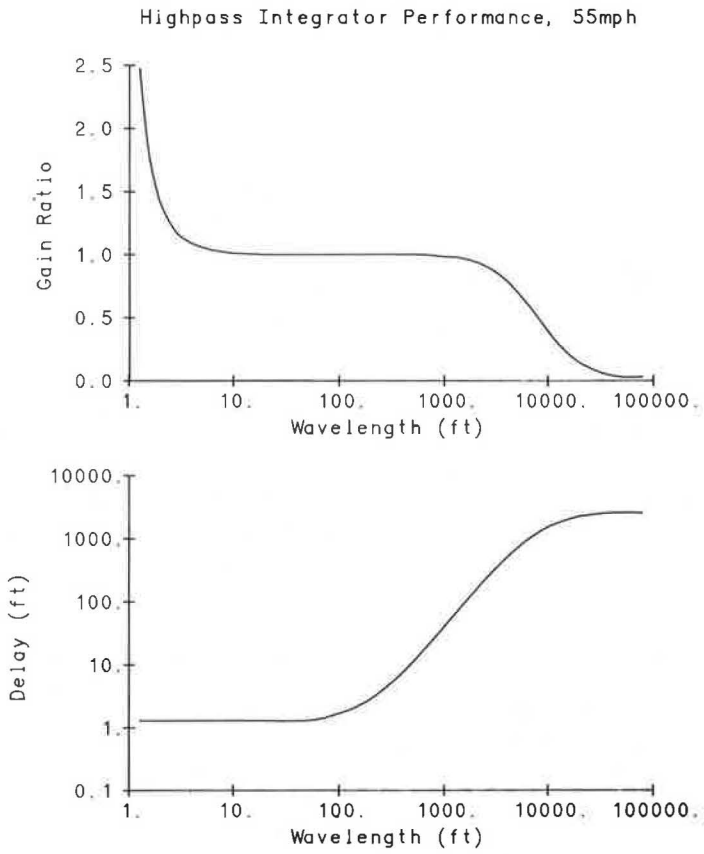

FIGURE 3 Gain ratio (defined as the ratio between amplitudes of computed and true displacement) and signal delay of digital high-pass double integrating filter at 55 mph.

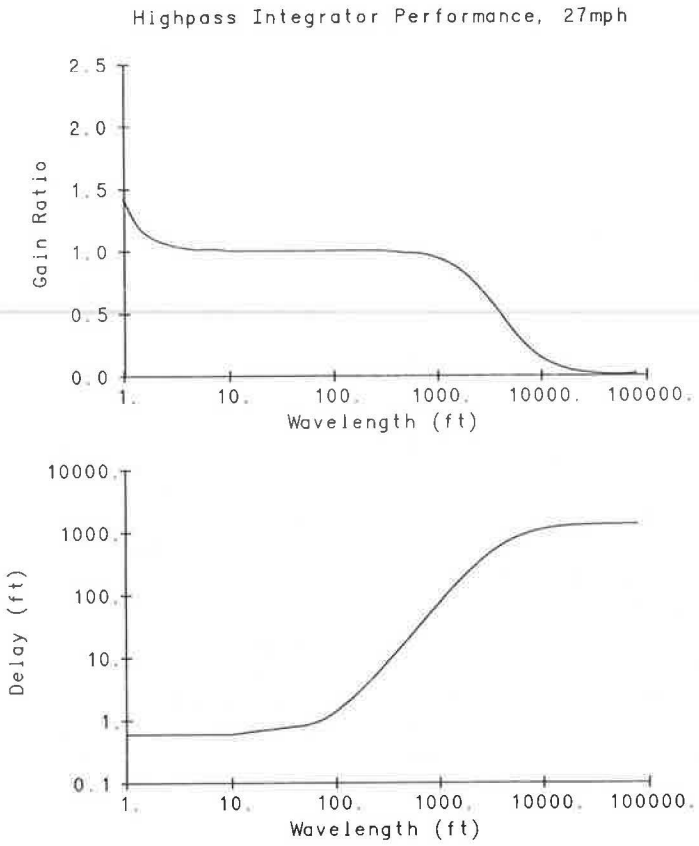

FIGURE 4 Gain ratio (defined as the ratio between amplitudes of computed and true displacement) and signal delay of digital high-pass double integrating filter at 27 mph.

Vehicle Height Measurement

The distance between the accelerometer location and the pavement surface is measured by an ultrasonic ranging device based on an instrumentation quality version of the electrostatic transducer used on autofocusing Polaroid cameras. The principle of operation is relatively simple; a short burst of 50-kHz sound waves is generated by the transducer, travels downward to the pavement surface, and is reflected back to the same transducer. The elapsed time t between sound generation and echo detection is proportional to the distance h between the transducer and the pavement surface, according to the relation

$$t = 2h/c \tag{8}$$

where c is the velocity of sound in air, approximately 1,087 ft/sec. At the equilibrium position of the transducer, approximately 1 ft above the pavement surface, the elapsed time is about 1.8 msec. To prevent interference resulting from multiple echoes, measurements must be performed at time intervals exceeding 10 msec.

Ultrasound generation and detection are performed by electronic circuitry located within the transducer, but control and timing are performed by an interface board installed in the profilometer computer. When the computer determines that the vehicle has traveled the specified sampling distance, software commands the interface to initiate the ultrasound transmission. Later, when the echo is detected, the interface provides a count which represents the elapsed time interval (in μsec).

The transducer's footprint—that is, the area of pavement which reflects the sound—is approximately 4 in. in diameter. Because timing stops on receipt of the earliest echo, any large object of cross section area exceeding 1 in.^{2} or so that protrudes above the surrounding surface may be detected instead of the background surface.

Coarse surface texture can affect the measurement is two ways. First, there is inherent uncertainty in defining the distance between transducer and coarse pavements. (Which surface elevation is the right one?) Second, the uneven and randomly oriented aggregate surfaces presented by a coarse pavement may scatter the ultrasound or cause destructive interference, leading to late echo detection. This problem occurs mainly on extremely coarse (⅝ in. or greater aggregate size) chip seals. Open-graded asphalt mixes, cracks, or smaller chips do not cause difficulty. Although timing accuracy allows measurement resolution of 0.001 ft, pavement surface effects limit accuracy to 0.005 ft on smooth pavement surfaces and 0.010 ft on coarse surfaces.

During the time between signal transmission and echo detection, the vehicle traveling 55 mph moves forward approx-

imately 1.7 in., a distance slightly greater than the transducer's diameter. No correction is made to compensate for an oblique sound path because any correction would be speed dependent and because of the impossibility of precisely identifying which areas on the transducer effectively transmitted and received the sound.

Likewise, no attempt is made to correct the distance measurement for effects of air temperature on sound velocity. The considerable variation of air temperature with height above pavement makes accurate temperature measurement over the entire sound path far more difficult than the expected measurement improvement would justify.

Because vehicle height measurements are taken at specified intervals, profile features shorter than twice that interval are inadequately sampled and are aliased into longer wavelengths. The severity of this problem depends on the short wavelength content of the profile being measured, and could only be diminished by increasing the sampling frequency or increasing the footprint of the transducer. The former alternative could be accomplished by using slower vehicle speeds or multiple transducers, but the latter is impossible without completely redesigning the transducer.

Synchronized Profile Computation

Because the times at which vehicle position $u(t)$ and vehicle height $h(x)$ are measured generally differ, it is necessary for the profilometer software to merge the two records and compute the profile $z(x)$ as their difference

$$z(x) = u(t) - h(x) \tag{9}$$

That is, the software must match vehicle position measurements to height measurements taken at or near the same time.

The situation is further complicated by the delays—25 msec in the analog low-pass filter and 16 msec in the numerical integration—that are introduced into the vehicle displacement record. These delays prevent the vehicle position from being known until approximately 40 msec after the vehicle height measurement is completed.

The measurement software overcomes this difficulty by saving the vehicle height measurements, along with measurement times, in a buffer area. When vehicle displacement is computed, its time minus the known delay time is compared to the time of the oldest stored height measurement. When the times match within one-half integration period, a profile value is computed. The error introduced by the maximum time mismatch of 4 msec is negligible because of the low frequency content of the vehicle displacement record.

Profile Recording

The computed profile is stored on one of the profilometer computer's floppy disks as the profile is recorded. To conserve storage space, profile elevations at each data interval are not stored. Instead, eight-bit signed integers representing elevation differences between successive points are recorded in arbitrary units of resolution. With this scheme, a 512-kilobyte diskette may contain up to 94 mi of profile sampled at 1-ft intervals.

Filtered Profile Computation

After the profile is recorded on diskette, it may be plotted or further analyzed for roughness ratings. For both processes, is desirable to filter the profile further to remove long-wavelength components. Plotting and rating programs use a digital recursive filter with the transfer function

$$H(w) = 1/[1 + \cot^2(\pi h/w)/\cot^2(\pi h/w_0)] \tag{10}$$

This filter is a spatial low-pass filter, where w denotes the wavelength, w_0 is the desired cutoff wavelength, and h is the data interval. Its formulation, similar to that of the high-pass filter employed in the double integration, is of the form

$$p_n = Az_n + Bz_{n-1} + Cz_{n-2} + Dp_{n-1} + Ep_{n-2} \tag{11}$$

That is, the filtered profile p_n is computed recursively as a linear combination of the unfiltered profile z_n at the present location, the two previous unfiltered profile points z_{n-1} and z_{n-2}, and the two previous filtered profile points p_{n-1} and p_{n-2}. The coefficients A through E are computed analytically from the data interval and the cutoff wavelength.

Because the filter is recursive, the signal phase and delay become exaggerated at wavelengths near and greater than the cutoff wavelength. Figure 5 shows the transfer function of the filter at the 500-ft cutoff wavelength commonly used for profile inspection, whereas Figure 6 shows the filter's transfer function for the 50-ft cutoff wavelength used for roughness evaluation.

ANALYSIS OF ERRORS

Identification of the causes of errors cited in the draft report was essential to determine whether they were correctable or whether the potential usefulness of the profilometer was restricted by inherent shortcomings.

Profile Initialization

The first error cited in the draft report—that the beginnings of plotted profiles suffer long-wavelength distortion—was known prior to the UMTRI study, and has its cause in the filtering method used when the profile is plotted or analyzed. Because the high-pass frequency used in the integration process is very low, the recorded profile may contain a considerable amount of long-wavelength information, especially if there is significant profile slope. The high-pass filter included in the profile analysis software effectively removes these low-frequency components, but only after a distance approximately equal to the cutoff wavelength has been processed. This problem can be eliminated by recording profile data points prior to the actual beginning of the test section. Alternatively, appropriate leading data could be synthesized when the profiles are plotted, but current software has no such capability. Consequently, the

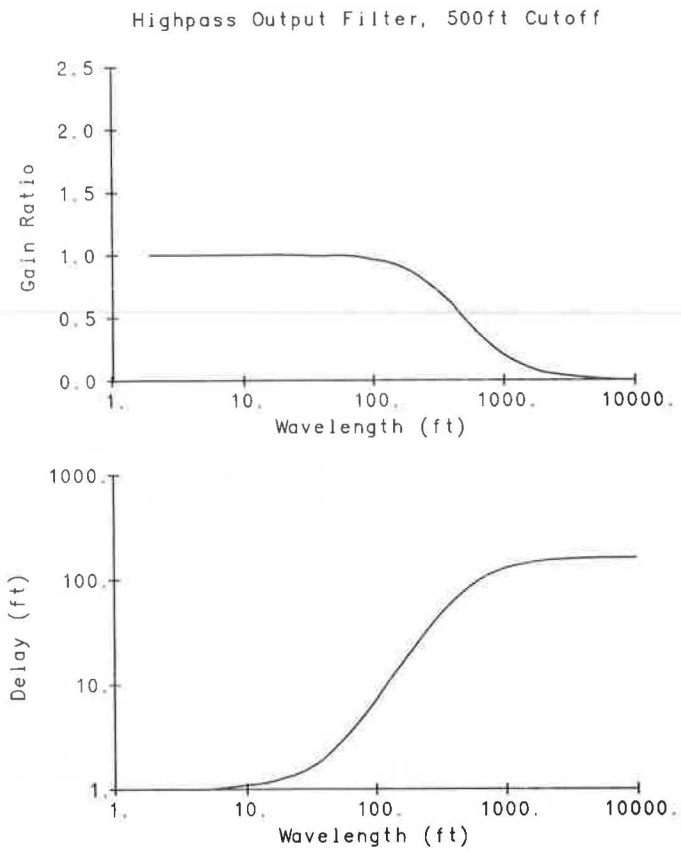

FIGURE 5 Characteristics of digital high-pass filter used to remove long-wavelength features from plotted profiles. Cutoff wavelength is 500 ft.

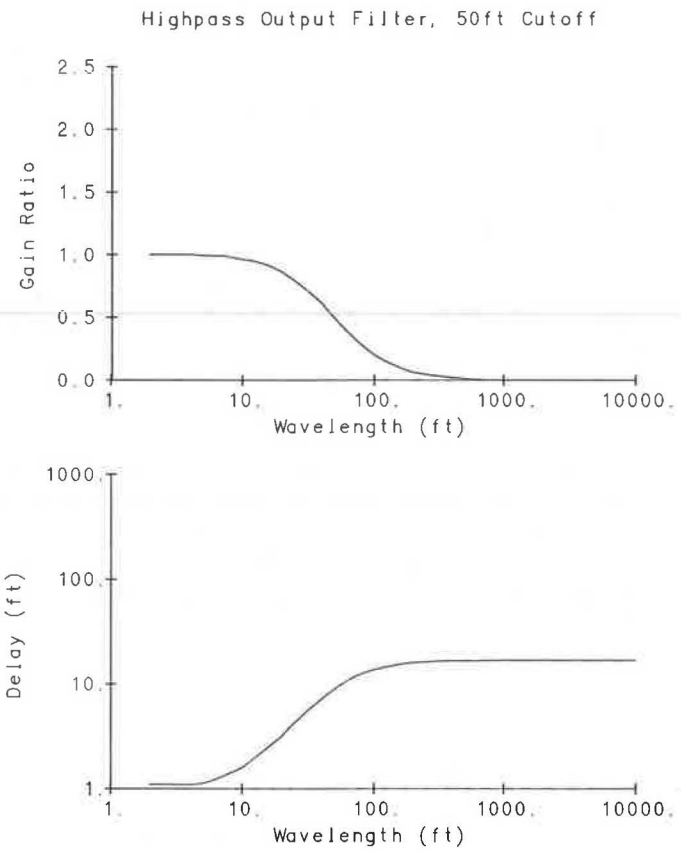

FIGURE 6 Characteristics of digital high-pass filter used to remove long-wavelength features from plotted profiles. Cutoff wavelength is 50 ft.

period during which the filtering procedure is stabilizing is characterized by a large-amplitude transient, the duration of which approximates the cutoff wavelength.

Because SDDOT has used the profilometer more as a pavement roughness measurement device then as a profile measurer, this problem has not previously been viewed as a serious error. For purposes of pavement evaluation, profiles are normally recorded in sections several miles long and filtered to remove wavelengths exceeding 50 ft. To eliminate any effect on roughness ratings, the computation software simply ignores the first 50 ft of data. When profiles are measured for plotting and inspection, testing is begun enough ahead of the area of interest to prevent transients from affecting the profile there.

Profile Underestimation

Although the problem of profile initialization was known prior to the study, profile underestimation was a completely unanticipated problem. It was apparent that the profile was either incorrectly computed or incorrectly stored, but discovery of the cause required that the entire system be checked component by component and procedure by procedure.

First, accelerometer operation was verified by inclining the unit at known angles from vertical and measuring the acceleration component from gravity. Both the primary accelerometer and a spare unit were determined to have calibration errors of less than 0.5 percent over the entire range of 0 to 90 degrees of inclination. Their offsets were close to zero, and observation of their output signal showed smooth indication of both positive and negative accelerations. The gain and frequency response of the 20-Hz low-pass antialiasing filter and the accuracy of the computer's analog-to-digital converters were also verified by direct comparison of output to controlled input signals.

The mathematical derivation of the high-pass integrating filter was checked next, without discovery of any formulation errors. Computational verification of the operation was accomplished by supplying the filter with numerical sine wave acceleration signals of various frequencies and comparing the integrated displacements to analytically computed displacements.

The accuracy of the integration timing was verified by measuring the time required to execute 10^4 integration steps. Regardless of vehicle speed, disk input-output operations, or any other circumstance, the integration interval did not vary from 8.00 msec.

Finally, inspection of the software that synchronizes vehicle position and vehicle height measurements and computes the profile revealed no logic or timing errors. Instructions that checked for synchronization failure were also verified, leading to the conclusion that the profile was being accurately computed.

Although all tests indicated that the profile computations

were correct, recorded profiles showed significant errors. When the accelerometer was mounted in a manually powered test jig that moved the accelerometer in periodic motion 1.5 in. peak-to-peak, and the vehicle height sensor was forced to measure a constant distance, the plotted profile amplitude was less than 1.5 in., especially at low frequencies of movement.

Inspection of the software that stores the profile on disk revealed the single problem responsible for general profile underestimation and more severe underestimation on smooth profiles and at low vehicle speeds in the UMTRI trials. As noted previously, the profile is stored as a series of integers, which, when multiplied by the unit of profile resolution, can be serially added to reconstruct the profile. The error involved truncation of this difference integer, which was computed according to the equation

$$N = G\{(z_n - z_{n-1})/R\} \tag{12}$$

where z_n and z_{n-1} are the current and previous computed profile elevations, R is the unit of resolution, and the function G denotes the greatest integer function. As a result of the truncation, a distance equal to the remainder of the division (between 0.000 and 0.005 ft) was lost from each difference representation. Had the difference equation been correctly written

$$N = G\{z_n/R\} - G\{z_{n-1}/R\} \tag{13}$$

the problem would not have occurred.

The fraction of profile amplitude lost by the truncation error depended on the magnitude of the profile difference. For a difference of five units of resolution (0.025 ft), the maximum error was one part in five, or 20 percent. However, for a difference smaller than one unit of resolution, the integer zero was stored, entirely eliminating the profile difference. The reason why smooth profiles and longer wavelengths were more severely underestimated was clear—in both cases, the elevation differences between succeeding data points were small, thus more drastically affected by the truncation.

In the case of the UMTRI tests, the same problem caused more severe profile underestimation at lower vehicle speeds. Because the profilometer allows the data interval to be decreased at lower vehicle speeds, the medium-speed runs were conducted at 0.5-ft intervals, and the low-speed runs at 0.3-ft intervals. Because of the shorter intervals, elevation differences tended to be smaller, resulting in more significant truncation errors.

During the profilometer's early development, its operation was checked against rod and level surveys, although not with the rigor of UMTRI's analysis. Later, the present profile storage method was adopted as a means to store the data more efficiently, but rod and level checks were not repeated. Operational checks in the laboratory, using bumps mounted on moving surfaces, did not reveal the error because the bumps were blocklike, not gradual enough to be significantly affected by the truncation.

SYSTEM CORRECTIONS

The information learned from the UMTRI Road Profilometer Meeting has been used to address the two problems cited in the draft report. First, the software that records the profile has been corrected so no profile amplitude is lost in truncation. In addition, the profile resolution unit has been changed from 0.005 to 0.001 ft; this improvement in resolution has come at the small expense of decreasing the maximum elevation change to ±0.127 ft per data interval.

Second, software will be modified to better initialize the digital filtering used to plot profiles. Because it is not always possible to record profile data ahead of the desired test section, work will concentrate on synthesizing data ahead of recorded profile data or using linear phase nonrecursive digital filters in the output programs. The latter alternative would offer the additional advantage of decreasing phase distortion at all profile wavelengths, but would also increase the profile computation time.

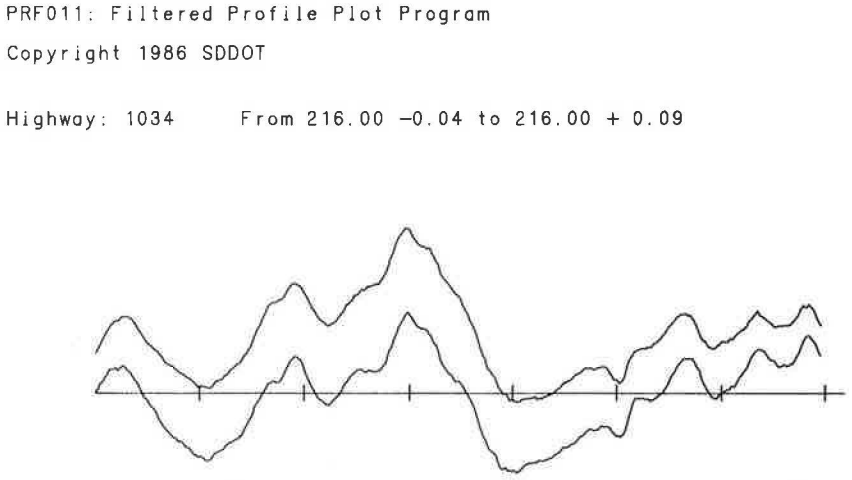

FIGURE 7 Comparison of surveyed profile (lower) and profile measured by profilometer. The horizontal distance between tick marks is 100 ft; the same distance represents 4 in. vertically.

Beyond these immediate changes, procedures have been developed within SDDOT that will minimize the possibility of similar errors' occurring. Test sections of diverse profile characteristics are being surveyed by rod and level and with an E.W. Face Dipstick, an inclinometer-based surface profiler. Profilometer measurements will be compared to surveyed profiles using the same methods employed during the UMTRI study (Figure 7). Detailed results on the current performance of the profilometer will be available in the spring of 1987. Similar checks of profilometer performance will be conducted periodically to ensure continued accuracy.

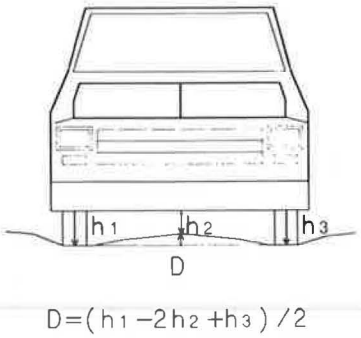

FIGURE 8 Method of rut depth measurement employed by the profilometer. Measurement approximates average of left and right wheelpath rut depths.

OTHER IMPROVEMENTS

SDDOT has worked to improve the system's performance in areas not addressed by the UMTRI study. First, the sensitivity of the ultrasonic ranging transducer has been improved, decreasing the errors caused by coarse pavement surfaces. Negligible differences presently exist between profiles measured on coarse surfaces such as chip seals and those measured on smoothly textured pavements.

Second, two additional ultrasonic transducers have been mounted in the center of the test vehicle and at the right wheelpath, and the software has been modified to measure rut depths simultaneously with profile (Figure 8). Rut depth is measured at every other profile data point; average rut depths are recorded at specified intervals, usually 50 ft. These interval averages can be used to generate rut depth summary reports for all of the state's highway system (Figure 9).

```
RUT020: Rut Depth Rating Document       Copyright 1986 SDDOT
30-DEC-86   15:37:51

Highway: 1034                                    Date: 04-AUG-86
   Lane: 2                                        Time: 11:04:10
Project: RUT DEPTH ILLUSTRATION    Average Speed(mph): 53.41
                                   Data Interval (ft): 50.00

Rut Depth Analysis

            From      To   Average --Rut Depth (inches)---
   MRM      Disp     Disp   Depth  0.0       0.5       1.0
 55.00     0.000    0.100    0.39   |    ----*---
           0.100    0.200    0.25   |  ---*---
           0.200    0.300    0.16   ---*----
           0.300    0.400    0.09   --*--
           0.400    0.500    0.06   -*-----
           0.500    0.600    0.24   |    -*-
           0.600    0.700    0.30   |    --*-
           0.700    0.800    0.23   |    -*--
           0.800    0.900    0.25   |----*---
           0.900    1.000    0.37   |------*-----------
 56.00     0.000    0.100    0.57   |     ------*-------
           0.100    0.200    0.30   |     -*--
           0.200    0.300    0.24   |  ---*---
           0.300    0.400    0.10   |-*--
           0.400    0.500    0.03   -*
           0.500    0.600    0.01   *-
           0.600    0.700    0.04   -*-
           0.700    0.800    0.05   -*
           0.800    0.900    0.05   -*-
           0.900    1.000    0.09   |-*
 57.00     0.000    0.100    0.09   |-*
           0.100    0.200    0.12   |-*
           0.200    0.300    0.05   -*-
           0.300    0.400    0.09   --*
           0.400    0.500    0.03   -*-
           0.500    0.600    0.09   |-*
           0.600    0.700    0.05   -*-
           0.700    0.800    0.06   -*-
           0.800    0.900    0.02   *-
           0.900    1.000    0.01   *-

          Project Average    0.15    ---*---------------
```

FIGURE 9 Sample computer output showing rut depth measurements at boundary of old rutted pavement and newer pavement. Average depth in each 0.1-mi interval is designated by an asterisk and the range of measurement by dashes.

In addition, the profile measurement software has been modified to allow simultaneous entry of various visual highway condition ratings during profile measurement. The profilometer computer maintains a record of the entire state's rating section locations and current ratings. As the test vehicle passes through these sections, the operator is prompted to verify or update the ratings. At the end of a testing season, the updated rating file is transferred back to the department's central data base.

Finally, new profile analysis software has been developed, including programs to compute the international roughness index and perform power spectrum analysis of the recorded profiles.

On the basis of the profilometer's performance following the corrections and recent improvements, SDDOT has decided to supply specifications, descriptions, and schematic diagrams to other state transportation departments. To date, two other states have decided to build similar instruments at an anticipated cost, excluding vehicles, of $20,000 each.

CONCLUSIONS

It is unfortunate that the profile underestimation error existed in the SDDOT profilometer during the UMTRI tests, because it completely precluded the possibility of determining the system's potential performance and prevented discovery of less significant errors. On the positive side, discovery of the error has enabled SDDOT to correct the problem and to verify that no other serious errors exist.

Above all, the experience has demonstrated the importance of independent verification of profilometer operation. Recent validation tests indicate that the corrected system provides valid and reliable profile and rut depth measurements. SDDOT will continue to test and improve its profilometer to achieve the highest possible performance consistent with its low cost.

REFERENCES

1. M. W. Sayers and T. D. Gillespie. *The Ann Arbor Road Profilometer Meeting Draft Report.* University of Michigan, Transportation Research Institute, Ann Arbor, 1985.
2. D. L. Huft. The South Dakota Profilometer. In *Transportation Research Record 1000*, TRB, National Research Council, Washington, D.C., 1984, pp. 1–8.

Publication of this paper sponsored by Committee on Surface Properties-Vehicle Interaction.

Incorporating the Effects of Tread Pattern in a Dynamic Tire Excitation Mechanism

T. G. CLAPP AND A. C. EBERHARDT

A basic understanding of dynamic tire tread response is provided and the information is incorporated in a method for predicting tire-pavement contact forces to excite dynamic tire models. Tire tread is analyzed to determine the response at the tire carcass line to external loading conditions. Results show that dynamic tread response below the natural frequency of the tread may be considered quasi-static. Static analysis shows negligible stress concentration effects at the tread edges along the carcass line. Noncontacting ribs produce vertical stress that is approximately 95 percent of the average stress along the carcass line directly below closely spaced tread elements. Tread and road surface input are combined to include the distributive effects of the tread with the higher-frequency surface effects. This is accomplished by discretizing the contact region into a finite number of equally sized elements. The pressure is computed for each element based on the tread pattern, the global pressure distribution, and the road surface input. The average pressure is determined by equating the axle loading force with the sum of the elemental pressures times elemental areas. Then the force distribution is computed over the tire-pavement contact region. Dynamic force response is determined by shifting the road and tread information and computing the force distribution for consecutive time steps.

When a loaded tire is rolled, time-varying stresses of an impulsive nature are exerted on the tire's contact surface due to rotation and the discrete nature of the tread element design. There also exists a spatial variation of the stress over the contact region due to the imposition and relaxation of loads on the tread elements while going through the footprint. A basic understanding of the excitation mechanism produced by tire-pavement interaction is an essential part of predicting the dynamic response created by tire design and construction. The dynamic nature of the forcing function is such that, as a rolling tire tries to maintain instantaneous equilibrium, fluctuating forces primarily at the leading and trailing edges of the tire produce a vibrational response that affects tire performance.

The trend by automotive manufacturers to produce small, lightweight vehicles has increased the significance of structure-borne vibration and acoustic radiation generated by a rolling tire. Road-tire-induced noise transmission paths are responsible for approximately 36 percent of the interior vehicle sound energy *(1)*. Tire noise is a major source of environmental pollution. Experimental evidence has identified tire surface vibration to be a dominant sound generation mechanism *(2)*.

North Carolina State University, Raleigh, N.C. 27695.

Tire noise, passenger comfort, and other performance criteria are affected by the dynamic response of the pneumatic tire at frequencies up to 2,000 Hz. Recent efforts to understand and predict dynamic response have led to the development of various tire models *(3–6)*. These models are attempting to predict dynamic tire response at frequencies in the audible range up to 1,000 Hz. Present dynamic models are limited in the complexity to which the tread pattern can be represented. Most tire models add tread structural properties such as stiffness and mass in the tread region, but no or very simple tread pattern information is included. The tire designer would like to model the dynamic response given a selected tread pattern. If a treadless tire model is to respond as if tread were present on the tire, the force input must reflect the tread pattern at the point where the forces enter the model and not the contact surface.

The tire excitation mechanism is dependent on many parameters such as external load, tire inflation pressure, road surface texture, and tread pattern. The tread pattern controls the transmission of tire-pavement contact forces to the tire carcass. Much work has been done to determine the global dynamic force distribution over the tire-pavement contact region *(7, 8)*. Other investigation have predicted road surface texture induced contact forces *(9, 10)*. The contact force or pressure at the tire-pavement interface must be combined with the tread pattern information to predict the excitation mechanism at the tire carcass line as required by treadless dynamic models. An important aspect in the development of an excitation mechanism is understanding how the forces are transmitted and transformed through the tread to the tire carcass.

This paper provides a basic understanding of tread response to dynamic contact forces. Dynamic analysis of a finite element tread model is performed to evaluate the carcass line response to an impulsive contact force. Stress concentrations at the carcass line are considered. The effects and influence of noncontacting ribs in the tread pattern are also investigated. The results of this paper are used to develop a tire excitation mechanism that predicts the excitation forces as they enter the tire carcass.

DYNAMIC TREAD ANALYSIS

Dynamic analysis is used to provide an understanding of the carcass line response to tread design features when loaded. Information concerning the dynamic response or transfer function of tire tread is obtained using transient finite element analysis. Nonlinear finite element analysis is required to model

the tire due to large deflections and large strains of the low-modulus rubber material. NASTRAN, NONSAP, and NIKE2D were computer codes considered. NIKE2D was selected because of the element formulation and graphical output capabilities.

NIKE2D is an implicit, static and dynamic, finite-deformation, finite element computer program for axisymmetric and plane strain problems in solid mechanics. The program has been developed at Lawrence Livermore Laboratory by J. O. Hallquist *(11)* by combining the latest algorithms available from a number of specialized finite element programs to increase the problem-solving capabilities while minimizing operating time and machine storage.

Developing a tread model for transient dynamic analysis is performed by understanding and then determining the governing parameters such as upper frequency of interest, material properties, and the number of time steps. The model is then built based on the combination of the finite element limitations and the model parameters.

Experimental evidence *(12)* shows that 16 elements per wavelength are needed to analyze transient excitation and that two time steps per element are needed to allow wave propagation without distortion. Thirty-two time steps per wavelength are therefore required. These strict limitations control the modeling parameters for the propagation of compressive waves.

The compressive wave speed is a material parameter determined by the following formula:

$$C = (Eg/r)^{1/2} \tag{1}$$

where

C = wave speed,
E = modulus of elasticity,
g = gravitational acceleration, and
r = weight density.

To illustrate Equation 1, an example using tread material properties for a typical radial passenger tire (*13*, p. 881) is presented. Other material properties may be used for particular tread compounds. The example material with properties of 520 psi (3.6 MPa) modulus and a weight density of 0.0415 lb/in.^{3} (1.15 g/cm^3) has a characteristic wave speed of 2,200 in./sec (55.9 m/sec). The shortest wavelength of interest is determined by the following formula:

$$L = C/f \tag{2}$$

where L is the wavelength and f is the upper frequency of interest.

The finite element limitation of 32 time steps per wavelength controls the time sampling increment t, which is given by

$$t = (L/C)/32 \tag{3}$$

A frequency of 2,500 Hz is selected as the upper range for proper finite element response. The resulting sampling time increment of 0.0125 msec produces a Nyquist frequency of 40 kHz. This large frequency range requires a sufficiently large number of time steps to achieve the frequency resolution necessary for analyzing frequency response in the 0- to 2,500-Hz range of interest. Computational restrictions limit the number of time steps that may be performed; consequently, 128 time steps are computed to produce a 64-line spectrum with a frequency bandwidth of 625 Hz.

With the characteristic wavelength and the number of time steps determined, the finite element tread model is constructed as shown in Figure 1. The characteristic finite element dimension of 0.060 in. (1.52 mm) is selected to obtain the limitation of 16 elements per wavelength. A symmetry boundary condition is applied along the left side of the model. The model height is determined so that a reflection of the initial wave propagation does not affect the nodal response at the carcass line.

An impulsive point force load is applied to the contact surface at the symmetry line to excite frequencies through the 2,500-Hz range as shown in Figure 2. The discrete load incre-

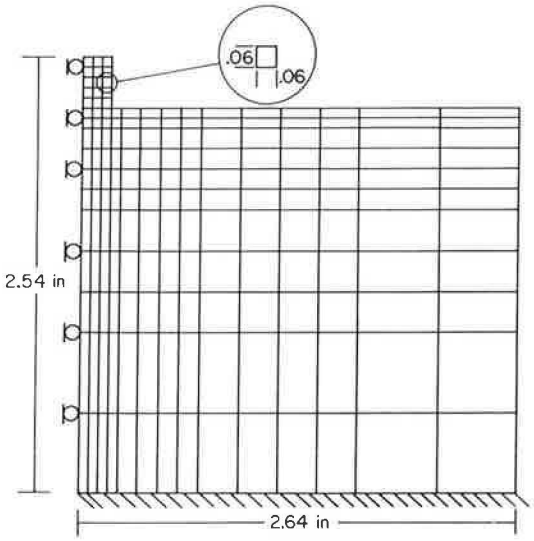

FIGURE 1 Finite element tread model for dynamic analysis.

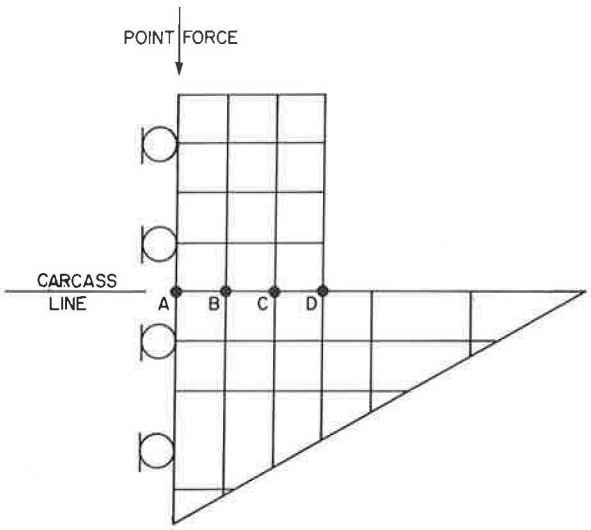

FIGURE 2 Dynamic finite element model of a tread's carcass line response to an impulsive point force.

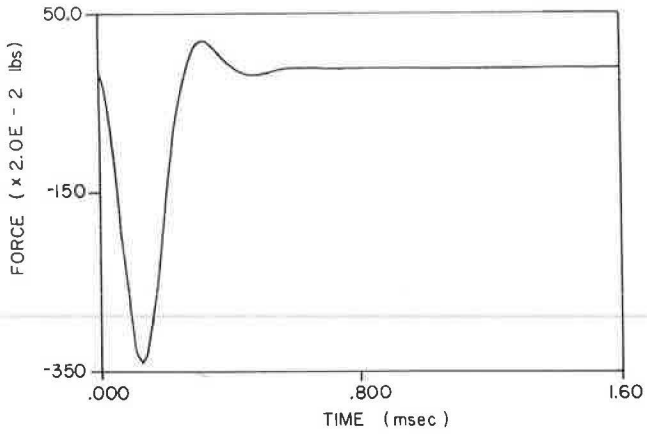

FIGURE 3 Impulsive point force input for dynamic analysis.

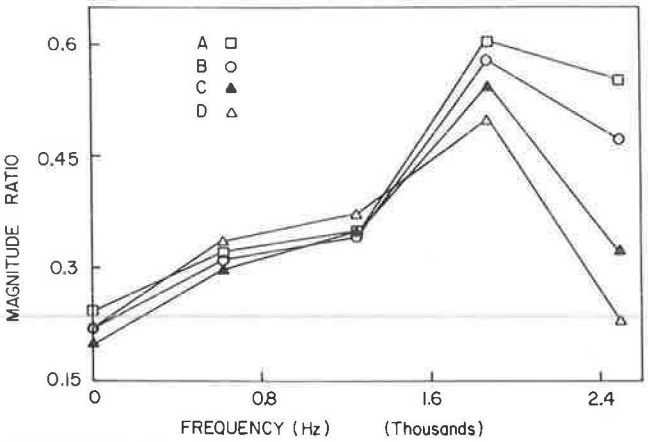

FIGURE 5 Magnitude frequency response of carcass line nodes to an impulsive point force.

ments for each time step are generated by inversely transforming a digitally filtered power spectrum in the frequency domain. The impulsive nature of the applied force input is shown in Figure 3.

The vertical stress at the driving point and at the four nodes along the carcass line is computed and stored for all 128 time steps. An example of the stress output of the driving point and a carcass line point is shown in Figure 4. The figure shows the impulsive nature of the driving point stress and the associated delayed response at the carcass line.

The four carcass line nodes located from the symmetry line to the edge of the tread are designated as *A*, *B*, *C*, and *D*, as shown in Figure 2. The magnitude and phase of the frequency response function are computed using the driving point vertical stress as input and the vertical stress at each of the carcass line nodal points as output.

The frequency response magnitude ratios are generally below 0.5 as shown in Figure 5. The phase results reflect an almost linear phase shift as shown in Figure 6. The frequency response at each nodal location is similar except for the magnitudes at 1,875 and 2,500 Hz. This fact implies that the dynamic response to a point force input is evenly distributed along the carcass line at frequencies below the 1,875-Hz bandwidth. The peak in magnitude at 1,875 Hz is of particular interest.

The simplest model of the tread element would be to treat the tread as a quarter-wavelength rod attached to an infinite medium as shown in Figure 7. Theoretically, the maximum-magnitude response occurs at the fundamental frequency of this system with lesser peaks at the higher harmonics. The theoretical natural frequency of the tread element model with a height of 0.3 in. (0.7 cm), or a 1.2-in. (3-cm) wavelength and a wave speed of 2,200 in./sec (55.9 m/sec), is 1,833 Hz, which falls within the 625-Hz bandwidth around the 1,875-Hz center frequency. Consequently, a simple rod model can provide a rough estimate of tread natural frequency and supports the dynamic finite element analysis of the tread.

This basic dynamic analysis allows a quasistatic assumption to be made as to the tread response at frequencies below the tread natural frequency. In this region, the dynamic tread response is similar to the static response. Static analysis can now be performed to understand how the contact forces are distributed below the tread at the carcass line.

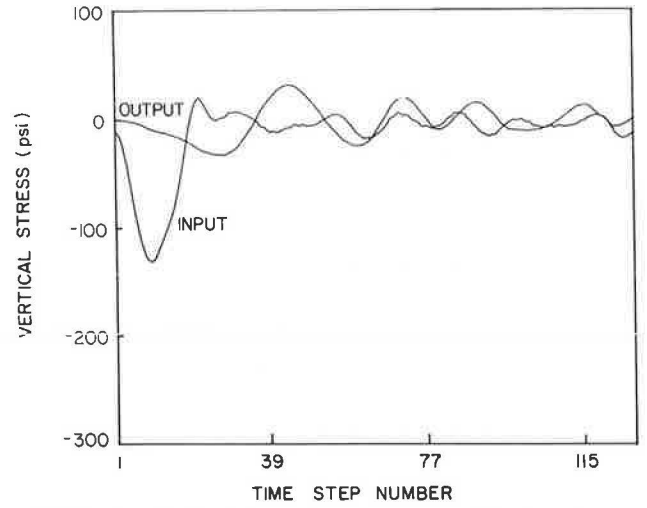

FIGURE 4 Vertical stress time response of the input driving point and an output carcass line node.

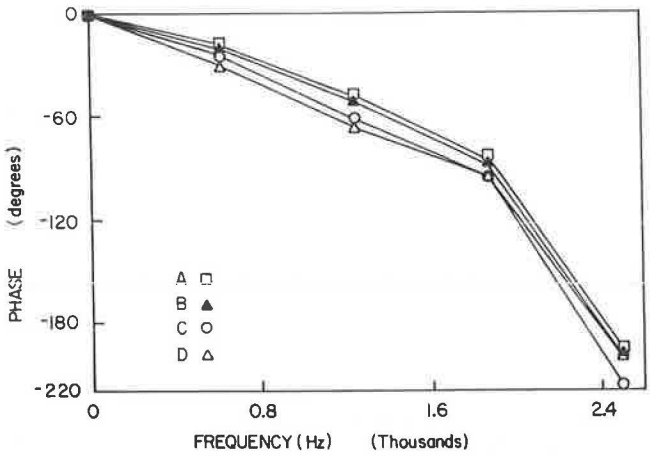

FIGURE 6 Phase frequency response of carcass line nodes to an impulsive point force.

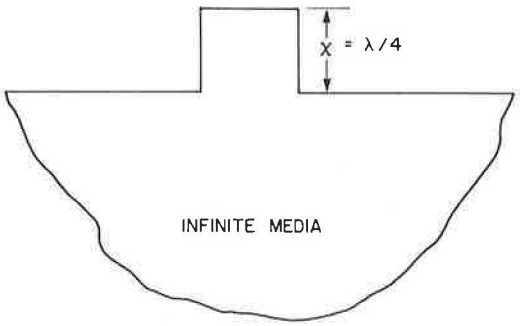

FIGURE 7 Quarter-wavelength rod model connected to an infinite medium.

STATIC TREAD RESPONSE

Various finite element tread models are analyzed statically to determine the effect of stress concentrations at the carcass line and the effect of noncontacting ribs that connect adjacent tread sections. The tread models are loaded using uniform displacement boundary conditions as shown in Figure 8. This loading condition closely simulates smooth road contact and produces a nonuniform vertical pressure distribution along the carcass line. Uniform displacement boundary conditions generate stress concentrations along the contact edges.

The significance of stress concentrations is determined by modeling the worse case, which is a tread with square edges as shown in Figure 8. The model is subjected to uniform displacement boundary conditions along the contact surface. The vertical stress produced at the carcass line is approximately 25 percent larger at the edges than at the center of the tread. Actual tread elements have a stress concentration factor much less than 1.25 because of the curved edges that must be present for the molding process; consequently, the nonuniform contact stress is distributed much more evenly across the carcass line than the contact line. This observation provides a basis for assuming that the stress concentration effect is not included in the force modeling process at the carcass line.

Tire tread design includes many considerations besides the actual contact surface involved. The assumption that the forces are transferred to the carcass line at locations only directly below the contact line excludes many sophisticated details associated with tread design. Tread designs include noncontacting ribs of various heights that connect tread elements. The noncontacting ribs produce vertical stress at the carcass that must be included in some fashion in the total tread-induced force model to ensure that these important design features are reflected in the force input.

Finite element models of differently sized and spaced ribs between two contacting tread elements are analyzed to determine the carcass line vertical stress response to uniform displacement of the contact surface. Tread spacing and rib height are the principal parameters of interest in the analysis.

The first set of finite element models has tread spacing of 0.2 in. (0.51 cm) with connecting rib height to tread height ratios of 0.25, 0.5, and 0.75. Each model is uniformly displaced at the contact surface. The vertical stress along the carcass is computed for five nodes located from the center of the rib into the tread element. The five nodes are labeled consecutively as shown in Figure 9. Nodes 2 through 5 are directly below the contact surface and Node 1 is a rib node. The vertical stress results are normalized to the minimum stress value directly below the contact surface to provide a relative scale factor at the nodal locations.

The normalized vertical stress results are graphically displayed in Figures 9–11 for rib height to tread height ratios of 0.25, 0.5, and 0.75 with a tread spacing of 0.2 in. (1.0 cm). The results show the carcass line stress carried by a noncontacting rib. The noncontacting rib with a rib height to tread height ratio of 0.25 produces carcass line stresses that exceed half the average stress under contacting tread. At rib height to tread

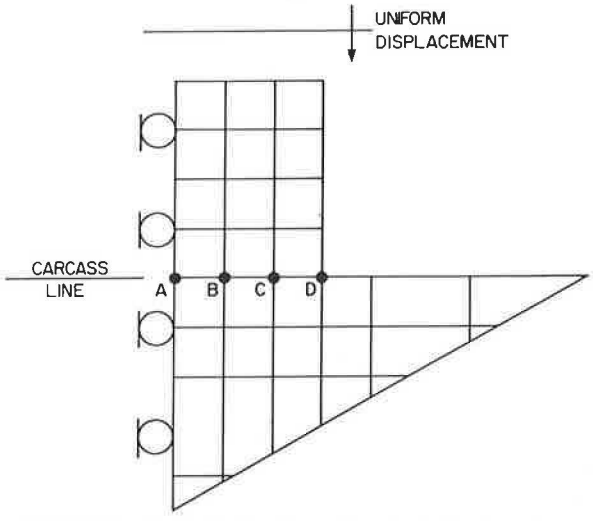

FIGURE 8 Static finite element model of a tread carcass line response to uniform displacement loading conditions.

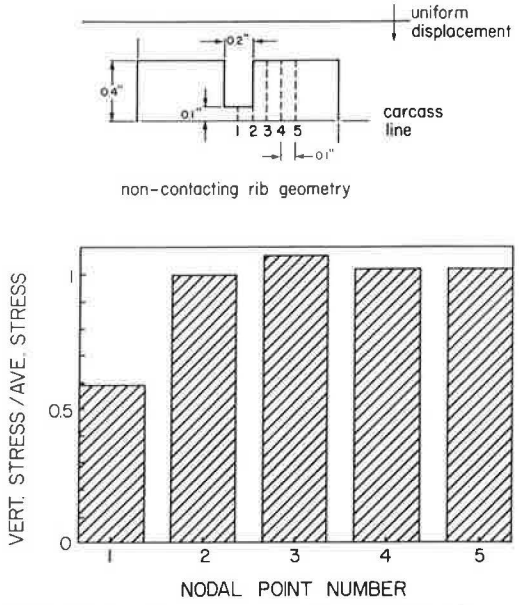

FIGURE 9 Carcass line nodal response of tread spaced 0.2 in. (0.51 cm) apart with a connecting rib of 25 percent height ratio.

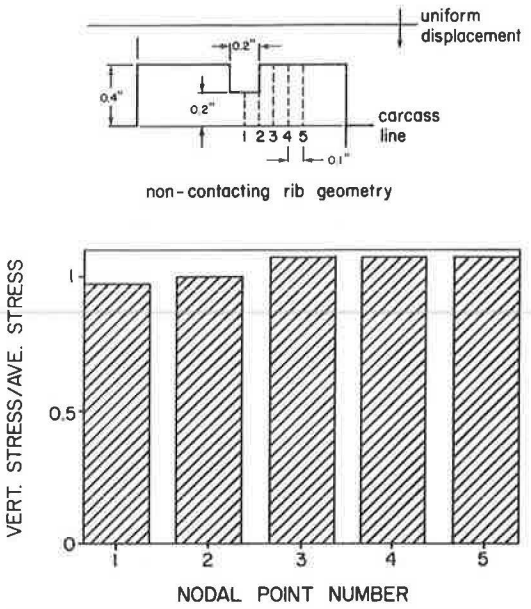

FIGURE 10 Carcass line nodal response of tread spaced 0.2 in. (0.51 cm) apart with a connecting rib of 50 percent height ratio.

height ratios of 0.50 and greater, the percentage of stress contribution to the carcass line is practically equal to the average stress over the contact region. A general statement can be made that the carcass line response of ribs with a height of greater than 50 percent of the tread height, and span between tread elements spaced less than 0.2 in. (0.51 cm) apart, is approximately equivalent to the average carcass line stress below the contact surface.

A second set of models has a tread spacing of 0.4 in. (1.0 cm) with connecting rib height to tread height ratios of 0.25, 0.50, and 0.75. Similar trends exist in distantly spaced tread elements with connecting ribs as with closely spaced tread elements except the stresses under the noncontacting ribs are lower at each rib height to tread height ratio.

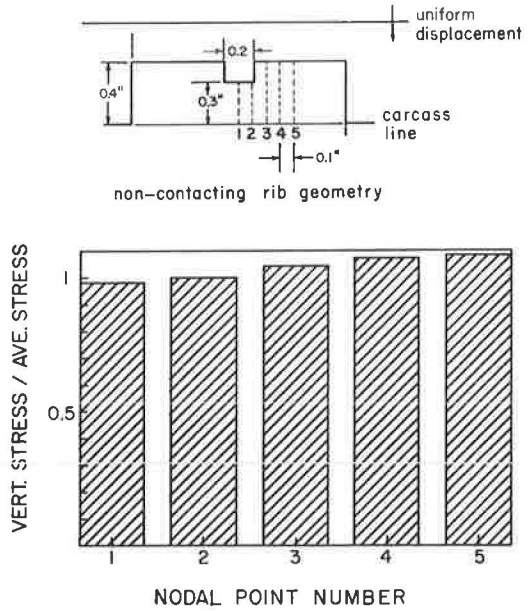

FIGURE 11 Carcass line nodal response of tread spaced 0.2 in. (0.51 cm) apart with a connecting rib of 75 percent height ratio.

The noncontacting rib results show how the vertical stress at the rib nodes increases as the height increases. The rib stress also decreases in magnitude as the tread spacing increases from the edge of the tread to the centerline of the rib. General estimates of the noncontacting rib contribution to vertical stress input at the carcass line can be made from these results.

DEVELOPMENT OF TREAD-INDUCED CONTACT FORCES

The analysis of noncontacting rib effects and tread edge effects at the carcass line provides information necessary to predict the tread-induced force input that is sensitive enough to characterize a detailed tread pattern. The way in which this information is incorporated into the tread-induced force model is by generating a tread pattern matrix. This matric has values that can range from 0 to 1, where 0 represents no tread contribution at the carcass line and 1 represents tread contact. Noncontacting ribs are represented as fractions according to rib height and tread spacing. Detailed estimates from the tread pattern values can be extracted from Figures 9–11. For passenger car tire design most of the noncontacting ribs are between contacting tread elements that are spaced less than 0.2 in. (0.51 cm) apart. When this is the case, general tread pattern scale factors for noncontacting ribs are assigned values of 0.95 and 0.6 for rib height to tread height ratios greater than 0.5 and less than 0.5, respectively.

The matrix of tread pattern values provides a scaling mechanism that can be combined with the contact region global pressure distribution. The global pressure distribution is defined as the distribution of contact pressure across the length and width of the contact patch of a rolling treadless tire. The global information is normalized to some unknown average pressure, resulting in a distribution of pressure ratios over the contact region. The unknown average pressure is determined from the equilibrium condition. Consequently, the tread-induced pressure input for an incremental area with center coordinates x and y is represented by the following formula:

$$P(x, y) = T(x, y)*G(x, y)*P_{avg} \quad (4)$$

where

$P(x, y)$ = elemental pressure,
$T(x, y)$ = tread pattern scale factor,
$G(x, y)$ = global pressure distribution, and
P_{avg} = average pressure.

In order to determine the elemental pressures, the average pressure P_{avg} must be computed. Equilibrium requires that the applied axle load must equal the sum of the incremental pressures times the incremental areas:

$$Ft = \Sigma [P(x, y)*A] \quad (5)$$

TABLE 1 SAMPLE ROAD AND TREAD DATA

Element No.	*R(x,I)* (psi)	*G(x,I)*	*T(x,I)*	IT*(x,I)*
1	0	1.2	1	1
2	20	1.3	1	1
3	30	1.4	1	1
4	15	1.5	1	1
5	0	1.5	0.95	0
6	9	1.3	0.95	0
7	0	1.2	1	1
8	7	1.2	1	1
9	15	1.2	0	0
10	4	1.1	0	0
11	0	1.1	1	1
12	0	1.0	1	1

NOTE: Ft = 75 lb; $A = 0.125$ in.^{3}.

where Ft is the static axle load and A is the element of area.

The average pressure is determined by substituting Equation 4 into Equation 5 and rearranging terms to obtain:

$$P_{avg} = (\text{Ft}/A)/\{\Sigma\,[T(x, y)*G(x, y)]\} \quad (6)$$

When no road-induced input is introduced, Equations 4 and 6 provide the basic force generation over the contact region.

When the texture-induced forces are considered, the pressure over an incremental area in the contact region is determined as

$$P(x, y) = G(x, y)*T(x, y)*P_{avg} + R(x, y)*\text{IT}(x, y) \quad (7)$$

where

$P(x, y)$ = elemental pressure,
$G(x, y)$ = global pressure distribution,
$T(x, y)$ = tread pattern data,
$R(x, y)$ = texture-induced pressure data,
IT(x, y) = integer tread pattern data, and
P_{avg} = average pressure.

Equation 7 includes the distributed contribution of the contact stress. An impulsive texture-induced pressure is included where road surface texture adds additional stress. This component is multiplied by an integer tread pattern value IT(x, y), which is either 0 or 1.

In order to determine the elemental input force, the average pressure must be determined. Equation 7 is substituted into Equation 5 and rearranged to obtain

$$P_{avg} = \{[\text{Ft}/A] - \Sigma\,[R(x, y)*\text{IT}(x, y)]\}/\{\Sigma\,[G(x, y)*T(x, y)]\} \quad (8)$$

An illustrative example is provided to explain the application of Equation 7 using a two-dimensional tread-road contact length. Necessary input data are provided in Table 1.

Recall that (a) the road-induced data $R(x, y)$ contain pressure information only at locations where the texture produces additional tire deformation, (b) the global pressure distribution $G(x, y)$ is a ratio of the global pressure at a particular location over some average pressure, (c) the tread pattern data $T(x, y)$ reflect not only the tread contact locations but also the noncontacting ribs (as seen by the two 0.95 values), and (d) the integer tread pattern IT(x, y) includes only the contacting tread locations.

For the sample data, Equation 8 is used to compute an average pressure of 41 psi (283 kPa), which is substituted into Equation 7 to produce the incremental pressure results presented in Table 2. The incremental force input is computed as the product of the pressure values times area.

This distribution of pressure values reflects the various parameter contributions, including important tread pattern information, while adding the road surface input that tends to randomize the output and to reflect the dynamic high-frequency response at the carcass line.

CONCLUSIONS

This research provides a method for developing a tire excitation mechanism that includes complex tread pattern effects. The tread effects are determined at the tire carcass to provide realistic input to treadless dynamic tire models.

Tread pattern information is generated from the tread response results by assigning a matrix of tread pattern values that range from 0 to 1 to describe the tread pattern design features over the tire-pavement contact region.

Tread and road surface texture-induced input are combined to include the distributive effects of the tread and the high-frequency road effects. This is accomplished by discretizing the contact region into a finite number of equally sized elements. The pressure is determined for each element from the tread pattern, the global pressure distribution, and the road surface input. The average pressure is determined by equating the axle loading force with the sum of the elemental pressures times element area. A discretized matrix of pressure values can be computed over the entire footprint. This would provide force data for one time stop of a dynamic tire model.

New tread and road surface information corresponding to the location of the tire contact region at the next time step can be input into the excitation model to compute the next force values required by the dynamic model. In this manner, the contact forces at the tire carcass line are predicted for a rolling tire on a desired road surface at a desired velocity.

The method developed within this report is based on many

TABLE 2 PRESSURE RESULTS FROM SAMPLE INPUT DATA

	Element No.											
	1	2	3	4	5	6	7	8	9	10	11	12
P(x, I) (psi)	49	75	93	80	58	51	49	57	0	0	45	41
P(x, I) (kPa)	305	519	644	548	403	349	339	392	0	0	311	283

simplifying assumptions. Much refinement is anticipated as knowledge is developed of true dynamic tire-pavement contact forces. This method does provide a means by which complex tread pattern information can be incorporated into sophisticated dynamic tire models.

ACKNOWLEDGMENT

The authors wish to thank Firestone Tire & Rubber Company for support of this research through the Department of Mechanical and Aerospace Engineering at North Carolina State University.

REFERENCES

1. S. K. Jha. Identification of Road/Tyre Induced Noise Transmission Paths in a Vehicle. *International Journal of Vehicle Design and Components*, Vol. 5, Nos. 1–2, Jan. 1984, pp. 143–158.
2. A. C. Eberhardt. *An Experimental and Analytical Investigation of the Vibration Noise Generation Mechanism in Truck Tires*. Report DOT-HS-8-02020. U.S. Department of Transportation, March 1981.
3. D. E. Southworth. *Finite Element Modeling and Verification of Heavy Vehicle Tire Transient Response*. Master's thesis. North Carolina State University, Raleigh, 1984.
4. M. C. Goff. *Development of a 3-Dimensional Finite Element Model of Orthotropic Laminate Tire Structures Under Initial Pressure Loading for Model Response*. Master's thesis. North Carolina State University, Raleigh, 1985.
5. F. Tabaddor and J. R. Stafford. Nonlinear Vibration of Cord-Reinforced Composite Shells. *Computers and Structures*, Vol. 13, 1981, pp. 737–743.
6. Y. B. Chang, T. Y. Yang, and W. Soedel. Dynamic Analysis of a Radial Tire by Finite Element and Model Expansion. *Journal of Sound and Vibration*, Vol. 96, No. 1, 1981, pp. 1–11.
7. S. A. Lippmann and K. L. Oblizajek. The Distributions of Stress Between the Tread and the Road for Freely Rolling Tires. *SAE Transactions*, 740072, 1974.
8. A. Browne, K. C. Ludema, and S. K. Clark. Contact Between the Tire and Roadway. *Mechanics of Pneumatic Tires*. NHTSA, U.S. Department of Transportation, 1981.
9. T. G. Clapp. *Approximation and Analysis of Tire/Pavement Contact Information Resulting from Road Surface Roughness*. Ph.D. dissertation. North Carolina State University, Raleigh, 1985.
10. T. G. Clapp and A. C. Eberhardt. Computation and Analysis of Texture-Induced Contact Information in Tire/Pavement Interaction. In *Transportation Research Record 1084*, TRB, National Research Council, Washington, D.C., 1986, pp. 23–29.
11. J. O. Hallquist. *NIKE2D—A Vectorized, Implicit, Finite Deformation, Finite Element Code for Analyzing the Static and Dynamic Response of 2-D Solids*. Report UCID-19677. Lawrence Livermore Laboratory, University of California, Berkeley, 1983.
12. A. C. Eberhardt. *Interaction of the Tire/Pavement Interaction Mechanism—Phase I and II*. Final Report, DOT/OST/P-34/86/036. U.S. Department of Transportation, June 1985.
13. J. R. Beatty. Physical Properties of Rubber Compounds. *Mechanics of Pneumatic Tires* (S. K. Clark, ed.), NHTSA, U.S. Department of Transportation, Washington, D.C., 1981.

Publication of this paper sponsored by Committee on Surface Properties-Vehicle Interaction.

External Methods for Evaluating Shock Absorbers for Road Roughness Measurements

JAMES C. WAMBOLD, DANIEL J. CHAPMAN, AND BOHDAN T. KULAKOWSKI

Two new experimental methods are described for the selection of shock absorbers for response-type road roughness meters. The methods allow for verification of the acceptability of the shock absorbers before they are mounted in the road roughness measuring vehicle. In the first method, a programmable shaker table is used to obtain the time response of the shock absorber. In the second method, a simple scotch yoke mechanism is used to produce the frequency response of the shock absorber. In both methods, the test results are compared with the corresponding time domain or frequency domain acceptability limits, which are determined from computer simulation and based on the relevant ASTM standards.

During the development of ASTM E 1082, *Test for Measurement of Vehicular Response to Traveled Surface Roughness (1)*, and of the proposed *Standard Specification for Trailers Used for Measuring Vehicle Response to Roughness (2)*, it became apparent that a method was needed to externally evaluate shock absorbers for cars and trailers used for measuring vehicle response to road roughness. Gillespie et al. *(3)* originally proposed an in-car test conducted on a fabricated calibration surface, but this test is essentially a trial-and-error method that allows an evaluation to insure that the shock absorber remains within specifications. In a companion paper, Kulakowski et al. *(4)* describe a greatly enhanced method for use in calibration of trailers.

The most important improvement of the latter method is that it does not require a specially fabricated calibration surface and can be applied on any road section for which the profile data have been acquired. (It is desirable that the selected test surface have a relatively high level of roughness uniformly distributed along its length.) A computer simulation program is used to calculate maximum and minimum acceptable values of the trailer suspension travel produced when it is towed over the test surface. If the measured suspension travel falls within the acceptable range for a given hysteresis of the axle-body displacement transducer, the shock absorber on board the trailer is then acceptable for roughness testing. If not, a new or different shock absorber would have to be mounted and the testing procedure repeated.

The method presented in this paper allows for testing the shock absorber before it is mounted so that the trial-and-error procedure can be avoided. This method can be used in selecting shock absorbers for both cars and trailers used in measuring road roughness.

Pennsylvania Transportation Institute, Pennsylvania State University, University Park, Pa. 16802.

THE EXTERNAL PROCEDURE

In the following external method for the selection of the shock absorber for the road roughness measuring vehicle, the shock absorber is tested outside the vehicle and is mounted only if found acceptable. The time and effort involved in this procedure can thus be considerably reduced in comparison with the internal method described by Kulakowski et al. *(4)*.

The proposed procedure requires the mounting of the shock absorber in a programmable shaker table or in a semiportable scotch yoke mechanism to test its dynamic characteristics. Either test apparatus must meet two specifications. First, the shock absorber should be subjected to forces of amplitudes and frequencies varying over a broad spectrum so that nonlinear effects are averaged out. Second, the particular range of amplitudes and frequencies of the excitation signal should be the same as would have been experienced by the shock absorber if it were mounted in the trailer and run over a calibration surface.

The schematic of the test apparatus is shown in Figure 1a, where C_s represents the damping coefficient of the tested shock absorber. The conditions experienced by the shock absorber in the system shown in Figure 1a should be similar those imposed on the shock absorber mounted in the vehicle represented by a standard quarter-vehicle model shown in Figure 1b. The dynamics of the two systems shown in Figure 1 are compared, first with the test apparatus driven by the shaker table and then by the scotch yoke mechanism.

PROGRAMMABLE SHAKER TABLE TESTING PROCEDURE

The acceptability limits for shock absorbers used in road roughness measurements have been defined in terms of the relative damping coefficient $\gamma = C_s/M_s$, where M_s is a sprung mass of a quarter-car or half-trailer *(1, 2)*. According to ASTM standards, the shock absorber is acceptable if its relative damping coefficient falls within specified limits, that is, if

$$\gamma_{min} \leq \gamma \leq \gamma_{max} \quad (1)$$

where, for a standard quarter-car,

$$\gamma_{min} = 4.0 \text{ sec}^{-1} \text{ and } \gamma_{max} = 9.5 \text{ sec}^{-1} \quad (2)$$

and, for a standard half-trailer,

$\gamma_{min} = 5.5$ sec^{-1} and $\gamma_{max} = 13$ sec^{-1} (3)

The standard values of γ are 6.0 sec^{-1} and 8.0 sec^{-1} for a quarter-car and a half-trailer model, respectively.

For the external testing procedure with a programmable shaker table, it is better to formulate an equivalent acceptability criterion in the time domain rather than in the domain of the relative damping coefficient. In order to transpose the criterion of Equation 1 to the time domain, assume that a specified calibration profile $x_p(t)$ is used as the input to the quarter-vehicle model shown in Figure 1b. Displacement of the sprung mass $Z_s(t)$ is considered as the output signal. The shock absorber having relative damping coefficient γ is considered acceptable if the quarter-vehicle time response $Z_s(t)$ satisfies the following condition:

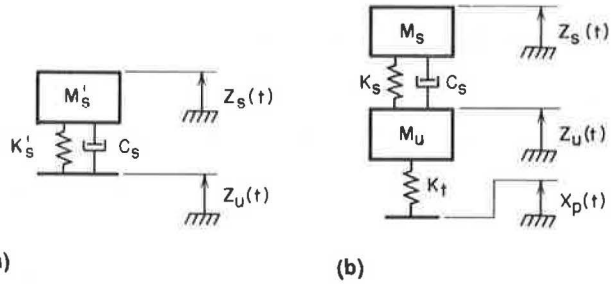

FIGURE 1 Schematic of the test apparatus (a) and of the general quarter-vehicle model (b).

$$Z_s'(t) \le Z_s(t) \le Z_s''(t), \text{ for } t_1 \le t \le t_2 \quad (4)$$

where

$Z_s'(t)$ = response with $\gamma = \gamma_{max}$,
$Z_s''(t)$ = response with $\gamma = \gamma_{min}$,
t_1 = time at beginning of the test, and
t_2 = time at end of the test.

Figure 2 presents time responses of the half-trailer model *(1)* for $\gamma = 5.5$, 8.0, and 13.0 sec^{-1} subjected to the ABAB pattern calibration profile proposed by Gillespie et al. *(3)*. The plots shown in Figure 2 were obtained using the computer simulation program CARTRA developed by Chapman *(5)*. It can be seen that the response of the sprung mass $Z_s(t)$ for $\gamma = 8.0$ sec^{-1} lies between the responses obtained for $\gamma_{min} = 5.5$ sec^{-1} and $\gamma_{max} = 13.0$ sec^{-1}.

In the testing procedure proposed here, the shock absorber is mounted in the test apparatus shown in Figure 1a. In order to subject the shock absorber to the same testing conditions as those generated in the quarter-vehicle model (Figure 1b), the displacement of the unsprung mass $Z_u(t)$, recorded when the standard trailer model ($\gamma = 8.0$ sec^{-1}) was run over the ABAB pattern, is used as the input signal to the test apparatus. If the mass and spring constant of the test apparatus are the same as the sprung mass and suspension spring constant ($M_s' = M_s$ and $K_s' = K_s$, respectively), the time domain acceptability criterion

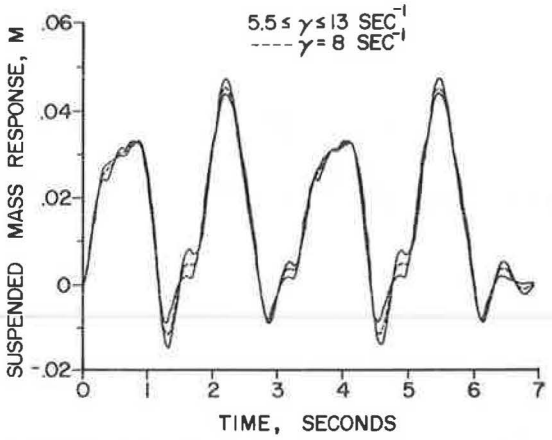

FIGURE 2 Trailer-suspended mass response to ABAB profile.

(Equation 4) can be applied to determine whether the shock absorber is acceptable. Similarly, any road profile $X_p(t)$, not necessarily the ABAB pattern, can be used as the input to the computer simulation program to obtain time responses $Z_u(t)$ and $Z_s(t)$. A programmable shaker table is then used to reconstruct $Z_u(t)$ as the input signal to the test apparatus shown in Figure 1a. In summary, the following step-by-step procedure is proposed.

Step 1: Simulate a standard quarter-vehicle model shown in Figure 1b subjected to a specified input profile $X_p(t)$, and record the response of the unsprung mass $Z_u(t)$. The computer program CARTRA *(5)* can be used.

Step 2: Simulate the quarter-vehicle model again, but now use the limiting values of the relative damping coefficient γ_{min} and γ_{max} and record the resulting displacements of the sprung mass, $Z_s'(t)$ and $Z_s''(t)$, respectively.

Step 3: Use a programmable shaker table to reconstruct $Z_u(t)$ recorded in Step 1.

Step 4: Apply the shaker table signal $Z_u(t)$ to the test apparatus with the tested shock absorber mounted as shown in Figure 1a and record $Z_s(t)$.

Step 5: Compare $Z_s(t)$ recorded in Step 4 with $Z_s'(t)$ and $Z_s''(t)$ obtained in Step 2. The shock absorber acceptability condition is given by Equation 4.

One difficulty with this testing procedure is that the displacements $Z_s(t)$ in the test apparatus and in the quarter-vehicle model can only be compared if the mass and spring constant of the test apparatus are the same as the sprung mass and the suspension spring constant of the vehicle model ($M_s' = M_s$ and $K_s' = K_s$, respectively). The sprung mass is 483.3 kg (1,063 lb) for the standard quarter-car and 304 kg (670 lb) for the standard half-trailer model. A programmable shaker table for such large masses is generally impractical, so a procedure using a reduced mass M_s' was developed for use in the test apparatus. For trailers, Chapman *(5)* proposes the following values of the parameters: $M_s' = 22.7$ kg (60 lb) and $K_s' = 470{,}000$ N/m (1,055 lb/in.). The system with these parameters has the same damping ratio as the suspension of the original trailer, but the resulting natural frequency ω_n' is approximately 13 times

higher than the original. Thus the system does not respond the same as the original system in terms of frequency or time. In fact, the small mass M_s' produces a small $Z_s(t)$ if the original $Z_u(t)$ is used to drive the test apparatus.

In order to remedy this problem, a time-scaled $Z_u'(t)$ must be obtained so that the input causes the test apparatus to respond in the manner in which the trailer did. In other words, if the original $Z_u(t)$ has harmonic components of frequencies near ω_n for the original trailer, these same corresponding portions of the new signal $Z_u'(t)$ must cause the test apparatus to respond in the same manner at frequencies near the new ω_n'. This calls for a frequency shift of the original $Z_u(t)$ signal, which can be accomplished through time scaling or time compression. If the old $Z_u(t)$ is compressed in time, all frequencies in the signal will be increased. With the time scaling determined by the compression factor set to the ratio (of 13) of the ω_n divided by the ω_n', the resulting $Z_u'(t)$ and the test apparatus simulate the original system well. Figure 3 shows the time-domain-based acceptability criterion in compressed time scale.

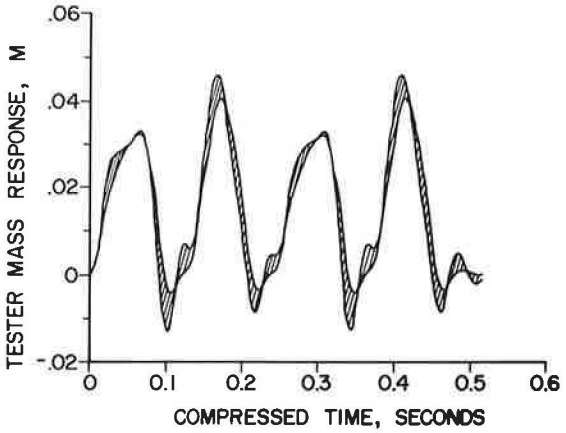

FIGURE 3 The external time-based acceptability criterion for a trailer.

A similar time scaling procedure should be applied for a quarter-car model. The acceptability criterion for shock absorbers mounted in cars is illustrated in Figure 4. The same five-step procedures are followed with the time compression.

Scotch Yoke Mechanism Testing Procedure

A programmable shaker table may not be available for testing shock absorbers as described in the previous section. A simple scotch yoke mechanism can then be used in a frequency-based test. This mechanism can be obtained from the Vehicle-Surface Interaction Program, Pennsylvania Transportation Institute, Pennsylvania State University, University Park, Pennsylvania.

The quarter-vehicle model (Figure 1b) is linear; therefore, if a sinusoidal input signal of frequency ω is applied, the displacements Z_s and Z_u of the sprung and unsprung masses are also sinusoidal of the same frequency, and of amplitudes $|Z_s(j\omega)|$ and $|Z_u(j\omega)|$, respectively. The ratio of the two amplitudes (the magnification factor) is a function of frequency and can be represented by the magnitude of the sinusoidal transfer function

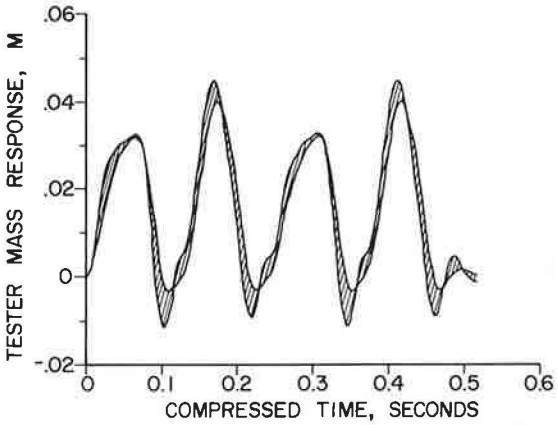

FIGURE 4 The external time-based acceptability criterion for a car.

$$M(\omega) = \frac{|Z_s(j\omega)|}{|Z_u(j\omega)|} \tag{5}$$

For the quarter-vehicle model the expression for $M(\omega)$ takes the form

$$M(\omega) = \left[\frac{\omega^2\gamma^2 + \omega_n^2}{\omega^2\gamma^2 + (\omega_n^2 - \omega^2)}\right]^{1/2} \tag{6}$$

where the natural frequency ω_n is

$$\omega_n = \left(\frac{K_s}{M_s}\right)^{1/2} \tag{7}$$

By substituting $\gamma = \gamma_{min}$ and $\gamma = \gamma_{max}$ into Equation 6, minimum and maximum magnification factor curves $M_{min}(\omega)$ and $M_{max}(\omega)$, respectively, are obtained. The curves calculated for a half-trailer are plotted in Figure 5, and the curves for a quarter-car are shown in Figure 6.

A scotch yoke mechanism can be used to apply a sinusoidal

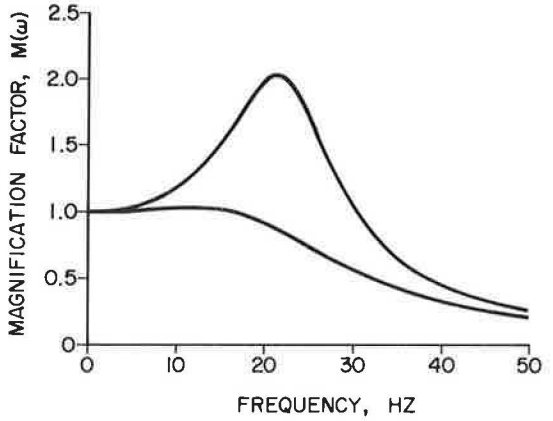

FIGURE 5 Trailer shock absorber acceptability criterion.

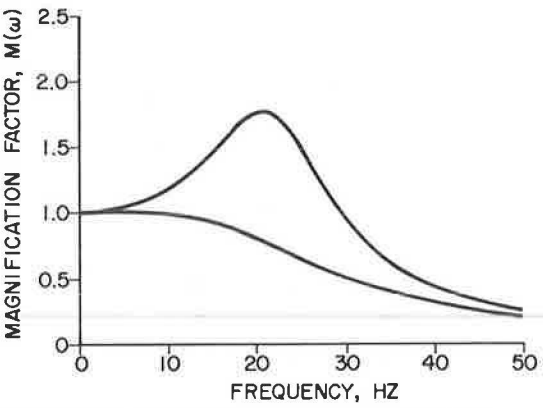

FIGURE 6 Car shock absorber acceptability criterion.

signal of amplitude $|Z_u|$ and frequency ω to the test apparatus shown in Figure 1a. If the amplitude of the steady state sinusoidal displacement of the mass $|Z_s|$ is such that the ratio $|Z_s|/|Z_u|$ lies within the minimum and maximum magnification factor curves shown in Figure 5 or 6, the shock absorber is acceptable. Mathematically, the acceptability condition in frequency domain can be written in the following form:

$$M_{min}(\omega) \leq M(\omega) \leq M_{max}(\omega) \text{ for } 0 \leq \omega \leq \omega_{max} \quad (8)$$

This form is equivalent to the original acceptability condition (Equation 1) as well as to the time domain criterion (Equation 4).

CONCLUSIONS

Two experimental methods for verification of acceptability of shock absorbers for use in road roughness measuring systems were described. In the two approaches, the general acceptability criteria for shock absorbers used in roughness-measuring cars and trailers stated in the ASTM Standards *(1, 2)* are transposed to the time and frequency domains. The testing procedures are simple and, more important, allow for the determination of shock absorber acceptability before it is mounted in a car or trailer. Also, the procedures are sufficiently flexible to be customized according to the type of equipment available and the specific needs of the user.

REFERENCES

1. *Test for Measurement of Vehicular Response to Traveled Surface Roughness.* ASTM Standard E1082, Annual Book of ASTM Standards, Vol. 04.03, American Society for Testing and Materials, Philadelphia, Pa., 1985.
2. *Standard Specification for Trailers Used for Measuring Vehicle Response to Road Roughness.* Proposed ASTM Standard, American Society for Testing and Materials, Warrendale, Pa., 1986.
3. T. D. Gillespie, M. W. Sayers, and L. Segal. *NCHRP Report 228: Calibration of Response-Type Road Roughness Measuring System.* TRB, National Research Council, Washington, D.C., 1980.
4. B. T. Kulakowski, D. J. Chapman, and J. C. Wambold. *Acceptability of Shock Absorbers for Road Measuring Trailers.* Pennsylvania Transportation Institute, Pennsylvania State University, University Park, June 1986.
5. D. J. Chapman. *Automobile Shock Absorber Acceptability.* M.S. thesis, Department of Mechanical Engineering, Pennsylvania State University, University Park, Dec. 1985.

Publication of this paper sponsored by Committee on Surface Properties-Vehicle Interaction.

Factor Analysis of Pavement Distresses for Surface Condition Predictions

J. J. HAJEK AND R. C. G. HAAS

Pavement distress information is needed to assess maintenance requirements and to plan rehabilitation. For immediate maintenance requirements, it is necessary that the details of individual distress types, severity, and density be known. However, for pavement design and long-range rehabilitation planning, more approximate and aggregated data are sufficient. Furthermore, due to correlation between individual distresses, it is only practical to predict aggregated rather than individual detailed distresses. The Ontario Ministry of Transportation and Communications currently uses 15 pavement surface distress types (characterized by five levels of severity and five levels of density) in their condition survey procedures for flexible pavements. In this paper, the distress types are aggregated into five fundamental uncorrelated categories (factors) using factor analysis techniques. The five factors are thermal cracking, edge cracking, surface instability, fatigue cracking, and random cracking. Analyses are based on data observed on about 350 pavement sections. In general, the pavement structure of these sections consisted of asphalt concrete on top of granular materials. The results show that of the variance associated with the original 15 distress types about 60 percent could be explained by the five fundamental factors. Although these five basic uncorrelated factors should be used for future surface distress predictions, the 15 individual distress types will still be required for the selection of specific maintenance treatments and for establishing the existing values of the five factors.

Because pavements deteriorate with time, traffic, and climate, not only is investment in preservation through timely maintenance and rehabilitation important today, but also for the future. Surface distress manifestations and their quantification, and measurements of surface roughness, structural adequacy, and friction provide much of the information for determining present and future needs and for planning maintenance and rehabilitation.

Distress manifestations are defined as visible consequences of various mechanisms that usually lead to a reduction in pavement performance *(1)*. At present, the Ontario Ministry of Transportation and Communications (MTC) uses the 15 distress manifestations presented in Table 1 to visually characterize pavement condition and to calculate the distress manifestation index as a measure of pavement structural performance *(2)*.

Although each of the 15 distress manifestations describes a unique, or at least different, visual pattern or characteristic, all 15 distresses still describe the same general phenomenon, that of pavement deterioration. As subsequently shown, the distress manifestations are interrelated and many are statistically highly correlated.

The principal objective of the research reported herein was to investigate if it is possible to identify some fundamental categories of distress manifestations and thus to simplify the existing method of describing and analyzing pavement distresses. The original impetus for this work was a need to develop a simplified method for describing and predicting distress manifestations, and for identification of pavement failure modes that would provide an expert system for selection of pavement preservation treatments *(3)*. However, this paper is mainly concerned with how the simplified method of describing pavement distress manifestations can be used for prediction of pavement performance.

INTERDEPENDENCY OF DISTRESSES

In order to illustrate statistical dependence among the 15 distress manifestation characteristics, a correlation matrix of these distresses based on 347 observations representing nearly all pavement management sections in three MTC districts (Huntsville, Kingston, and Stratford) is presented in Table 1. The section lengths ranged from 0.3 to 25.7 km, with an average of 9.9 km. The sections were selected to exhibit a uniform pavement performance. The distresses were identified and rated by using the procedures described by Hajek et al. *(2)*, and were measured in terms of their density and severity on interval and ordinal scales, respectively, both scales ranging from 0 to 5 *(4)*. Final values of the distress manifestation variables were obtained by adding scaled values of density and severity. For example, if the severity of wheel track rutting was moderate (i.e., rutting depth was in the range of 12 to 19 mm) and its density was throughout (i.e., moderate rutting occurred on 80 to 100 percent of the section length), the severity was assigned a value of 3, the density a value of 5, and the final value was 8. This procedure was originally developed for calculation of the distress manifestation index *(2)*.

The coefficients of the correlation matrix for the 15 variables (Table 1) appear reasonable and as expected in both sign and magnitude. For example, variable B, flushing, is positively correlated with variable E, distortion ($r = 0.316$). This correlation suggests that excess asphalt, which results in flushing, also contributes to distortion. On the other hand, the lack of significant correlation between flushing and variable L (single and multiple transverse cracking), $r = -0.002$, suggests that flush-

J. J. Hajek, Ministry of Transportation and Communications, 1201 Wilson Ave., Downsview, Ontario, Canada M3M 1J8. R. C. G. Haas, Department of Civil Engineering, University of Waterloo, Waterloo, Ontario, Canada N2L 3G1.

TABLE 1 SIMPLE CORRELATION MATRIX OF MTC'S 15 DISTRESS MANIFESTATIONS

VARIABLE NAME	A	B	C	D	E	F	G	H	I	J	K	L	M	N	O
A Ravelling & Coarse Aggregate Loss	1.000														
B Flushing	-0.042	1.000													
C Rippling & Shoving	-0.113	0.132	1.000												
D Wheel Track Rutting	0.238	0.084	0.040	1.000											
E Distortion	0.066	0.316	0.310	0.313	1.000										
F Long. Wheel Track- Single & Multiple Cracking	0.232	0.189	0.059	0.459	0.426	1.000									
G - Alligator Cracking	0.010	0.025	0.096	0.204	0.194	0.319	1.000								
H Centreline - Single & Multiple Cracking	0.272	0.062	-0.085	0.343	0.243	0.468	0.145	1.000							
I - Alligator Cracking	0.155	0.032	0.095	0.153	0.207	0.245	0.291	0.224	1.000						
J Pavement Edge - Single & Multiple Cracking	0.218	0.099	0.137	0.300	0.256	0.302	0.225	0.334	0.190	1.000					
K - Alligator Cracking	0.120	0.060	0.220	0.202	0.321	0.252	0.179	0.141	0.081	0.340	1.000				
L Transverse - Full, Half & Multiple Cracking	0.251	-0.002	-0.077	0.400	0.101	0.419	0.101	0.586	0.122	0.292	0.059	1.000			
M - Alligator Cracking	-0.006	-0.029	0.021	0.041	-0.023	0.056	0.158	0.081	0.139	0.146	0.105	0.096	1.000		
N Longitudinal Meander & Midlane Cracking	0.096	0.204	0.177	0.331	0.404	0.537	0.213	0.464	0.249	0.366	0.178	0.430	0.203	1.000	
O Random Cracking	0.048	0.047	0.079	0.148	-0.006	0.239	0.149	0.090	0.085	0.185	0.176	0.159	0.222	0.173	1.000

Note: Correlation coefficients are based on 347 observations and are significant at the 1% level if their value exceeds approximately |0.15|.

ing does not have any effect on the formation of transverse cracks.

Detailed examination of the correlation matrix suggests that the distresses are highly correlated in many complex ways. For example, half, full, and multiple transverse cracking have statistically significant correlations with, among other variables:

- Wheel track rutting (r = 0.40),
- Single and multiple longitudinal wheel track cracking (r = 0.42),
- Single and multiple centerline cracking (r = 0.59), and
- Longitudinal meander and midlane cracking (r = 0.43).

Wheel track rutting has, in turn, statistically significant correlation with yet other distresses such as distortion (r = 0.31).

Variables that are highly correlated may actually measure similar characteristics and may be interchangeable to a certain degree. Also, correlation between variables masks specific influences of individual variables and often prevents their use in multiple regression models, particularly those obtained by stepwise regression.

A question then arises: What is the minimum number of distresses (variables) capable of describing distress manifestations in a concise, elucidative manner? Preferably, these variables should be uncorrelated and should attempt to identify fundamental distress categories.

The task of summarizing interrelationships among many variables in a concise basic manner can be tackled very effectively by factor analysis techniques *(5, 6)*. These techniques were first applied in the area of psychology in the early 1900s. Since the 1940s, factor analysis has been used in many other fields such as sociology, medicine, business, and transportation planning *(7)*. However, it appears that this technique has realized limited, if any, application to pavement technology.

FACTOR ANALYSIS TECHNIQUES

The basic factor model represents variables as additive composites of several weighted factors or loadings using a set of linear equations called the total factor pattern:

$$Z_1 = a_{11}F_1 + a_{12}F_2 + \ldots a_{1m}F_m + b_1S_1 + e_1E_1$$
$$Z_2 = a_{21}F_1 + a_{22}F_2 + \ldots a_{2m}F_m + b_2S_2 + e_2E_2$$
$$\ldots$$
$$Z_n = a_{n1}F_1 + a_{n2}E_2 + \ldots a_{nm}F_m + b_nS_n + e_nE_n \quad (1)$$

where, using index j to designate variables and index i to designate individuals (observations):

- Z_j = Observed variable, total number of variables being n.
- F_j = New uncorrelated components called common factors. The total number of common factors is m, which is usually much smaller than n. F_j is a factor common to all variables.
- S_j = Specific factor.
- E_j = Error factor; $S_j + E_j$ values are called unique factors.
- a_{ji} = Common factor coefficients; $a_{ji}F_j$ is the contribution of factor F_j to the linear composite.
- b_j = Specific factor coefficient.
- e_j = Error factor coefficient.

The factor analysis model resembles regression analysis insofar as a variable is described as a linear combination of another set of variables plus a residual. However, in regression analysis this set of variables (i.e., the set of independent variables) are

observable quantities, whereas in factor analysis they are hypothetical constructs that can only be estimated from the observed data *(6)*. The important property of factors as hypothetical constructs is that they are independent (and uncorrelated) even though the original variables themselves may be related.

The objective of factoring, which constitutes the basic part of factor analysis, is to find the coefficients of the factor pattern a_{ji}, b_j, and e_j. Because a system of orthogonal (uncorrelated) factors consistent with observed data and satisfying Equation 1 may be chosen in an infinite number of ways, the coefficients of the factor pattern cannot be uniquely determined. Consequently, many factor analysis techniques have been developed to extract factors and to transform the extracted factors in order to obtain the factor solutions that are most amenable to interpretation.

The factoring operation is usually done on dimensionless standardized values of variables Z_j for all individuals i. The standardized variables have zero means and variances equal to unity. Using the notation of Equation 1, the composition of the unit variance of variable Z_j is defined as

$$\sum_{i=1}^{m} a_{ji}^2 + b_j^2 + e_j^2 = 1 \qquad (2)$$

where

$\sum_{i=1}^{m} a_{ji}^2$ = communality of variable Z_j, defined as the proportion of the unit variance explained by m common factors;

b_j^2 = specificity of the observed variable Z_j; and

e_j^2 = error variance associated with variable Z_j.

Because e_j^2 is usually unknown, the sum $b_j^2 + e_j^2$ represents the uniqueness of the observed variable, that is, that proportion of the unit variance unexplained by common factors.

Factor analyses were performed using the SAS computer program package *(8)*. Three extraction techniques were investigated:

- Principal component analysis,
- Principal factor analysis, and
- Maximum-likelihood factor analysis.

Detailed results are reported only for the principal component analysis because the results obtained by this technique appeared to permit the best interpretation of the resulting factor solution. The factors obtained by this technique yield the best least-square estimates of the entire correlation matrix and each succeeding common factor accounts for the maximum obtainable amount of variation in the correlation matrix *(9)*. In other words, the factors are selected in a stepwise manner.

The indeterminacy of factor solutions may result in factors with loadings (i.e., a_{ji} coefficients) that may be difficult to interpret. This situation can be radically improved by rotating the axes of the reference frame on which the factors are measured. Because the objective of this research was to obtain simplified factors and to maintain orthogonality of the factors, the varimax method of rotation was used. The varimax method alters individual factor coefficients, as well as the variance explained by each factor, whereas the total variance explained by the rotated and the original factor patterns remains unchanged. The method also strives for a simplified factor solution by making the small-factor loadings approach zero and the large-factor loadings approach unity *(9, 10)*.

DATA ANALYSIS

Factor analysis was carried out on distress manifestation data obtained for three MTC districts. The procedure used for collecting the distress data was referenced previously; their correlation matrix was presented in Table 1. The three MTC districts were selected with the intention of obtaining a representative sample of distress manifestations associated with conventional flexible pavements (asphalt concrete on top of granular material) subjected to a variety of traffic and environmental exposures. Nearly all asphalt concrete pavements (about 3,000 km, centerline) on the King's highways in the three districts were included in the study.

The frequency of occurrence of distress manifestations in the three districts is illustrated in Figure 1 using the final values (sums of scaled values of density and severity) of the 15 distress variables. The most frequent distress was transverse cracking—half, full, and multiple—which occurred, in one form or another, on about 90 percent of all sections. On the other hand, alligator transverse cracking occurred on only 2 percent of the sections.

The factor solution obtained by principal component analysis and rotated using the varimax method is shown in Table 2. Table 2 (Part a) gives the rotated factor pattern for only five factors, or principal components, and thus gives results for a truncated component solution. The remaining 10 factors (there are 15 variables) were not included in the solution based on the Mineigan criterion, which states that the variance explained by a factor included in the solution must be at least equal to unity *(8)*. The number of factors required to represent the 15 variables was also tested using maximum-likelihood analysis. The probability level based on the chi-square test for the hypothesis of five factors being sufficient was 0.026; for that of six factors the probability was 0.500. This difference indicates that the five-factor model provides an appropriate representation of the data.

The entries of the factor pattern in Table 2 (Part a) are the a_{ji} coefficients of Equation 1. They are also regression coefficients between variables Z_j and factors F_m. These entries, which are referred to as factor loadings, theoretically can range from −1 to +1. The further the factor loading for a given variable is from 0, the more one can generalize from that factor to the variable.

Final communality estimates of the 15 variables explained by the five factors are given in Table 2 (Part b). These estimates, multiplied by 100, yield the percentage of the variance for a given variable, explained by the factors. With the exception of variables D and J (wheel track rutting and pavement edge single and multiple cracking), the factors explained more than 50 percent of the variance. The best results were obtained for distortion (68.9 percent) and for pavement edge alligator cracking (68.7 percent).

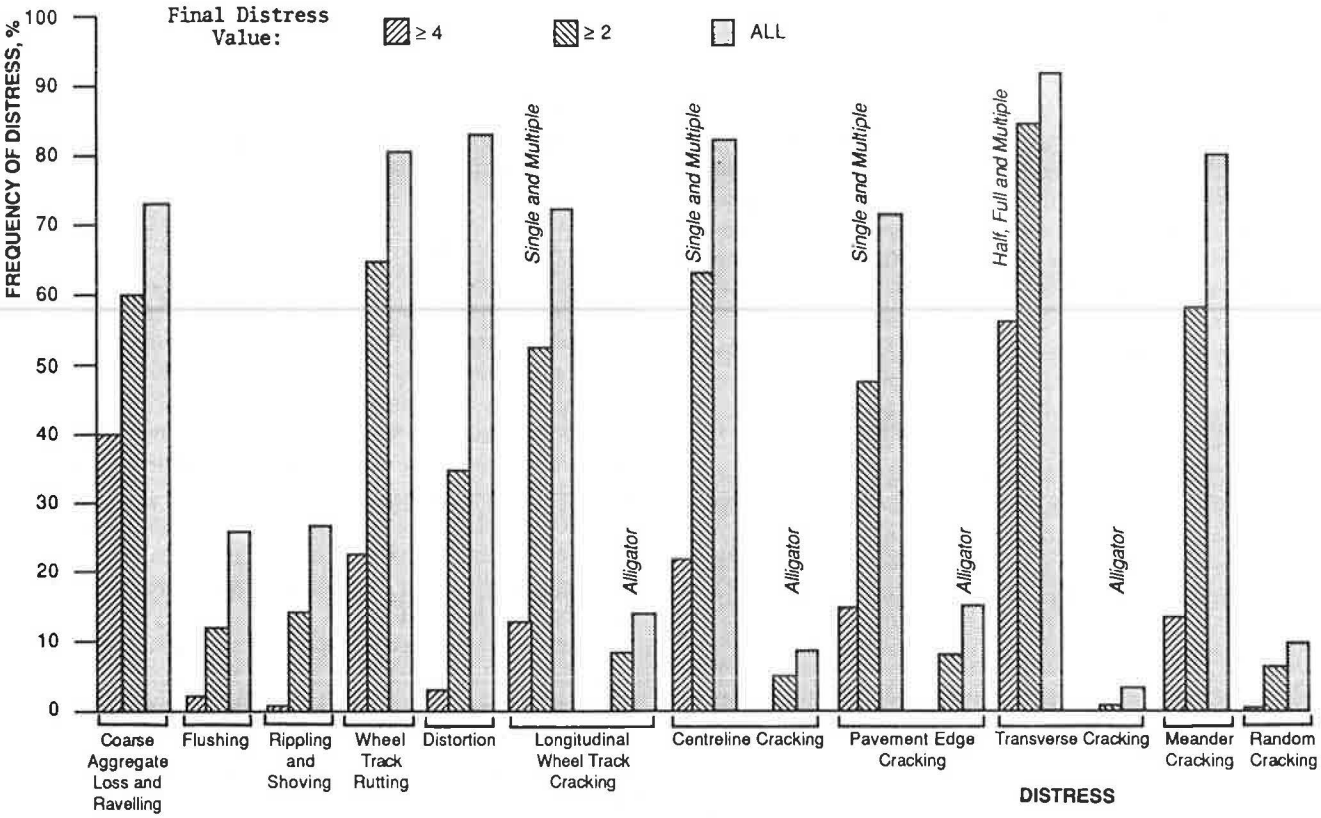

FIGURE 1 Occurrence of distress manifestations.

TABLE 2 VARIMAX SOLUTION FOR PRINCIPAL COMPONENT ANALYSIS

Part (a) Rotated Factor Pattern						Part (b) Final Communality Estimates[1]
	FACTORS					
VARIABLE NAME	1	2	3	4	5	
A Ravelling & Coarse Aggregate Loss	0.443	0.335	-0.455	0.036	-0.250	0.579
B Flushing	0.146	-0.018	0.719	-0.101	-0.049	0.551
C Rippling & Shoving	-0.214	0.448	0.492	0.143	0.062	0.553
D Wheel Track Rutting	0.595	0.284	0.054	0.095	-0.032	0.448
E Distortion	0.281	0.390	0.582	0.252	-0.236	0.689
F Long. Wheel Track- Single & Multiple Cracking	0.670	0.196	0.255	0.247	0.056	0.617
G - Alligator Cracking	0.094	0.143	0.049	0.708	0.184	0.567
H Centreline - Single & Multiple Cracking	0.796	-0.003	-0.008	0.115	0.018	0.648
I - Alligator Cracking	0.173	0.017	-0.019	0.802	-0.022	0.674
J Pavement Edge - Single & Multiple Cracking	0.399	0.527	0.009	0.131	0.180	0.486
K - Alligator Cracking	0.072	0.815	0.057	0.040	0.113	0.687
L Transverse - Full, Half & Multiple Cracking	0.805	-0.060	-0.080	-0.039	0.154	0.683
M - Alligator Cracking	0.038	-0.020	-0.048	0.231	0.731	0.592
N Longitudinal Meander Midlane Cracking	0.614	0.066	0.411	0.219	0.225	0.649
O Random Cracking	0.157	0.239	0.007	-0.069	0.703	0.581

Part (c) Variance Explained by Each Factor						
	FACTORS					
	1	2	3	4	5	Total[2]
Variance Explained (Eigenvalues)	3.035	1.613	1.556	1.448	1.311	8.963
Percent of Total Variance	20.2	10.8	10.4	9.7	8.7	59.8

[1] One minus communality gives variable uniqueness.

[2] Total unit variance for 15 observations is equal to 15.

Table 2 (Part c) presents the variance explained by each factor. These variances, which are equal to factor eigenvalues, can be calculated as

$$\sum_{j=1}^{15} (a_{jm})^2 \tag{3}$$

For example, the standardized variance for Factor 1 was equal to 3.035 and represented about 20 percent of the total variance. (The total variance for the 15 standardized variables is equal to 15). The variance explained by the five factors of 8.93 accounted for about 60 percent of the total variance of the original 15 variables.

This 60 percent of the total variance explained by the five factors is reasonable, but not as large as may be desired, indicating the following:

1. Additional variables should be included in the analysis to better define the common factors.
2. The variables have a high degree of uniqueness.

Because uniqueness consists of a specific variance and an error variance in unknown proportions, it may be interpreted in many ways. For example, by attributing the main portion of uniqueness to the specific variance, the results suggest that many distress manifestation variables tend to measure unique specific pavement deterioration properties not common to other variables. On the other hand, by attributing the main portion of uniqueness to the error variance, the results indicate the presence of substantial measurement errors. The most likely interpretation is somewhere between these two extremes. The presence of these errors in the pavement distress rating process has been documented before *(11)*.

At any rate, the construction of five new, uncorrelated, hypothetical variables, which contain 60 percent of the information previously transported by the 15 original correlated variables, is a significant accomplishment, particularly in view of the purpose of the work, which was to provide an aggregated, approximate, and practical basis for predicting distresses.

The effect of varimax rotation is graphically illustrated in Figure 2, which shows a plot of the factor pattern in the common-factor space of two dimensions represented by Factors 1 and 2. The actual factor space is five-dimensional. The plot is an example of several possible projections of this space to a cartesian coordinate system.

The varimax rotation strives to simplify factor solution by concentrating variable loadings on as few factors as possible. Considering for example variable *H* (centerline single and multiple cracking), its loadings before rotation were 0.67 on Factor 1 and 0.40 on Factor 2. After the rotation, the corresponding loadings were 0.80 and 0.

INTERPRETATION OF FACTORS

An important step in factor analysis is interpretation of factor meanings. Because factors are unobservable hypothetical variables, their identification and interpretation are based upon observations of which variables are, and which are not, related to the factors and what these relationships may conceptually indicate. In other words, possible quantitative distinctions based on statistical results as well as qualitative distinctions based on intuitive evaluation of the underlying physical phenomena are sought.

The basic guide for factor interpretation is provided by the coefficients (factor loadings) of the factor pattern. These coefficients, as regression coefficients between factors and variables, reflect the importance of the factors in predicting the observed variables. To facilitate the interpretation, a list of salient factor loadings is given in Table 3. The salient (or prominent) factor loadings were defined as correlation coefficients equal to or greater than 0.4. This definition guarantees that the correlations are statistically significant ($P < 0.025$) even after making allowances for the possibility of increased errors of orthogonally rotated factor solutions *(9)*.

The main motivation for applying the technique to pavement distress data is its potential to explain the relationship among many variables in terms of more basic concepts. These concepts should, in turn, help to explain the overall problem. Pavement damage in Ontario occurs because of the following four basic damage attributes related to load and environment:

1. Traffic loads,
2. Temperature changes,
3. Moisture effects, and
4. Construction flaws due to materials and construction techniques.

Ideally, for explanatory purposes, one should strive to construct the factors so that each factor combines and isolates the effects of only one of the damage attributes. However, all damage attributes act on the pavement structure simultaneously in many complex ways. For example, a frost heave is the result of combined damage attributes of temperature changes, moisture effects, and construction flaws. On the top surface, the resulting pavement damage is aggravated by traffic loads. The frost heave itself would be described by the MTC distress survey in terms of distortion and perhaps also in terms of several different types of cracking. For these reasons, the ideal explanatory solution, based on the factor loadings of Table 3, is difficult to achieve.

By way of introduction to interpreting and naming factors, Factor 4 is considered first. This factor has only two salient (statistically significant) factor loadings and both of them are with variables describing alligator cracking: longitudinal wheel track alligator cracking (0.71) and centerline alligator cracking (0.80, Table 3). The remaining 13 variables do not have statistically significant loadings on Factor 4. Also, the two variables with salient loadings on Factor 4 do not have salient loadings on any other factor. Thus, Factor 4 can be considered a factor describing alligator cracking. However, the 15 original variables contain two additional variables describing other types of alligator cracking not included in Factor 4: pavement edge alligator cracking and transverse alligator cracking.

The first variable associated with alligator cracking—transverse alligator cracking—is rare (it occurs on less than 4 percent of the sections shown in Figure 1) and was included, as discussed later, in Factor 5. The second variable, pavement edge alligator cracking, loads strongly only on Factor 2 (0.81) and thus appears to be unrelated to the two types of alligator

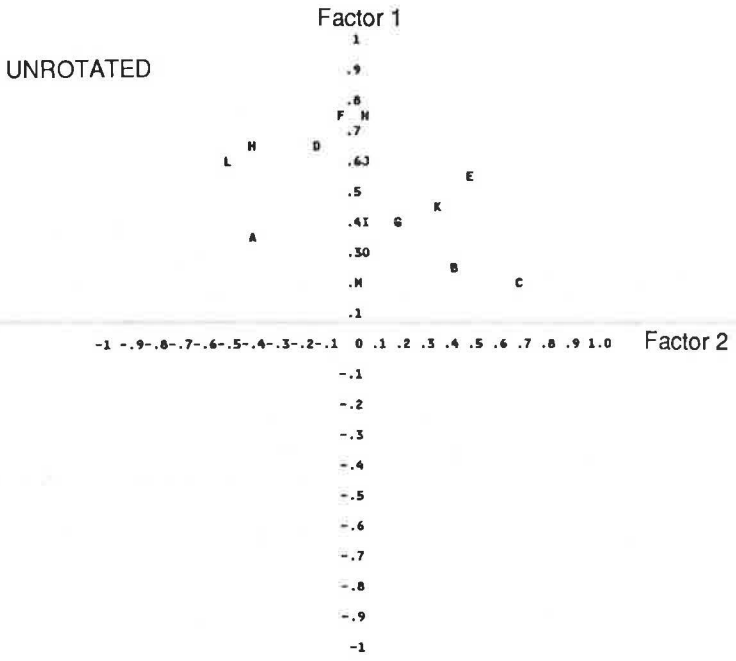

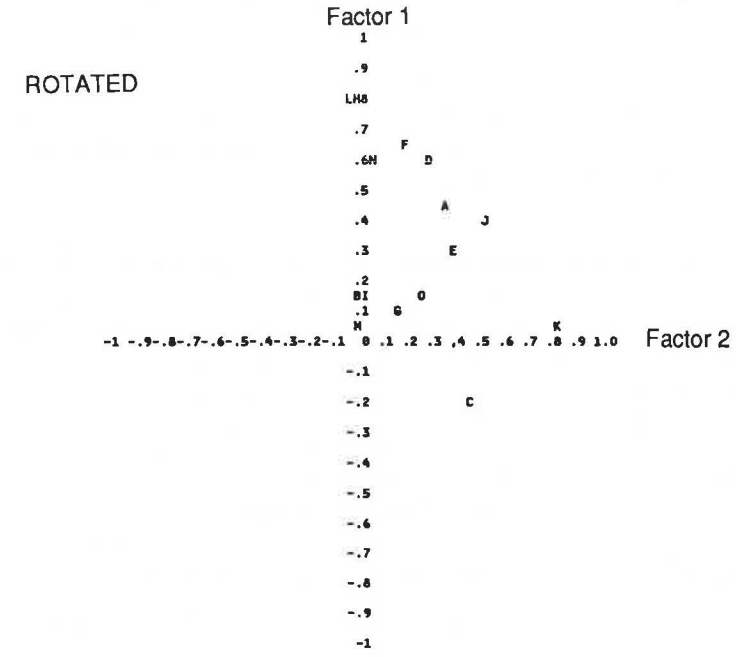

LEGEND
A,B,C...O are variables defined in Tables 1 to 4.

FIGURE 2 Graphical representation of varimax rotation.

cracking associated with Factor 4. It may be hypothesized that Factor 4 describes alligator cracking caused by pavement structural fatigue, whereas Factor 2 describes alligator cracking caused by insufficient strength of the pavement edge typical for pavements with thin asphalt concrete surfaces. This assumption is supported by the next highest loading for Factor 2, which is single and multiple pavement edge cracking. The two types of pavement edge cracking (single and multiple, and alligator) are related to each other and with Factor 2, but are unrelated to fatigue cracking described by Factor 4. Factor 4 was thus named fatigue cracking and Factor 2 was named pavement edge cracking.

Factor 1 has high salient or statistically significant loadings on all four variables describing different types of single and multiple cracking (longitudinal wheel track, centerline, pavement edge, and transverse) and was named thermal cracking

TABLE 3 SALIENT FACTOR LOADINGS

VARIABLE NAME	Factor 1 Thermal Cracking	Factor 2 Edge Cracking	Factor 3 Surface Instability	Factor 4 Fatigue Cracking	Factor 5 Random Cracking
A Ravelling & Coarse Aggregate Loss	0.44		-0.45		
B Flushing			0.72		
C Rippling & Shoving		0.45	0.49		
D Wheel Track Rutting	0.60				
E Distortion		0.40	0.58		
F Long. Wheel Track- Single and Multiple Cracking	0.67				
G - Alligator Cracking				0.71	
H Centreline - Single and Multiple Cracking	0.80				
I - Alligator Cracking				0.80	
J Pavement Edge - Single and Multiple Cracking	0.40	0.53			
K - Alligator Cracking		0.81			
L Transverse - Full, Half & Multiple Cracking	0.81				
M - Alligator Cracking					0.73
N Longitudinal Meander Midlane Cracking	0.61		0.41		
O Random Cracking					0.70

[1] For factor loadings higher than 0.40.

factor. Evidently, single and multiple pavement edge cracking contributes both to the thermal cracking factor (Factor 1) with a loading of 0.40 and to the pavement edge cracking factor (Factor 2) with a loading of 0.53. The variance of this variable must then be subjectively divided for interpretive purposes. Because the two factors are orthogonal, it may be hypothesized that one portion of the single and multiple pavement edge cracking is related to the same causes as, for example, the transverse cracking and centerline cracking of Factor 1 that have been linked in the past to high asphalt concrete stiffness at low temperature and to other causes *(12)*. The other portion of the single and multiple pavement edge cracking would then be hypothesized to have the same causes as Factor 2, that is, insufficient strength of the pavement edge. The thermal cracking is also associated with raveling and coarse aggregate loss (loading of 0.44). This association appears to indicate that the low asphalt content and stripping, usually associated with raveling, also contributes to general cracking *(13)*.

Factor 3 has the highest positive loading on flushing (0.72) and the highest negative loading on raveling and coarse aggregate loss (–0.45). The two variables are related in the opposite directions. Flushing is associated with the absence of raveling and coarse aggregate loss, whereas the raveling and coarse aggregate loss tend to be associated with the thermal cracking factor (loading of 0.44). Other salient loadings of Factor 3 are for the variables rippling and shoving, distortion, and longitudinal meander and midlane cracking. For this reason, Factor 3 was named surface instability factor. Pavement damage caused by frost heaves is usually described in terms of distortion and longitudinal meander and midlane cracking. Both these variables are associated with Factor 3.

Longitudinal meander and midlane cracking is associated with both the surface instability factor (loading 0.41) and with the thermal cracking factor (loading 0.61). This association suggests, quantitatively, how the cause for this distress manifestation may be proportioned.

Factor 5 explained the lowest amount of variance (Table 2, Part c) and was the most difficult to interpret. Because it had high loadings from transverse alligator cracking (0.73) and from random cracking (0.70), it was named "random cracking" factor. The name was selected because the occurrence of transverse alligator cracking is low compared even to that of random cracking, as shown in Figure 1. Transverse alligator cracking usually develops from a single transverse crack by formation of additional parallel cracks alongside the original crack and by subsequent gradual formation of an alligator pattern. It is probably caused by all four basic damage attributes. Transverse alligator cracking was only marginally related to the fatigue cracking factor (0.231 in Table 2, Part a).

In summary, the following factors were identified. They are listed in order of their contribution in explaining the sample variance, together with their possible causes:

Factor	*Factor Name*	*Possible Principal Cause*
1	Thermal cracking	Temperature changes, traffic loads
2	Pavement edge cracking	Effect of load on thin AC pavement
3	Surface instability	Construction flaws (frost heaves)
4	Fatigue cracking	Traffic load
5	Random cracking	All causes

The factors can be viewed as uncorrelated fundamental operational representatives of all 15 distress manifestations. Because the factors are orthogonal, information provided by any given factor is uncorrelated and independent of that provided by any other factor or factors.

Factor analysis techniques lie somewhere between a science and an art *(14)*. Different analysts may use different techniques that yield somewhat different results and different researchers may interpret even the same results differently. Therefore, the results should be viewed as only one of the possible interpretations of statistical data. Nevertheless, they can also be explained in term of qualitative reasonableness of the basic physical phenomena involved.

FACTOR SCORES

The factors as hypothetical constructs can be also be expressed in terms of the 15 observed variables. It is thus possible to characterize, quantify, and predict pavement distress manifesta-

TABLE 4 SCORING COEFFICIENTS

VARIABLE NAME	Factor 1 Thermal Cracking	Factor 2 Edge Cracking	Factor 3 Surface Instability	Factor 4 Fatigue Cracking	Factor 5 Random Cracking
A Ravelling & Coarse Aggregate Loss	0.151	0.283	-0.396	-0.012	-0.260
B Flushing	0.061	-0.133	0.517	-0.161	-0.018
C Rippling & Shoving	-0.185	0.277	0.271	0.041	0.027
D Wheel Track Rutting	0.190	0.119	-0.030	-0.045	-0.082
E Distortion	0.021	0.153	0.316	0.093	-0.241
F Long Wheel Track- Single & Multiple Cracking	0.201	-0.019	0.113	0.057	-0.020
G - Alligator Cracking	-0.093	-0.017	-0.048	0.539	0.061
H Centreline - Single & Multiple Cracking	0.307	-0.129	-0.034	-0.018	-0.036
I - Alligator Cracking	-0.045	-0.115	-0.091	0.652	-0.112
J Pavement Edge - Single & Multiple Cracking	0.061	0.323	-0.095	-0.037	0.078
K - Alligator Cracking	-0.098	0.602	-0.093	-0.103	0.030
L Transverse - Full, Half & Multiple Cracking	0.336	-0.152	-0.060	-0.149	0.091
M - Alligator Cracking	-0.049	-0.093	-0.035	0.119	0.563
N Longitudinal Meander & Midlane Cracking	0.189	-0.145	0.252	0.028	0.134
O Random Cracking	0.006	0.125	-0.015	-0.187	0.551

tions in terms of the five fundamental uncorrelated factors rather than in terms of the 15 highly correlated original variables.

Table 4 gives a matrix of scoring coefficients that can be used to calculate factor scores S_{ki} for individual observations from the following formula:

$$S_{ki} = \sum_{j=1}^{n} (s_{kj} \cdot Z_{ji}); \; k = 1, 2, \ldots 5 \tag{5}$$

where

S_{ki} = factor score for factor k and observation i;
s_{kj} = scoring coefficient for factor k and variable j;
Z_{ji} = value of variable j for observation i; and
n = number of variables, 15 in this case.

The matrix of scoring coefficients can be roughly approximated by dividing factor loadings by factor eigenvalues. The factor scores estimated by the scoring coefficients are also uncorrelated for all practical purposes *(8)*. These scores can be used to characterize and quantify the state of visual pavement deterioration instead of the original 15 variables. For example, the factor score for the general cracking factor (Factor 1) is

$$S_{1i} = 0.151 \cdot Z_{Ai} + 0.061 \cdot Z_{Bi} - 0.185 \cdot Z_{Ci} + \ldots + 0.006 \cdot Z_{Oi} \tag{6}$$

where subscripts A, B, C, . . . O refer to variables (distress manifestations) defined in Tables 1 to 4, and subscript i identifies an observation. Thus, for example, Z_{Ai} is a value of raveling and coarse aggregate loss for observation i, and Z_{Bi} is a value for flushing for the same observation.

The concept of characterizing, quantifying, and ultimately predicting visual pavement distresses in terms of factor scores is examined first for Factor 4. Factor 4 was named fatigue cracking and its two variable loadings are unique: longitudinal wheel track alligator cracking and centerline alligator cracking have salient, or statistically significant, factor loadings only on Factor 4. Furthermore, both variables measure the same phenomenon of cracking and are measured on the same scale. Thus, this type of fatigue cracking can be predicted independently of virtually any other distress manifestation. This prediction, of course, has been a common practice in the past; the present results provide further statistical justification for the practice.

Factor 1, named thermal cracking, is affected by two variables that do not provide unique loadings (raveling and coarse aggregate loss and pavement edge single and multiple cracking) as well as by heterogeneous variables—variables that are measured on different scales and that generally measure different deterioration phenomena such as rutting and cracking. Overall, Factor 1 loadings indicate that it is not possible to examine and predict the associated variables in isolation. For example, raveling and wheel track rutting both contribute to longitudinal wheel track cracking, transverse single and multiple cracking, and to other distresses. The prediction of any one of these distresses (rutting, for example) is questionable without taking into account the influence of the other distresses. Similarly, considering Factor 3 and its salient loading, it appears unattainable to predict roughness (in terms of distortion, rippling, and shoving) without taking into account flushing and longitudinal meander and midlane cracking.

The prediction of factor scores overcomes this limitation because the scores encompass the contributions of all relevant variables and provide uncorrelated fundamental measures of pavement visual distresses. Also, if the factor scores are known (or predicted), the scoring coefficients of Table 4 can be used to calculate values of the individual pavement distress variables.

CONCLUSIONS AND RECOMMENDATIONS

1. The evaluation of visible pavement distresses benefits from the application of factor analysis techniques. Factor analysis techniques, which can identify fundamental and uncorrelated categories of pavement distress manifestations, are useful in explaining and investigating relationships between highly correlated pavement distresses. As with any statistical procedure, factor analysis is a valuable tool only if used correctly. In addition, because of the skills required for factor interpretation, the successful user must have an in-depth technical knowledge of the problem domain.

2. Principal component analysis identified five basic independent factors that together explained about 60 percent of the variance previously explained by 15 observed variables. These five factors were named thermal cracking, pavement edge cracking, surface instability, fatigue cracking, and random cracking.

3. The results of factor analysis helped to quantify statistically associations between various distresses (such as raveling and cracking or distortion and flushing) in terms of more basic concepts. However, because of the interaction between the pavement damage attributes (e.g., traffic loads and temperature changes) and pavement structures, it was not possible to isolate the effects of the individual damage attributes (expressed as visible pavement surface distress manifestations) and assign them only to specific factors.

4. Due to the complex interdependency of individual pavement distresses, predictions of pavement distresses should be done in terms of the fundamental factors (i.e., factor scores) rather than in terms of the traditional distresses. The prediction of pavement distresses in terms of five factor scores will

provide sufficiently detailed data for the selection and timing of pavement rehabilitation treatments and for life-cycle economic analysis. For planning purposes, the separate prediction of pavement distresses in terms of the 15 pavement distress manifestation variables appears to be both impractical (because too many prediction models would be required) and logically incorrect (because distresses are interdependent).

5. All 15 distress manifestation variables currently used to characterize visible pavement deterioration contribute significantly to one or more of the fundamental factors and should be retained. Also, the individual distress variables are required for the selection of specific maintenance treatments and for establishing the existing values of the five factors.

ACKNOWLEDGMENTS

The authors express their appreciation to members of the MTC regional geotechnical sections for providing the pavement condition data that made this report possible. Appreciation is also extended to W. A. Phang, Manager of Pavement and Roadway Research, MTC, and to G. W. Bennett, Statistical Consulting Service, University of Waterloo, for many valuable comments and suggestions.

REFERENCES

1. W. R. Hudson, F. N. Finn, R. D. Pedigo, and F. L. Roberts. *Relating Pavement Distress to Serviceability and Performance*. Report FHWA-RD-80-098. FHWA, U.S. Department of Transportation, July 1980.
2. J. J. Hajek, W. A. Phang, G. A. Wrong, and G. M. Scott. *Pavement Condition Index (PCI) for Flexible Pavements*. Report PAV-86-02. Ontario Ministry of Transportation and Communications, Downsview, Ontario, Canada, July 1986.
3. J. J. Hajek. *Life-Cycle Pavement Performance Modelling Using a Knowledge-Based Expert System Technology*. Unpublished report. Department of Civil Engineering, University of Waterloo, Waterloo, Ontario, Canada.
4. B. G. Hutchinson. Principles of Subjective Rating Scale Construction. In *Highway Research Record 46*, HRB, National Research Council, Washington, D.C., 1964, pp. 60–70.
5. S. A. Mulaik. *The Foundations of Factor Analysis*. McGraw-Hill Book Company, New York, 1976.
6. H. H. Harman. *Modern Factor Analysis*. The University of Chicago Press, Chicago, Ill., 1968.
7. G. E. Mouchahoir. The Use of Multivariate Statistics in Transportation Planning. *Traffic Engineering*, Oct. 1971, pp. 44–48.
8. SAS Institute Inc. *SAS User's Guide: Statistics*. Version 5 Ed., SAS Institute, Cary, N.C., 1985.
9. R. L. Gorsuch. *Factor Analysis*. 2nd ed., Lawrence Erlbaum Associates, Inc., Hillsdale, N.J., 1983.
10. R. J. Harris. *A Primer of Multivariate Statistics*. Academic Press, Inc., New York, 1975.
11. R. L. McHattie and B. G. Connor. Description and Evaluation of Alaska's Pavement Rating Procedure. In *Transportation Research Record 938*, TRB, National Research Council, Washington, D.C., 1985, pp. 61–72.
12. J. J. Hajek and R. C. G. Haas. Predicting Low Temperature Cracking Frequency of Asphalt Concrete Pavements. In *Transportation Research Record 407*, TRB, National Research Council, Washington, D.C., 1972, pp. 39–54.
13. V. J. Marks and C. L. Huisman. *Reducing the Adverse Effects of Transverse Cracking*. Final Report, Iowa Department of Transportation, Ames, Jan. 1985.
14. L. L. Dickinson and J. W. Hall. Factor Analysis of Pedestrian Accidents. In *Transportation Research Record 605*, TRB, National Research Council, Washington, D.C., 1986, pp. 35–41.

Publication of this paper sponsored by Committee on Monitoring, Evaluation and Data Storage.

Development of a Utility Evaluation for Nondestructive Testing Equipment Used on Asphalt Concrete Pavements

SHELLEY M. STOFFELS AND ROBERT L. LYTTON

Nondestructive testing of pavements has become a cost-effective and invaluable aid in determining the actual condition of pavement sections in a highway network. Because the number of nondestructive testing devices in use grows each year, the choice of the best method involves a complex comparison of alternatives involving the test equipment itself, the resulting data, and the available methods of analyzing the data provided. All of these factors are considered in a systematic way by the application of utility theory. A hierarchical weighting system is developed using nonlinear utility curves. Each of the independent decision criteria is carefully defined. Weighting factors are developed using the Churchman-Ackoff technique. The analysis is performed with uncertainty obtained by using a beta probability distribution. The calculated results are expressed in terms of an expected value and a 95 percent confidence interval. Five generic nondestructive testing devices are evaluated for use on asphalt concrete pavements for both project-level design and network-level planning. The characteristics of these devices used in the calculations were deliberately revised so that none of them represent actual commercially available equipment. The generic devices are used to demonstrate the evaluation technique. The formulated utility analysis framework can be applied to real devices. Furthermore, the analysis can be extended to other situations by appropriate modification of the criteria, weights, or utility curves.

Nondestructive testing of pavements has become a cost-effective and invaluable aid in determining the actual condition of pavement sections in a highway network. However, the number of nondestructive testing devices that are in common use grows each year, and new devices are being developed. The choice of the best method to use involves a complex comparison of alternatives involving the test equipment itself, the available methods of analyzing the data provided, and a knowledge of the assumptions and limitations in the analysis. This paper provides guidelines and recommendations for the selection of nondestructive testing devices for use on asphalt concrete pavements.

The analysis of the usefulness of a device entails consideration of a variety of criteria. These criteria should include economic factors and operational characteristics as well as the quality of the resulting data. Because many of the factors that should be considered are noneconomic, they are thus difficult to compare. It is, however, important to consider all of the factors in a systematic way; this is done by the application of utility theory.

The formulation of the utility analysis decision framework included the following steps:

1. Identification and definition of important, independent attributes,
2. Assignment of weights of relative importance to attributes, and
3. Development of a utility curve for each attribute showing the relative desirability of values and the location of optimum values.

These steps required the input of personnel involved in the use of the testing devices. Once the decision framework is formulated, it can be used to objectively evaluate any nondestructive testing device. It can also be modified to evaluate other types of equipment.

DESCRIPTIONS OF NONDESTRUCTIVE TESTING EQUIPMENT

The nondestructive testing equipment used to collect data on existing pavements can be divided into four general categories:

1. Static deflection.
2. Steady state deflection.
3. Impulse load deflection.
4. Wave propagation.

Measurement systems that determine pavement response to slowly applied loads are generally termed static deflection systems. Loads are applied by slowly driving to or away from a measurement point with a loading vehicle, or they may be applied by reacting against a stationary loading frame. The measurement of static deflection under a slowly moving load to ascertain structural capacity must be done with care and attention to detail in order to achieve consistent results.

Steady state dynamic deflection measurement systems use a dynamic force generator and measure the deflection response of the pavement with inertial motion sensors. For pure sinusoidal motion at any fixed frequency, the output of such sensors is directly proportional to deflection. Thus, to measure deflection, it is only necessary to determine the calibration factor for the measurement frequency. The integrated output of a geophone is

S. B. Stoffels, ERES Consultants, Inc., P.O. Box 1003, Champaign, Ill. 61820. R. L. Lytton, Texas Transportation Institute, Texas A&M University, College Station, Tex. 77840.

the most common type of motion sensor employed when deflections are measured over a range of frequencies. The calibration factor is constant in its flat response range, which generally begins at a frequency value that is about three or four times higher than the resonant frequency of the sensor.

Pavement deflection in response to dynamic loads at any specific driving frequency is approximately proportional to the amplitude of the load. The proportionality factor (dynamic stiffness) is not independent of driving frequency. At low driving frequencies the dynamic pavement stiffness approaches the value of the static (or elastic) pavement stiffness.

Essentially all impulse load testing methods deliver some type of transient force impulse to the pavement surface and measure its transient response. In principle, this method is rapid. Force impulses are normally generated by dropping a weight from a known height onto an impact plate that has been placed on the surface of the pavement. The pavement response is normally measured with inertial motion sensors.

The response of the pavement structure to transient loads is explained in the literature *(1, 2)*. Szendrei and Freeme *(3)* discuss the direct relationship in linear viscoelastic systems between impulse testing and steady state sinusoidal testing. Any impulsive force *f(t)* that is a function of time can be represented through the inverse Fourier transform as a function of frequency *(4)*.

By far the major advantage in this testing approach is that the actual duration required for measurements is only a few seconds. One disadvantage is the problem of obtaining accurate response information in the low frequency range because of characteristic low output of inertial motion sensors in this range of frequencies. Also, to obtain reliable response information in the significant frequency range of the pavement requires force impulses that have a short duration. Such impulses are difficult to produce. Nevertheless, considerable pavement characterization information can be obtained when force impulses of longer duration are used.

Wave propagation techniques offer methods for the determination of the elastic properties of individual pavement layers and subgrades. There are two basic techniques for propagating waves through pavement structures: (1) steady state vibration tests, and (2) impulse tests. A good description of both steady state vibration tests and impulse tests is provided by Green and Hall *(5)*. The wave propagation method involves the measurement of the velocity and wavelength of the surface waves propagating away from the vibratory source placed on the surface. Generally, three types of waves are transmitted when a surface is subjected to a vibration source.

1. Compression *(P)* waves,
2. Shear *(S)* waves, and
3. Rayleigh *(R)* waves.

Rayleigh waves are dominant as about 67 percent of the energy is dissipated in Rayleigh waves. *P* and *S* waves attenuate rapidly. *R* waves are the principal type that are measured in wave propagation techniques.

Only limited use has been made of wave propagation techniques for pavement evaluation. Interpretation of wave velocity test results to obtain elastic constants of pavement layers is the greatest obstacle. Two approaches have been used, the dispersion curve method and an empirical method that associates the wave length with the depth of the layer below the surface where the wave energy travels. The dispersion curve method has been found successful in determining the moduli of the two layers closest to the surface *(6)*. The depth-of-wave travel empirical technique has been used successfully to determine the moduli of multiple layers below the surface *(7)*. Both methods require the signals reaching the sensors to be analyzed by using a Fourier transform to express the wave speed data as a function of frequency.

EVALUATION METHODOLOGY

The analysis of the usefulness of a nondestructive testing device entails consideration of a variety of criteria. Many of these factors are noneconomic, and are thus difficult to compare. It is, however, important to consider all of the factors in a systematic way; this can be achieved by the application of utility theory. Numerous texts on utility theory exist *(8–10)*, and the theory has been successfully used in the analysis of a number of extremely complex engineering problems. As an example, the optimum configuration for the supersonic transport was arrived at by use of utility theory *(11)*.

Basically, utility theory is a way to compare apples and oranges with bananas. Two important terms used in utility theory are value and utility. Value is defined as the worth or importance attached to an object or a service. Utility is defined as the power or efficiency of satisfying wants. A previously developed utility analysis program was modified to suit the needs of the project *(12)*. Provisions for alternative methods of weighting were incorporated.

Decision Criteria

The major attributes of the decision were first identified. The attributes are

1. Cost,
2. Operational characteristics,
3. Data quality,
4. Versatility,
5. Reliability and maintenance downtime, and
6. Time in service and degree of development.

These attributes were further divided into decision criteria that contribute to satisfying the objectives associated with the attributes. The resulting decision flowchart is shown in Figure 1. Each decision criterion had to be carefully defined so that objective values could be determined. The final definitions are given in Table 1.

In order for the utility evaluation to be valid, the criteria must be independent of one another. Any interdependence may sway the outcome by overlapping or repeating the consideration of a certain criterion or subcriterion. This factor was carefully considered when selecting the criteria and developing the definitions. It might appear that a better evaluation could be provided by adding more criteria or by further subdividing the criteria. However, if such actions are taken, independence must

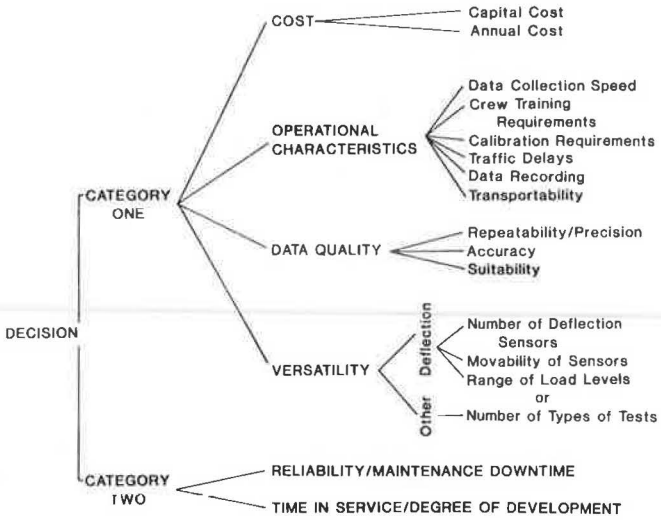

FIGURE 1 Flowchart of utility decision criteria.

be maintained. For example, a criterion for type of sensors could be added. Certainly, LVDTs and geophones are preferable to dial gauges. However, when the independence of such a criterion is examined, its validity is doubtful. The advantages of the better sensors are to a great extent included in the criteria for accuracy, reliability, repeatability and precision, data collection speed, and calibration requirements. Therefore, type of sensors would have to be defined and weighted in such a manner as to exclude such factors. Upon examination of this definition, it may well be found that such a factor is, in fact, already incorporated into the utility analysis and therefore unnecessary. Similarly, ease of operation could be considered. However, this criterion is almost totally incorporated into crew training requirements, data collection speed, and annual cost. In this manner, a wide variety of criteria were considered, defined, divided, and combined to result in the system given in Table 1. Totally independent criteria are not realistically possible, but the independence can be maximized by careful adherence to the definitions.

The attributes were divided into two major categories. Category 1 attributes are generally concerned with specific device characteristics, whereas Category 2 attributes involve reliability, time in service, and degree of development. Therefore, the utility of Category 1 reflects the potential of the devices; the combination of the two categories gives the current utility of the device to a user.

Weighting Factors

Next, weighting factors were developed for the decision criteria. The weighting factors provide a measure of the value of each criterion.

Several types of weighting factors are possible. Weights can be multipliers in an additive system, for example.

$$w_1A + w_2B + w_3C \quad (1)$$

or weights can be exponents in a multiplicative system, as in

$$A^{w1}\, B^{w2}\, C^{w3} \quad (2)$$

A combination of hierarchical additive and multiplicative weighting methods was chosen for application to this problem. The attributes and criteria within Category 1 and within Category 2 were combined using the additive method. However, the total utility was determined by combining the utilities of Category 1 and 2 multiplicatively with exponential weights. This weighting was done because if a device has either a low Category 1 utility or a low Category 2 utility, its present use value is also low. The multiplicative scheme allows values to have a more noticeable impact. However, it was desirable to keep Category 1 characteristics separate and obtain the utility for Category 1 additively in order to provide some indication of the potentials of the devices at current cost levels.

Two separate sets of weights were developed to allow for the possibility that different devices could be optimal in different situations. The two situations considered were used for network-level analysis and planning and use for project-level analysis for design.

After the weighting system was decided upon, the weights had to be determined. The weights were determined using the Churchman-Ackoff point-allocation method as shown in Figure 2. The method was chosen because of its relative simplicity *(13)*. Furthermore, Schoemaker and Waid have experimentally examined multiple regression, analytic hierarchies, direct trade-offs, point allocations, and unit weighting, and have found that the point allocation method was more than adequate and, in fact, exhibited the narrowest distribution of correlations *(14)*. As previously explained, the method requires independence of the decision criteria.

Weights were determined independently by each of the following individuals who are familiar with the equipment:

1. Roger E. Smith, ERES, Inc., Champaign, Illinois;
2. Harold L. Von Quintus, Brent Rauhut Engineers, Inc., Austin, Texas;
3. Jim Hall of the Waterways Experiment Station, Vicksburg, Mississippi;
4. Robert L. Lytton of the Texas Transportation Institute, College Station, Texas; and
5. Freddy L. Roberts of the Highway Research Center, Auburn, Alabama.

Each individual was asked to fill out a form, using the Churchman-Ackoff method. Weights were then normalized so that the weights in each division totaled one. The five normalized weights for each criterion were then analyzed to determine the mean and standard deviation. Using this information, the final weights were determined in a group session. These final weights are given in Table 2.

Utility Curves

Utility curves show the function of efficiency of each criterion in satisfying the corresponding want. They enable us to mea-

TABLE 1 DEFINITIONS OF DECISION CRITERIA

Criterion	Definition
CATEGORY ONE:	
Capital Cost	Determination of capital costs shall include consideration of the following components: 1. Initial Cost -- The cost to purchase the equipment and accessories. 2. Salvage Value -- The expected salvage value of the NDT equipment and accessories at the end of its service life. 3. Equipment Life -- The expected life anticipated for the NDT equipment and its accessories.
Annual Data Collection Cost	Determination of annual data collection cost shall include consideration of the following components: 1. Maintenance Cost -- Average annual maintenance costs over the life of the equipment, including both parts and labor. 2. Crew Costs -- The costs of the crew required to operate the equipment for one day of testing (an eight-hour day).
Data Collection Speed	The total time required to test a pavement station from the time the tow vehicle stops until it starts again after the measurement is completed. This time includes set-up, testing, data collection, and reloading.
Crew Training Requirements	Personnel training includes actual time operating the equipment as well as reviewing the operations manual provided by the manufacturer. It should include familiarization with equipment operation, trouble-shooting, data interpretation for verification, and calibration procedures. Requirements should be expressed as the total number of man-hours of training required for an entire crew.
Calibration Requirements	The estimated number of hours of calibration required per week of use.
Traffic Delays	This factor is a measure of the inconvenience to other road users. It is dependent upon the travel speed of the testing vehicle and upon the space occupied by the required equipment. It will be evaluated on a continuous scale from 0 to 1: 0 = No traffic delays. 0.5 = Complete obstruction of a single lane. 1 = Complete obstruction of two lanes.
Data Recording	A measurement of the degree of automation and the ease of data acquisition, storage, and retrieval. It will be evaluated on a continuous scale from 0 to 1. 0 = No automation; all data must be hand recorded. 0.5 = Data is recorded automatically, but does not include test section or other relevant information. 1 = Equipment must be transported over distances by a specially equipped additional vehicle.
Repeatability/ Precision	The expected coefficient of variation of a measurement repeated at a single location.
Accuracy	The expected error of the measured quantities. For deflection-type devices, this should incorporate the accuracy of both load measurements and deflection measurements.

TABLE 1 continued

Criterion	Definition
Suitability	Are the pavement responses measured the same as would occur when a 9-kip moving wheel load is applied? It will be evaluated on a scale from 0 to 1: 0 = No. 0.4 = Procedure to convert to 9-kip moving wheel load requires use of assumed material properties of the layers. 0.7 = Accurate procedure available for conversion from the applied load to a 9-kip moving wheel load. 1 = Yes.
For deflection-type devices:	
Number of Deflection Sensors	The actual number of deflection sensors used for each test.
Movability of Sensors	Are the sensors movable, for the evaluation of load transfer, etc.? It will be evaluated on a continuous scale from 0 to 1: 0 = No. 0.5 = Yes. Requires sensors to be moved manually. 1 = Yes. Sensors can be moved automatically.
Range of Load	The range of load levels that the deflection-measuring equipment can exert on the pavement. The rating will be on a continuous scale from 0 to 1 as follows: 0.0 = No load. 0.2 = One light load level. 0.4 = One heavy load level. 0.6 = A range of loads from light to medium. 0.8 = A range of loads from medium to heavy. 1.0 = A range of loads from light to heavy. The light loads shall be 0-4000 lb.; medium loads, 4000-10,000 lb.; and the heavy loads, 10,000-24,000 lb. or more.
For other NDT devices:	
Versatility	Versatility shall be defined as the number of types of measurements that can be made by a single device.
CATEGORY TWO:	
Reliability/ Maintenance Downtime	The estimated time, in number of days per year, that the equipment will be out of service due to equipment failures, malfunctions, etc. This includes waiting time required to obtain necessary parts and service.
Time in Service/ Degree of Development	It will be evaluated on a continuous scale from 0 to 1: 0 = Equipment is in developmental stages and has not been field tested for pavement studies, and equipment or software is not yet developed for production testing. 0.5 = Equipment has been developed and field tested on a limited basis but is not in production or available commercially. Some software has been finalized. 1 = Equipment and software is in fully-developed use, accepted nationwide, available commercially, and in use for production testing.

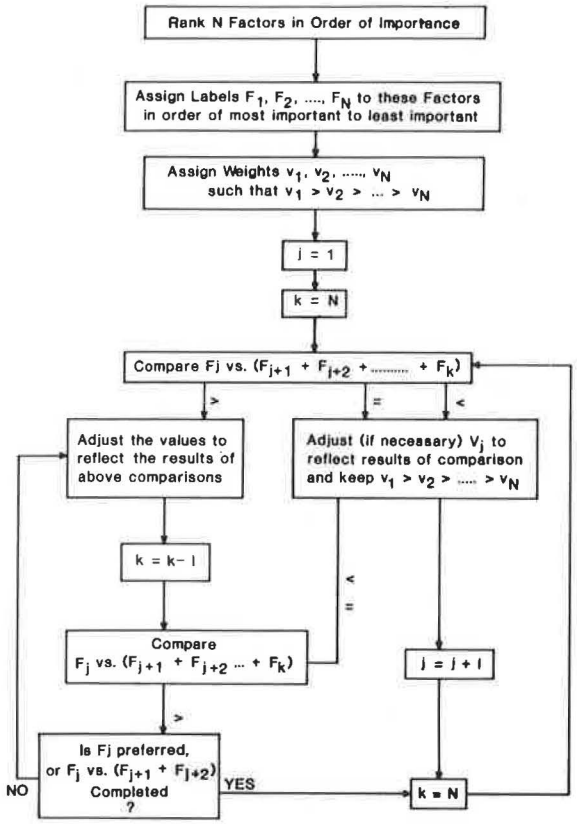

FIGURE 2 Graphical illustration of the Churchman-Ackoff Method to determine the weights of the factors.

TABLE 2 WEIGHTING FACTORS

Factor	Project-Level Relative Weight	Network Level Relative Weight
Category One	1.00	1.00
Category Two	0.50	0.50
Cost	0.19	0.23
Operational Characteristics	0.22	0.34
Data Quality	0.35	0.28
Versatility	0.23	0.15
Reliability/Maintenance Downtime	0.48	0.60
Time in Service/Degree of Development	0.52	0.40
Capital Cost	0.52	0.43
Annual Cost	0.48	0.57
Data Collection Speed	0.22	0.23
Crew Training Requirements	0.14	0.10
Calibration Requirements	0.15	0.14
Traffic Delays	0.20	0.19
Data Recording	0.19	0.20
Transportability	0.09	0.13
Repeatability/Precision	0.28	0.38
Accuracy	0.41	0.30
Suitability	0.31	0.32
Number of Deflection Sensors	0.30	0.43
Movability of Sensors	0.30	0.27
Range of Load Levels	0.40	0.30

sure the utility for a given level of an attribute. A utility function $u(x)$ represents the utilities of a group of decision makers for various values of an attribute. Utility curves may assume a variety of shapes. In this project, both linear and nonlinear utility functions were used. The utility values range from 0 to 1, with 0 being of no value and 1 satisfying the want perfectly. The shapes of the utility curves indicate preferences. Curves that are convex upward are representative of personal preferences of those people who are willing to take a chance. This risk proneness is due to an expectation that the method, if successful, will more than justify the expenditure of additional amounts of the independent decision variable plotted along the abscissa. Curves that are concave upward represent risk aversiveness in personal preferences, indicating a less than optimistic expectation of a successful outcome. Straight-line curves represent a set of personal preferences that is convinced of neither an optimistic nor pessimistic outcome. Actual curves may be any combination of these shapes *(8, 12, 15)*.

One set of utility curves was used for both project-level and network-level analyses. Each of the five expert participants constructed a set of utility curves, drawing one curve for each decision criterion. Points on these curves were averaged, the curve shapes were examined, and a tentative set of combined curves were drawn. These curves were later refined in a group session. Example curves shown in Figure 3 were fitted with an exponential equation of the form

$$u = a + bx^c \tag{3}$$

where

u = utility,
x = decision variable, and
a, b, c = constants computed to fit the points.

These utility functions $u(x)$ were used for the integration in the utility analysis program.

Consideration of Uncertainty

Many of the nondestructive testing devices considered are still in a developmental stage. Furthermore, even if detailed knowledge of a particular technique were known, the actual values of the criteria could vary significantly, depending upon the specific use and user. In order to be confident of the decisions made in this condition of uncertainty, the decision criteria were described as a distribution of values instead of as a single value. Each decision criterion was assumed to have a beta probability density function. At some value of a decision criterion x, the beta probability density is

$$f(x) = [\Gamma(\alpha - \beta)x^{\alpha-1}(1 - x)^{\beta-1}]/[\Gamma(\alpha)\,\Gamma(\beta)] \tag{4}$$

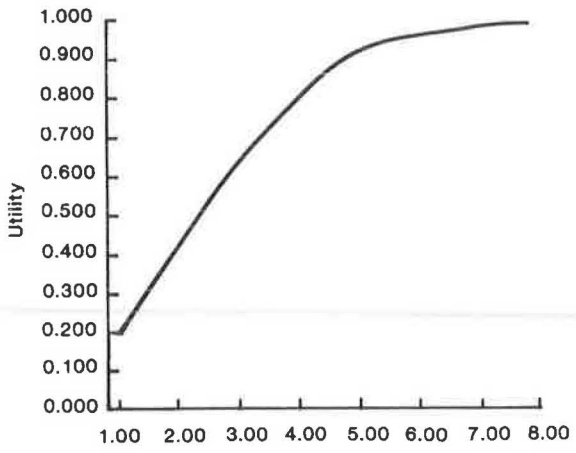

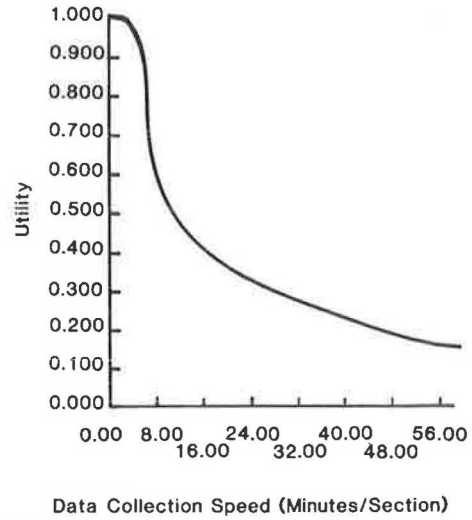

FIGURE 3 Two of the utility curves developed for the decision analysis.

where $\Gamma(\alpha)$, $\Gamma(\beta)$ are gamma functions of α and β, respectively, and α, β are distribution parameters that can be determined if the mean and standard deviation of the variable x are known.

The beta distribution is convenient for determining the mean and standard deviation if estimates of optimistic, most probable, and pessimistic values of the decision variable are known. The mean is given by

$$\bar{x} = (o + 4m + p)/6 \tag{5}$$

where o, m, p are optimistic, most probable, and pessimistic values of x. The variance of a beta distribution is given by (9):

$$\sigma_x^2 = (p - o)^2/6 \tag{6}$$

The distribution parameters α and β are

$$\alpha = \mu\,[\mu(1 - \mu)/\sigma_x^2 - 1] \tag{7}$$

$$\beta = (1 - \mu)\,[\mu(1 - \mu)/\sigma_x^2 - 1] \tag{8}$$

With these values of α and β known, it is possible to calculate $f(x)$ for any value of x.

The expected value of the utility of x is given by the integral

$$E(u_x) = \int_{x_{min}}^{x_{max}} f(x)\,u(x)\,dx = \mu_u \tag{9}$$

and the variance of the utility of x is

$$\text{var}(u_x) = \int_{x_{min}}^{x_{max}} f(x)\,u^2\,(x)\,dx - \mu_u^2 \tag{10}$$

Simpson's rule is used in the computer program to numerically evaluate the two integrations in Equations 9 and 10. The reason for calculating variances as well as expected values of the utilities is to provide the option of comparing the nondestructive testing devices at various degrees of certainty.

If the utility distribution is assumed to be normal, a confidence interval (L, U) for u is given by

$$\left.\begin{matrix} L \\ U \end{matrix}\right\} \quad E(u) \mp Z_{(1 + \gamma)/2}\,[\text{var}(u)]^{0.5} \tag{11}$$

where $Z_{(1 + \gamma)/2}$ is the $100(1 + \gamma)/2$ fractile of the standard normal distribution. To compute the 95 percent confidence interval, $(1 + \gamma)/2 = 0.975$ and $Z = 1.96$.

EVALUATIONS OF NONDESTRUCTIVE TESTING DEVICES

For purposes of demonstrating the use of the utility analysis, five generic devices were evaluated. The characteristics of these devices are given in Table 3. These characteristics have been set deliberately so as not to represent actual devices; therefore, the resulting rankings as obtained here do not necessarily represent realistic comparisons between the various types of devices.

The utility analysis program was run for each of the generic devices. The resulting total utilities, one being optimal, are given in Table 4. The expected value of utility is shown for each device; the range given represents the 95 percent confidence interval.

The decision process as presented reflects the viewpoints of the panel of experts involved. However, the decision process for other groups may vary. For example, one significant change might occur if an organization already owned one or more NDT devices. The decision analysis for purchasing additional devices would probably still be similar to that presented here; perhaps compatibility of data and software would require consideration. However, such an organization might also wish to examine the net utility of replacing the devices already in use. The primary difference would be in the evaluation of capital cost; the capital cost would be zero for the device or devices already owned, thus improving their utility relative to the device being considered for purchase. Crew training requirements might also be taken as zero. With capital cost and crew training requirements equal to zero for each of the devices, the utility analyses were repeated. The resulting total and Category 1 utilities are presented for project-level and network-level use in Table 5. The utilities from Table 5 for a device already owned can be compared to those in Table 4 for other devices. For example, the total utilities for a previously purchased static

TABLE 3 CHARACTERISTICS OF GENERIC DEVICES

		Static Deflection			Steady-State Vibration I			Steady-State Vibration II			Impulse Device			Wave Propagation		
Characteristic	Unit	Low	Most Probable	High	Low	Most Probable	High	Low	Most Probable	High	Low	Most Probable	High	Low	Most Probable	High
Capital Cost	Dollars	1,000	2,000	3,000	40,000	45,000	50,000	20,000	25,000	30,000	55,000	60,000	70,000	50,000	75,000	100,000
Annual Cost	Dollars/yr	40,000	45,000	55,000	40,000	45,000	50,000	40,000	45,000	55,000	40,000	45,000	50,000	45,000	50,000	55,000
Data Collection Speed	Minutes/ Station	5	10	15	0.75	1.30	2.75	1.88	2.75	11.00	0.75	1.30	2.75	15	35	55
Crew Training Requirements	Man-hours	1	4	6	21	42	70	16	40	80	40	60	95	60	80	100
Calibration Requirements	Hours/week	.25	.50	2	2	4	6	2	4	6	4	6	9	3	5	7
Traffic Delays	---	0.4	0.6	1.0	0.36	0.50	0.66	0.36	0.47	0.66	0.36	0.47	0.66	0.6	0.8	1.0
Data Recordings	---	0.0	0.1	0.2	0.33	0.55	0.77	0.50	0.85	1.0	1	1	1	1	1	1
Transportability	---	0.0	0.25	0.50	0.67	0.70	0.75	0.5	0.5	0.5	0.5	0.5	0.5	0	0	0
Repeatability/ Precision	---	0.3	0.05	0.10	0.005	0.01	0.02	0.005	0.01	0.02	0.005	0.01	0.02	0.005	0.01	0.02
Accuracy	Percent	4	11	20	4.5	8.6	13.2	4	11	20	3.6	7.0	10.6	5	10	15
Suitability	---	0.0	0.3	0.6	0.43	0.57	0.70	0.6	0.7	0.8	1	1	1	0.3	0.4	0.5
No. of Deflection Sensors	Sensors	1	1	1	5	5	5	3	3	3	3	5	7	4	4	4
Movability of Sensors	---	0	0	0	0.5	0.5	0.5	0.5	0.5	0.5	0.5	0.6	0.7	0.5	0.5	0.5
Range of Load Levels	---	0.4	0.4	0.4	0.2	0.2	0.2	0.6	0.6	0.6	1	1	1	0.1	0.1	0.1
Reliability/Maintenance Downtime	Days/year	0	3	5	5	7	15	5	7	15	7	10	18	14	18	27
Time in Service/ Degree of Development	---	0.90	0.95	1.0	1	1	1	1	1	1	0.6	0.7	0.8	0.1	0.1	0.1

deflection device are 0.553 and 0.575 for project level and network level, respectively. In both cases, there are still three devices with higher total utilities, including capital cost. Although the utility for the static deflection device is improved, the owner might still wish to consider the purchase of one of the higher-ranking devices.

SUMMARY AND CONCLUSIONS

A utility analysis framework has been formulated for the evaluation of nondestructive testing devices on asphalt concrete pavements. This analysis enables a variety of factors, both economic and noneconomic, to be considered in an objective,

TABLE 4 UTILITIES OF GENERIC NONDESTRUCTIVE TESTING DEVICES

Device		Project-Level Use		Network-Level Use	
		Category One	Total	Category One	Total
Static Deflection	Expected Value	.565	.552	.587	.573
	95% Confidence Interval	.513-.617	.500-603	.547-.627	.533-.614
Steady-State Vibration I	Expected Value	.701	.664	.704	.657
	95% Confidence Interval	.672-.730	.627-.701	.683-.726	.619-.695
Steady-State Vibration II	Expected Value	.717	.679	.723	.675
	95% Confidence Interval	.670-.764	.627-.731	.690-.757	.630-.720
Impulse Device	Expected Value	.810	.668	.776	.638
	95% Confidence Interval	.790-831	.626-.710	.760-792	.593-.684
Wave Propagation	Expected Value	.605	.325	.615	.349
	95% Confidence Interval	.570-.639	.292-.358	.589-.647	.312-.385

TABLE 5 UTILITIES OF GENERIC NONDESTRUCTIVE TESTING DEVICES ALREADY OWNED

Device		Project-Level Use		Network-Level Use	
		Category One	Total	Category One	Total
Static Deflection	Expected Value	.567	.553	.589	.575
	95% Confidence Interval	.515-.619	.502-605	.549-.630	.535-.616
Steady-State Vibration I	Expected Value	.718	.680	.722	.674
	95% Confidence Interval	.689-.747	.642-.717	.700-.743	.635-.712
Steady-State Vibration II	Expected Value	.729	.690	.736	.687
	95% Confidence Interval	.682-.776	.639-.742	.603-.770	.641-.733
Impulse Device	Expected Value	.833	.687	.799	.658
	95% Confidence Interval	.812-853	.644-.730	.783-815	.611-.704
Wave Propagation	Expected Value	.636	.342	.647	.367
	95% Confidence Interval	.603-.669	.308-.376	.624-.671	.329-.405

consistent manner. The analysis is concerned with the selection of a device for either project-level design or network-level planning by highway and transportation officials. The analytical framework consists of a hierarchical weighting method with nonlinear utility curves and consideration of uncertainty.

This analysis can be easily modified to suit other specific needs. For example, if a device is to be selected for use in a research study monitoring pavement performance, the requirements would probably differ in some ways. The availability of technical support from the manufacturer might become a significant criterion. Perhaps accuracy would be more important. Factors can be added and weights changed without altering the overall framework. However, when these changes are made, the independence and relative overall importance of the criteria must be reevaluated.

An objective, extendable, and repeatable decision analysis method has been developed for selecting nondestructive pavement analysis devices. This utility analysis should prove useful to highway and transportation agencies or firms contemplating the purchase of a nondestructive testing device for use on asphalt concrete pavements. Officials and consultants are able to see objective and comprehensive comparisons of a much wider variety of devices than any one agency could compare by trial use. The method should be applied to the actual characteristics of real devices.

ACKNOWLEDGMENT

The work discussed in this paper was sponsored by the NCHRP. The assistance of the expert panel consulted is gratefully acknowledged.

REFERENCES

1. E. Volterra and E. C. Zachmanoglou. *Dynamics of Vibrations.* Charles E. Merrill Books, Inc., Columbus, Ohio, 1965, pp. 101–107.
2. W. Heukelom and C. R. Foster. Dynamic Testing of Pavements. In *Proc., American Society of Civil Engineers,* Vol. 86, No. SM1, Feb. 1960, pp. 1–28.
3. M. E. Szendrei and C. R. Freeme. Road Response to Vibration Tests. In *Proc., American Society of Civil Engineers,* Vol. 96, No. SM6, Nov. 1980, pp. 2099–2124.
4. H. Hansen and P. Chenea. *Mechanics of Vibrations.* John Wiley and Sons, Inc., New York, 1956, pp. 287–304.
5. J. L. Green and J. W. Hall. *Nondestructive Vibratory Testing of Airport Pavements.* FAA-RD-73-205-1. FAA, U.S. Department of Transportation, Aug. 1974.
6. B. O. Hardin. *Effects of Strain Amplitude on the Shear Modulus of Soils.* AFWL-TR-72-201. Air Force Weapons Laboratory, Albuquerque, N.M., March 1973.
7. J. S. Heisey, K. H. Stokoe III, and A. H. Meyer. Moduli of Pavement Systems from Spectral Analysis of Surface Waves. In *Transportation Research Record 852,* TRB, National Research Council, Washington, D.C., 1982, pp. 22–31.
8. P. C. Fishburn. *Decision and Value Theory.* John Wiley and Sons, Inc., New York, 1964.
9. D. D. Meridith et al. *Design and Planning of Engineering Systems.* Prentice Hall, Englewood Cliffs, N.J., 1973.
10. R. Schlaifer. *Analysis of Decisions Under Uncertainty.* McGraw-Hill Book Co., New York, 1969.
11. *Request for Proposals for the Development of a Commercial Supersonic Transport.* FAA, Aug. 15, 1963 (amended by Addendum I, Oct. 4, 1963).
12. W. B. Ledbetter et al. *Techniques for Rehabilitating Pavements Without Overlays—A Systems Analysis.* FHWA-RD-78-108. FHWA, U.S. Department of Transportation, Sept. 1977.
13. C. W. Churchman and R. L. Ackoff. An Approximate Measure of Value. *Journal of Operations Research,* Vol. 2, 1954, pp. 172–187.
14. P. J. H. Schoemaker and C. C. Waid. An Experimental Comparison of Different Approaches to Determining Weights in Additive Utility Models. *Management Science,* Vol. 28, No. 2, Feb. 1982, pp. 182–196.
15. R. L. Keeney. Utility Functions for Multi Attribute Consequences. *Management Science,* Vol. 18, No. 5, Jan. 1972, pp. 276–287.

Publication of this paper sponsored by Committee on Monitoring, Evaluation and Data Storage.

Estimating the Life of Asphalt Overlays Using Long-Term Pavement Performance Data

J. J. HAJEK, W. A. PHANG, AND A. PRAKASH

Asphalt concrete overlays of flexible pavements are the most common pavement rehabilitation treatment in Ontario. In this paper the development of mathematical models for the performance prediction of these overlays is described. The modeling approach was based on a statistical evaluation of observed overlay performance and used readily available data. Its objective was to develop performance prediction models that would fit the existing pavement management system and could be used for life cycle economic analyses. The duration of overlay life cycle, for a predetermined terminal serviceability, was estimated as a function of overlay thickness, traffic (in number of equivalent single axles), maintenance patching, and life cycle duration of the initial pavement. The latter variable was included in the model to capture the influence of local field conditions and to characterize the strength of the underlying support structure. Maintenance patching was included to quantify the effect of pavement maintenance on overlay performance. The proposed models are preliminary and should be updated when more data become available. The modeling approach developed in this paper may be used for performance prediction of other pavement rehabilitation treatments. The paper also illustrates some of the benefits and limitations of a long-term pavement performance monitoring program for pavement performance prediction.

One of the basic building blocks of any pavement management system is the prediction of pavement performance. The process of pavement performance prediction, within the pavement management framework, encompasses *(1)*

1. The time when a pavement preservation action will be required,
2. What this preservation action should be, and
3. The consequences (benefits) of this action.

The last item, the consequences of pavement preservation actions for the most common rehabilitation treatment, asphalt concrete overlays over asphalt concrete pavements, is addressed in this paper. The objective was to develop models that would permit (a) estimation of the immediate effect of an overlay on pavement serviceability, and (b) estimation of its life cycle period. The selection of prediction modeling techniques was strongly influenced by data availability and by the type of results required in the context of the pavement management system of the Ministry of Transportation and Communication (MTC) *(2)*. A determined effort has been made to capitalize fully on the advantages of a pavement management information database, particularly on the availability of long-term pavement performance data.

Ontario Ministry of Transportation and Communications, 1201 Wilson Ave., Downsview, Ontario, Canada M3M 1J8.

DATA COLLECTION

The objective of the data collection process was to obtain, for a number of pavement sections, a complete record of pavement serviceability data spanning its initial life cycle following a new construction or reconstruction, as well as its subsequent life cycle following an overlay. An example of the two pavement performance life cycles is shown in Figure 1. In addition to the long-term pavement serviceability data, other data deemed to influence overlay life, such as traffic data, overlay thickness, life span of the initial pavement *(3)*, and the pavement condition before resurfacing in terms of roughness and various pavement distresses, were also collected.

The estimated lives of the initial and overlaid pavements were not actual lives, but the ages of the pavements when serviceability reaches a pavement condition rating (PCR) of 55. The PCR is a measure of overall pavement serviceability on a scale 0 to 100 *(4)*. Newly constructed pavements generally have a PCR of 95; rehabilitation is mostly done anywhere between 40 and 60.

Data Sources

Because the pavement information data bank was not yet fully functional, additional data had to be obtained from a variety of sources including pavement performance records *(4)*, contract drawings, and traffic files. The requirement of long-term pavement serviceability data for two pavement life cycles, covering up to 40 years, posed considerable problems of data collection.

Because of incomplete records and rather demanding data requirements, it was not possible to obtain the required data for pavement sections selected randomly. Rather, in assembling the data set used for modeling, all readily available observations were used. Altogether, data for 50 pavement sections, ranging in length from 5.0 to 26.7 km, were used for the development of prediction models. Each section had a uniform pavement structure and exhibited a uniform pavement performance. Detailed data on all observation sections are described by Hajek et al. *(5)*.

Data Description

In view of the modeling objectives, and uncertainties as to which variables may significantly influence overlay perfor-

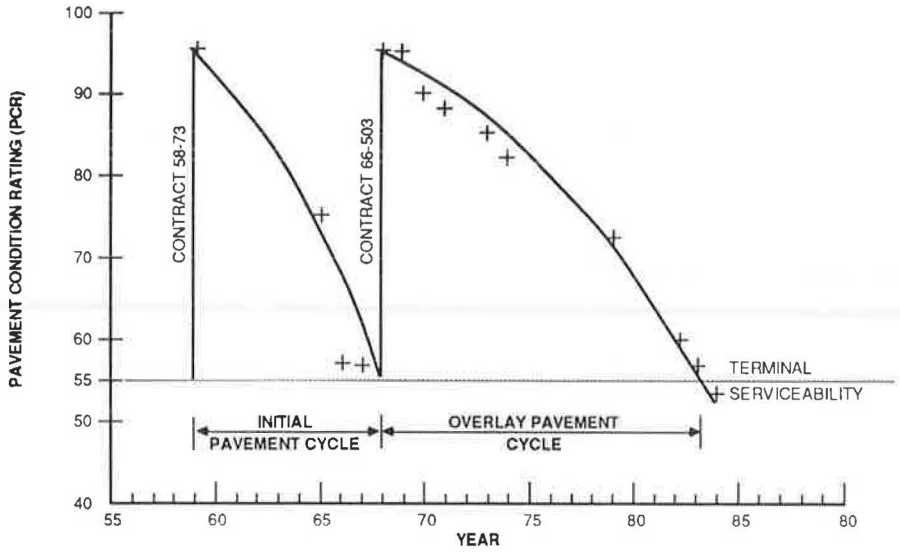

FIGURE 1 Pavement life cycles.

mance, each pavement observation section was initially characterized by more than 30 variables or factors. These variables were grouped into the following categories:

1. Traffic and environmental characteristics,
2. Initial pavement structure and its maintenance,
3. Initial pavement performance,
4. Overlay structure and its maintenance, and
5. Overlay performance.

Some principal characteristic variables collected for the observation sections are described in the following text. Additional variable definitions and detailed data are given by Hajek et al. *(5)*.

Traffic and Environmental Characteristics

System variables were as follows:

AADT83. The 1983 annual average daily traffic volume ranged from 1,000 to 8,000 vehicles; the average was 3,700 vehicles.

TRUCK. The percentage of trucks in 1983 traffic flow ranged from 4 to 24 percent; the average was 14 percent.

FREEZE. The freezing index *(6)* ranged from 420 to 2,040 degree-days Celsius.

Initial Pavement Structure and Its Maintenance

The initial pavement structure was usually a new construction or a reconstruction. In four cases, the initial pavement structure was an overlay. The maintenance of the initial pavement structures was recorded only in terms of patching. System variables were as follows:

GRANA. The average thickness of granular base, expressed as granular base course (Granular A) equivalent thickness *(7)*, ranged from 125 to 510 mm; the average was 300 mm.

BEFAC. The total average thickness of asphalt concrete ranged from 50 to 200 mm; the average was 100 mm.

PATCH. The extent of machine (full-width) patching was measured before rehabilitation.

Initial Pavement Performance

In general, pavement performance was characterized by a performance curve and by the results of a detailed pavement distress survey conducted just before overlay placement. System variables were as follows:

BEF55. The life span of the initial pavement was defined as the number of years required for the initial pavement structure to reach a terminal serviceability. The terminal serviceability was arbitrarily set at a PCR level of 55 (Figure 1). This normalized definition of the life cycle length was adopted in order to define pavement life span solely in terms of pavement performance rather than in terms of actual construction timing. If the rehabilitation took place before the pavement reached the 55 level, its BEF55 was obtained by extrapolating the performance curve. The average BEF55 was 13.1 years.

RCR. The riding comfort rating was measured on a scale from 0 to 10, just before rehabilitation; the average RCR was 5.1.

DMI. The distress manifestations index *(4)* was determined just before overlay placement. DMI was calculated as the sum of 25 individual pavement distresses, characterized by their severity and extent, and weighted according to their contribution to the PCR. Pavements without distresses have DMI equal to 0; pavements with many distresses, such as surface deformation and cracking, may have DMI exceeding 100.

ALLIG. The total alligator cracking, a portion of DMI summarizing all types of alligator cracking, was determined just before overlay placement.

Overlay Structure and Its Maintenance

System variables were as follows:

THOV. The total overlay thickness (mm) was measured including surface and binder courses but not including padding. The overlay thickness ranged from 40 to 175 mm; the average was 70 mm.

PATCH. The extent of patching was measured before rehabilitation. Crack sealing was also recorded but virtually all patched overlays also underwent some crack sealing.

Overlay Performance

The overlay performance was characterized by the performance curve in terms of PCR. System variables were as follows:

AFT55. The life span of the overlay cycle was defined as the number of years before the overlay reached the PCR level of 55 (Figure 1). The reasons for this normalized definition of overlay life were the same as those for BEF55. The average overlay life span was 14.8 years, 1.7 years longer than the average life span of the initial pavement structure.

ΔPCR5. The change in PCR during the first 5 years was measured following overlay placement.

DEVELOPMENT OF PREDICTION MODELS

The result of the data collection phase was a detailed record of pavement performance and pavement structural changes, including major maintenance activities, covering a period of two pavement life cycles. This record was available for 20 pavement sections; the record covering a period of 1½ pavement cycles was available for an additional 30 sections. These records were used to predict overlay performance in terms of the following performance characteristics:

1. Immediate increase in PCR after overlay placement,
2. Duration of overlay life cycle, and
3. PCR change (drop) during the first 5 years after overlay placement.

Immediate Increase in PCR Following Overlay Placement

The PCR directly after an overlay depends on the design intentions for the treatment as well as the workmanship of the contractor. Based on 50 observations, the average increase of PCR after overlay placement, or average PCR jump, was 53 PCR units. The range was from 32 to 66 PCR units. The plot of the PCR jump versus overlay thickness shown in Figure 2 indicates that there was no correlation between these two variables.

The only factor with a statistically significant influence on the PCR jump was the PCR level (or also RCR level) before the overlay. The PCR jump increased as the PCR level before the overlay decreased. This action reflects the fact that the PCR can theoretically reach a level of only 100 regardless of overlay

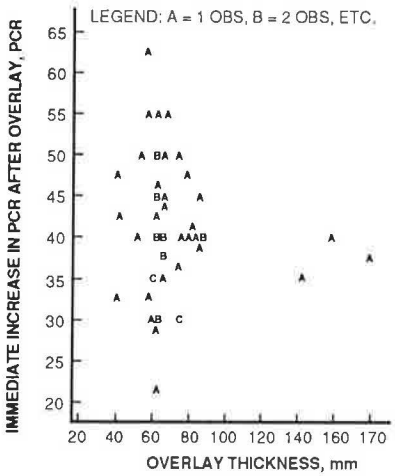

FIGURE 2 Relationship between increase in PCR and overlay thickness.

thickness. Thus, pavements with low PCR level before the overlay have greater opportunity to realize large PCR jumps. Furthermore, the PCR is subjectively assigned and PCR raters, influenced by the halo effect *(8)*, may be inclined to rate all newly overlaid pavements near the top of the PCR scale. This overrating may explain why the average PCR level of newly overlaid pavements was 94.3 with the standard deviation of only 3.2. At any rate, no useful prediction model for the PCR jump could be constructed.

Duration of Overlay Life Cycle

The period an overlay will last before reaching terminal serviceability is a basic performance characteristic necessary for any life cycle economic evaluation. In order to normalize results and eliminate the influence of construction timing, the duration of overlay life cycle must be linked to the terminal serviceability. In this analysis, the terminal serviceability was set at the PCR level equal to 55.

The prediction of the overlay life cycle duration required pavement performance data for two pavement life cycles. Of 50 observation sections, 20 were found to satisfy this condition.

Model Development

Statistically, the modeling approach was based on linear regression techniques. The selection of independent variables was based on past experience that suggests that the prediction of overlay life span depends on the following factors:

- Overlay strength (i.e., overlay thickness, quality of overlay materials, and quality of their placement),
- Strength and condition of pavement structure being overlaid,
- Maintenance effort, and
- Traffic and environment exposures.

Several different models were constructed and evaluated. The

evaluation was based on rational formulation, behavior of the model, and its statistical parameters. The following model was selected for the prediction of the overlay life cycle:

$$AFT55 = 1.32 \cdot BEF55^{0.33} \cdot THOV^{0.47} \cdot ESAL^{-0.097} \cdot 1.14^{PATCH} \quad (1)$$

where

AFT55 = duration of overlay life cycle corresponding to the terminal PCR level of 55 years,
BEF55 = duration of initial pavement structure life cycle corresponding to the terminal PCR level of 55 years,
THOV = thickness of overlay (mm), and
ESAL = number of equivalent single axle loads per day calculated using the equation.

$$ESAL = (AADT83 \cdot TRUCK \cdot TRUCKF \cdot LDF)/200 \quad (2)$$

where

AADT83 = 1983 annual average daily traffic,
TRUCK = truck percentage,
TRUCKF = truck factor, and
LDF = lane factor.

The final variable is PATCH, an indicator (dummy variable) used to account for the presence of patching during the initial cycle. PATCH introduced into the regression analyses patching information originally measured on a nominal (nonnumerical) scale *(9)*. PATCH was set to 0 for no or a limited amount of patching and to 1 for all other cases.

The selected model was not the one with the best statistical parameters, but was the best model when both the statistical parameters and rational model formulation were considered.

Model Evaluation

Statistical parameters of the model represented by Equation 1 are summarized in Tables 1–3. The model was highly statistically significant with R^2 *(10)* of 0.72. This means that 72 percent of the total variance was explained by the model. The model root mean square error, an estimate of the standard deviation of the error term, was 1.12 years. All partial regression coefficients of the independent variables were statistically significant; the intercept was not statistically significant (Table 1).

The data in Table 3 show values and statistical significance of correlation coefficients for variables of Equation 1. There was only a limited amount of intercorrelation between the independent variables. The overlay thickness, although exhibiting no significant correlation with PCR jump ($R = -0.11$) or with PCR before resurfacing ($R = 0.19$), had somewhat significant correlation with RCR ($R = 0.24$). This indicates that overlays tended to be thicker when the RCR of the initial pavement was lower, and to allow for distortion.

A plot of measured versus calculated overlay life spans is shown in Figure 3. The residuals, differences between the predicted and observed AFT55 values, were normally distributed.

The prediction model defined by Equation 1 can be advantageously used to isolate and quantify the effects of the model variables. The effect of individual variables and evaluation of rational behavior of the model, in view of the factors known to influence the overlay performance, are discussed in the following.

Overlay Thickness

The overlay thickness was the only variable used to characterize the overlay strength. Equation 1 can be rearranged to

TABLE 1 ANALYSIS OF VARIANCE IN OVERLAY LIFE PREDICTION MODEL

Source of Variance	Degrees of Freedom	Sum of Squares	Mean Square	*F* Value	Level of Significance (%)
Regression model	4	0.0919	0.0230	9.84	0.04
Error	15	0.0350	0.0023	—	—
Corrected total	19	0.1270	—	—	—

TABLE 2 PARTIAL REGRESSION COEFFICIENTS IN OVERLAY LIFE PREDICTION MODEL

Parameter	Estimate	Std. Error of Estimate	Student's *t* Value for HO: Para = 0	Level of Significance (%)
Intercept	0.121	0.264	0.46	65.0
log THOV	0.472	0.140	3.37	0.4
log ESAL83	–0.097	0.026	–3.74	0.2
log BEF55	0.331	0.098	3.38	0.4
PATCH	0.058	0.022	2.62	1.9

TABLE 3 CORRELATION COEFFICIENTS IN OVERLAY LIFE PREDICTION MODEL[a,b]

	THOV	ESAL83	BEF55	PATCH	AFT55
THOV	1.00				
ESAL83	0.25	1.00			
BEF55	0.03	0.05	1.00		
PATCH	−0.14	−0.01	0.16	1.00	
AFT55	0.41	−0.41	0.45	0.35	1.00

[a] All correlation coefficients are based on 46 to 50 observations with the exception of correlation coefficients involving AFT55, which are based on 20 observations.

[b] Correlation coefficients based on 50 observations are significant at 10 percent level of significance if their value exceeds 0.24. The corresponding value for correlation coefficients based on 20 observations is 0.36.

predict overlay thickness for a desired length of overlay life cycle:

$$THOV = \left(\frac{AFT55}{1.32 \cdot BEF55^{0.33} \cdot ESAL^{-0.097} \cdot 1.14^{PATCH}} \right)^{2.13} \quad (3)$$

The relationship between overlay thickness and overlay life is illustrated in Figures 4*a* and 4*b*. Both figures assume that the initial pavement life cycle was 13 years, the data set average. Furthermore, Figure 4*a* assumes that none or only a small amount of maintenance patching was done in the first cycle; Figure 4*b* assumes that more extensive patching was done. For a typical range of overlay thickness, the doubling of thickness results in a 5- to 7-year increase in overlay life. However, the relationship between overlay thickness and overlay life is not linear.

Figures 4*a* and 4*b* also show a corresponding relationship obtained by inputting average data set values and a subgrade layer coefficient M_s, equal to 5,000, to a mechanistically based OPAC prediction method *(7)*. The model results from Equation 3 and the OPAC results are quite similar, particularly for the case with the maintenance patching.

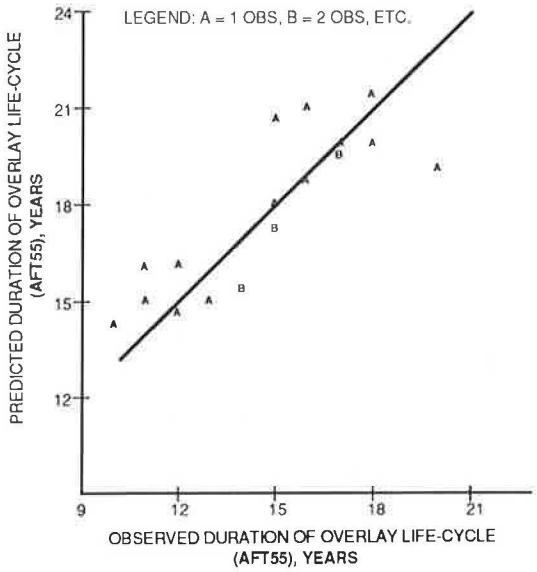

FIGURE 3 Comparison of observed and predicted length of overlay life cycle (AFT55).

The compatibility of the two prediction methods may be attributed, to some extent, to coincidental selection of average OPAC input data. However, the shapes of curves relating overlay thickness to overlay life are similar. Also, the empirical model of Equation 1 requires only readily available data, whereas the mechanistically based OPAC prediction method requires considerably more detailed data that is not always available.

Figures 4*a* and 4*b* can be used for rough estimation of overlay thickness requirements. An example is shown from Figure 4*a*. For a desired overlay life of 15 years and assuming

- No significant amount of patching,
- Initial pavement life of 13 years, and
- 100 ESAL/day (approximately an AADT of 3,000 with 14 percent of trucks),

the recommended overlay thickness is 70 mm.

Patching

According to Figure 5, the presence of patching during the initial pavement cycle increased the overlay life by about 2 years. It appears that patching, usually done near the end of the initial pavement cycle, strengthened the pavement structure where such strengthening was most required. The overlay performance benefited from this action, assuming that patches were overlaid before they deteriorated.

Patching during the initial pavement cycle occurred about 15 or 20 years ago and data describing patching extent and timing lack many details. Nevertheless, even in this crude form, the effect of patching was statistically significant (Tables 2 and 3).

Equation 1 represents a pavement damage equation that includes the effect of maintenance. Historically, pavement damage functions have been unable to include and quantify the effect of maintenance *(10, 11)*. Equation 1 does this in a format fully compatible with the requirements of life cycle economic analyses.

The effect of maintenance patching in the second (overlay) cycle was also evaluated but could not be quantified. There were also problems with data. Patching is usually done at the end of the pavement life. Thus, the effect of the second cycle patching may not be fully accounted for if the serviceability limit is set at the PCR level equal to 55 or if the patching has not been done yet.

Traffic

The traffic exposure was characterized by the number of equivalent single axles in 1983 (Equation 2). The relationship between traffic and overlay life (AFT55), illustrated in Figure 6, is expressed both in terms of number of equivalent single axle loads (ESALs) and annual average daily traffic (AADT) volumes. AADT volume is assumed to contain 14 percent of trucks and to have a typical truck factor.

Duration of Initial Pavement Structure Life Cycle

Variables related to the strength of the pavement being overlaid and variables characterizing environmental exposure could be expected to be useful in predicting the overlay life. These types

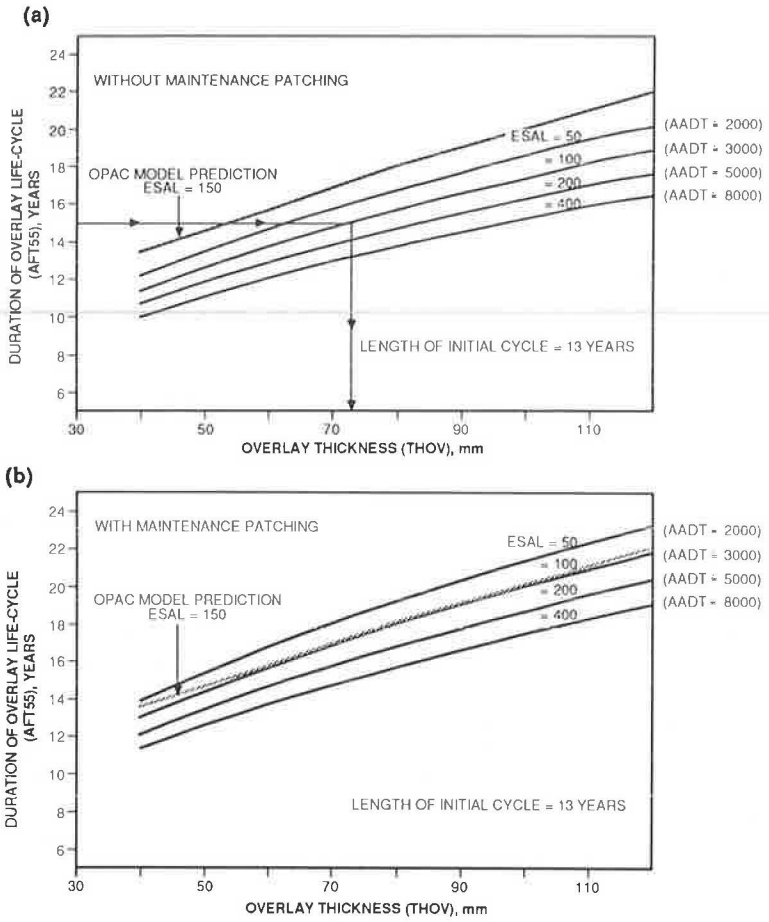

FIGURE 4 (a) Effect of overlay thickness on overlay life, no maintenance patching. (b) Effect of overlay thickness on overlay life, with maintenance patching.

of variables available in the data bank included, for example, thickness of asphalt concrete, granular base equivalency thickness, subgrade type, and freezing index, but did not include any results of pavement deflection tests *(5)*. None of the available variables exhibited any predictive potential with the exception of the duration of the initial pavement life cycle. It appears that it is more important to know the life span of the initial pavement than its thickness.

Figure 7 illustrates the observed relationship between the duration of the initial pavement life cycle and the subsequent overlay cycle, both cycles being referenced to the same terminal performance level of PCR equal to 55. The effect of the initial cycle is quite pronounced; on average, all other variables being equal, a 5-year increase in the initial pavement life resulted in a 2-year increase in the overlay life.

The life span of the initial pavement structure embodies site-

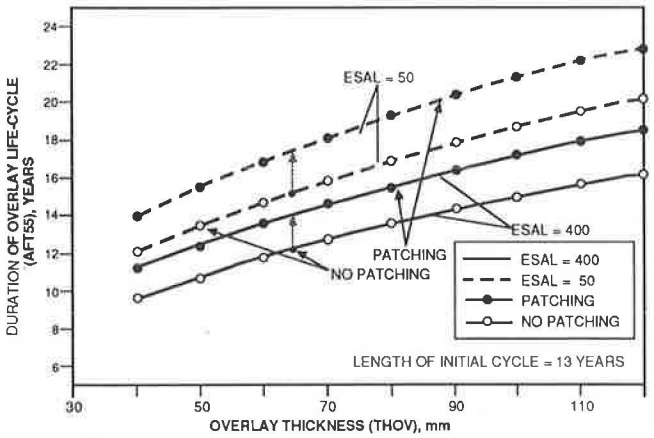

FIGURE 5 Effect of maintenance patching on overlay life.

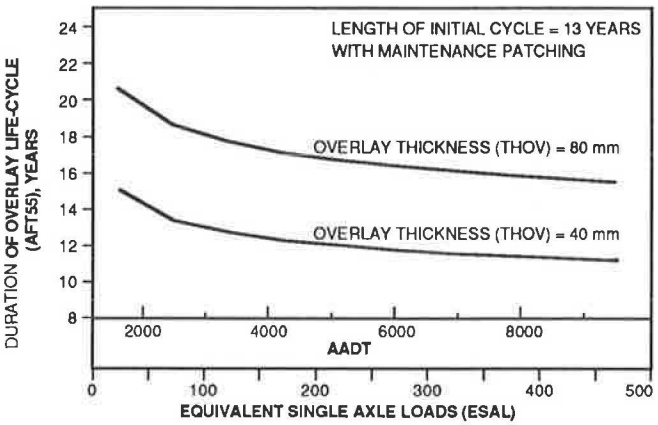

FIGURE 6 Effect of traffic on overlay life.

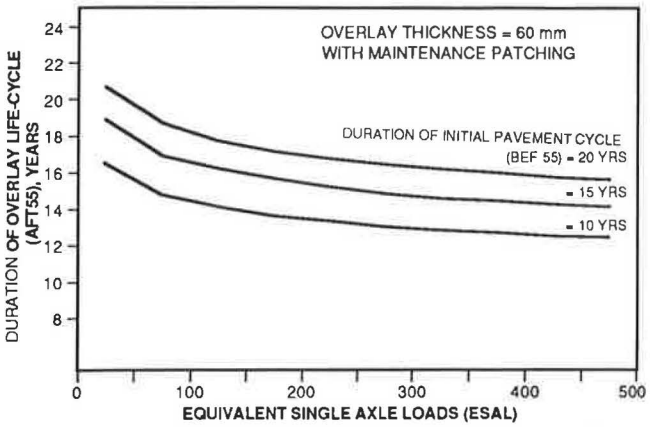

FIGURE 7 Effect of initial pavement life on overlay life.

specific, long-term interaction between the pavement structure, including maintenance, and traffic and environmental exposures. If, for example, the initial pavement structure performs poorly, perhaps because of local soil or drainage conditions or unusually heavy traffic loads, chances are that the overlay performance is also negatively influenced by the same conditions. The duration of the initial pavement life cycle is thus a comprehensive, site-specific, and readily available predictor of overlay performance that should not be overlooked even by mechanistically based overlay design methods.

Model Verification

Because of the relatively small number of observations available for the model development *(20)* and the method used for their selection, an additional six observations were selected in a random manner to evaluate the model accuracy independently.

The results of this evaluation, presented in Table 4, indicate that the accuracy of the model is roughly in line with expectations. The standard deviation of the difference between measured and predicted overlay life spans for the six additional observations was 2.07 years, comparable to the model root mean square error of 1.12 years.

PCR Change During the First 5 Years After Overlay (ΔPCR5)

The prediction of PCR change during the first 5 years of overlay life (ΔPCR5) complements the prediction of overlay life cycle span and was motivated by two reasons.

Data Availability

The development of the overlay life cycle prediction model required pavement performance data for the same basic pavement structure spanning two pavement life cycles or approximately 25 to 40 years. Because the ΔPCR5 prediction modeling required considerably less historical data, an additional 30 observations were available for a total of 50 observations. Also, it was hoped that the ΔPCR5 prediction could serve as a surrogate of the total life cycle prediction.

Performance Curve

Prediction of ΔPCR5 helps to define the shape of the pavement performance curve. The shape of the performance curve, in addition to its length, is often used in economic analyses.

Model Description

A number of ΔPCR5 prediction models were constructed and evaluated. These models related ΔPCR5 with variables characterizing pavement structure and pavement condition before overlay, as well as overlay itself. The following prediction model for ΔPCR5 was selected because of its rational structure, statistical parameters, and simplicity.

$$\Delta PCR5 = 36.31 \cdot THOV^{-0.65} \cdot ESAL^{0.16} \cdot DMI^{0.21} \quad (4)$$

Statistical parameters of the model represented by Equation 4 are summarized in Tables 5–7. Even though the multiple correlation coefficient of the model was relatively low (R^2 = 0.26), the model itself and its partial regression coefficients

TABLE 4 MODEL VERIFICATION

Observation No.[a]	Initial Cycle Life BEF55 (years)	Overlay Thickness THOV (mm)	Traffic Loads ESAL (axles)	Maintenance Patching PATCH (0 or 1)	Overlay Life AFT55		Difference, Observed-Predicted (years)[c]
					Observed (years)	Predicted[b] (years)	
1	16	55	102	1	18	16.0	2.0
2	8	60	37	1	16[d]	14.6	1.4
3	6[e]	60	15	1	11	14.5	–3.5
4	11	50	177	0	12	11.2	0.8
5	16	60	77	0	17[d]	15.0	2.0
6	13	40	50	1	14	13.8	0.2

[a] Listed as observation sections 51 through 56 in Reference 5.
[b] Using Equation 1.
[c] Avg = 0.48; SD = 2.07
[d] Extrapolated for next 5 years.
[e] Pavement structure before overlay included 100 mm of cold mix.

TABLE 5 ANALYSES OF VARIANCE OF ΔPCR5 MODEL

Source of Variance	Degrees of Freedom	Sum of Squares	Mean Square	*F* Value	Level of Significance (%)
Regression model	3	0.398	1.33	5.08	0.4
Error	42	1.098	0.026		
Corrected total	45	1.496			

TABLE 6 PARTIAL REGRESSION COEFFICIENTS OF ΔPCR5 MODEL

Parameter	Estimate	Std. Error of Estimate	Student's *t* Value for HO: Para = 0	Level of Significance (%)
Intercept	1.555	0.367	4.24	0.1
log THOV	–0.655	0.208	–3.15	0.3
log ESAL83	0.161	0.060	2.68	1.0
log DMI	0.211	0.116	1.82	7.6

were statistically significant. There was no intercorrelation between model variables. The correlation coefficient between ΔPCR5 and the duration of overlay life cycle (AFT55) was –0.47, indicating that ΔPCR5 can serve as a surrogate for AFT55.

The prediction of ΔPCR5 suffered more from the subjectiveness of the PCR scale than did the prediction of the overlay life. The change in ΔPCR5 starts at the top of the PCR scale which may be also influenced by the halo effect.

Equation 4 is graphically represented in Figures 8*a* and 8*b*. Figure 8*a* illustrates the influence of overlay thickness on ΔPCR5. Figure 8*b* shows that DMI at the time of overlay placement influences the rate at which the overlay deteriorates, at least in the first 5 years of its life. Equation 4 thus quantifies, on a statistical basis, the effects of deferring overlays: A postponement of overlay placement increases DMI and the increase in DMI accelerates pavement deterioration (ΔPCR5). Alligator cracking (ALLIG) had a similar influence on ΔPCR5 and was also highly correlated with DMI (Table 4).

CONCLUSIONS AND RECOMMENDATIONS

1. Long-term pavement performance data can be used to develop reliable empirical models for performance prediction of various rehabilitation treatments. These models can include the effect of maintenance effort and can be used for life cycle economic analyses.

2. Using long-term pavement performance monitoring data, a damage model has been developed for asphalt concrete overlays over existing asphalt concrete pavements. The model predicts the span of the overlay life cycle for a predetermined terminal serviceability as a function of overlay thickness, traffic, maintenance patching, and the life cycle span of the initial pavement. The last variable, included in the model to characterize the interaction between the initial pavement structure and its traffic and environmental exposures, appears to be useful, readily available, and site specific.

3. The model developed for prediction of the drop in pavement serviceability during 5 years following the overlay placement (ΔPCR5) quantifies the influence of pavement distress conditions before overlay placement on the overlay performance. Deterioration in the overlay occurs at an accelerated rate when there is a delay in placing the overlay.

4. The proposed overlay performance prediction models and their coefficients were statistically significant despite many assumptions, simplifications, and possible sources of error (e.g., variability due to section length, subjective nature of PCR, and difficulties in quantifying maintenance effort). These problems can be eliminated or considerably reduced by better

TABLE 7 CORRELATION COEFFICIENTS OF ΔPCR5 MODEL[a,b]

	THOV	ESAL83	DMI	ΔPCR5	ALLIG	RCR
THOV	1.00					
ESAL83	0.25	1.00				
DMI	0.27	0.15	1.00			
ΔPCR5	–0.28	0.12	0.19	1.00		
ALLIG	–0.16	–0.07	0.54	0.30	1.00	
RCR	0.24	0.13	0.13	–0.08	–0.03	1.00

[a] Correlation coefficients are based on 46- to 50-observation sections.
[b] Statistical significance of correlation coefficients is outlined in footnote *b*, Table 3.

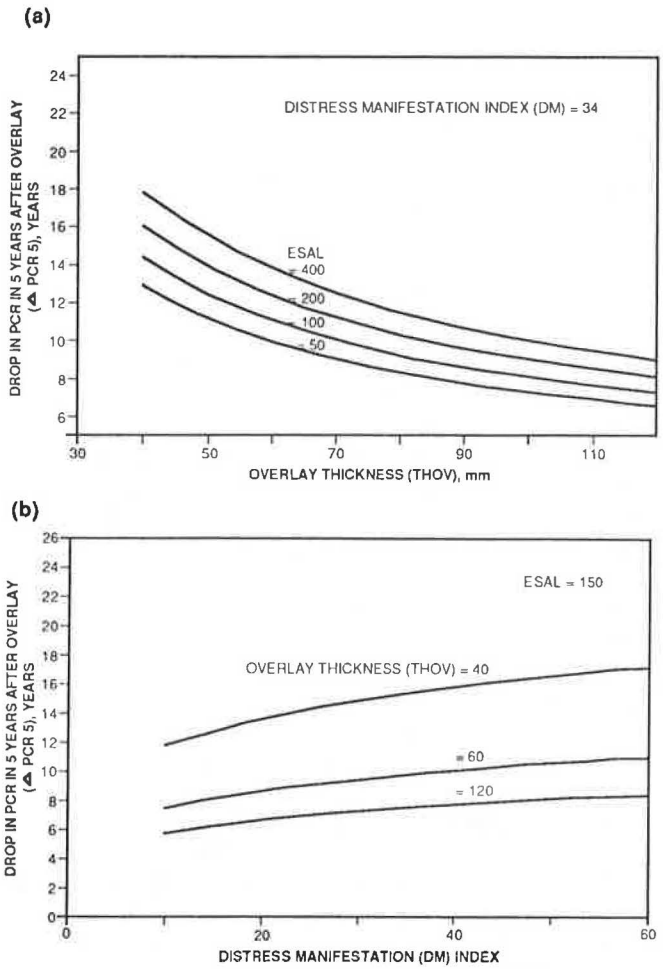

FIGURE 8 (a) Effect of overlay thickness on PCR drop. (b) Effect of DMI on PCR drop.

designed and executed long-term pavement performance programs *(13)*.

5. The proposed models should be updated when more data become available both to increase the model database and as an ongoing adjustment to reflect overlay design changes. The modeling can be also improved by developing different prediction equations for different climatic regions. Additional models should be developed for other rehabilitation treatments.

6. The prediction models developed in this study are based on statistically documented experience obtained by a long-term pavement performance monitoring program. The results detail some of the significant benefits such programs can provide for pavement performance prediction. However, the results also indicate some limitations of using long-term pavement performance data for prediction purposes. Because the span of overlay life cycle appears to depend on the life span of the initial pavement, the duration of time the pavement should be monitored may exceed 20 years. During this time, the pavement construction technology and traffic loads may undergo some significant changes. Yet, the results of the long-term pavement performance monitoring apply to the pavements built at the beginning of the program. At the end of the program, perhaps 20 years later, new materials may be already used (e.g., asphalt additives and granular materials) for which the long-term monitoring results may not fully apply. Similarly, in the early 1960s, typical truck tire pressures were in a range of 70 to 90 psi, whereas the current range may be closer to 100 to 130 psi. While some limitations are unavoidable, a judicious selection of pavement sections for long-term monitoring may ameliorate some of the limitations.

ACKNOWLEDGMENTS

The authors wish to express their appreciation to University of Waterloo engineering students, R. Little and A. Lane-Smith, for their help with data collection and to A. Lane-Smith and C. Kingdon for conducting statistical analysis. Appreciation is also extended to members of the MCT regional geotechnical sections for providing invaluable long-term pavement performance data.

REFERENCES

1. J. J. Hajek, W. A. Phang, A. Prakash, and G. A. Wrong. Performance Prediction for Pavement Management. In *Proc., North American Pavement Management Conference,* Toronto, Canada, March 1985, pp. 4.122–4.134.
2. W. A. Phang and G. A. Wrong. *Maintenance of the Highway Infrastructure, Pavement Management and Preservation.* Report ONT-014. Ontario Ministry of Transportation and Communications, Downsview, Ontario, Canada, March 1985.
3. T. L. Nelson and R. V. LeClerc. *Development and Implementation of Washington State's Pavement Management System.* Report WA-RD 50.1. Washington State Department of Transportation, Olympia, Feb. 1983.
4. G. J. Chong, W. A. Phang, and G. A. Wrong. *Manual for Condition Rating of Flexible Pavements.* Report SP 004. 2nd ed., Ontario Ministry of Transportation and Communications, Downsview, Ontario, Canada, April 1982.
5. J. J. Hajek, W. A. Phang, and A. Prakash. *Estimating the Life of Asphalt Overlays.* Report PAV-86-02. Ontario Ministry of Transportation and Communications, Downsview, Ontario, Canada, May 1986.
6. R. A. Chisholm and W. A. Phang. Measurement and Prediction of Frost Penetration in Highways. In *Transportation Research Record 918,* TRB, National Research Council, Washington, D.C., 1983, pp. 1–10.
7. R. Kher, and W. A. Phang. OPAC Design System. In *Proc., 4th International Conference on Structural Design of Asphalt Pavements,* Ann Arbor, Mich., Aug. 1977, pp. 841–854.
8. B. G. Hutchinson. Principles of Subjective Rating Scale Construction. In *Highway Research Record 46,* HRB, National Research Council, Washington, D.C., 1964, pp. 60–70.
9. D. B. Suits. Use of Dummy Variables in Regression Equations. *American Statistical Association Journal,* Dec. 1957, pp. 548–551.
10. SAS Institute Inc. *SAS User's Guide: Statistics, Version 5 Edition.* SAS Institute, Cary, N.C., 1985.
11. R. D. Pedigo, W. R. Hudson, and F. L. Roberts. Pavement Performance Modelling for Pavement Management. In *Transportation Research Record 814,* TRB, National Research Council, Washington, D.C., 1981, pp. 14–21.
12. D. R. Luhr, B. F. McCullough, and A. Pelzner. Development of an Improved Pavement Management System. In *Proc., 5th International Conference on Structural Design of Asphalt Pavements,* Vol. 1, University of Michigan, Ann Arbor, 1982, pp. 553–563.
13. Strategic Highway Research Program. *Section 2: Research Design Summary.* TRB, National Research Council, Washington, D.C., May 1986, pp. 8–20.

Publication of this paper sponsored by Committee on Monitoring, Evaluation and Data Storage.

Present Serviceability-Roughness Correlations Using Rating Panel Data

RAYMOND K. MOORE, G. NORMAN CLARK, AND GARY N. PLUMB

The Kansas Department of Transportation (KDOT) has completed an extensive study of pavement serviceability using 24-member rating panels. The AASHTO five-point segmented rating scale and the three-point segmented rating scale designed to develop serviceability estimates directly related to KDOT pavement management system roughness levels were used. The average standard deviation of individual panel ratings over all pavement types was approximately 12 percent of the maximum scale value. This value corresponds to 0.60 for the AASHTO five-point scale and 0.36 for the KDOT three-point scale; these standard deviations appear to be consistent for panel sizes ≥24. The standard deviation of the individual panel ratings for a given test section appears to be independent of the mean panel rating. Although statistically significant linear, log-log linear, and exponential linear models were developed, they were not completely satisfactory for the prediction of the present serviceability index (PSI), given Mays ride meter (MRM) roughness values. None of these functions are conceptually correct for smooth pavements (low MRM values). A statistically significant correlation was established between the AASHTO five-point and KDOT three-point present serviceability rating (PSR) values. It appears that the three-point PSR data are consistent at terminal serviceability values associated with the AASHTO five-point scale.

The Kansas Department of Transportation (KDOT) has completed an extensive present serviceability study of selected in-service pavement sections using 24-member rating panels. The ratings were made during November and December in 1985. The strategic goal of the research effort was to develop statistical relationships between present serviceability rating (PSR) as estimated by the mean panel rating and pavement management system (PMS) survey data including roughness as measured by the Mays ride meter (MRM) in inches per mile. Two segmented rating scales were needed to fulfill research objectives.

The KDOT PMS network optimization system (NOS) uses three levels of pavement roughness based on MRM data *(1)*. Level 1 roughness is associated with comfortable or satisfactory ride quality. Level 2 roughness is tolerable for the highway user. Level 3 roughness is judged to be uncomfortable and generally indicates a need for scheduling a pavement preservation action (although primary and secondary distress conditions are also considered).

A 0 to 3 scale was developed to study the relationship between PSR and NOS roughness levels that were initially assumed using prior research and engineering judgment. The panel rating card is shown in Figure 1. Numbers were omitted from the segmented scale, but numerical values were scaled from the cards after the rating survey was completed. The use of this particular rating card has not been previously reported in the technical literature.

The second rating card used the five-point segmented scale developed by Carey and Irick *(2)* for the AASHO (now AASHTO) road test *(3)*. Although initially criticized for many potential shortcomings by Hutchinson *(4)* and more recently by Weaver *(5)*, this segmented scale has been the basis for most PSR reporting in the United States. Recent research reported by Nick and Janoff *(6, 7)* indicates that the AASHTO scale does not violate good psychometric principles if panel members are properly instructed and the survey is competently administered. The KDOT panel rating study incorporated the five-point scale for two reasons. First, an algorithm was needed to relate PMS survey data to PSR using a five-point scale as reported to the FHWA for Highway Performance Monitoring System (HPMS) pavement sections. Second, another objective was to correlate the PSR data using both scales to ascertain if the NOS roughness levels were consistent with the more frequently used AASHTO scale. The rating card is illustrated in Figure 2.

SCOPE OF RESEARCH RESULTS

The research reported herein concerns five major topics related to the collection and analysis of panel data. These topics are (a) panel and test circuit design, (b) survey administration, (c) panel data statistics, (d) PSI-MRM roughness correlations, and (e) PSR_3-PSR_5 correlations. The use of these data within the

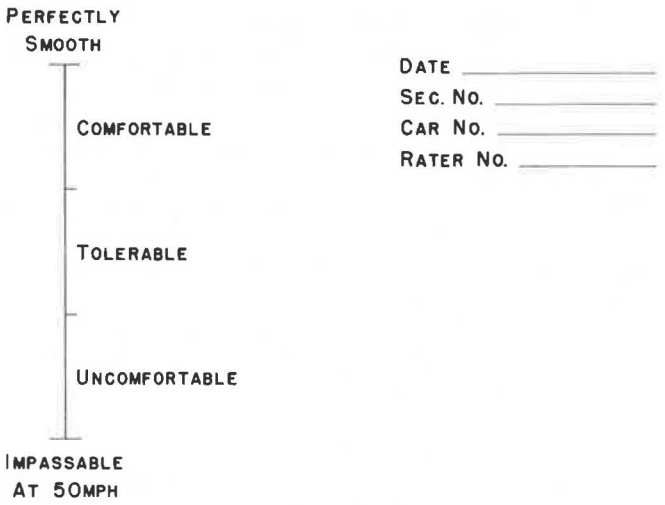

FIGURE 1 KDOT scale rating card.

R. K. Moore, Department of Civil Engineering, University of Kansas, Lawrence, Kans. 66045. G. N. Clark and G. N. Plumb, Pavement Management Task Force, Kansas Department of Transportation, Topeka, Kans. 66611.

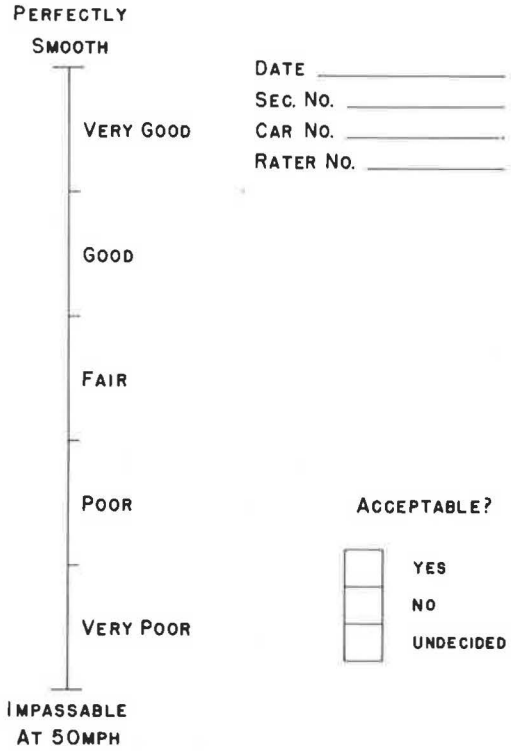

FIGURE 2 AASHTO scale rating card.

KDOT PMS system is beyond the scope of this paper because preparatory work has not been completed.

PANEL AND TEST CIRCUIT DESIGN

A panel size of 24 was selected using parametric theory of estimation as recommended by Zaniewski and Hudson *(8)*. Panel size was determined based on the AASHTO scale because panel data have been previously published. Because the three-point scale was to be correlated with the AASHO scale, the same panel size was used for both surveys.

Nick and Janoff *(6)* published data using the AASHTO scale and 36-member rating panels that had an average standard deviation of 0.61 for all pavement sections. Furthermore, Nick and Janoff *(6)* used a subset of Weaver's data *(9)* to calculate a standard deviation of 0.60. Although the exact panel size for Weaver's data was not given, his panels were much larger than 36. Therefore, using an assumed standard deviation of 0.60 with a maximum allowable error of 0.25, a minimum sample size of 23 is necessary to be 95 percent confident that the population mean falls within the allowable error relative to the mean panel rating.

The 24 panel members were assigned 3 to a car. Each car had a driver who served as part of the survey administration and did not rate pavements. Therefore, eight cars were used. The automobiles were 1985 Ford Tempo four-door sedans.

Three test circuits were designed to reflect the pavement design, traffic, and environmental differences that occur in Kansas. A circuit of test sections was developed from in-service pavements in KDOT Districts I and IV to represent eastern Kansas, in KDOT Districts II and V to represent central Kansas, and in KDOT Districts III and VI to represent western Kansas. Each circuit comprised 36 0.5-mi test sections selected to represent the diversity in observed pavement condition. This selection criteria created large distances between test sections in some cases. Dummy sections were added when necessary to reorient panel members following extended travel times.

The central circuit comprised 8 to 10 sections of each of the four major pavement types used in the KDOT PMS. These are full-design bituminous pavement (FDBit), partial-design bituminous pavement (PDBit), portland cement concrete pavement (PCCP), and composite (COMP) pavement. FDBit and PCCP pavement sections were constructed based on conventional engineering thickness design. Composite pavements are PCCP pavements that have been overlaid; these are also fully designed. PDBit sections have built-up thicknesses that have evolved through repeated application of surface treatments or overlays. Although hot mix overlay or recycled resurfacing mixture and thickness design is based on current engineering practice, the complete pavement cross section has been constructed with only partial reliance on formal design procedures.

A balanced design (approximately the same number of test sections for each pavement type) was necessary for the central circuit because the three-point scale was used only on this circuit. Central Kansas has enough diversity in the four pavement types that a balanced circuit could be developed in this region, as presented in Table 1. However, PCCP and COMP sections are scarce in western Kansas. The western circuit had a majority of FDBit and PDBit sections (Table 2) and the eastern circuit was designed with emphasis on PCCP and COMP sections (Table 3).

The design was based on having a minimum of 24 test sections of each pavement type over all three circuits. From a statistical standpoint, correlations using 24 pairs of correlates are statistically significant ($\alpha = 0.05$) if the absolute value of the correlation coefficient equals or exceeds 0.40 *(10)*. However, the minimum absolute value of the correlation coefficient for engineering significance was set at 0.70 because a simple linear regression between the correlates would only account for about one-half of the total variation in the data set (i.e., $r^2 = 0.49$). This assumption is particularly important if the data are to be used as the basis of a predictive model to estimate future values of PSI given MRM roughness data.

SURVEY ADMINISTRATION

The panel members were all KDOT employees who volunteered from the districts and from the headquarters organization in Topeka. Different panels were used for all four surveys (AASHTO scale applied to the eastern, central, and western circuits and the three-point scale applied only to the central circuit). The panel instructions were adapted from those used by Nick and Janoff *(6, 7)*. A special effort was made to insure that the raters concentrated only on ride quality. They were instructed to ignore pavement appearance, cracking, patching, and so forth. As previously noted, the drivers were part of the survey administration and did not rate pavements.

The eastern and central circuits each required 2 days for evaluation. In the western circuit, 3 days were needed because of the location of the test sections. Each test section was rated

TABLE 1 CENTRAL KANSAS CIRCUIT, THREE-POINT SCALE

Test Section	PSR_3	Standard Deviation	MRM Roughness (in./mi)
FDBIT			
C–9	1.08	0.30	148
C–10	0.95	0.33	137
C–11	0.95	0.28	141
C–12	1.07	0.35	84
C–13	0.87	0.30	124
C–14	1.95	0.38	77
C–15	1.97	0.38	70
C–26	1.15	0.33	131
C–33	2.33	0.26	31
C–38	1.26	0.37	165
PDBIT			
C–20	2.05	0.37	39
C–21	1.74	0.50	42
C–24	0.80	0.32	140
C–25	0.92	0.29	128
C–27	1.49	0.47	109
C–28	2.26	0.32	60
C–34	1.52	0.36	159
C–40	2.46	0.31	35
PCCP			
C–4	1.14	0.30	144
C–5	1.32	0.40	88
C–17	1.30	0.35	111
C–18	1.32	0.43	126
C–19	1.40	0.41	110
C–23	1.11	0.40	169
C–35	1.41	0.41	109
C–36	1.33	0.37	174
C–41	1.75	0.43	59
COMP			
C–6	1.70	0.38	38
C–7	1.71	0.38	47
C–8	1.72	0.41	31
C–22	1.38	0.43	108
C–29	1.42	0.37	129
C–30	1.76	0.39	90
C–31	1.70	0.42	90
C–37	1.22	0.26	108
C–39	2.18	0.28	54

at 50 mph by all panel members within a 30-min time period on the same day. NOS survey data, including roughness of the pavement sections, were collected within 2 days of the panel rating. The MRM roughness data represent the average of three runs over the 0.5-mi test section. Although the eastern circuit originally had 36 test sections, 5 of the sections were omitted from the data analysis because they were snow covered at the time of the survey.

PANEL DATA STATISTICS

Central Circuit, Three-Point Scale

Panel rating data for the three-point scale are given in Table 1. The average standard deviation over all pavement sections is 0.36. This represents 12 percent of the maximum scale value (3.0). Figure 3 illustrates the association between PSR_3 (mean panel rating) and the standard deviation of the panel ratings for all test sections. The correlation coefficient of 0.11 was not statistically significant ($\alpha = 0.05$). The variation in the panel ratings is independent of the mean present serviceability although extreme roughness and smoothness (PSR_3 near 0.0 or 3.0) were not represented in the data set. None of the correlation coefficients were significant ($\alpha = 0.05$) when the data were stratified by pavement type.

Western Circuit, AASHTO Scale

The panel rating statistics are given in Table 2. The average standard deviation over all pavement types is 0.63, or 13 percent of the maximum scale value of 5.0. The correlation coefficient between PSR_5 (mean panel rating) and the standard

TABLE 2 WESTERN KANSAS CIRCUIT, AASHTO SCALE

Test Section	PSR_5	Standard Deviation	MRM Roughness (in./mi)
FDBIT			
W–4	2.58	0.55	84
W–13	2.22	0.78	166
W–16	2.64	0.68	130
W–17	3.32	0.62	74
W–19	2.10	0.71	97
W–20	1.81	0.63	171
W–24	3.00	0.60	68
W–25	1.95	0.61	88
W–26	2.08	0.92	180
W–29	1.96	0.65	143
W–30	3.00	0.62	135
W–41	3.27	0.64	106
W–42	2.47	0.64	44
PDBIT			
W–7	3.55	0.42	31
W–8	3.14	0.67	41
W–9	3.14	0.79	33
W–10	2.46	0.62	151
W–11	2.31	0.79	150
W–12	2.40	0.64	133
W–14	1.77	0.60	225
W–15	2.83	0.52	128
W–21	2.94	0.69	103
W–22	2.33	0.49	206
W–23	2.40	0.59	171
W–27	3.65	0.59	67
PCCP			
W–5	3.35	0.75	80
W–6	3.67	0.63	49
W–34	2.29	0.57	103
W–35	2.73	0.57	86
COMP			
W–31	1.87	0.68	165
W–33	2.95	0.57	37
W–36	3.08	0.52	61
W–37	2.75	0.60	94
W–38	2.85	0.62	89
W–39	2.92	0.51	94
W–44	3.98	0.58	38

TABLE 3 EASTERN KANSAS CIRCUIT, AASHTO SCALE

Test Section	PSR_5	Standard Deviation	MRM Roughness (in./mi)
FDBIT			
E–4	3.08	0.59	50
E–5	2.91	0.61	50
E–6	2.77	0.62	39
E–23	2.78	0.65	107
PDBIT			
E–29	2.05	0.55	172
E–31	1.42	0.59	401
E–36	2.63	0.41	170
E–37	2.37	0.51	128
PCCP			
E–10	1.95	0.78	170
E–11	1.92	0.77	183
E–13	2.79	0.63	144
E–24	2.35	0.86	125
E–27	3.66	0.60	55
E–28	3.29	0.68	92
E–32	2.28	0.82	168
E–33	2.68	0.71	88
E–34	3.58	0.56	117
E–35	3.36	0.66	129
E–38	1.48	0.70	269
E–39	2.00	0.55	181
E–40	2.33	0.48	147
E–41	2.23	0.57	189
COMP			
E–7	2.15	0.54	86
E–8	2.25	0.67	141
E–9	2.90	0.52	65
E–14	3.86	0.49	72
E–15	3.55	0.68	84
E–20	2.27	0.62	94
E–21	2.57	0.57	149
E–25	2.82	0.67	164
E–26	3.20	0.57	116

deviation is –0.28, which is not significant ($\alpha = 0.05$). Furthermore, none of the correlation coefficients for the data when stratified by pavement type were significant ($\alpha = 0.05$). The dispersion of panel data is unaffected by the serviceability of the pavement as estimated by the mean panel rating.

Eastern Circuit, AASHTO Scale

The panel rating statistics are given in Table 3. The average standard deviation over all pavement sections is 0.62, or 12 percent of the maximum scale value of 5.0. The correlation coefficient between PSR_5 (mean panel rating) and the standard deviation of the panel ratings for all test sections is –0.20, which is not statistically significant ($\alpha = 0.05$). None of the correlation coefficients were significant ($\alpha = 0.05$) when the data were stratified by pavement type.

Central Circuit, AASHTO Scale

The panel rating statistics are given in Table 4. The average standard deviation over all pavement sections is 0.50, or 10 percent of the maximum scale value of 5.0. The correlation coefficient between PSR_5 (mean panel rating) and the standard deviation of the panel rating shown in Figure 4 for all test sections is –0.47, which was statistically significant ($\alpha = 0.01$). This correlation suggests that the dispersion of individual ratings decreases as pavement smoothness increases. The correlation may have been the result of a data set representing a relatively smooth group of pavements. Only test section C–13 had a PSR_5 less than 2.0. When the data are subdivided by pavement type, the 10 FDBit pavement sections had a correlation coefficient of –0.75, which was significant ($\alpha = 0.05$). None of the correlations between PSR_5 and standard deviation were significant ($\alpha = 0.05$) for the other three pavement types.

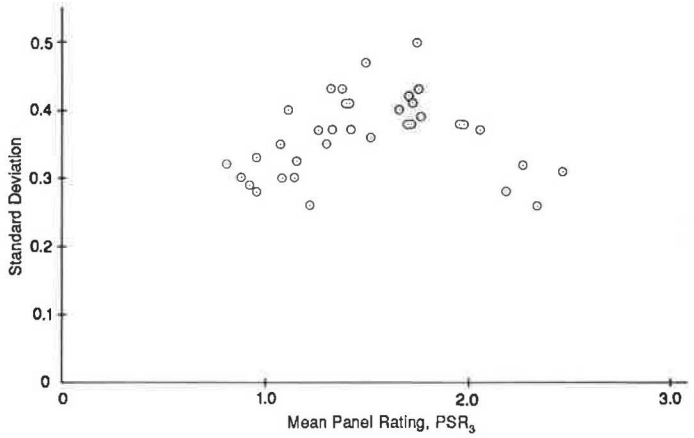

FIGURE 3 Standard deviation and PSR_3 correlation, Central Circuit.

TABLE 4 CENTRAL KANSAS CIRCUIT, AASHTO SCALE

Test Section	PSR_5	Standard Deviation	MRM Roughness (in./mi)
FDBIT			
C–9	2.24	0.61	148
C–10	2.21	0.70	137
C–11	2.26	0.58	141
C–12	2.34	0.71	84
C–13	1.99	0.60	124
C–14	3.37	0.48	77
C–15	3.22	0.48	70
C–26	2.58	0.52	131
C–33	3.95	0.49	31
C–38	2.53	0.60	165
PDBIT			
C–20	3.52	0.40	39
C–21	3.14	0.48	42
C–24	2.05	0.52	140
C–25	2.22	0.57	128
C–27	3.03	0.47	109
C–28	3.90	0.42	60
C–34	3.04	0.65	159
C–40	4.27	0.40	35
PCCP			
C–4	2.65	0.52	144
C–5	2.68	0.41	88
C–17	2.76	0.52	111
C–18	2.76	0.52	126
C–19	2.73	0.51	110
C–23	2.31	0.48	169
C–35	2.66	0.37	109
C–36	2.72	0.38	174
C–41	3.36	0.38	59
COMP			
C–7	2.99	0.47	47
C–8	2.92	0.42	31
C–9	2.98	0.46	38
C–22	2.50	0.47	108
C–29	2.71	0.51	129
C–30	2.86	0.48	90
C–31	3.05	0.55	90
C–37	2.41	0.43	108
C–39	3.54	0.51	54

Discussion

The dispersion of individual ratings can be reasonably assumed to be independent of the mean panel rating. Although the central circuit had a statistically significant negative correlation, this finding was not persuasive. A simple linear regression accounts for only 22 percent of the total variation in the data set.

A reasonable estimate of the standard deviation for a 24-member panel is about 12 percent of the maximum scale value using both the three-point and AASHTO scales. This characteristic appears to extend to larger panel sizes. As previously stated, data developed by Nick and Janoff *(6)* using 36-member and larger panels had average standard deviations of 0.60 using the AASHTO scale. This value of standard deviation also corresponds to 12 percent of the maximum scale value. As panel sizes become smaller, the standard deviation may increase as indicated in early research reported by Nakamura and Michael *(11)*. For example, a table of recommended panel sizes that used a standard deviation of 0.84 was based on 10-member panels. However, this finding may be useful in planning future panel rating studies that focus on pavement ride quality.

Using theory of estimation, the three-point scale has a maximum allowable error of 0.15 at the 95 percent confidence level. This error for 24-member panel sizes is certainly satisfactory for PSR determinations.

PSI-MRM ROUGHNESS CORRELATIONS

The following list of equations provides the various linear and transformed models developed from central circuit data that estimate present serviceability index PSI_3 given MRM roughness values (in inches per mile).

FDBIT

$$PSI_3 = 2.47 - 0.0100MRM \quad (r = -0.82)$$

$$\log PSI_3 = 1.24 - 0.56 \log MRM \quad (r = -0.82)$$

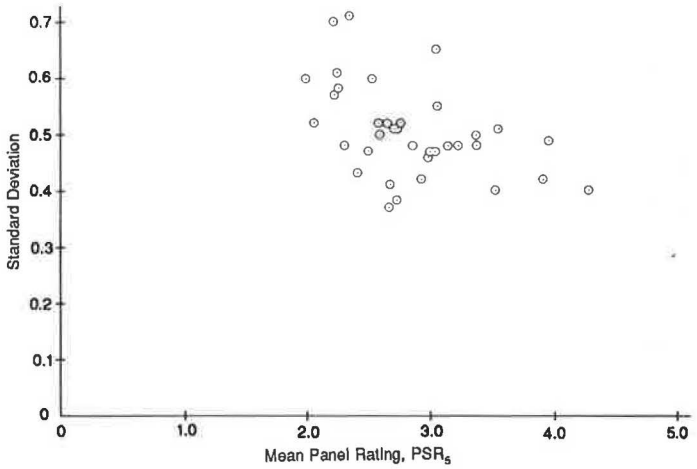

FIGURE 4 Standard deviation and PSR_5 correlation, Central Circuit.

$[PSI_3 = 17.38\ (MRM^{-0.56})]$

$\ln PSI_3 = 0.96 - 0.00647MRM \quad (r = -0.78)$

$[PSI_3 = 2.61e^{-0.00647MRM}]$

PDBIT

$PSI_3 = 2.50 - 0.00949MRM \quad (r = -0.80)$

$\log PSI_3 = 1.14 - 0.51 \log MRM \quad (r = -0.78)$

$[PSI_3 = 13.80\ (MRM^{-0.51})]$

$\ln PSI_3 = 0.99 - 0.00623MRM \quad (r = -0.77)$

$[PSI_3 = 2.69e^{-0.00623MRM}]$

PCCP

$PSI_3 = 1.81 - 0.00384MRM \quad (r = -0.77)$

$\log PSI_3 = 0.79 - 0.32 \log MRM \quad (r = -0.82)$

$[PSI_3 = 6.17\ (MRM^{-0.32})]$

$\ln PSI_3 = 0.62 - 0.00274MRM \quad (r = -0.77)$

$[PSI_3 = 1.86e^{-0.00274MRM}]$

COMP

$\ln PSI_3 = 0.73 - 0.00319MRM \quad (r = -0.67)$

$[PSI_3 = 2.08e^{-0.00319MRM}]$

The following list of equations provides the models that estimate PSI_5 given MRM roughness values.

FDBIT

$PSI_5 = 3.49 - 0.00799MRM \quad (r = -0.68)$

$\log PSI_5 = 0.933 - 0.26 \log MRM \quad (r = -0.66)$

$[PSI_5 = 8.57\ (MRM^{-0.26})]$

$\ln PSI_5 = 1.28 - 0.00302MRM \quad (r = -0.68)$

$[PSI_5 = 3.60e^{-0.00302MRM}]$

PDBIT

$PSI_5 = 3.65 - 0.00697MRM \quad (r = -0.83)$

$\log PSI_5 = 1.08 - 0.031 \log MRM \quad (r = -0.85)$

$[PSI_5 = 12.02\ (MRM^{-0.31})]$

$\ln PSI_5 = 1.34 - 0.00276MRM \quad (r = -0.87)$

$[PSI_5 = 3.82e^{-0.00276MRM}]$

PCCP

$PSI_5 = 3.87 - 0.00925MRM \quad (r = -0.81)$

$\log PSI_5 = 1.32 - 0.44 \log MRM \quad (r = -0.81)$

$[PSI_5 = 20.89\ (MRM^{-0.44})]$

$\ln PSI_5 = 1.44 - 0.00370MRM \quad (r = -0.84)$

$[PSI_5 = 4.22e^{-0.00370MRM}]$

COMP

$PSI_5 = 3.53 - 0.00732MRM \quad (r = -0.57)$

$\log PSI_5 = 0.83 - 0.20 \log MRM \quad (r = -0.55)$

$[PSI_5 = 6.76\ (MRM^{-0.20})]$

$\ln PSI_5 = 1.28 - 0.00264MRM \quad (r = -0.58)$

$[PSI_5 = 3.60e^{-0.00264MRM}]$

These regressions are based on data collected from all three circuits and aggregated for the analysis. The correlation coefficients are significant ($\alpha = 0.05$).

In general, the linear and exponential linear models underestimate serviceability for smooth pavements. A perfectly smooth pavement (MRM = 0 in./mi) should yield a PSI that approaches 3.0 or 5.0, depending on the present serviceability scale. None of the linear or exponential models have this characteristic. The log-log linear model has a limit of infinity for MRM values approaching 0, which is obviously inconsistent with maximum serviceability of 3.0 or 5.0.

PSR_3-PSR_5 CORRELATIONS

The central circuit used two different rating panels to evaluate the test sections. The first panel used the three-point scale and the second used the AASHTO scale. Figure 5 illustrates the correction which has a statistically significant ($\alpha < 0.01$) correlation coefficient of 0.97. The simple linear regression to estimate PSR_3 is as follows:

$$PSR_3 = -0.72 + 0.78PSR_5$$

AASHTO present serviceability values of 2.0 and 2.5 have been used as terminal serviceability indices for pavement design applications. If these values are used in the regression, PSR_3 estimates of 0.84 and 1.23 are obtained. These values are slightly less than and greater than 1.00, which represents the lower bound of NOS Level 3 roughness and indicates that pavement preservation actions are needed. This indication suggests that the three-point scale produced reasonable serviceability results that correspond conceptually with the AASHTO scale.

CONCLUSIONS

1. For panel sizes of 24, the average standard deviation of individual panel ratings over all pavement types is approximately 12 percent of the maximum scale value. This corre-

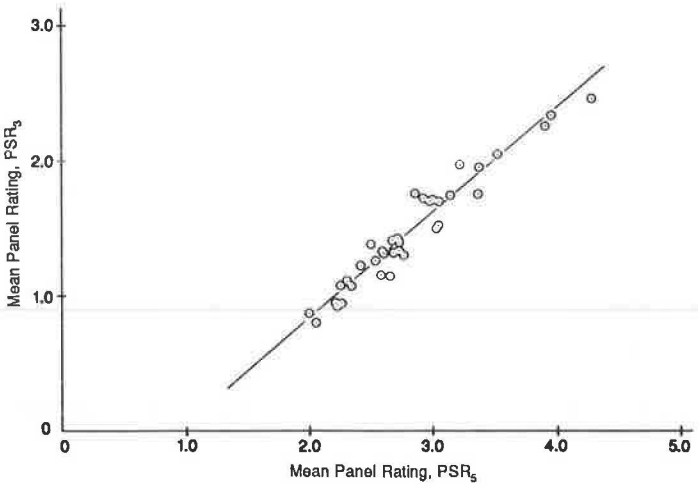

FIGURE 5 PSR_3-PSR_5 correlation.

sponds to 0.60 for the five-point AASHTO scale and 0.36 for the three-point scale developed in this research effort.

2. The standard deviation of individual panel ratings appears to be independent of the mean panel rating for a given pavement section. The dispersion of individual panel ratings for a test section is not linearly associated with the mean panel rating.

3. Statistically significant linear, log-log linear, and exponential linear models are not completely satisfactory for the prediction of PSI given MRM roughness values. None of these functions are conceptually correct when the pavements are smooth (low MRM roughness values).

4. A statistically significant correlation was established between the AASHTO five-point scale and the KDOT three-point scale. The KDOT scale for Level 3 roughness ($PSR_3 \leq 1.0$) corresponds well with the AASHTO estimates of terminal serviceability.

5. Survey administration guidelines as reported by Nick and Janoff *(6, 7)* and Zaniewski and Hudson *(8)* were successfully implemented. The recommendations relating to panel design, driver instructions, panel instructions, and test circuit construction were in part responsible for a successful serviceability study.

ACKNOWLEDGMENTS

J. Freund, A. Gisi, S. Woolington, and D. Gamble of the KDOT Roughness Technical Group had major responsibilities for project planning and field coordination of the panel rating activities. Members of the KDOT Geotechnical Group served as drivers and collected the NOS roughness and pavement condition survey data for the test sections. Eighty-five KDOT employees served as members of the rating panels. Without the enthusiastic cooperation of these individuals, this study would not have been possible.

REFERENCES

1. R. Kulkarni, F. Finn, E. Alviti, J. Chuang, and J. Rubinstein. *Development of a Pavement Management System.* Final Report-Phase II. Kansas Department of Transportation, Topeka, Sept. 1983.
2. W. N. Carey and P. E. Irick. The Pavement Serviceability-Performance Concept. *Bulletin 250*, HRB, National Research Council, Washington, D.C., 1960.
3. The AASHO Road Test: Report 5—Pavement Research. In *Special Report 61-E*, HRB, National Research Council, Washington, D.C., 1962.
4. B. G. Hutchinson. Principles of Subjective Rating Scale Construction. In *Highway Research Record 46*, HRB, National Research Council, Washington, D.C., 1964, pp. 60–70.
5. R. J. Weaver. Quantifying Pavement Serviceability as It Is Judged by Highway Users. In *Transportation Research Record 715*, TRB, National Research Council, Washington, D.C., 1979, pp. 37–44.
6. J. B. Nick and M. S. Janoff. Evaluation of Panel Rating Methods for Assessing Pavement Ride Quality. In *Transportation Research Record 946*, TRB, National Research Council, Washington, D.C., 1983, pp. 5–12.
7. M. S. Janoff, J. B. Nick, P. S. Davit, and G. F. Hayhoe. *NCHRP Report 275: Pavement Roughness and Rideability.* TRB, National Research Council, Washington, D.C., 1985.
8. J. P. Janiewski, S. W. Hudson, and W. R. Hudson. Pavement Condition Rating Guide. FHWA, U.S. Department of Transportation, 1985.
9. R. J. Weaver and R. O. Clark. *Psychophysical Scaling of Pavement Serviceability.* Manual SEM–9. Soil Mechanics Bureau, New York State Department of Transportation, Albany, May 1977.
10. G. W. Snedecor and W. G. Cochran. *Statistical Methods.* 6th ed., Iowa State University Press, Ames, 1967.
11. V. F. Nakamura and H. L. Michael. Serviceability Ratings of Highway Pavements. In *Highway Research Record 40*, HRB, National Research Council, Washington, D.C., 1963, pp. 21–36.

The opinions, findings, and conclusions expressed in this paper are those of the authors and do not necessarily reflect the policy or views of the Kansas Department of Transportation.

Publication of this paper sponsored by Committee on Monitoring, Evaluation and Data Storage.

Video Image Distress Analysis Technique for Idaho Transportation Department Pavement Management System

JIM BAKER, BASIL DAHLSTROM, KEITH LONGENECKER, AND TRI BUU

The Idaho Transportation Department (ITD) is developing and implementing an automated highway management system, the Pavement Performance Management Information System (PPMIS). The system consists of structural adequacy data, present serviceability data, and surface distress data. Field data for the first two modules are obtained using automated collection techniques. However, surface distress data are still gathered manually and are incorporated into a visual and subjective methodology. The ITD is pursuing a low-cost, technically sound methodology to automate the collection and analysis of surface distress data. The primary objective is to investigate the feasibility of automating the acquisition and subsequent analysis of pavement condition data. Two basic questions are being examined: First, can high-quality video images of road surfaces be filmed at average highway speeds? Second, can computer software be developed to use those images to calculate crack size and crack type, and to assign a severity rating to specific sections of road surface? VideoComp, an Idaho corporation, is assisting the ITD in efforts to answer these and related questions. Preliminary findings indicate that automation of the distress data module is feasible. During 1985 and 1986, VideoComp videotaped more than 2,400 lane-mi of Idaho's Interstate highways and 380 lane-mi of principal arterial highways. In addition, computer software capable of determining crack type and size has been successfully demonstrated.

Transportation departments throughout the United States are faced with a growing problem: the adequate maintenance of the nation's highways in the face of severely restricted maintenance budgets and shrinking maintenance staffs. Simply put, the nation's transportation departments are being asked to do more with less.

The response of the Idaho Transportation Department (ITD) to this challenge is the aggressive development and implementation of an automated pavement management system. The Pavement Performance Management Information System (PPMIS) is an automated highway maintenance model used for annual analysis and programming of projects and budget requirements for the maintenance and rehabilitation of the Idaho highway system.

The PPMIS consists of three major data elements: structural adequacy data, present serviceability data, and surface distress data *(1)*. To satisfy the data requirements of these three elements, the ITD is continuing efforts to implement a fully automated field data collection system. Data collection and analysis for two of the elements (structural adequacy and present serviceability) are fully automated. However, surface distress data collection and analysis remain manually based techniques relying on visual and subjective ranking methodology.

In this paper, efforts underway by VideoComp and the ITD to automate the surface distress data element of the PPMIS are examined. Specifically, the use of video image equipment to collect field data and computer-assisted analysis of those data are discussed.

The major feature of the video image system is that field data are collected, processed, analyzed, and passed on to the PPMIS in a totally automated fashion. The video image process reduces human intervention in the data collection required for surface distress analysis, reduces measurement error associated with labor intensive data collection techniques, and leads to significant cost savings.

BACKGROUND INFORMATION

The Idaho state highway system consists of approximately 5,000 mi of paved or oiled highways including about 612 mi of Interstate highways. During the past several years, the Transportation Management Services Section of the ITD has been developing and implementing new management information systems designed to enhance the ability of managers to make timely, well-informed decisions regarding the construction and maintenance of Idaho's roads and highways.

These efforts have led to the development of a number of interrelated information management subsystems. Together, these subsystems form the ITD program analysis system including computer programs and models such as PPMIS, HWYNEEDS, and HIAP, which can be used to provide the ITD with a very flexible and powerful set of program planning and budgeting analysis tools. For example, PPMIS is used to develop resurfacing, restoration, and rehabilitation (3R) improvement proposals; HWYNEEDS is used to develop capital improvement proposals; and HIAP is used to analyze funding allocations. Funding allocation options are analyzed by types of improvement within both the 3R and capital program improvement categories, federal-aid systems, and state districts.

Pavement Management System

The focus of this paper is the Pavement Management System (PMS) currently in use by the ITD. PMS ranks highway sec-

J. Baker and B. Dahlstrom, VideoComp, Boise, Idaho 83709. K. Longenecker and T. Buu, Idaho Transportation Department, Boise, Idaho 83707.

tions based on the severity of pavement deflections, roughness, cracking, and friction deficiencies. A composite index of deflection, roughness, and cracking for each highway section is also produced as a measure of overall performance.

At the heart of the PMS is the PPMIS, a computerized pavement evaluation information system *(2)*, developed to aid the ITD maintenance and district personnel in making the most appropriate rehabilitation decisions and in estimating the volume of work and cost of improvement on pavement condition problems.

The PPMIS model consists of three main computer programs: SYSTDY, SUMMARY, and POD *(2)*. SYSTDY and SUMMARY are used for network level analysis, whereas POD is used for analysis at the project level. SYSTDY and SUMMARY programs are designed to use any combination of structural adequacy, present serviceability, and distress data, whereas the POD program is limited to structural adequacy data.

Analysis at the network level begins with the program SYSTDY, which edits and processes the deflection, present serviceability, distress, and friction database information of the pavement network. SYSTDY transforms these inventory data into indices such as structural index (SI), present serviceability index (PSI), and cracking index (CI) and produces a report for each pavement section in the network. Summarized data are then passed to the SUMMARY program. This program combines the SI, PSI, and CI into a composite index (final index, FI), which represents the overall pavement condition of each section. Currently, data are collected for approximately 1,700 distinct sections of Idaho roadways. Pavement sections are logical units based on a number of selection criteria as identified by ITD. Criteria include jurisdictional boundaries (i.e., city and county), changes in pavement type (from concrete to asphalt), functional classification (e.g., principal arterials and secondary roads), time period of construction, terrain, and a number of other geometric characteristics. Pavement sections, as defined by the ITD are variable in length ranging from a minimum length of 0.3 mi to a maximum length of 9.3 mi.

Pavement sections form the basic units of analysis for ITD pavement management decisions. In comparing and assessing identified pavement sections, weighting factors are introduced on the various indices with functional classification, traffic volumes, and speeds being the influencing factors. In-depth descriptions of PSI, SI, CI, FI, and criteria used to establish pavement sections are available from the Management Services Section of the ITD *(3)*.

SUMMARY produces a ranked list of sections that can be used for programming improvement priorities. The POD program at project level is used to estimate overlay requirements for sections of highway that have a structural adequacy problem. The overall PPMIS model output is used in the yearly analysis and programming of projects and budget requirements for maintenance and rehabilitation of the Idaho state highway system.

Data Collection for the PPMIS Model

The PPMIS model requires a significant level of data acquisition. Pavement condition surveys include pavement deflection (Dynaflect measurements), pavement roughness (Cox roadmeter), pavement cracking (subjective evaluation using reference photographs), and pavement friction (locked-wheel tests). Supplementary data such as temperature, date, and route number are added through a Hewlett-Packard 85 microcomputer in the field.

Although the amount of data required to support PPMIS is quite large, the ITD has a small staff available to collect those data. Accordingly, the ITD has acquired several automated data collection and processing systems to provide computerized data management capabilities. All of the data necessary to support PPMIS with the exception of cracking (distress) data are collected and processed using automated techniques. At present, the PPMIS cracking index is a modification of a cracking rating scheme developed by the Arizona DOT. The rating crew has a series of pictures that are compared to the pavement. Different ratings correspond to different types (transverse, longitudinal, and alligator) and different degrees of cracking. The rater records the index from the pictures that most resemble the pavement in question; the averaging of ratings is allowed when appropriate.

ITD personnel perceive this manual and subjective data collection process as a weakness in the overall data collection methodology of PPMIS. Problems associated with the current system of data collection include a high cost of acquiring data, difficulty in replicating the collection efforts over time, and in general accumulation of data that are not as accurate or reliable as deemed necessary. The ITD, through a series of contracts with VideoComp, an Idaho consulting firm, is attempting to resolve this problem. VideoComp has developed a data collection and analysis system that helps ensure more cost-effective, timely, and accurate data for input into the PPMIS model.

The remainder of this paper describes the data collection system developed by VideoComp, examines how those data are analyzed, and discusses future research efforts to be undertaken by the Idaho Transportation Department and VideoComp.

SURFACE DISTRESS DATA ACQUISITION: AN AUTOMATED APPROACH

As discussed earlier, the ITD is vigorously pursuing the development of a low-cost, technically sound methodology for the automated collection and analysis of surface distress data. Four basic objectives have guided development of the ITD research agenda:

Objective 1. To determine if video image processing techniques can be used to provide severity measures (distress index) on the extent of the distress-cracking problem of any given pavement section.

Objective 2. To determine the capability of an automated system to classify, measure, and record the area and extent of a crack problem for any given pavement section.

Objective 3. To ensure that automated data collection techniques satisfy data reliability requirements, and that they can be replicated over time.

Objective 4. To determine the cost-effectiveness of automated data collection compared to more traditional manual surveys.

In the fall of 1985, VideoComp began work designed to meet the first two objectives. Those efforts, as well as subsequent work performed in 1986, are examined in more detail in the following paragraphs.

Data Acquisition

During the spring and summer of 1985, VideoComp designed and constructed a prototype vehicle for use in videotaping the travel lane of Idaho's Interstate highways. Since that time, the prototype vehicle has been used to videotape more than 2,400 lane-mi of Interstate highway for the travel lane as well as 380 lane-mi of principal arterial highways. In addition, project level taping has been performed on selected sections of Interstate highway.

The prototype, a trailer towed by a truck, features a video camera, video recorder, and controlled lighting. The initial videotaping project focused on four major activities:

1. Capture pavement surface images while traveling at highway speeds.
2. Film the outside wheelpaths of the outside (travel) lane with images of pavement surface covering at least 5 ft (width) of the outside lane starting from the lane-shoulder joints.
3. Edit the videotapes to provide a continuous record of the Interstate surface as it existed in October 1985 (with images recorded on videotapes that can be shown frame-by-frame on a television screen).
4. Preparation of a final report that discussed project methodology and findings.

Videotaping was completed in October 1985; a report documenting the project was presented to ITD in November 1985 *(4)*.

After reviewing results of the initial videotaping, ITD personnel determined that a width of 8 ft was more desirable than that of 5 ft as originally selected, and that location and distance information such as mile post location and direction of travel should be encoded on each videotape during subsequent videotaping projects.

In response to these requests, VideoComp modified the prototype vehicle. The modified vehicle (Figure 1) features two cameras and two recorders, and supports the videotaping of a field 8 ft wide. In addition, the vehicle supports a sophisticated distance-measuring scheme (in thousandths of a mile), and allows for character insertion through a keyboard directly on to each videotape that provides the viewer with critical information such as name of road, direction of travel, MACS code, and other required or desirable information (Figure 2).

Data acquisition using the original and modified prototype vehicles enabled ITD and VideoComp to acquire 2 years of visual analog benchmark data for Idaho's Interstate highways. ITD plans to use the data in a number of ways including studies of change of pavement condition over time. More importantly, the project served as a field demonstration of the concept of acquiring high-quality visual pavement surface condition data at highway speeds. Important findings from the project included

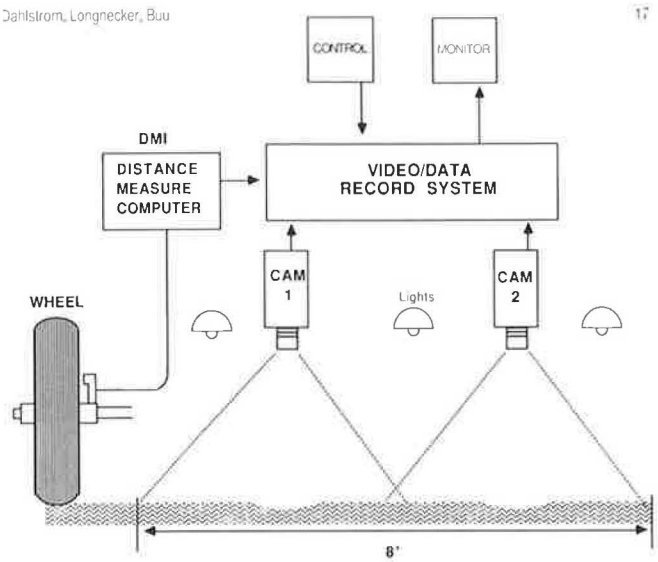

FIGURE 1 System overview.

1. Acquiring pavement condition data at highway speeds even in heavy traffic is relatively simple.
2. Visual data acquired are of a quality that allows surface images including cracking to be well defined and stable. Image quality tends to be better if videotaping occurs during the night. The angle of the sun in early morning and late afternoon results in some minor lighting problems.
3. Most of the prototype equipment used in the project is readily available for over-the-counter purchase. The mobile equipment used to gather data proved to be sturdy, dependable, and tolerant of a wide range of environmental conditions such as varying temperatures and dust.
4. Time and costs involved in gathering data appear to be quite reasonable.
5. It is apparent that the technology exists that will allow for the cost-effective, objective, and consistent collection of highway pavement condition data.
6. Collected data is of sufficient quality to be used as input data converted to digital data for computer software being developed to analyze the type, extent, and severity of cracking.

In all, 53 videotapes produced in Beta II format have been taped since 1985. Those tapes are currently archived at the Management Services Section of the ITD.

Data Analysis

After successfully demonstrating the ability to videotape road surfaces at highway speeds, VideoComp began the process of developing computer software necessary to analyze those videotapes. The software was designed to (a) accept videotaped frame-by-frame images as input; (b) digitize and store frames that exhibit evidence of cracking; (c) determine the type of crack (i.e., longitudinal, transverse, or alligator); (d) calculate the size of existing cracks; (e) classify the extent and severity of cracking; (f) incorporate findings from individual frames into an algorithm designed to classify the extent of cracking from the crack index for any given pavement section; and (g)

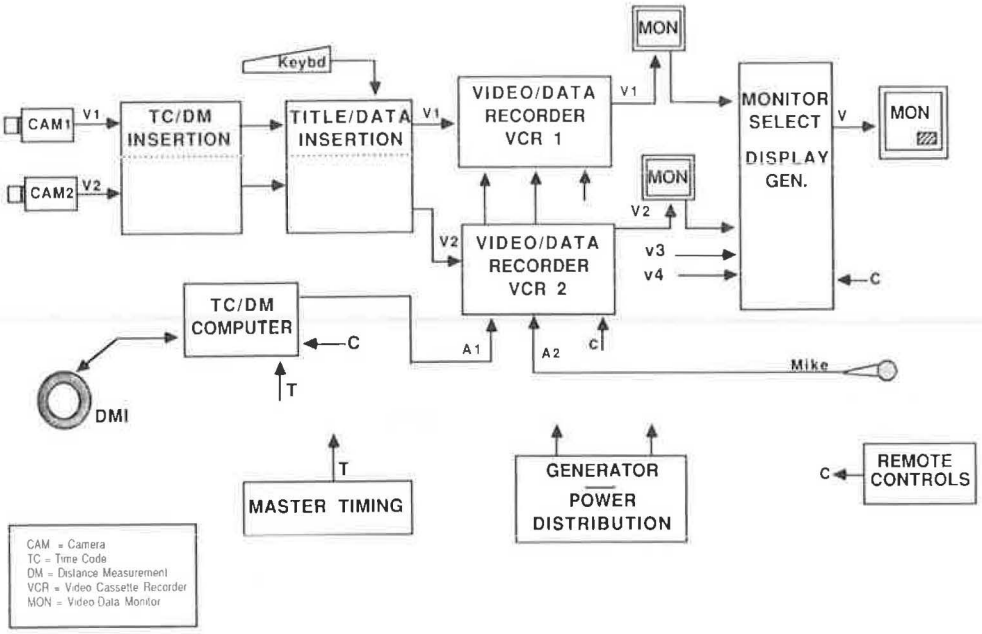

FIGURE 2 Highway data capture system.

pass the assigned crack or distress index on for use as input into PPMIS.

Figures 3 and 4 are reproductions of printouts taken from a randomly selected section of videotaped Idaho Interstate highway. Figure 3 is the digitized image of one frame of the selected videotape. The frame for concrete surface exhibits both transverse and longitudinal cracking. Figure 4 is the product of computer software that extracts the crack features, determines crack type, calculates the length of the cracks, and calculates total area for each of the cracks.

Ongoing Research and Development

Two of the four objectives of the ITD-VideoComp research agenda, automated data collection and computerized data analysis, formed the bulk of the research and development efforts of VideoComp to date. Over the next several months, efforts were to be directed toward the improvement of existing data collection and analysis processes. Work was also to begin on Objectives 3 and 4. To satisfy Objective 3, VideoComp was to assess the reliability of data and findings when an automated approach is used. Specifically, sections of Idaho Interstate highway designated as "long-term pavement monitoring sections" (LTMs) were to used for calibration studies. VideoComp has videotaped both lanes in one direction of four LTMs located in southern Idaho for project level analysis. Computer software developed by VideoComp was being used to establish a crack index for each LTM. Results were to be compared with existing pavement condition records for calibration purposes. The final objective of the ITD-VideoComp effort was to determine if automated collection and analysis is more cost-effective than current practices.

Included in the calibration efforts was to be a thorough examination of sampling techniques and strategies to be followed. A fundamental issue is the sample size necessary to develop a crack index at the network level. Each mile of

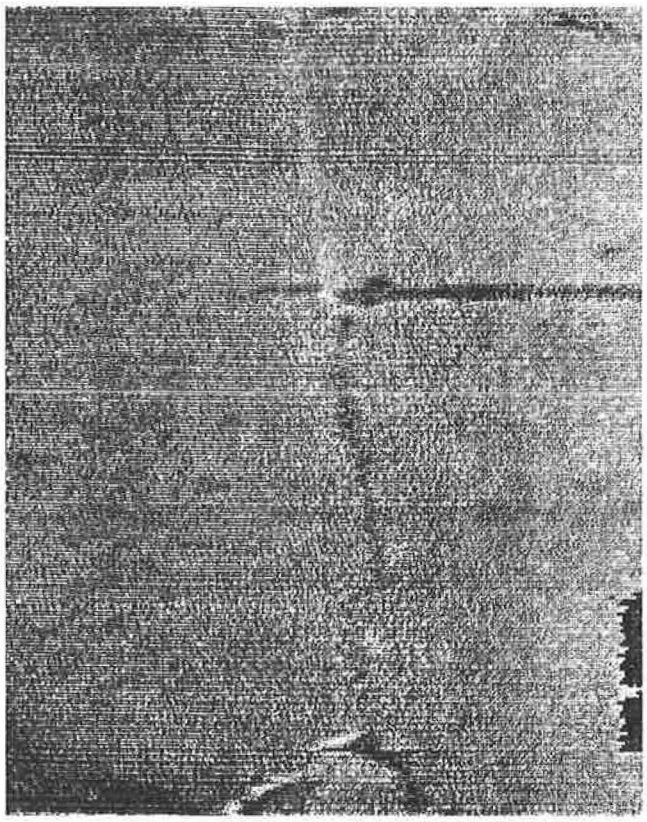

FIGURE 3 Digitized image—Idaho Interstate highway.

videotaped road surface is uniquely identified and each frame on the videotape has a reference distance measure. This measurement of distance is crucial for subsequent sample selection, especially for repeated sampling techniques; data analysis such as conversion of milcage data to pavement section data; and for replication studies over time. In playback mode, a cut-in win-

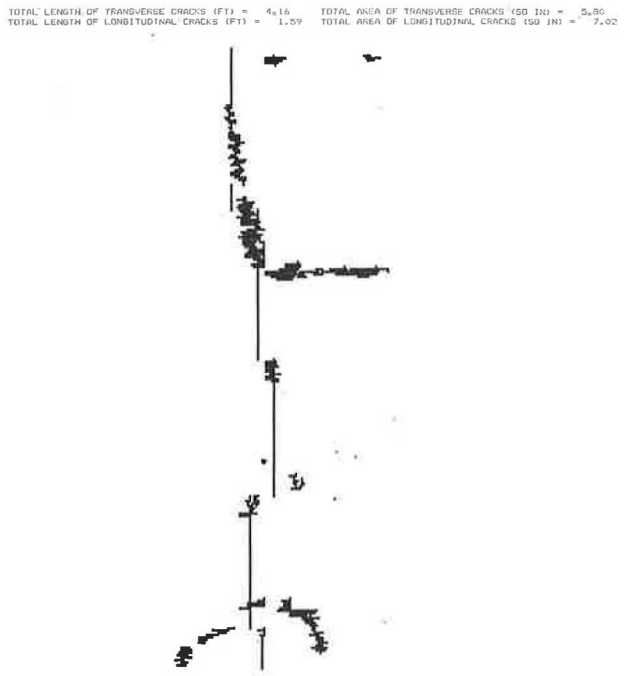

FIGURE 4 Computer-generated image of pavement surface cracking.

dow serving as a distance indicator appears on the screen. ITD data analysts have the option of using the window or simply turning it off. The window should prove useful during visual examination of various road surfaces.

Developing a sampling strategy is a crucial element of the ITD-VideoComp research agenda. VideoComp was to continue to develop and assess sampling strategies to be employed for network analysis. For example, the adequacy of a sample 100 ft long by 8 ft wide for classifying 1 mi of road surface in a statistically meaningful way was to be assessed. Numerous sample sizes and sampling techniques were to be examined during this phase of the research project. Using VideoComp computer software, a number of samples were to be selected from the LTM videotapes. Sample data were then to be compared with population data, and confidence intervals and levels calculated for various sample sizes. The product of this phase of the research was to be a detailed set of recommendations for the ITD to follow when using sampling procedures to assess the conditions at network level of Idaho's highways.

A second and related aspect of work to be undertaken in completing Objective 3 was to be the use of VideoComp computer software in conjunction with computer-assisted drafting (CAD) software to produce computer-generated maps of selected road surfaces. Those maps were to include features such as mileage markers and were also to include the location, type, and size of cracks on any given road surface. In addition to the detailed maps, a crack index was to be calculated for the entire road surface. VideoComp analysts were to work with ITD analysts to assess the reliability and usefulness of the output generated during this research phase.

Work on cost-effectiveness, the final objective of the ITD-VideoComp research agenda, was to focus on the costs associated with collecting and analyzing data using automated techniques versus the costs incurred in using manual collection and analysis techniques. Also addressed in this assessment was to be the reliability of data collected by automated processes versus manual collection techniques.

SUMMARY

The ITD is developing and implementing an automated highway management model, the PPMIS. A key input into the model is surface distress data. At present, those data are gathered manually and incorporated into a visual and subjective methodology. Department personnel consider the current collection and analysis techniques inadequate.

As a result, the ITD, in cooperation with VideoComp, is pursuing development of a low-cost, technically sound methodology to automate the collection and analysis of surface distress data. The research agenda jointly formulated by ITD and VideoComp is designed to answer two basic questions. First, can high-quality video images of road surfaces be collected at average highway speeds? Second, can computer software be developed to use those images to determine crack characteristics such as type and size and assign a reliable severity rating to specific sections of road surface?

In preliminary research efforts, the answer to both questions is yes. The next level of work is to refine existing data collection and analysis techniques, conduct numerous reliability calibration studies on various road surfaces in varying environmental conditions, and develop a sampling strategy for network level analysis. Finally, efforts will be focused on a thorough assessment of the costs and benefits associated with the automated collection and analysis of pavement surface condition data.

ACKNOWLEDGMENT

The information presented in this paper is the product of a cooperative effort between the ITD and VideoComp. A number of people have been involved in these research efforts and deserve recognition and our appreciation. Chief among the persons contributing to our efforts is R. Manubay, ITD, and D. Graybeal, Audio and Video Systems Engineer, Boise State University.

Finally, the authors would like to express appreciation to the Director of the ITD and to the Idaho Transportation Board, whose enthusiastic support and commitment made this pavement condition research project possible.

REFERENCES

1. R. B. Manubay. *Description of Models, Databases, and Operation Function, Advance Planning and Statistics Information Handout.* Idaho Transportation Department, Boise, 1981.
2. R. B. Manubay, C. Kerr, and J. Obenchain. Computerized Pavement Performance Evaluation Database Development for Structural Adequacy, Present Serviceability, and Distress Analysis. In *Transportation Research Record 1048*, TRB, National Research Council, Washington, D.C., 1985, pp. 37–42.
3. R. B. Manubay. *Program Analysis System.* Idaho Transportation Department, Boise, 1986.
4. J. Baker and B. Dahlstrom. *Inventory of the Idaho Interstate Highway Pavement Surface Fall 1985.* VideoComp, Boise, Idaho, Nov. 1985.

Publication of this paper sponsored by Committee on Monitoring, Evaluation and Data Storage.

Acceptability of Shock Absorbers for Road Roughness Measuring Trailers

BOHDAN T. KULAKOWSKI, DANIEL J. CHAPMAN, AND JAMES C. WAMBOLD

The accuracy of the response-type road roughness meters depends primarily on how the dynamic characteristics of the test vehicles adhere to prescribed standards. The standards for shock absorbers used in roughness-measuring vehicles as defined by ASTM are discussed in this paper. A new acceptability criterion is proposed that assures a higher overall accuracy of the measuring system and at the same time allows for larger deviations of the shock absorber parameters from the standard values. The method allows for verifying the acceptability of shock absorbers mounted in road roughness measuring vehicles. The effects of typical nonlinearities in shock absorber characteristics are also presented.

Road roughness is evaluated in most states on the basis of the dynamic response of a vehicle of specified parameters subjected to the road profile. For the accuracy of the measurements it is essential that the dynamic characteristics of the test vehicle adhere strictly to prescribed standards. ASTM is developing such standards for cars and trailers used in measuring road roughness. A car is represented by a quarter-car or a half-car simulation model, which is specified in a proposed ASTM standard *(1)*. A trailer is represented by a half-trailer simulation model of the same structure as the quarter-car model but of different parameters *(2)*, which are also given in the proposed standard *(1)*. The standard models are useful in calibrating actual test vehicles.

The characteristics of the actual vehicles used in measuring road roughness never exactly match the characteristics of the standard model. The deviations between the actual and standard model parameters cause measurement errors. In this paper the effects of two parameters of roughness-measuring trailers—shock absorber damping coefficient and hysteresis in axle-body displacement transducer—are investigated. A relatively simple procedure is presented that allows for verification of the acceptability of trailer shock absorbers. Although the acceptability criterion formulated by ASTM *(2)* is discussed, a modified criterion is recommended.

HALF-TRAILER MODEL

The main characteristics of the trailers used in simulating vehicle response to road roughness are specified in the new ASTM standard *(2)*. The trailers are two-wheeled, single-axle vehicles that are towed on highways at typical traffic speeds while the relative movement between the axle and body is transduced and recorded as an indication of road roughness.

The structure of the trailer simulation half-trailer model is shown in Figure 1, and its frequency response is plotted in Figure 2. The values of the parameters used in the two standard vehicle models are given in Table 1.

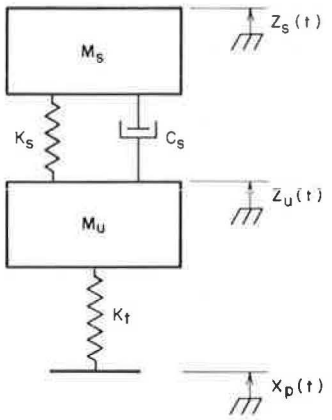

FIGURE 1 Half-trailer model.

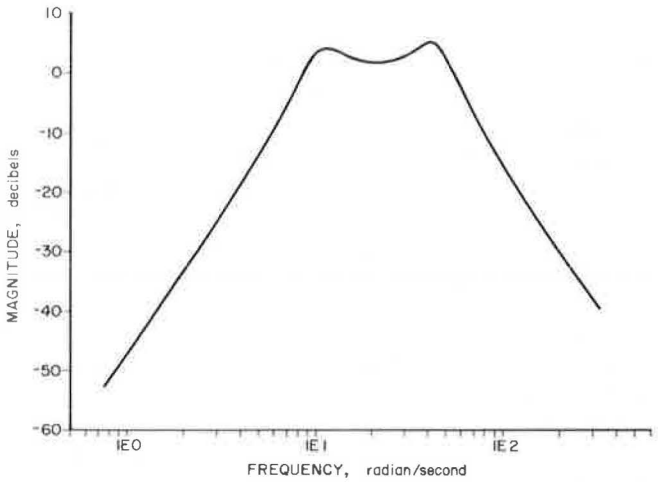

FIGURE 2 Magnitude versus-frequency-response of a half-trailer model.

Department of Mechanical Engineering and Pennsylvania Transportation Institute, Pennsylvania State University, University Park, Pa. 16802.

TABLE 1 PARAMETER VALUES FOR THE STANDARD QUARTER-CAR AND HALF-TRAILER MODELS

Model	k_s/M_s (sec^{-2})	k_T/M_s (sec^{-2})	M_u/M_s	C_s/M_s (sec^{-1})
Quarter-car	62.3	653	0.15	6.0
Half-trailer	125.0	622	0.26	8.0

The motion of the half-trailer model is governed by the following differential equations:

$$\ddot{z}_s = -\frac{C_s}{M_s}\dot{z}_s - \frac{k_s}{M_s}z_s + \frac{C_s}{M_s}\dot{z}_u + \frac{k_s}{M_s}z_u \tag{1}$$

$$\ddot{z}_u = -\frac{C_s}{M_u}\dot{z}_u - \frac{k_t + k_s}{M_u}z_u + \frac{C_s}{M_u}\dot{z}_s + \frac{k_s}{M_u}z_s + \frac{k_t}{M_u}x_p \tag{2}$$

The main output variable from the model is an axle-body displacement (for suspension travel) $\Delta_z(t)$:

$$\Delta_z(t) = z_s(t) - z_u(t) \tag{3}$$

The normalized absolute value of the suspension travel accumulated over a period of time t_f yields a measure of road roughness ST, which is defined as

$$ST = \frac{1}{L}\int_0^{t_f} |\dot{\Delta}_z(t)|\, dt \tag{4a}$$

or in a discrete form

$$ST = \frac{1}{L}\sum_{k=1}^{N} |\Delta_z(k) - \Delta_z(k-1)| \tag{4b}$$

The trailer suspension travel is measured by a displacement transducer that introduces a measuring error due to hysteresis in its input-output characteristics. As a result, the signal $\Delta_z(t)$ produced by the transducer differs from the actual axle-body displacement, as shown in Figure 3. Figure 4 shows a simplified block diagram of the entire measuring system. In order to investigate the performance of the trailer-based measuring system, the computer program CARTRA has been developed at the Pennsylvania Transportation Institute. The program allows for simulation of the half-trailer model given by Equations 1 and 2, together with the assumption that the displacement transducer has a nonlinear characteristic with hysteresis of width 2δ. The program calculates an accumulated suspension travel of the half-trailer model subjected to an arbitrary road profile, which is measured by the displacement transducer with hysteresis in the input-output characteristic. Again, for consistency with the quarter-car model analysis, the same road profile as that used in verifying the acceptability of the quarter-car parameters introduced by Gillespie et al. *(3)* is used as the input. The profile, called the ABAB pattern, is shown in Figure 5. According to Gillespie et al. *(3)*, this profile has the spectral properties of an average bituminous road at 50 mph when the profile is actually traversed at 15 mph. The same test conditions as specified in Gillespie et al. *(3)* were used in the computer simulation. The velocity of the trailer was 15 mph, and the period of integration of the suspension travel was equal to the time it takes to traverse the profile plus 1 sec for the transient motion of the trailer to cease. Although many states have found that these ABAB bumps do not provide good calibrations, the bumps provide a good basis for comparisons with simulations. Alternative methods are also given for actual calibration.

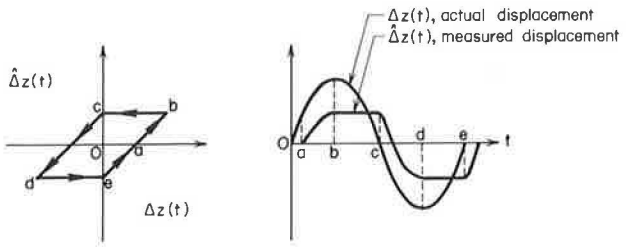

FIGURE 3 Transducer hysteresis and its effect on measured displacement.

FIGURE 4 Block diagram of a trailer-based system.

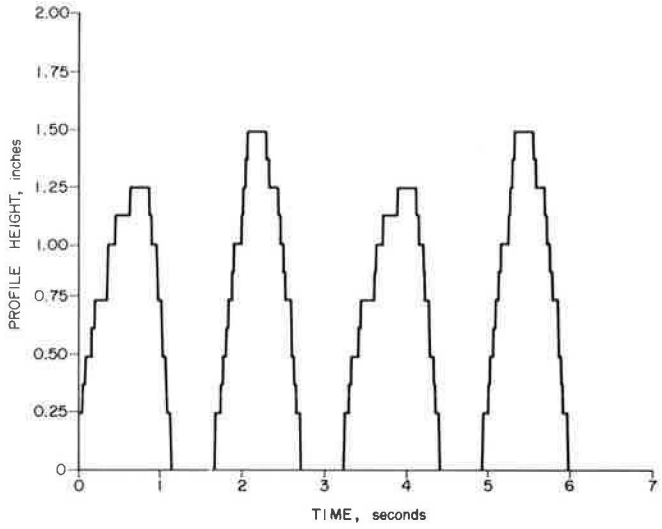

FIGURE 5 ABAB calibration surface profile.

The results of computer simulation of the half-trailer system subjected to the conditions just described are shown in Figure 6. The parameters that are of greatest concern in determining the acceptability of a road roughness measuring system—the relative damping coefficient of the shock absorber $\gamma = C_s/M_s$ and the transducer hysteresis δ—were varied over the ranges 5 to 13 sec^{-1} and 0 to 1.27 mm (0.05 in.), respectively.

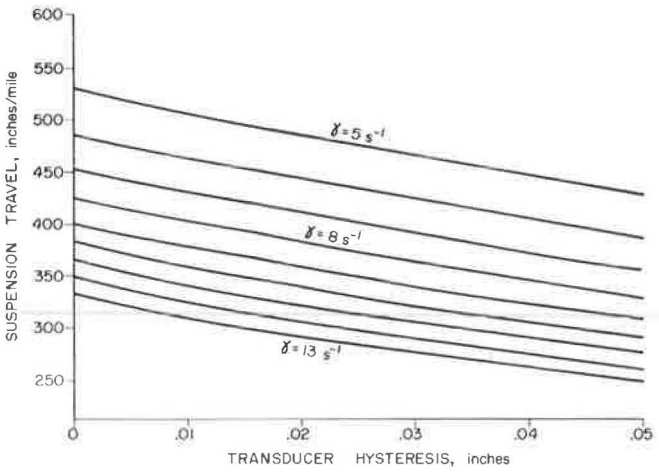

FIGURE 6 Computer simulation of suspension travel versus transducer hysteresis for different damping coefficients.

Effect of Shock Absorber Nonlinearities

In the trailer simulation program used to generate suspension travel data, a linear model of the trailer given by Equations 1 and 2 was used. Actual shock absorber characteristics are nonlinear and concern over how these nonlinearities affect the trailer performance is justified. The confidence with which the results obtained for a linear model can be applied to actual trailers are certainly affected by the shock absorber nonlinearities.

In order to investigate the problem, a nonlinear force-versus-velocity characteristic for a typical shock absorber was incorporated in the trailer simulation program. Figure 7 shows the characteristics of a shock absorber installed in a 1967 midsized Chevrolet; the force-velocity relationship is indeed strongly nonlinear. In addition, the shock absorber exhibits much greater damping in extension than it does in compression, as is shown by different slopes of the two dashed straight lines representing linear approximations for the positive and negative applied velocities.

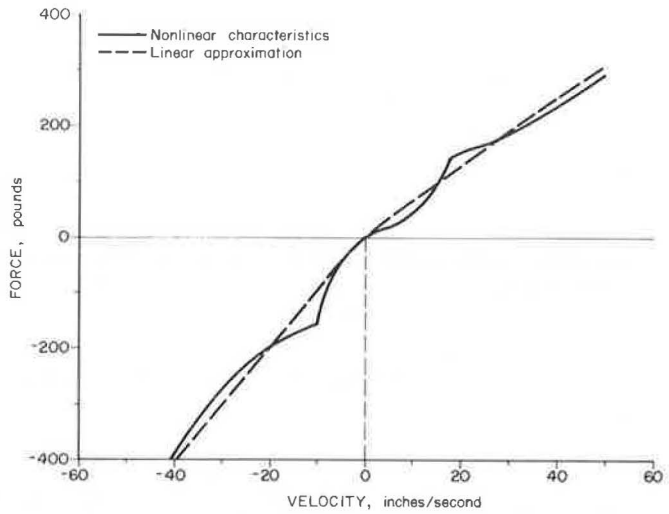

FIGURE 7 Nonlinear shock absorber characteristic.

The results of the computer simulation for a trailer with linear and nonlinear shock characteristics are shown in Figure 8. The dashed line represents the accumulated suspension travel of the trailer with the nonlinear shock absorber. The solid line indicates the results obtained using the linear trailer model with relative shock absorber damping $\gamma = 3.58$, which is the value that yields a suspension travel versus hysteresis characteristic closest to that of the nonlinear characteristic. A good agreement between the nonlinear and linear model performance can be observed from Figure 8. The following explanation is offered for this observation. The ABAB profile contains a broad spectrum of frequencies and a large range of amplitudes. The response of the nonlinear trailer model is integrated over the length of the profile and normalized with respect to the unit length. The mathematical operations of integration and division by the integration range yield an average value of the integrated variable, the trailer suspension travel in this case. All the partial responses of the trailer to all the components of the ABAB profile are averaged out. On the other hand, the linearized characteristic of the shock absorber represents an average damping coefficient of the nonlinear shock absorber. If the amplitudes contained in the road profile are equally distributed, averaging of the damping characteristic and averaging of the trailer response yield similar results. Therefore, the effect of shock absorber nonlinearity is negligible. Considerable care should, however, be exercised if profiles other than ABAB are used. If the distribution of amplitudes of different frequency components in the road profile is not uniform, the process of averaging the trailer response is disturbed, and significant discrepancies may occur between the linear and nonlinear cases. This possibility should be taken into consideration when a new road surface is selected for the calibration of road roughness measuring systems.

Another source of nonlinear effects in shock absorber performance is variation in air temperature, which causes changes in the temperature and thus in the viscosity of the shock absorber fluid. In a study by Croteau (private communication), the analysis of 300 pairs of roughness and temperature data collected on five different pavements indicates that a 10°F change in air temperature causes a measurement error of about 3 in./mi. In

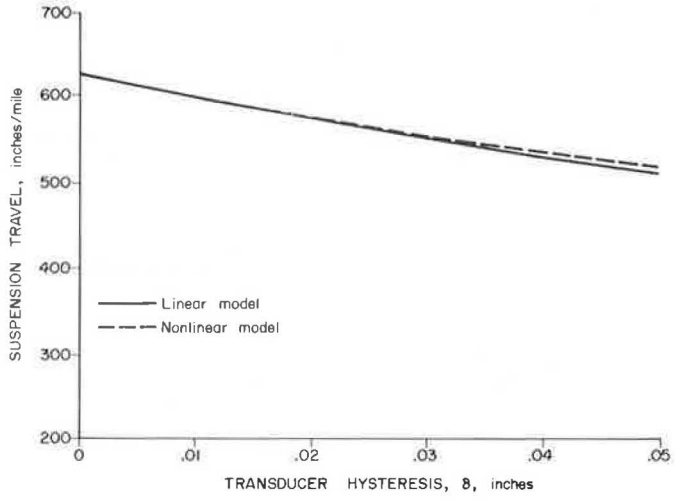

FIGURE 8 Effect of nonlinear shock absorber characteristics.

conjunction with this study, temperature correction equations are currently being developed.

Shock Absorber Acceptability Criterion

The accuracy of road roughness measurements obtained with a trailer system is dependent primarily on the extent to which the actual trailer parameters agree with the parameters of the standard model given in Table 1. The measuring error is also affected by the hysteresis of the axle-body displacement transducer. The proposed ASTM standard establishes the following limits for the deviations of the relative shock absorber damping coefficient γ, and for the hysteresis of the displacement transducer δ:

$$5.5 \text{ sec}^{-1} \leq \gamma \leq 13.0 \text{ sec}^{-1} \tag{5a}$$

and

$$0 \leq \delta \leq 0.05 \text{ in. } (1.27 \text{ mm}) \tag{5b}$$

The limiting values of the relative damping coefficient were selected so that the values of the accumulated suspension travel generated by the half-trailer models with $\gamma = 5.5$ and 13.0 sec^{-1} towed over the ABAB surface differ by ±20 percent, respectively, from the accumulated suspension travel obtained with the standard model ($\gamma = 8.0$) towed over the same surface. The 20 percent deviations occur for $\delta = 0$ in the displacement transducer. The maximum acceptable value for hysteresis, $\delta = 0.05$ in. (1.27 mm), also causes a 20 percent deviation in the accumulated suspension travel value when the relative shock absorber damping coefficient is equal to its standard value $\gamma = 8.0$ sec^{-1}. The dashed area in Figure 9 represents the acceptable combinations of the relative damping coefficient γ and the transducer hysteresis δ. The acceptability criterion can also be stated in a more general form as follows: a trailer is considered acceptable if the normalized suspension travel measured while the trailer is towed over the ABAB surface lies within the acceptable area marked in Figure 9. This is the equivalent of the requirements for a car presented in *NCHRP Report 228 (3)*.

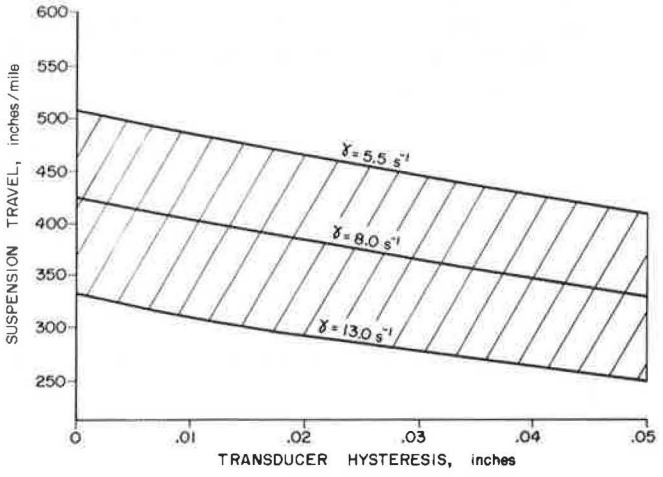

FIGURE 9 Shock absorber acceptability area.

The acceptability criterion raises doubts whether indeed one can distinguish good or acceptable trailers from bad or unacceptable ones. The measuring error of a trailer having relative damping coefficient γ and transducer hysteresis δ, towed over the ABAB surface, can be calculated as

$$\varepsilon(\gamma, \delta) = \frac{|ST(\gamma, \delta) - ST(8.0, 0.0)|}{ST(8.0, 0.0)} \times 100 \text{ percent} \tag{6}$$

The limits for the shock absorber damping γ and transducer hysteresis δ given by Equation 5 were established separately for the two parameters. In actual measurements, the error is determined by a combined effect of the deviations of γ and δ from their reference values. To illustrate this effect, the measuring error defined by Equation 6 was plotted versus hysteresis for several values of shock absorber damping coefficient. Figure 10 shows that the error is zero even in instances where both

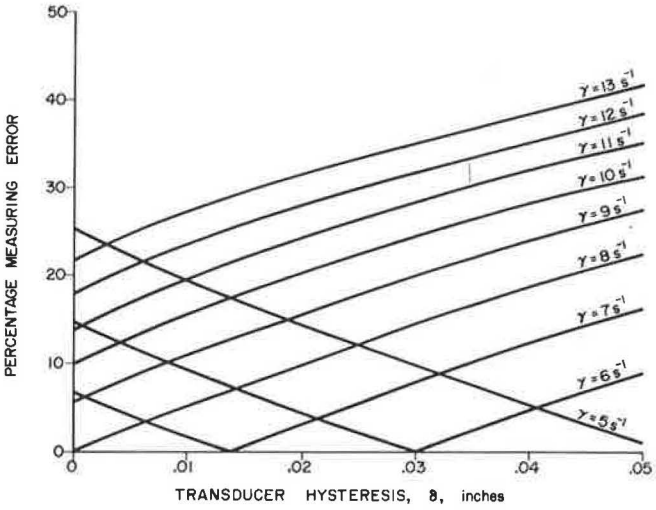

FIGURE 10 Measuring error curves for different values of system parameters.

parameters do not have the values prescribed by the standard. In fact, for each value of relative damping coefficient γ less than 8.0 sec^{-1} there is a nonzero value of transducer hysteresis δ for which the error is zero. This effect is caused by the two error components, one from the damping coefficient and the other from the transducer hysteresis, that cancel each other. Physically, this fact can be explained by noting that if a softer shock absorber is used, $\gamma < 8.0$ sec^{-1}, the trailer suspension overreacts, producing larger values of accumulated suspension travel, which can be partially or even totally compensated by a loss of motion in increased hysteresis of the axle-body motion transducer. For harder shock absorbers, the two error components always add up, contributing to the increased value of the overall measuring error. It can therefore be concluded that, in general, softer shocks are more likely than harder shocks to produce accurate results. This conclusion must not be extended too far to prevent drastic nonlinear effects such as hitting shock absorber end limits from interfering in the measuring process.

The ASTM acceptability criterion for road roughness measuring trailers establishes limits on shock absorber damping and transducer hysteresis, neglecting the effect of interaction

between γ and δ. In its present form, the criterion is cause-oriented and not result-oriented. To illustrate the consequences of such a formulation of the acceptability criterion, consider two systems. In the first system, the hysteresis $\delta = 0.05$ in. (1.27 mm) is within the acceptable limits, and the damping coefficient $\gamma = 5.0$ sec^{-1} is outside the acceptable limit. Therefore, according to the criterion, the trailer is unacceptable. From Figure 10, the measuring error for this unacceptable trailer is less than 2 percent. On the other hand, a trailer with a transducer hysteresis $\delta = 0.04$ in. and damping coefficient $\gamma = 13.0$ sec^{-1} is acceptable according to the proposed criterion. The measuring error of this trailer on the ABAB surface is about 38 percent (Figure 10).

It is proposed that the acceptability criterion be based on the measuring error of the trailer rather than on deviations of the trailer parameters from the standard values. A trailer acceptability would then be decided solely on the basis of the difference between the accumulated suspension travel when the trailer is towed over the ABAB surface and the suspension travel generated by the standard half-trailer model. Figure 11 shows the acceptable area as determined by a 20 percent

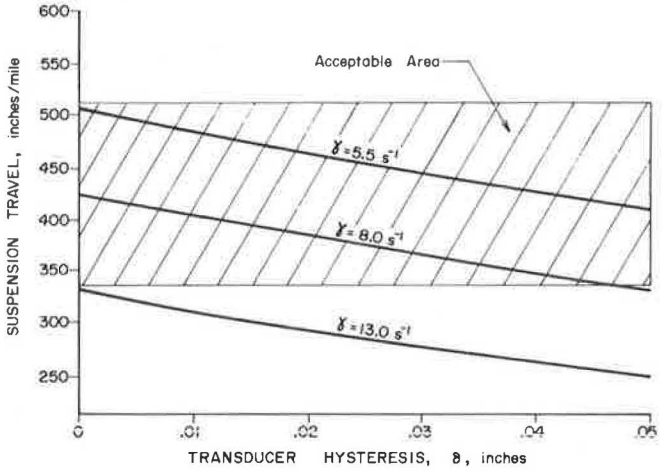

FIGURE 11 Modified acceptability criterion.

maximum acceptable difference between the suspension travel values. According to this acceptability criterion, the transducer hysteresis must be less than 0.05 in. (1.27 mm), but an acceptable value of damping coefficient depends on the actual value of the hysteresis

$$\gamma_{min}(\delta) \leq \gamma \leq \gamma_{max}(\delta)$$

The two limiting curves $\gamma_{min}(\delta)$ and $\gamma_{max}(\delta)$ are plotted in Figure 12. The following regression equations have been developed for the limiting curves:

$$\gamma_{min} = 5.49 - 55.4\delta + 341\delta^2 \quad (7)$$

$$\gamma_{max} = 12.8 - 159\delta + 1{,}078\delta^2 \quad (8)$$

Verification of Shock Absorber Acceptability

A practical procedure to be employed in the verification of trailer acceptability in terms of the ASTM standard depends on

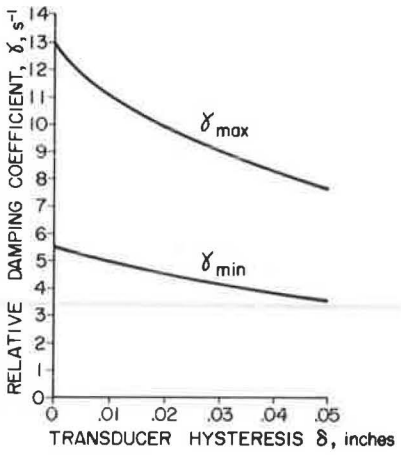

FIGURE 12 Minimum and maximum relative damping coefficients for the modified acceptability criterion.

whether the ABAB calibration surface is available or not. Both situations will now be considered. The procedure is the same, regardless of which of the two acceptability criteria discussed in the previous section is used.

The first step in the verification procedure involves a determination of the transducer hysteresis. This step is the same, regardless of what calibration surface is used. If the hysteresis δ_a is acceptable, that is, less than 0.05 in. (1.27 mm), the corresponding maximum and minimum values of the accumulated suspension travel ST_{max} and ST_{min} are found from Figure 9, where

$$ST_{max}(\delta_a) = ST(\delta_a)\,|_{\gamma = 5.5} \quad (9)$$

and

$$ST_{min}(\delta_a) = ST(\delta_a)\,|_{\gamma = 13.0} \quad (10)$$

If the ABAB surface is available, the trailer is towed over it and the generated suspension travel is measured. The trailer is considered acceptable if the measured accumulated suspension travel falls between the minimum and maximum values corresponding to the transducer hysteresis. Mathematically, the acceptability condition can be presented as

$$ST_{min}(\delta_a) \leq ST(\delta_a) \leq ST_{max}(\delta_a) \quad (11)$$

This procedure is illustrated in Figure 13.

For most users of road roughness measuring trailers, the ABAB surface is not readily available. It is therefore desirable that the proposed ASTM acceptability criterion be applied to other surfaces.

The following procedure is proposed for verification of shock absorber acceptability on a user-selected pavement surface.

1. Select a road section subject to some regimen and obtain profile data for it.

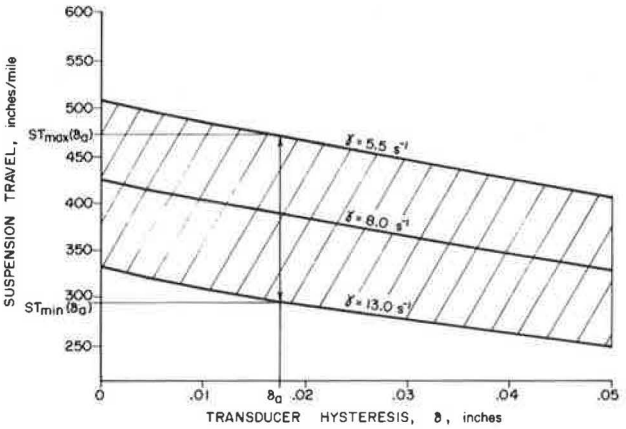

FIGURE 13 Verification of shock absorber acceptability.

2. Determine hysteresis δ_a in the axle-body displacement transducer.

3. Simulate a half-trailer model subjected to the road profile obtained in Step 1 with transducer hysteresis δ_a for two values of damping coefficient, γ_{min} and γ_{max}. Record the accumulated suspension travel values obtained for the limiting values of the damping coefficient, $ST_{min}(\delta_a)$ and $ST_{max}(\delta_a)$.

4. Tow the trailer over the selected road test section and measure the generated suspension travel $ST(\delta_a)$. The trailer, and in particular its shock absorbers, will be considered acceptable if the acceptability condition is satisfied, that is, if

$$ST_{min}(\delta_a) \leq ST(\delta_a) \leq ST_{max}(\delta_a)$$

In order to employ this procedure, a profile of the selected road test section must be provided. Also, a computer program will be necessary in Step 4 to simulate a half-trailer model.

To illustrate the procedure, a complete shock absorber acceptability area was developed for the Pavement Roughness Research Facility of the Pennsylvania Transportation Institute (PTI) *(4)*. The results are shown in Figure 14. The PTI profile is composed of 11 sinusoidal sections of different amplitude and wavelength. The amplitudes and wavelengths in the 11 sections were selected to approximate a white noise frequency spectrum when the profile is traversed three times at 30, 60, and 90 ft/sec. When the results obtained with the ABAB and with the PTI surfaces are compared, some interesting observations can be made. First, the level of roughness of the PTI surface is considerably higher. In fact, the PTI surface is much rougher than most actual road surfaces. This causes the ABAB curves to decline faster with increased hysteresis, because the effect of hysteresis is more visible at the lower level of surface roughness. The relative effect of the shock absorber damping coefficient is most pronounced on the ABAB surface. The sensitivity of the accumulated suspension travel to changes in the damping coefficient can be defined as

$$\frac{(ST|_{\gamma = 5.5}) - (ST|_{\gamma = 13.0})}{ST|_{\gamma = 8.0}} \times 100 \text{ percent}$$

which is equal to 40 percent for the ABAB surface and 30 percent for the PTI profile.

These observations should be taken into consideration when a road section is to be selected for testing shock absorbers. The test surface should be sufficiently rough to ensure the required sensitivity of the measuring system. From the results obtained on both the ABAB and the PTI surfaces, the normalized accumulated suspension travel will change by about 20 percent when the value of the damping coefficient changes from its standard value, $\gamma = 8.0\ sec^{-1}$, to the maximum or minimum admissible value, $\gamma = 13$ or $\gamma = 5.5\ sec^{-1}$, respectively. The higher the level of roughness, the better the resolution of the measurements obtained with a trailer. In addition, the road roughness should be fairly uniformly distributed along the length of the selected section. If a selected road has only a few severe bumps that contribute to high average roughness, the results of the measurements may be disturbed by nonlinearities in the trailer suspension.

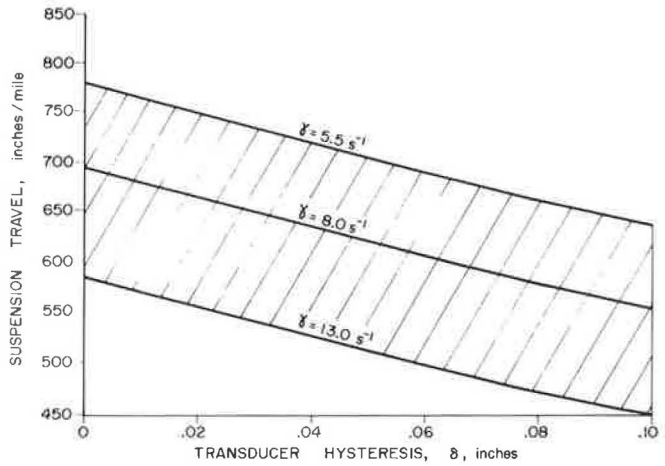

FIGURE 14 Acceptability area for the PTI Pavement Roughness Research Facility.

CONCLUSION

A procedure for verifying the acceptability of shock absorbers for use in road roughness measuring trailers has been presented. The testing procedure is simple and can be conducted on any road section for which the profile data have been acquired. It is desirable that the test surface have a high level of roughness uniformly distributed along its length. A computer simulation program is also necessary to calculate maximum and minimum acceptable values of the trailer suspension travel produced when the trailer is towed over the test surface. The ASTM acceptability criterion should be modified to address the problem of the accuracy of the entire trailer. In its present form, the criterion determines the acceptable limits of the shock absorber damping coefficient, which constitutes but one element of the trailer. The accuracy of the trailer does not depend exclusively on its shock absorber nor on any other single component of the system, but is a result of interaction among all the trailer elements. A new modified criterion has been proposed, based on the relative measurement error rather than on the values of selected trailer parameters.

REFERENCES

1. J. C. Wambold and J. J. Henry. *Standard Practice for Simulating Vehicular Response to Longitudinal Profiles of a Vehicular Traveled Surface*. ASTM Task Group E17.33.80.1, American Society for Testing and Materials, Philadelphia, Pa., Oct. 1, 1985.
2. *Standard Specification for Trailers Used for Measuring Vehicle Response to Road Roughness*. Draft Specification, ASTM Committee E-17. American Society for Testing and Materials, Philadelphia, Pa., Sept. 1984.
3. T. D. Gillespie, M. W. Sayers, and L. Segel. *NCHRP Report 228: Calibration of Response Type Road Roughness Measuring System*. TRB, National Research Council, Washington, D.C., 1980.
4. D. W. Ahn. *Simulation of the Quarter-Car Model on a Reference Road*. Master's thesis, Pennsylvania State University, University Park, Dec. 1984.

Publication of this paper sponsored by Committee on Surface Properties-Vehicle Interaction.